SYNTHESIS, CHARACTERIZATION AND DEVICE STUDIES OF CONJUGATED FOLADMERS

A DISSERTATION IN

Chemistry

And

Pharmaceutical science

Presented to the Faculty of the University
Of Missouri- Kansas City in partial fulfillment of
The requirements for the degree

DOCTOR OF PHILOSOPHY

By
KULDEEP CHANDRASHEKHAR SHETYE
M. Sc. (Thesis) University of Mumbai, 2008

Kansas City, Missouri
2017

SYNTHESIS, CHARACTERIZATION AND DEVICE STUDIES OF CONJUGATED FOLADMERS

KULDEEP SHETYE, Candidate for the Doctor of Philosophy Degree

University of Missouri-Kansas City, 2017

ABSTRACT

Conjugated polymers have found a wide range of electronic applications in last few decades due to their superior combination of optoelectronic, mechanical properties, and solution processability. In the past few years, significant advancement has been achieved in developing organic semiconductors with high charge mobility, which are used in solar cells, organic light emitting diodes, and organic field effect transistors. Two of the main challenges of organic semiconductors, for commercialization are their efficiency and lifetime. Although the power conversion efficiency (PCE) of organic solar cells has improved to above 10%, device stability has remained a major issue. Conjugated foldamers can be considered as a viable option to achieve the desired stability. Conjugated foldamers are generally driven by secondary interactions such as π-π stacking, H-bonding, and solvophobic interactions. We have designed foldamers based on polycyclic aromatic systems (PCA) that have large aromatic sizes. PCA containing conjugated polymers may form π-stacked columns after folding. These conjugated foldamers exhibit efficient charge transport that is an essential property for optoelectronic devices. We envision that in a composite containing a conjugated foldamer and doped electron acceptors (such as PCBM), the dopants may be encapsulated inside the folded

polymers, leading to improved morphological stability, and thus, device stability. We have synthesized triphenylene-based conjugated foldamers **58** and **59** with and without imide functionalization and studied their optoelectronic properties. Their optical data in different solvents showed interesting results that provided folding possibilities of **59** also supported by their theoretical calculations.

In the next chapter, we report the synthesis and characterization of a new conjugated foldamer based on imide-functionalized naphthodithiophene (INDT) building blocks. We also synthesized naphthalene dithiophene (NDT)-based D/A conjugated polymers **31** and **36** for comparison with INDT based polymers. Their UV/vis absorption and fluorescence emission properties with respect to solvents and concentrations have been carefully studied to shed light on their folding process. CD spectroscopy was used to confirm the presence of helical folding present in the polymers. The device properties of INDT-based polymers were found to be 0.026 and 0.18% for polymers **20** and **22,** respectively.

In the last chapter, we have synthesized organic-inorganic hybrid conjugated copolymer **56** wherein hexamolybdate clusters are covalently embedded in the main chain with diene and have characterized their properties using ^{1}H-NMR, GPC and CV spectroscopy.

APPROVAL PAGE

The faculty listed below, appointed by the Dean of the College of Arts and Sciences have examined a dissertation titled "Synthesis, Characterization and Device Studies of Conjugated Foldamers", presented by Kuldeep Shetye, candidate for the Doctoral of Philosophy degree, and certify that in their opinion is worthy of acceptance.

Supervisory Committee

Zhonghua Peng, Ph.D.
Committee Chair
Department of Chemistry

James R. Durig, Ph.D.
Department of Chemistry

Keith Buszek, Ph.D.
Department of Chemistry

Kathleen V. Kilway, Ph. D.
Department of Chemistry

Simon Friedman, Ph.D.
Department of Pharmacy

William G. Gutheil, Ph.D.
Department of Pharmacy

CONTENTS

ILLUSTRATIONS

SCHEMES

TABLES

ABBREVIATIONS

OLED	Organic light emitting diode
OFET	Organic field effect transistor
PCE	Power conversion efficiency
PCA	Polycyclic aromatic compounds
PCBM	[6, 6]-phenyl-C_{61}-butyric acid methyl ester
INDT	Imide functionalized naphthalene dithiophene
CD	Circular dichroism
OPV	Organic photovoltaics
PVD	Photovoltaic device
EDOT	Ethylene dioxythiophene
HOMO	Highest occupied molecular orbital
LUMO	Lowest uncoccupied molecular orbital
PBI	Perylene bisimide
PAH	Polycylic aromatic hydrocarbon
DLC	Discotic liquid crystal
SCLC	Space charge limited current
TPA	Triphenylene aromatic
THF	Tetrahydrofuran
NDT	Naphthalene dithiophene
DMF	*N*,*N*-Dimethyl formamide
DFT	Density functional theory
TEG	Triethylene glycol

POM	Polyoxometalate
$PC_{71}BM$	[6, 6]-phenyl-C_{71}-butyric acid methyl ester
RFID	Radio frequency identification
CdTe	Cadmium-telluride
CIGS	Copper-indium-gallium-selenide
GaAs	Gallium arsenide
OSC	Organic solar cell
PV	Photovoltaic
ITO	Indium tin oxide
V_{OC}	Open circuit voltage
J_{SC}	Short current density
FF	Fill factor
P_{max}	Maximum power
J_m	Current density
V_m	Voltage
η_p	Power conversion efficiency
P_0	Incident light intensity
EQE	External quantum efficiency
IPCE	Incident photon collected electron
D/A	Donor- acceptor
CT	Charge transfer
E_g	Energy gap
LED	Light emitting diode

L_{AB}	Bond length alteration
CV	Cyclic voltammetry
DSC	Diffraction scanning calorimetry
XRD	X-ray diffraction
PR-TRMC	Pulse radiolysis time resolved microwave conductivity
TOF	Time of flight
NBS	*N*-Bromosuccinamide
H_2SO_4	Sulfuric acid
TFA	*tri*-Fluoroacetic acid
NMR	Nuclear Magnetic Resonance
$Ni(COD)_2$	Bis(1,5-cyclooctadiene) nickel(0)
COD	*cis,cis*-1,5-Cyclooctadiene
$Pd(PPh_3)_4$	Tetrakis(triphenylphosphine)palladium(0)
$p\text{-}(o\text{-tolyl})_3$	Tri(*ortho*-tolyl)phosphine
MeOH	Methanol
$Pd_2(dba)_3$	Tris(dibenzylideneacetone)dipalladium(0)
DCM	Methylene chloride
DMSO	Dimethyl sulfoxide
Mn	Number average molecular weight
Mw	Weight average molecular weight
PDI	Polydispersity index
GPC	Gel permeation chromatography
Fc	Ferrocene

TLC	Thin layer chromatography
RBF	Round bottomed flask
n-BuLi	n-Butyllithium
CH_3COOH/ AcOH	Acetic acid
$MoCl_5$	Molybdenum pentachloride
$FeCl_3$	Iron (III) chloride
BHJSC	Bulk heterojunction solar cell
PEDOT	Poly(3,4-ethylenedioxythiophene)
PSS	Poly(styrenesulfonate)
IR	Infrared spectroscopy
KOH	Potassium hydroxide
$MgSO_4$	Magnesium sulfate
PSC	Polymer based solar cell
BHJ	Bulk heterojunction
POSS	Polyhedral oligomeric silesquioxane
TMSP	Transition metal substituted polyoxometalate
DCC	Dicyclohexylcarbodiimide
CH_3CN	Acetonitrile

ACKNOWLEDGEMENTS

I would like to take this opportunity to thank primarily my advisor and chair of my committee, Prof. Zhonghua Peng. Without his guidance and continuous encouragement, this dissertation could not have been possible. He has always encouraged us to think of any problem independently and objectively, plan ahead of time, and execute to minimize errors. He has been patient and supportive with me and shaped as well as helped to grow the analytical thinking and research attitude in me.

I would like to extend my thanks to other dissertation committee members, Prof. James R. Durig, Prof. Kathleen Kilway, Prof. Keith Buszek, Prof. Simon Friedman, and Prof. William G. Gutheil, for their professional guidance and valuable support in reviewing my dissertation.

I am grateful to Dr. Nikoloy Gerasimchuk, Department of Chemistry, Missouri State University for his kind assistance with the CD measurements. I specially wish to express my earnest thanks to Dr. Yong Li at Department of Chemistry, UMKC. He has been of great help for photovoltaic device fabrications and has been a good mentor in assisting me with difficult concepts. I would also like to thank Dr. Tanmoy Dutta for helping me in the initial stage of my graduate studies. I would like to thank all the members of Dr. Peng's group, both past and present: Dr. Ching-en Chou, Dr. Shaohua Li, Dr. Jin Lu, Dr. Ruixin Wang, Mr. John Oster, Mr. Kyle Scheel and Mr. Xiaodong Yan. They all have been very helpful, and I have had great time working with them. My special thanks to all the staff of the Department of Chemistry: Ms. Josephine Maningat, Ms. Asia Williams, Mr. John Whitchurch, Mr. Michael Sykora, and Ms. Kathy Garrison.

I would also like to thank my previous advisor Prof. Suhas Pednekar, Ramnarain Ruia College, University of Mumbai, under whose guidance I finished my Master degree in Organic

chemistry (by Research) in India. I was first introduced to organic reactions in his laboratory, and his positive as well as professional approach towards his life and career has always inspired me to do well.

It would be incomplete if I forget to mention two of my favorite professors under whose guidance I learned many innovative things not only in Chemistry but also in general towards life. Late Dr. J. N. Gadre, from Ruia College, University of Mumbai, with whom I had lots of friendly discussions, had always wished well for all his students including me. Late Prof. Dr. K. D. Deodhar, IIT Bombay, was one of the most generous and knowledgeable persons I have ever came across in my life. He would always help us to find solutions to any difficult problems and showed us how to lead a successful life. Both have left an unforgettable impression in my life. I have tried to inculcate those principles in my life and hope to follow the path they have shown me.

I wish to acknowledge all those people who have helped me in my professional career, Dr. R. N. Ganguly, Prof. Sanjay Mahajani, Dr. Aashish Hingole, Dr. Jignesh Trivedi, Dr. Junaid Shaikh, Dr. Vibhuti Dukhande, Dr. Minal Naik, Dr. Ganesh Mule, Dr. Bhushan Deodhar, Dr. Sudhanunshu Purohit, and Mr. Dattatray Sawant.

My friends have also shown faith in me and helped me in times of need: Mr. Kapil Kulkarni, Mr. Pradnesh Vaidya, Mrs. Tejashree Vaidya, Dr. Aashima Khosla, Dr. Vikram Panwar, Dr. Neena Kanwar, Miss Gunjan Shetye, Miss Mayuri Patil, Mr. Tejas Bhosle, and all my relatives, especially Mr. Swapnil Shetye and Mrs. Neha Shettigar, and all others who have blessed and showered me with unconditional love and support.

Finally, I would like to express my deepest love, respect and gratitude towards my parents, Mr. Chandrashekhar Shetye and Mrs. Sheela C. Shetye for their love, caring and support that helped me to face all the difficulties and stay focused on my study towards Ph.D.

Dedicated to my dear parents for their unconditional love and support

CHAPTER 1

INTRODUCTION

Organic electronics deals with the study of design, synthesis, characterization, and applications of small organic molecules or polymers that are capable of transporting charges. This area has attracted significant research efforts in the last two decades due to the pressing need of finding alternative clean energy sources and improving the current electronics market. With the ever-growing electronics market, it is essential to come up with materials that are highly efficient and are cost effective. The global flexible electronics market is expected to reach around USD 27.21 billion by the year of 2024 as per the recent market analysis report.[1] These devices are attractive due to their ability to curve, roll, flex, adapt and fold.

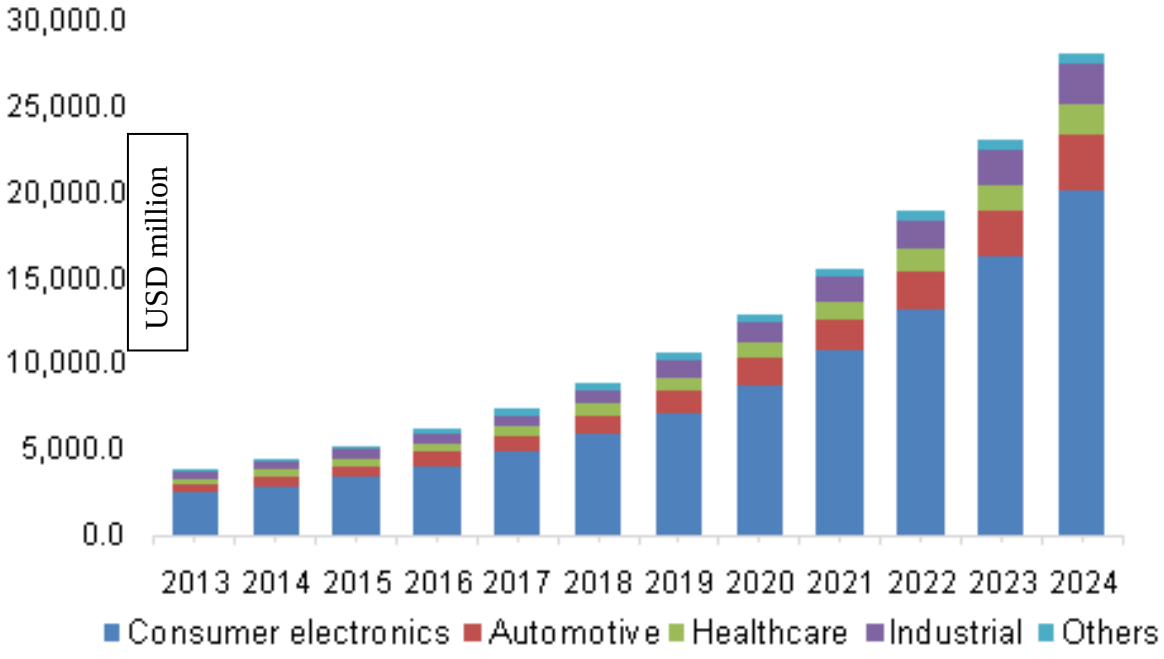

Figure 1: Asia specifc growth of flexible electronics market in the near future (2013-2024).[1]

Traditionally, those semiconducting materials were made of inorganic materials. These inorganic materials have delocalized electrons, which can move freely through interatomic spaces and hence have good electrical conductivity. On the other hand, organic materials, which may possess lower charge carrier mobility, have some advantages. With organic materials, it is easy to alter the band gap via chemical modifications; they have lower fabrication cost, they are much lighter in weight, less fragile, and resistive to corrosion. These organic materials include organic molecules and polymers; fullerenes, nanotubes, graphene, and other carbon based molecular structures; ensembles of molecules and molecular structures; and hybrid materials. While most organic electronic devices are still in the early stage of prototype demonstration, some are being commercialized as competitive products. For example, displays based on organic light emitting diodes (OLED) have entered the market for years. Ching W. Tang[2] and Steven van Slyke from Eastman Kodak in (1980) first demonstrated OLED. Companies like Sony,[3] Samsung,[4] and LG[5] are frontiers in OLED research and occupy major commercial market for OLED TV. Television screens study predicts that the total market for OLED materials will grow from about $450 million in 2013 to over $4.6 billion by the end of 2020. Organic materials, thus whether used in combination with inorganic materials or without, hold the potential to expand our electronic horizon in ways unimaginable.

Conducting polymers have some unique properties such as good mechanical strength, ease in processing, and remarkable flexibility (bendable and reversibly stretchable), making them a better choice for certain electronic applications. Conducting polymers were first reported in 1977 by Shirakawa,[6] Alan Heeger, and Alan MacDiarmid, who discovered that iodine-doped polyacetylene could be highly conductive. Because of this discovery, they won the 2000 Nobel Prize in Chemistry.[7] The 2010 Millennium Technology Prize, one of the

world's most prestigious technology prizes was awarded to Michael Graetzel for his invention of dye-sensitized solar cells[8] and Sir Richard H. Friend for his work on plastic electronics.[9] Organic electronics have broad applications as organic light emitting diodes (OLED),[10] organic field effect transistors (OFET),[11] solar cells,[12] radio frequency identification (RFID) tags, memory devices etc.[13]

1.1 Organic photovoltaics

Out of the various applications of organic electronics, renewable sources of energy like solar has been one of the most prominent uses that could be achieved using organic photovoltaics (OPVs). Solar energy is one of the cleanest sources of energy available today and offers inexhaustible supply that is pollution free.[14] Solar cells and solar module arrays have predominantly made of inorganics like crystalline silicon, germanium (Generation I technology). A. E. Becquerel, a French physicist in 1839, was the first to understand the photovoltaic effect and proposed the idea of photovoltaic cell.[15] In 1883, Charles Fritts built solar cell using semiconductor material selenium after coating it with a thin layer of gold, but it had efficiency of only 1%.[16] Daryl Chapin, Fuller, and Pearson from Bell laboratories reported the first practical silicon solar cell in 1954 with efficiency about 6%.[17]

There are generally two types of 1st generation solar cells, namely single crystalline and multi crystalline silicon solar cells. They have high efficiencies, approximately 25% and 20%, respectively, and have been used for commercial production.[18] Organic solar cells (OSCs) still suffer from low efficiency. However, due to the promise of providing solar to electrical energy conversion in portable, lightweight, and flexible substrates at a lower cost, there is a push for the development of OSCs.

The Generation II materials used in the manufacture of solar cells include CdTe (cadmium-telluride) and copper-indium-gallium-selenide (CIGS), gallium arsenide (GaAs), amorphous silicon (a-Si:H)[19-22] that are deposited by vacuum or chemical vapor deposition techniques, since they are less expensive and can be made in thinner films as compared to silicon solar cells. The efficiencies of these kind of solar cells has reached up to 28.1% for GaAs single junction devices and 42.3% for GaAs triple junction metamorphic cells.[23-25] However, their broader applications are limited as compared to Generation I materials due to their high fabrication costs. Also, there are issues such as toxic nature of these compounds like Cd, Te, Ga, and Se and the waste materials produced after their usage as well as the limited supply of these materials regarding their earth-abundance.

Organic photovoltaics (OPVs) or organic solar cells are generally viewed as one of the most exciting near-future applications of organic electronics (Generation III materials). OPVs are attractive due to their flexibility, large area coverage, and low cost. However, a key challenge to organic solar cells is its still relatively low efficiency. The harvesting of solar energy relies on chemical and physical interactions at the interfaces between materials that harvest the light and materials that transport electrical current. While the current OPV technologies boasts conversion efficiencies that exceed 10 %, reaching even 12%, it is not yet higher enough to be competitive with silicon-based solar cells.

OPVs have some key advantages:[26]

1. Low weight and flexibility of the PV modules,
2. Semitransparency,
3. Easy integration into other products,
4. Exciting and newer future applications like wearable PV,

5. Significantly lower production costs as compared to current inorganic technologies,
6. Manufacture of OPV is a continuous process using state of the art printing tools, and
7. Short energy payback times and lower environmental impact during the manufacturing and disposal steps.

1.2 Concept of foldamers in optoelectronics

While the efficiency of OSCs (~ 10% until today) has continued to improve, the device stability has remained a major issue. Foldamers[27] can be considered as a viable option to achieve this desired stability. The term foldamer, which was coined by Moore *et al* defines it as, "a foldamer is any oligomer that folds into a conformationally ordered state in solution, the structures of which are stabilized by a collection of noncovalent interactions between nonadjacent monomer units." [27e] In the interdisciplinary nature of today's research, it is advantageous to look beyond mere covalent interactions and study the secondary interactions such as hydrogen bonding and π-π interactions that would open an array of supramolecular architectures. Examples of these non-covalent interactions can also be found in natural *α*-helices and their *β*- peptide analogues, which involves hydrogen bonding and solvophobicity. The helical nature as seen in DNA or RNA has inspired most of the foldamer research. Earlier work on natural peptides implies that folding from random coil into the helical secondary structure is the result of numerous subtle interactions of the backbone, side chains, and solvent, which are difficult to control.[28] It was found in the study of the folding of proteins from random coil to ordered secondary structures as reported by Zimm and Bragg.[29] Thus, the shape and stability of the foldamers can be attributed to the following major factors namely, solvophobicity, hydrogen bonding, and Van der Waals interactions. The study of this process would eventually lead to the control of the folding process.

The natural world has always significantly attracted human interest for the variety of examples of fascinating regularity and symmetry of which it is capable. Helical structures are very common in biological materials such as proteins and nucleic acids. Mostly, the vast number of complex shapes found in case of DNA and RNA inspired all the initial research; especially the helix structure has gained a lot of attention. The breakthrough in the field of molecular biology came when, α-helix, the best-known natural helical architecture, the right-handedness of which in natural polypeptides, was determined by Pauling in 1951.[30] Watson and Crick later found the double helical structure of DNA (Figure **2**).[31]

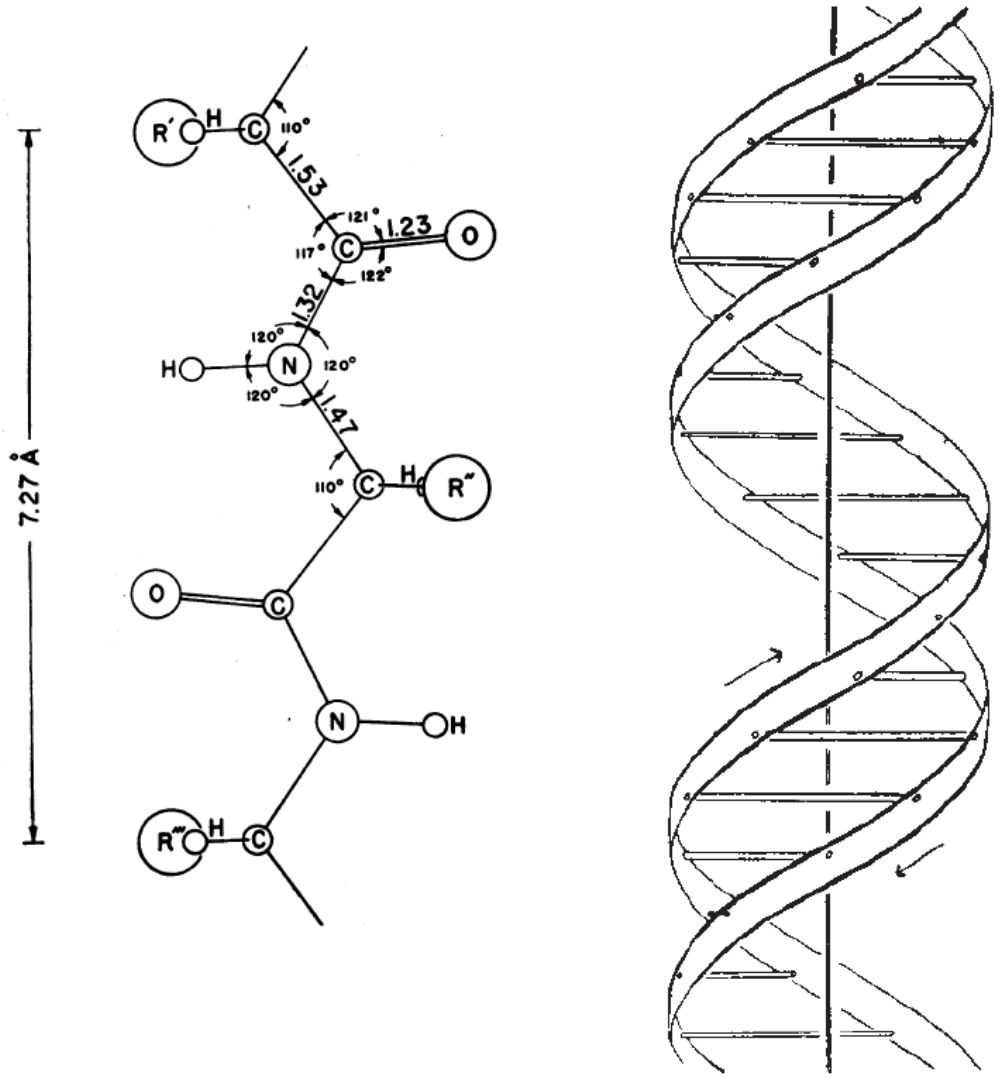

Figure 2: Dimension of polypeptide chain by Pauling[30] (left) double-stranded helix structure of DNA proposed by Watson[31] (right).

In 1955, Natta[32] discovered that stereoregular isotactic polypropylene has a helical structure in the solid state, which marked the beginning of the field for synthetic helical molecules. Doty *et al* showed helix formation of poly(γ-benzyl-*l*-glutamate) resulting from polymerization of N-carboxyanhydride of the corresponding α-amino acid, where random coil conformation changed into an α-helix structure with increasing chain length.[33] In 1960, Pino demonstrated helical structure for vinyl polymers, isotactic poly(3-methyl-1-pentene) in solution.[34] In 1969, Millich[35] showed the helical conformation of polyisocyanides with bulky

side groups, which was confirmed by Drenth and Nolte.[36] It was also later studied by Green,[37] Hoffman,[38] and Salvadori.[39] Schmidt[40] proposed *β*-structures for poly[(S)-*β*-amino-butyric acid] and later also by Goodman[41] in 1974, in addition *β*-structures was proposed for poly(*α*-isobutyl-L-asparate) by Yuki[42] although experimental results that confirmed helical conformation for poly(*α*-isobutyl-L-asparate) were obtained by Subirana[43] later. Okamoto and Yuki prepared first vinyl polymer,[44] poly(triphenylmethyl methacrylate), from an achiral monomer that had single-handed helical structure stable in solution. In addition, this polymer was commercially successful which proved the practical applicability of such synthetic helical molecules.[45]

The complexity of the folding process can be simplified by understanding the interactions, which govern folding, and eventually that knowledge would lead to control of the folding process. Among the synthetic helical structures that were synthesized, *β*-peptides are most similar to *α*-helix.[46] The folding in their structures was also governed by forces, such as hydrophobicity and intramolecular hydrogen bonding between non-adjacent amino acids. The *β*-peptides were extensively studied by Gellman[47] and Seebach,[48] and was shown that the extra carbon in the *β*-amino acid building block was the pivotal point for their synthetic architecture. Various functionalities can be incorporated in the backbone to influence the properties of the secondary architecture. While *α*-amino acids can adopt in *α*-helical motif of proteins, *β*-peptides constructed from *β*-amino acids can also adopt a different, stable helical conformation defined by interwoven 14-membered ring hydrogen bonds (a 14-helix) [trans-ACHC]. Gellman *et. al.*, designed 12-helix structure [trans-ACPC]. (as shown in Figure **3**)

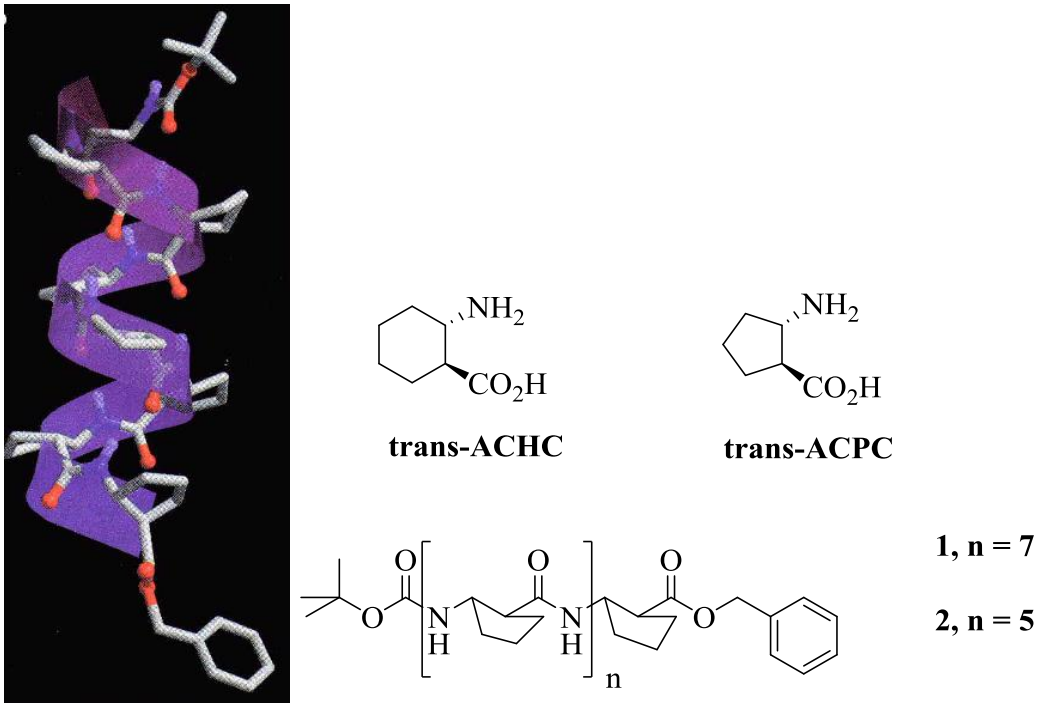

Figure 3: An example of the β-peptide capable of folding as reported by Gellman *et. al.*[47]

Based on these natural helical architectures, many synthetic strategies have been developed over the years, helicenes being one of them, that was reported by Newman in 1955.[49] They also reported the resolution of hexahelicene by selective complexation with one of the enantiomers of 2-(2,4,5,7-tetranitro-9-fluorenylideneaminooxy)propionic acid, which was also followed by Wynberg *et al* in solution.[50] The helix is a chiral structure, that may be right or left handed, i.e., *P* (plus) and *M* (minus) helix that are nonidentical mirror images. When there are no structural influences that prefer one handedness over the other, the resultant compound would be a racemic mixture of *P* and *M* helices. While if one of the two helices is selectively synthesized, then the polymer would be optically active although it may not contain any chiral group in the side or main chain. This approach for the design of helical architectures can be also extended to thiophene rings or heliphene (Figure **4**). Han *et al* first synthesized helical phenylenes (heliphenes) with 6 and 7 units of cyclobutadiene units fused with benzene. They

also studied the temperature dependent ^{1}HNMR study of [7]heliphene which resulted in remarkably low energy barrier corresponding to $\Delta G^{\neq} = 12.6 \pm 0.4$ kcal/mol, (cf. [6]- and [7] helicene: $\Delta G^{\neq}_{-27^{\circ}C} =$ 36.2 and 41.7 kcal/mol respectively) for inversion of the helical handedness.[51]

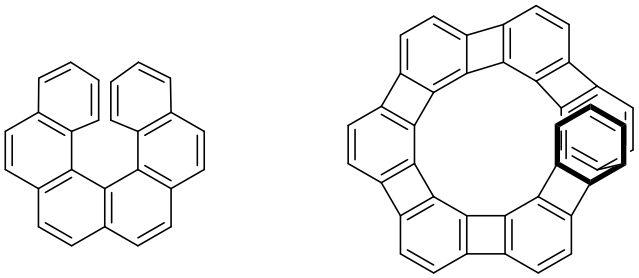

Figure 4: Structure of helicene (left) and heliphene (right).

In addition to these examples, notable progress in the field of helical conformations were also found for helical complexes of oligomeric ligands and metals, also known as helicates by Lehn in 1987,[52] oligoarylenes by Lehn in 1995,[53] and oligo(aryleneethynylene)s by Moore in 1997.[54] The helicenes are thus important in the study of field of foldamers as they demonstrate that structural constraints are essential while synthesizing these helical architectures.

The proclivity of molecules to fold mainly depends on the structural constraints present among them as well as solvophobicity and π-π stacking. Lehn *et al* synthesized oligomer units consisting of pyridine-pyrimidine units **(1)** that spontaneously arrange into multiturn helical superstructures both in solution and in solid state,[55] and the crystal structure of the structure showed a helical pitch of 3.75 Å and an interior void of about 2 Å diameter. In 2002, they also further synthesized an alternating pyridine-pyridazine heterocyclic strand that yielded hexagonal structure **2** with twelve heterocycles per turn. It has outside diameter of 25 Å and

an interior void of 8 Å respectively.[56] Lehn *et al* also proved that replacement of pyridine group in the previously synthesized pyridine-pyrimidine helicity condon **1** by 1,8-naphthyridine results in an increase of the size. In addition, the presence of highly polar 1,8-naphthyridine entity in the interior void promoted helix aggregation and assisted in the binding with various cationic species. The inner diameter in compound **3** helped to increase the inner diameter to ~ 5Å.[57] These demonstrated helical conformations, were based upon the design of helicity condons and enforced helical winding of the stand due to transoid conformation imposed around the interheterocyclic bonds, which were energetically favored over the cisoid conformation. In addition, these molecules also showed that by carefully selecting the building blocks for these helical architectures one could adjust the size of the inner void (Figure **5**).

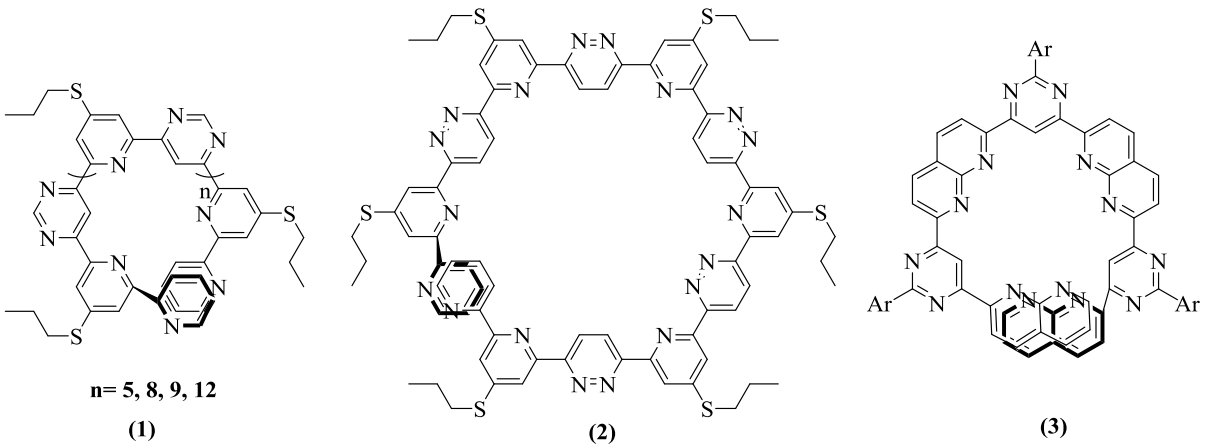

Figure 5: Aromatic N-heterocyclic helices based on π-π interactions by Lehn *et al.*[57]

Moore and coworkers deigned another type of foldamers that relied on the folding properties of the molecules based upon their π-π interactions and solvophobicity.[54] The chains in those molecules did not form intramolecular hydrogen bonds, and solvophobic interactions drove the folding transition, which was sensitive to chain length, solvent quality, and temperature. These oligo(meta-phenylenethynylene) (mPE) constructs, which are capable of

folding, were reported first time in 1997 (Figure **6**).[54] The folding nature of mPEs was based on the effect of solvophobicity, such that ethynyl linkages can adopt favorable cisoid conformation that induces folding if the compound has poor solubility. In these solvents, the system shielded the apolar benzene moieties from the solvent by adopting the cisoid form, and vice versa. The large number of π-π interactions present in the molecules helped to provide the stability to the architecture and the ethylene oxide side chains improved the solubility.

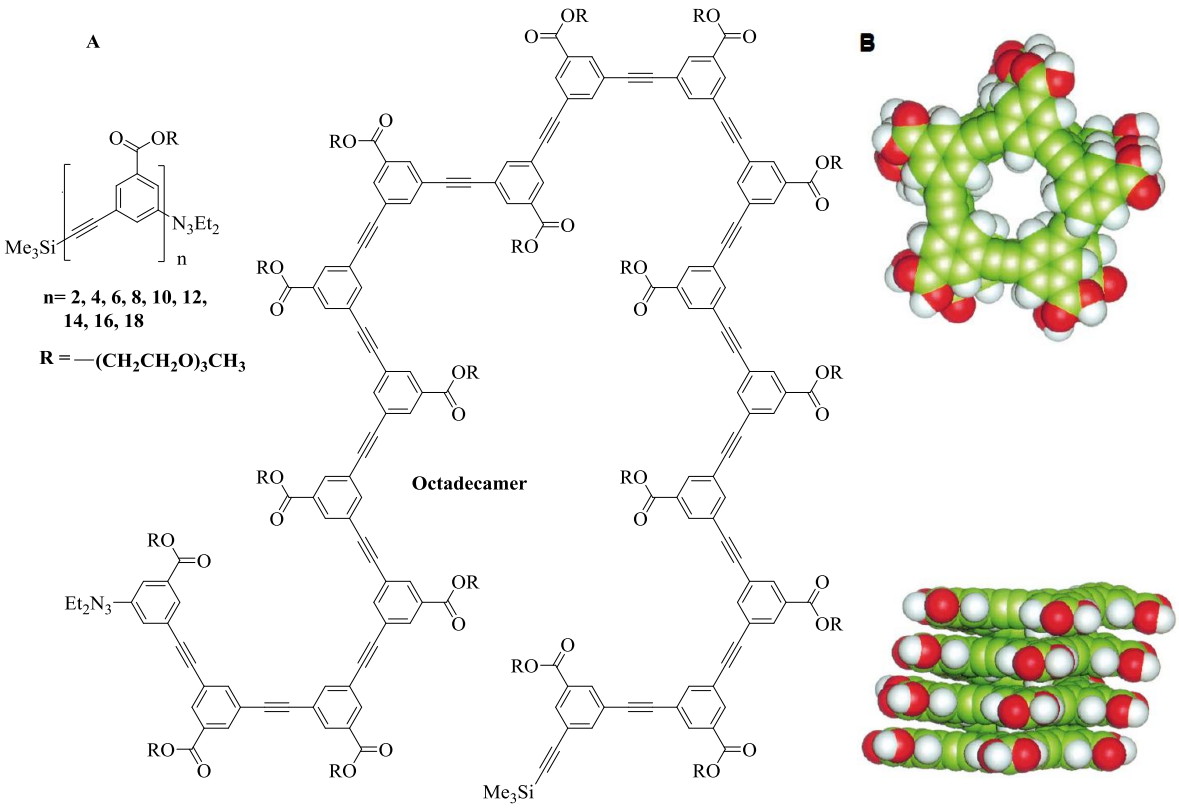

Figure 6: (A) mPEs oligomers 1 to 9, octadecamer with random coil conformation (B) helical conformation of mPE with n=18.[54]

Thus, Moore *et al* were able to develop an elegant system of folding mPEs in polar organic solvents based on a solvophobically driven mechanism.[54] In addition, the results obtained based on these findings showed that different aromatic N-heterocycles, oligo(*m*-PEs),

and oligo(*o*-PEs) were capable of folding without additional functionalities like hydrogen bonding. However, additional external structural elements capable of hydrogen bonding between the repeating units produced an increase in the strength (approximately 1 kcal/mol for every one hydrogen bond) of the folded conformation of m-PEs.[58, 59] Gong *et al* were able to develop a different strategy for folding oligo(*m*-PEs) in nonpolar organic solvents through hydrogen bonding and thereby inducing backbone rigidification (Figure **7**).[60] Thus, even in solvents like chloroform in which only random coil conformations were expected, due to hydrogen bonding, folding conformations were observed.

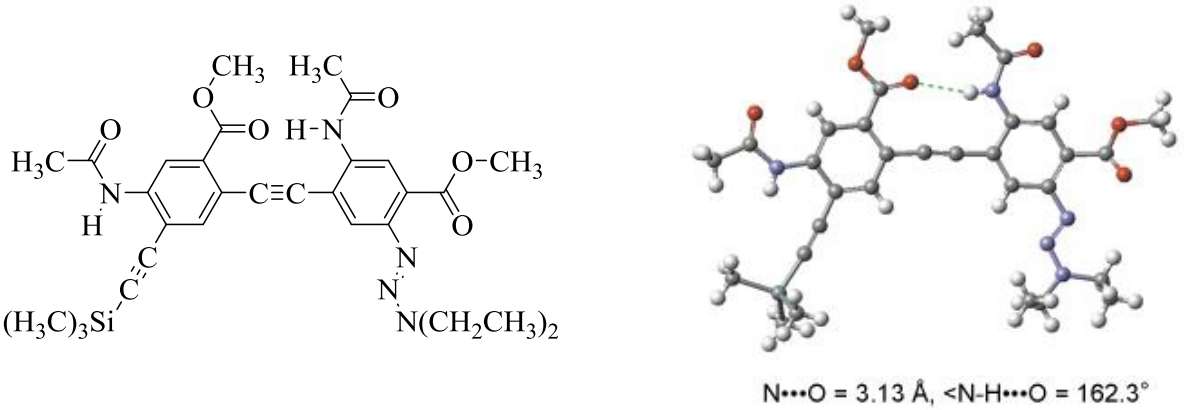

Figure 7: Backbone rigidification by H-bonding in oligo(m-PEs).[60]

In 2005, Tew *et al* synthesized oligomers based on *o*-phenylene ethynylene (oPE) backbone with polar substituents using Sonogashira coupling (Figure **8**).[61] The oligomers formed with polar triethylene glycol monomethyl ether (Teg) side chains were found to adopt folded conformation in polar solvents like acetonitrile. The aspect ratios of the folded mPEs and oPEs oligomers would be considerably different based on computational and simple torsional considerations, and hence would lead to different geometrical shapes upon folding. The larger backbone curvature created by smaller bond angle for oPEs formed a full turn with three repeating units.

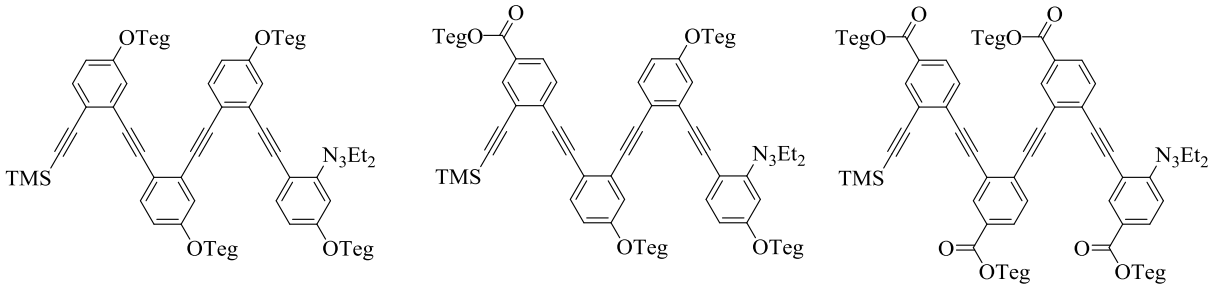

Figure 8: oPE tetramers with different substituents synthesized by Tew *et al.*[61]

Aromatic oligoamides have also shown a folding nature due to the presence of intramolecular hydrogen bonding capabilities of the amide units, and the π-π interactions present between the molecules upon folding help to stabilize the structures. Aromatic polyamides, such as poly(*p*-phenylene terephthalamide) and poly(*p*-benzamide) possessed rod like or planar structures.[62] However if the nitrogen of the amide bonds could be alkylated, the resultant polymers would form coiled structures.[63] Tanatani *et al* synthesized N-alkylated poly(p-benzamide) using chain-growth polycondensation that formed helical conformation in solution with three monomer units per turn (Figure **9**).[64]

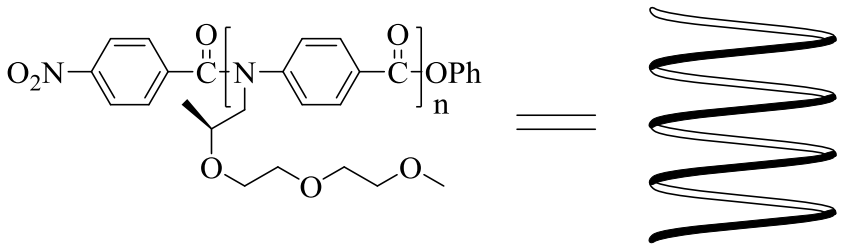

Figure 9: Poly(*p*-benzamide) with chiral side chain formed helical conformation.

The scope of aromatic oligoamide for helical polymers was expanded by Huc and coworkers when they determined the structures of oligo(quinolone)[65] (Figure **10**). They

synthesized aromatic foldamers from quinoline amino acid that formed stable helical conformation in solution as determined by ^{1}H and ^{1}H-ROSEY NMR experiments.[65]

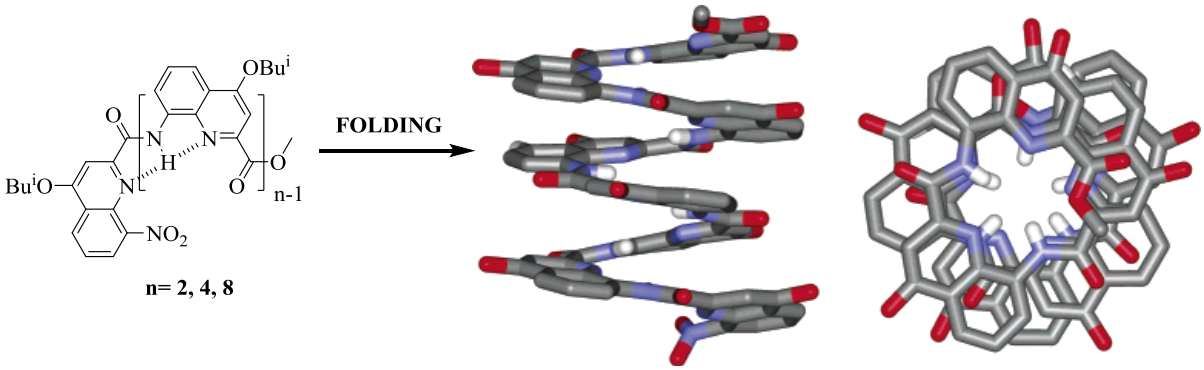

Figure 10: The oligo(quinoline) that adopted helical conformations prepared by Huc *et al.*[65]

Similar to oligo(quinolones), another group in which the folding is governed by the H-bonding and π-π interactions are the aromatic oligoureas. Bing Gong and coworkers also synthesized foldamers based on aromatic oligoureas (Figure **11**).[66] The backbone of this class of oligomers involve benzene rings linked by *N*,*N*'-disubstituted urea groups. The presence of ester groups ortho to the urea nitrogen atoms lead to the formation of intramolecularly H-bonded, six-membered ring. It is combined with the *cis*, *cis* conformation of the urea group resulted to rigidification of the oligourea backbone structure. The molecular modeling studies have shown that for oligomers with more than four residues, a helical conformation with an inner diameter of ~4 Å occurs. The smaller radius of the inner pitch has been advantageous for binding or transporting ions, like sodium ion.[66] The replacement of the ester group with ether linkages resulted in a five-membered, intramolecularly H-bonded ring. The backbone of the structures resulted by these ether linkages would be more flexible due to the weaker H-bonds in the five-membered rings.

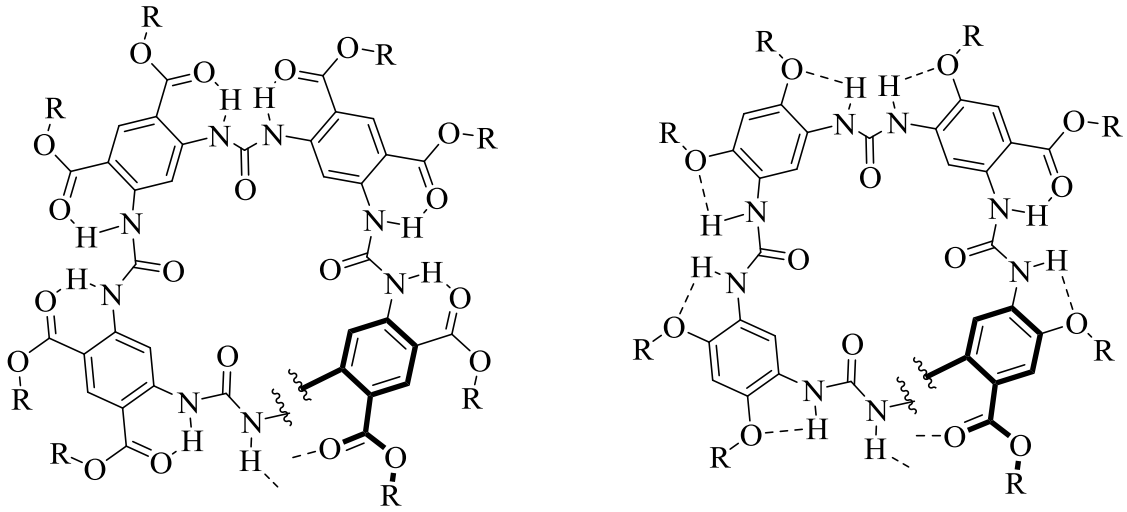

Figure 11: General structures of folded oligourea.[66]

Similar to this research by Bing Gong and coworkers, Meijer, *et al*[67] reported the helical polyureas based on the same design principles (Figure **12**). They synthesized poly-ureidophthalimide via condensation that folded into a chiral, helical folded structure based on the CD spectroscopy results. The consecutive monomeric units of diamino-functionalized monomer upon condensation introduced a curvature in the ureidophthalimide backbone because of intramolecular H-bonding. The interactions of the urea protons with the imide carbonyl oxygens gave almost 120° bend creating a helix.

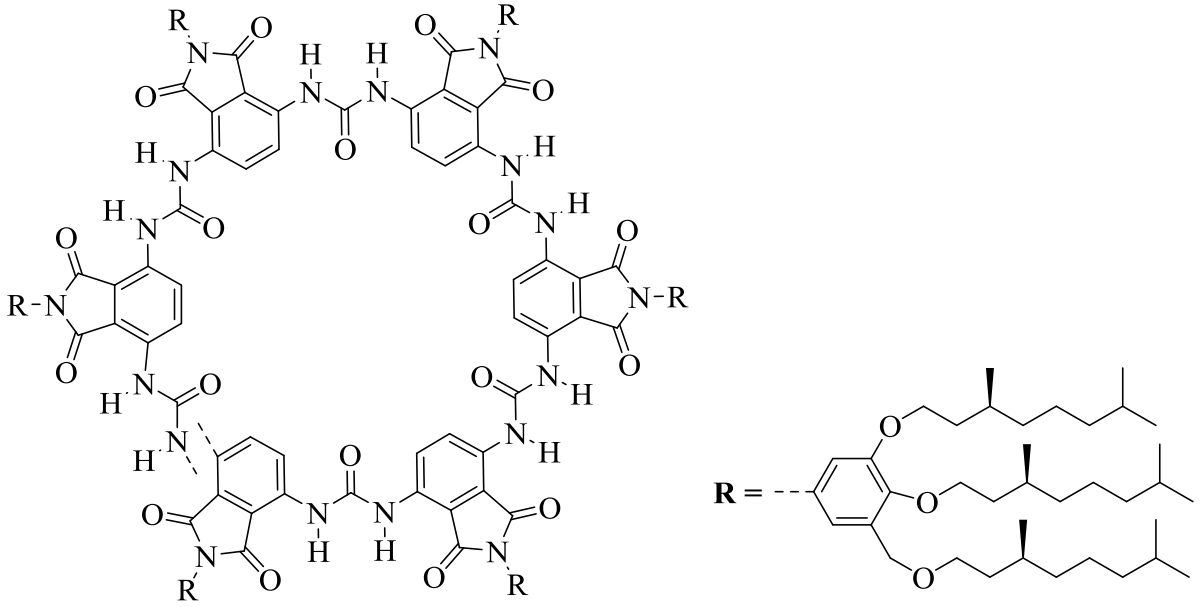

Figure 12: Chemical structure of a turn of the poly(ureidophthalimide) by Meijer *et al*.[67]

Shido *et al* were amongst the initial efforts to demonstrate the helical structures when five benzene rings connected at meta positions by cis-urea or guanidine formed aromatic layered helices in the crystal state.[68,69] The *cis*-preference of the *N*-methylated urea and guanidine bonds was general instead of aromatic rings and showed unique properties, such as lipophilic or water-soluble character. The methyl groups on the urea functionalities in them prevented the H-bonding, and the folding was governed by π-π interactions alone in their oligomer formations (Figure **13**).

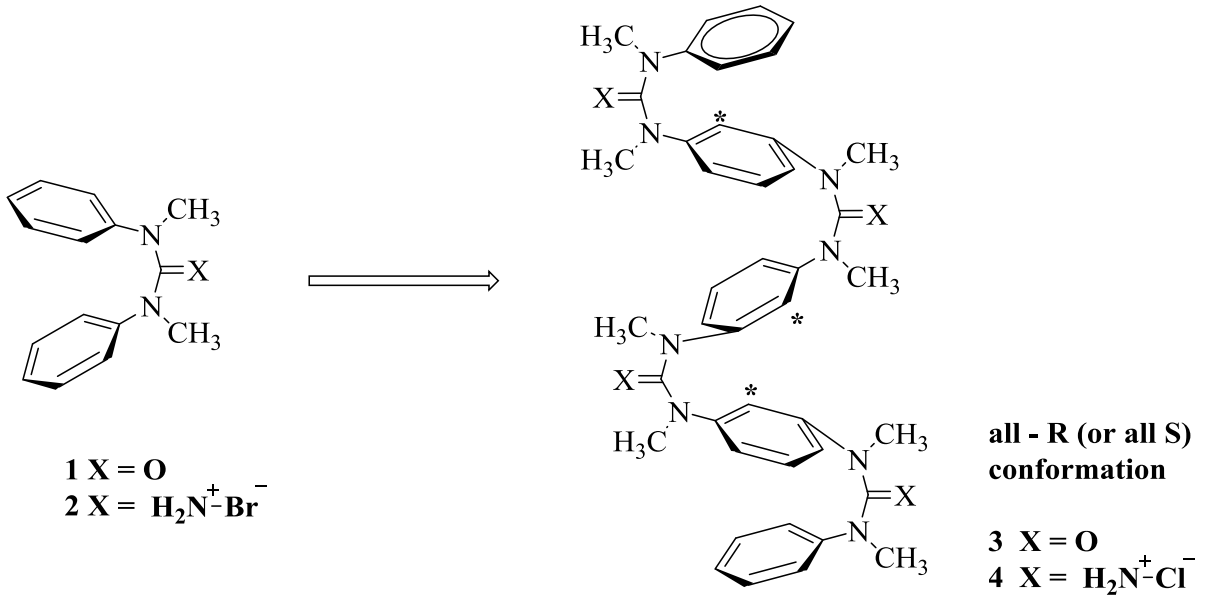

Figure 13: Folded structures of *N,N′*-dimethyl-*N,N′*-diphenylurea and *N,N′*-dimethyl-*N,N′*-diphenylguanidium bromide.[68]

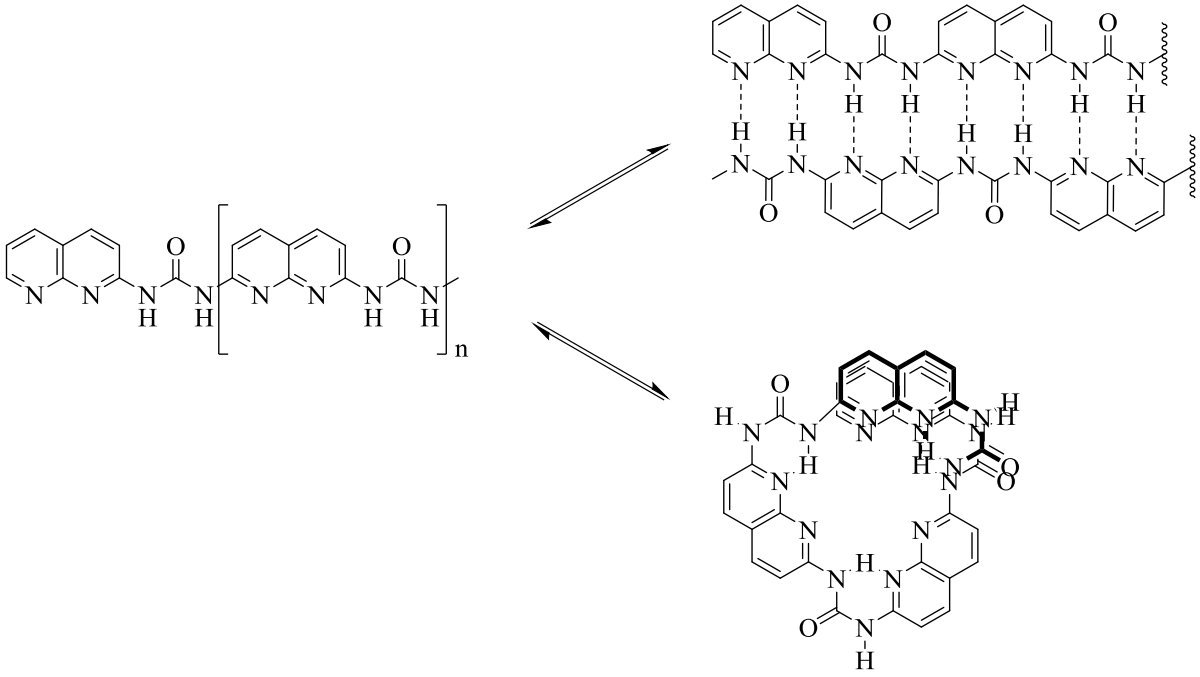

Figure 14: Structure of oligo(naphthyridinylurea) into helix and sheet form.[70]

Zimmerman *et al* showed the conformational and experimental studies of heterocyclic ureas (amides) and their concentration dependent unfolding to form multiply hydrogen-bonded

complexes.[70] Their work was the initial step towards construction of naphthyridinylurea oligomers that could exist as unfolded β-sheets and folded helical structures.[70] (Figure **14**)

In our laboratory, Ching-en Chou and coworkers synthesized polymers containing triphenylene units as backbones in their structures.[71] These conjugated polymers with different side chains namely ethynyl, diethynylphenyl, and divinylphenyl attached to the bridging phenyl rings showed either interchain aggregation and/or folding conformation depending on the solvents used for them (Figure **15**).[71] Additionally, these triphenylene-containing conjugated polymers were connected to each other at the 7 and 10 positions. The polymer with ethynyl linkage (PTPT) showed strong folding propensity in both good and poor solvent; and the polymer with diethynylphenyl (PTPA), two long alkyl chains attached to bridging phenyl rings folded in only poor solvents. Whereas, the one with divinylphenyl (PTPV) has lower folding propensity because of the geometrical flexibility of the added vinyl bonds.

The ^{1}HNMR spectroscopy study of these polymers gave broad aromatic signals along with the upfield shift indicating the presence of strong intertriphenylene π-π stacking. The thermal properties of the polymers showed that the backbone flexibility of these polymers, PTPT being more rigid since it had high glass transition temperatures (T_g) well above 300 °C, while PTPV with the divinyl linkage being more flexible due to lower glass transition temperatures (T_g). The optical data for these compounds agreed with other data, PTPT showed broad structureless emission in dilute conditions indicating highly aggregated structure driven by strong π-π interaction among stacked triphenylene rings. The concentration and solvent dependence of these polymers also corroborated the previous observation. It showed red shift (50 nm) in PTPT after changing from less polar solvents like chloroform to more polar solvents like acetonitrile. PTPA showed two different absorption bands in $CHCl_3$ and CH_3CN

suggesting the adoption of random coil conformation and folding conformations in different solvents. While for PTPV there was broad absorption peaks in all the solvents, the emission peak was blue shifted after changing the solvent from $CHCl_3$ to CH_3CN.[71]

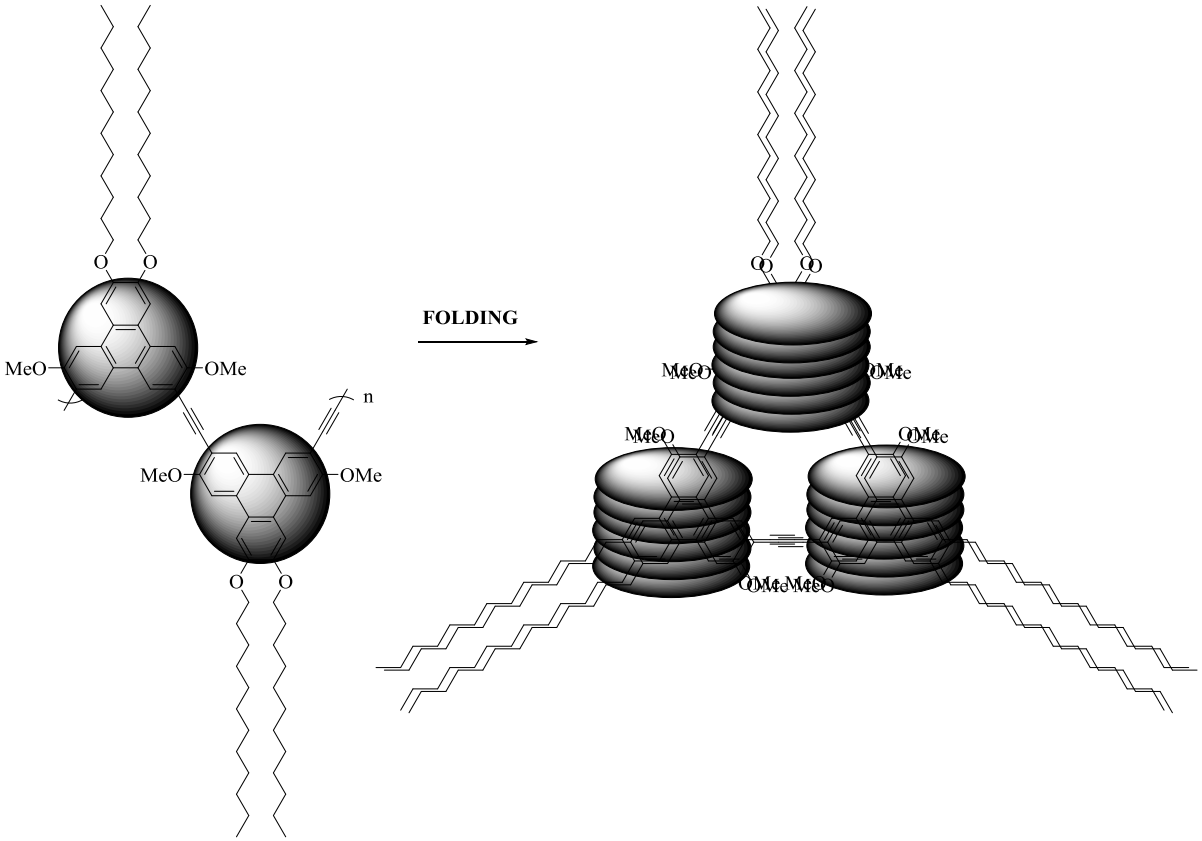

Figure 15: Intrachain folding effect seen in triphenylene containing conjugated polymers.

CHAPTER 2

SYNTHESES AND OPTICAL PROPERTIES OF TRIPHENYLENE BASED CONJUGATED FOLDAMERS

2.1 Introduction to polycyclic aromatic compounds (PACs)

Polycyclic aromatic compounds (PACs) contain two or more benzene rings, which are fused together either in linear, angular, or in a cluster arrangement. They are one of the most important classes of optoelectronic organic materials due to the π electron cloud and the planar structure. Some commonly used PACs like naphthalene (bicyclic aromatic hydrocarbon), anthracene, phenanthrene, or large PACs, such as coronene are listed in Figure **16**.

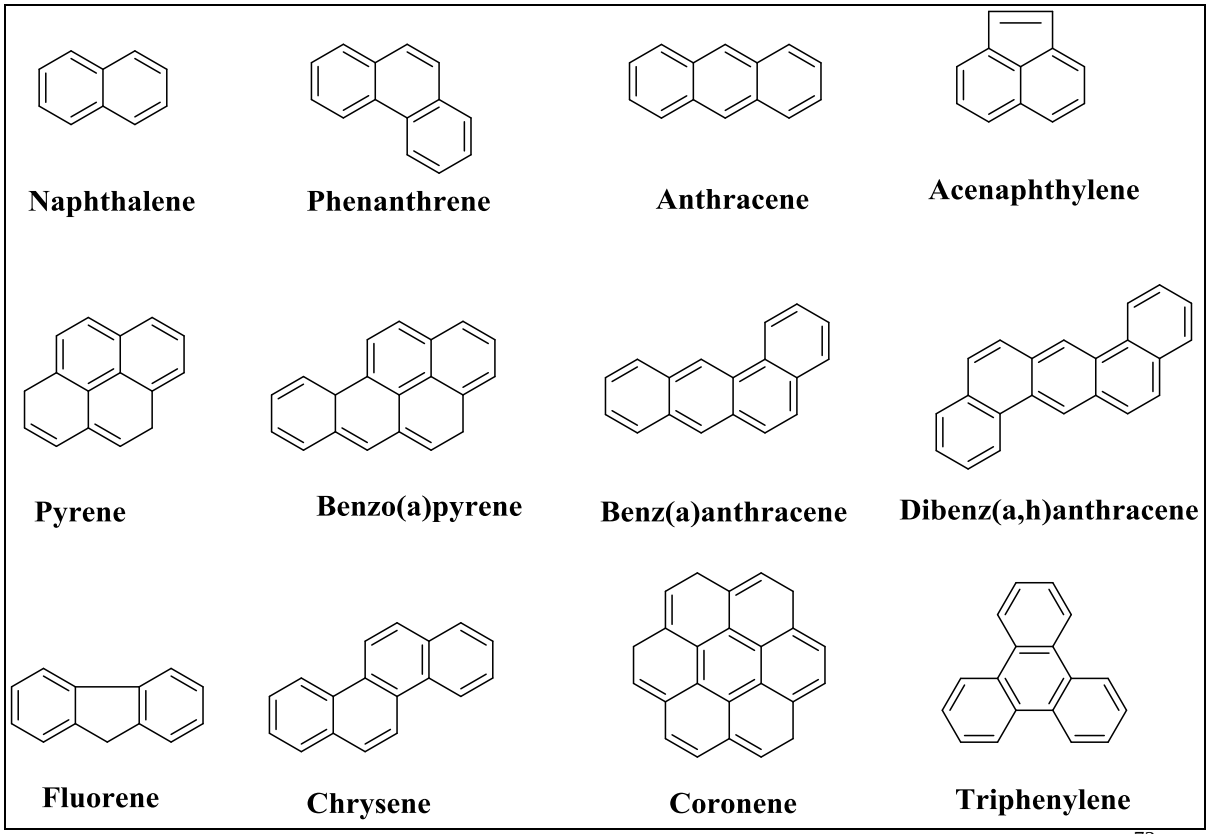

Figure 16: Examples of some commonly used polycyclic aromatic hydrocarbons PACs.[72]

The main source of these PACs is usually incomplete combustion of organic materials such as coal, wood, oil, and petrol.[73] In general; PACs have high melting and boiling points. They also have lower vapor pressure and lower solubility in water, which tend to decrease with the increase in their molecular weights.[74] PACs are largely readily soluble in organic solvents being lipophilic in nature and possess properties, such as good light sensitivity, emission, resistivity to corrosion, and heat.[75] They are mostly used as intermediates in agricultural products, pharmaceuticals, thermosetting plastics, photographic products, lubricating materials, dyes, pigments, and other chemical industries.[76] In the last decade, PACs have emerged as efficient materials for optoelectronic applications including organic field effect transistors (OFETs) or organic solar cells (OSCs) because of the extended π-conjugation which allows for reduced HOMO-LUMO gap and possibility of self-assembly because of π-π interactions.[77] Scholl,[78-80] Clar,[81-84] and Zander[85-87] made the pioneering work towards the synthesis of PAHs. Earlier, these reactions were carried out under harsh conditions of temperature and pressure but now the emphasis has been more towards performing them under mild conditions.

Elbs reaction[88] is generally the preparation of polyaromatic compounds like anthracene by intramolecular condensation of diaryl ketones containing methyl or methylene substituent *ortho* to the carbonyl group. The first practical synthesis of 3-methylcholanthrene was achieved by this reaction by Fieser and Seligman.[89] Diels-Alder reaction (intermolecular or intramolecular) has been widely used in the synthesis of small or large sized PACs system.[90,91] Also, ring closing metathesis is one of the efficient route for synthesis of double bonds in cyclic organic compounds[92] or in PACs[93] due to its ability to form multiple aromatic rings in a single step. The Scholl reaction[94] is acid catalyzed oxidative condensation of aryl groups and used to

prepare hexaalkoxytriphenylenes from *o*-dialkoxybenzenes. The theoretical studies suggest that the reaction follows either radical cation or arenium cation mechanism.[95] In one of the examples, Klaus Mullen and co-workers from Max-Planck Institute for polymer research via oxidative cyclodehydrogenation synthesized hexa-*peri*-hexabenzocoronene[96] (HBC) and its derivatives (Figure **17**) as well as much larger all-benzoid PACs with up to 222 carbons. The Kovacic conditions,[97] which uses transition metals such as $MoCl_5$, $CuCl_2$ or $FeCl_3$, are commonly used.

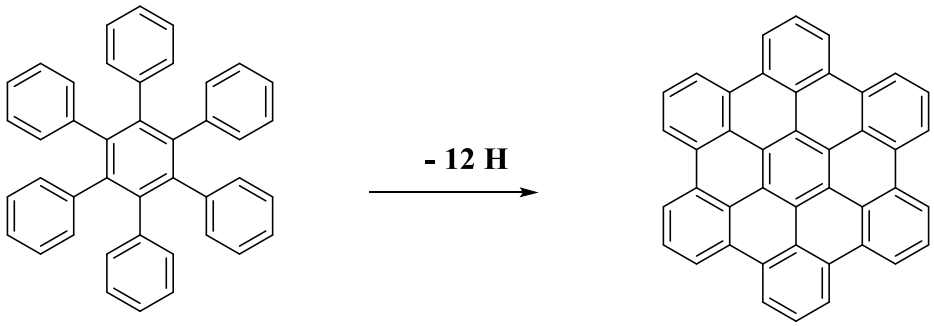

Figure 17: Preparation of hexabenzacoronene (HBC) using Scholl reaction.

Photocyclization of arylethylenes is one of the preferred methods for the synthesis of PAHs as reported in the literature.[98] The photochemical conversion of stilbene-type molecules to phenanthrene was discovered in 1930s and was widely used for preparation of their analogues. In a typical Mallory type photocyclization, stilbenes, *o*-terphenyls, and related derivatives undergo intramolecular cyclization to afford phenanthrene-containing products. Iodine is used as an oxidant, as well as, other mild oxidants such as diphenyldiselenide[99] or copper salts[100] have also been employed, as shown by the recent literature for the synthesis of regiospecifically fluorinated[101] PAHs in Figure **18**.

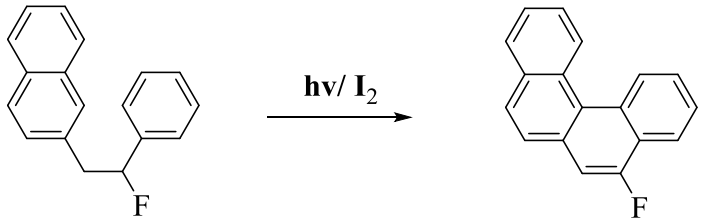

Figure 18: Example of oxidative photocyclization for synthesis of PAHs.[101]

There are also few other useful methods such as Wagner-Meerwin rearrangement,[102] Wittig olefination,[103] flash vacuum pyrolysis,[104] and Friedel-Crafts type reactions such as Haworth synthesis,[105] extrusion of heteroatoms that can be used to synthesize kekulene,[106-108] which have been reported in the literature for the preparation of PACs.

2.2 Discotic nature of PACs

The major driving force for folding in the case of π-conjugated molecules is π-π stacking which makes it enthalpically favorable. As these π interactions are directly related to the size of the aromatic core, larger PACs would be expected to have much stronger propensity for folding. Additionally, these PACs could be arranged in the form of π-stacked columns, which would then exhibit strong electron delocalization[109] and high charge carrier mobility through these stacked columns.[110] Hence, foldamers which are capable of forming stacked columns, provide efficient charge transporting properties that are crucial for polymer based electronic devices, such as OLED, OFET, and OSCs.[111] These discotic molecules, such as triphenylenes, can self-assemble into 1-D columns due to strong π-π interactions between neighboring aromatic cores and the nanophase segregation of aliphatic chains (Figure **19**).[112] These π-π interactions are characteristically stronger than van der Waal's forces and lower than hydrogen bonding, approximately 0-50 kcal/mol.[113] The π-π stacking distance between the neighboring aromatic rings is generally about 3.5 Å. In these triphenylene derivatives, for

example, the formation of 3-D crystal is hindered, and the flow of electrons is maintained unidirectional, due to high entropy and disorder of the flexible aliphatic chains on the periphery.[114] In these oriented columnar stacks of discotic molecules, there is a preferential direction for charge transfer along the columnar direction.[115] Therefore the discotic molecules are considered to possess high charge carrier mobilities and are found to have wide applications in LEDs,[116] PVDs,[117,118] and organic semiconductor transistors.[119, 120]

In this chapter, we have designed the syntheses of triphenylene-based conjugated foldamers and studied their optoelectronic properties. Due to the tendency of triphenylene derivatives to form discotic structures, they can act as excellent energy and hole transporters.[121]

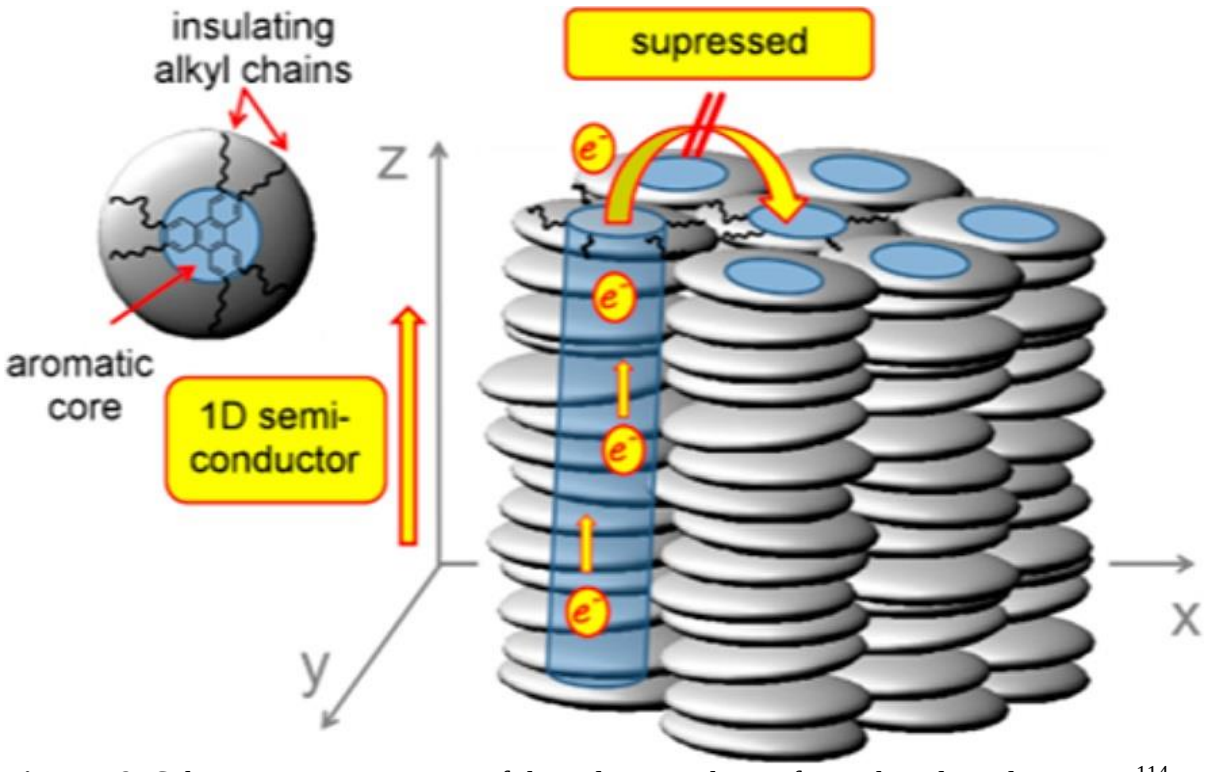

Figure 19: Schematic representation of the columnar phase of a triphenylene derivative.[114]

There are two different types of columnar discotic molecules alignment, homogeneous or ‘edge-on’ orientation and homeotropic or ‘face-on’ orientation. The ‘edge-on’ orientation

in which the column axis is parallel to the substrate is preferable. In case of OFETs while 'face-on' orientation where columnar axis is perpendicular to the substrate is ideal in case of OPVD or OLEDs (Figure **20**).[122] For OFETs, high charge carrier mobility of the semiconductor material and minimal concentration of charge trap sites are crucial parameters for higher performance. Both above-mentioned factors are functions of the morphology and the order of semiconductor molecules. If the columns of discotic molecules can be placed between two electrodes with a perpendicular π-stacking axis, a relatively defect-free conductive pathway can be obtained and results in higher device performance.

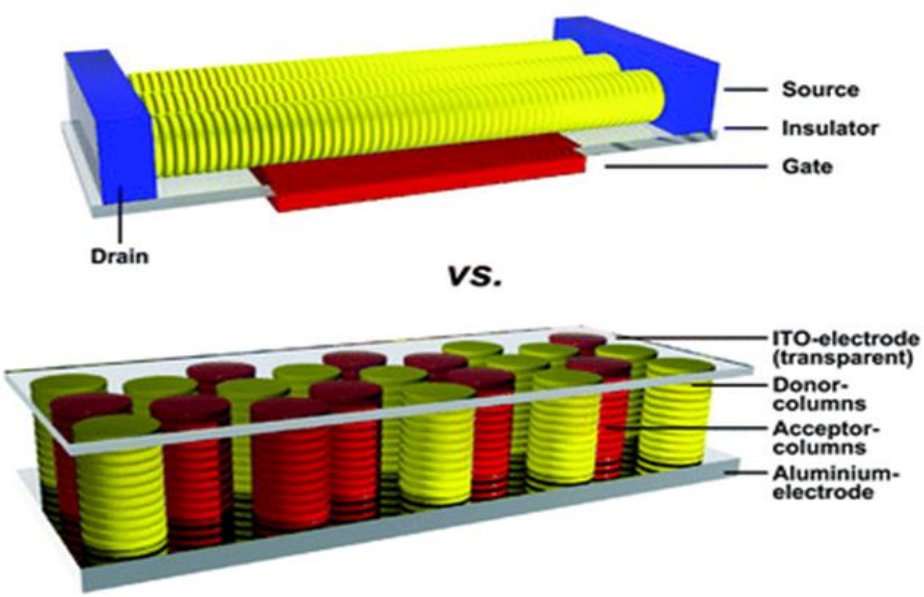

Figure 20: The orientation of discotic molecules in OFET (above) and in OLED (below).[122]

In case of OPVDs, discotic molecules are preferred for producing higher performing solar cells. The operating principle of these OSCs is given in Figure **21** and can be summarized into few basic steps. The active layer consisting of semiconducting organic molecule such as small molecule, or polymer, absorbs the light from the sun and generates coulombically bound electron-hole pairs called excitons. This neutral exciton diffuses in the active layer and at the

donor-acceptor interface; the exciton dissociates to form electron and hole, which is energetically favorable. For efficient photovoltaic devices, the created charges need to be transported to the appropriate electrodes within their short lifetime (about 45 fs). Hence, in case of OPVDs, as the semiconductor is sandwiched between two electrodes, and charge migration perpendicular to the substrate is required, which demands 'face on' orientation of the discotic molecules on the substrate.[123]

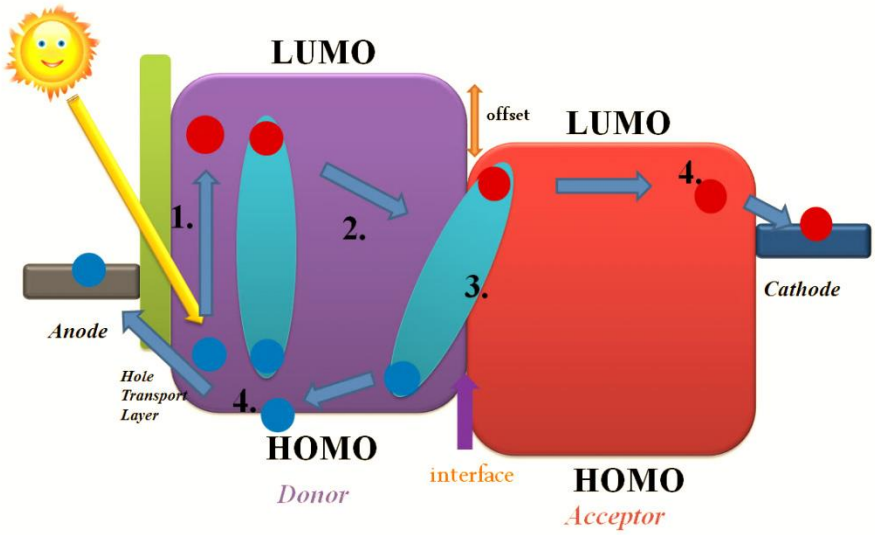

Figure 21: Operations of organic photovoltaic devices.[124]

OLEDs also have similar working principle to that of OPVDs, and hence, the 'face-on' or homeotropic orientation where the organic semiconductor is sandwiched between two electrodes is carried out. The molecular units in these materials (such as hexahexylthiotriphenylene) are self-organized into columnar stacks providing a favorable face-to-face orientation of the aromatic cores that leads to a large π overlap between adjacent units. Similar to OPVDs, a multilayer structure where the hole or electron transporting material is contained in a separate layer provides better control of charge-carrier injection properties.

Zhiquen He *et al* have recently reported of an electron transporting anthraquinone derivative that demonstrated stable large scale 'face-on' orientation on an open substrate that substantially improved its charge-carrier mobility.[125] The electron mobility for the film without alignment was 3.1x 10^{-4} $cm^2V^{-1}s^{-1}$ initially, which was increased by two orders of magnitude when it was heomeotropically aligned 1.2x 10^{-2} $cm^2V^{-1}s^{-1}$.[125]

2.3 Significance of imide functionalization

Many experimental and theoretical studies have shown that inclusion of an electron deficient imide moiety in the system will have various advantages. It will increase the electron affinity of the system significantly and increase the thermal and chemical stability of the system along with the lowering of sensitivity towards mobile electron traps. The nitrogen of the imide group can be functionalized easily without actually disturbing the electronic properties of the system. This introduction of side chains that will affect the solubility of the molecule since the LUMO of the optimized structure have nodes passing through the imide nitrogen. Additionally, the solubilizing groups in the imide position that are far from the main polymer backbone will decrease the backbone twisting of the successive units ($\mathbf{E^{\theta}}$). Further, the imide functionalization will introduce an inherent dipole moment, which will reduce the steric crowding around the polymer backbone and enhance interchain π–π stacking ($\mathbf{E^{int}}$). This is due to the polymer with higher intrinsic dipole moment exhibit higher solar cell performance than a similar polymer with no or low intrinsic dipole.[126]

Among the electron deficient discotic molecules, perylene-diimide (PDI) derivatives are one of the best candidates for electron-transporting discotic liquid crystals (DLCs).[126] The DLC-based molecules have a natural tendency to stack in a columnar "face-on" pattern. This will be beneficial to minimize the charge trapping sites. This tendency results in higher

crystallinity that assures higher crystalline domains, columnar arrangement of the acceptor units of the neighboring polymer chains (higher interchain charge transport and higher interchain coupling in solid state ($\mathbf{E^{int}}$), and higher aromatic resonance energy ($\mathbf{E^{Res}}$) and thereby achieve high mobility.

Table 1: Computational studies for the imide functionalized triphenylene derivatives

Compound	**HOMO (eV)**	**LUMO (eV)**	**E_g (eV)**
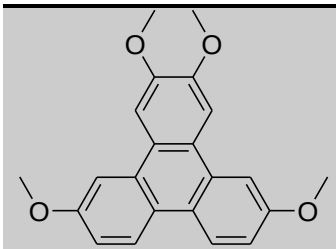	-5.197	-0.816	4.38
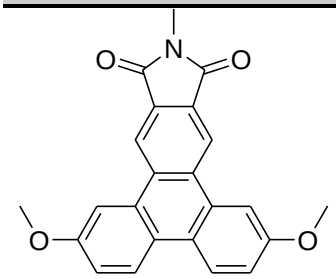	-5.63	-2.34	3.29

In addition, computational studies were performed on these aromatic systems containing triphenylene derivatives using DFT-B3LYP calculation with the basis set 6-31G. The theoretical study as shown in Table **1** indicated that inclusion of imide moiety decreased both HOMO and LUMO as compared to the dialkoxy derivatives, thereby lowering the band-gap. In addition, the presence of a nodal plane passing through the imide nitrogen would help introduction of solubilizing alkyl side chains without affecting its electronic nature.

2.4 Target molecules for triphenylene based conjugated polymers

With the aforementioned synopsis of the discotic molecules containing triphenylene cores, we have decided to synthesize the following polymers (Figure **22**). The series of various other polymers with branched or hydrophilic side chains could be attached further to create an array of polymers and their comparative data could be obtained later.

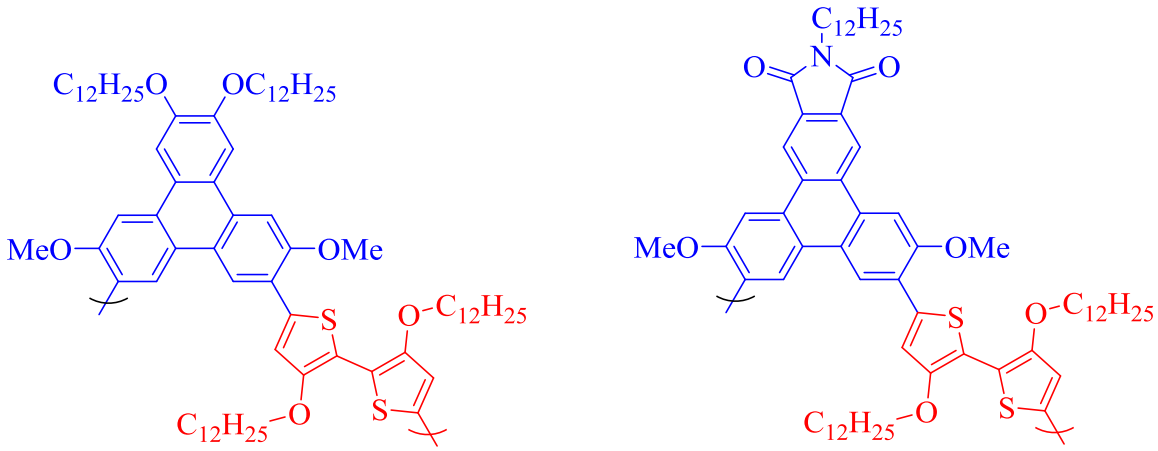

Figure 22: Target polymers of triphenylene core with alkoxy chains and imide functionalization.

2.5 Synthesis and characterization of triphenylene based conjugated polymers

In this chapter, *o*-xylene was used as the starting material because of the low cost and commercial availability. *o*-Xylene was first subjected to bromination, followed by oxidation to give 4,5-dibromophthalic acid in about 60% yield. It was then converted to 4,5-dibromophthalic anhydride by treatment with acetic anhydride, and then upon reaction with dodecylamine gave N-(dodecyl)-4,5-dibromphthalic anhydride. Various other amines could also be used in place of dodecylamine to synthesize corresponding imide compounds that could be further utilized to make a library of organic molecules. Further inclusion of amines with branched side chains or with heteroatoms would help to improve the solubility and processability in the next chapters. The imide with straight chain amine was used as a precursor for other reactions and due to its high stability was synthesized in multigrams scale (Scheme **1**) and stored for future use.

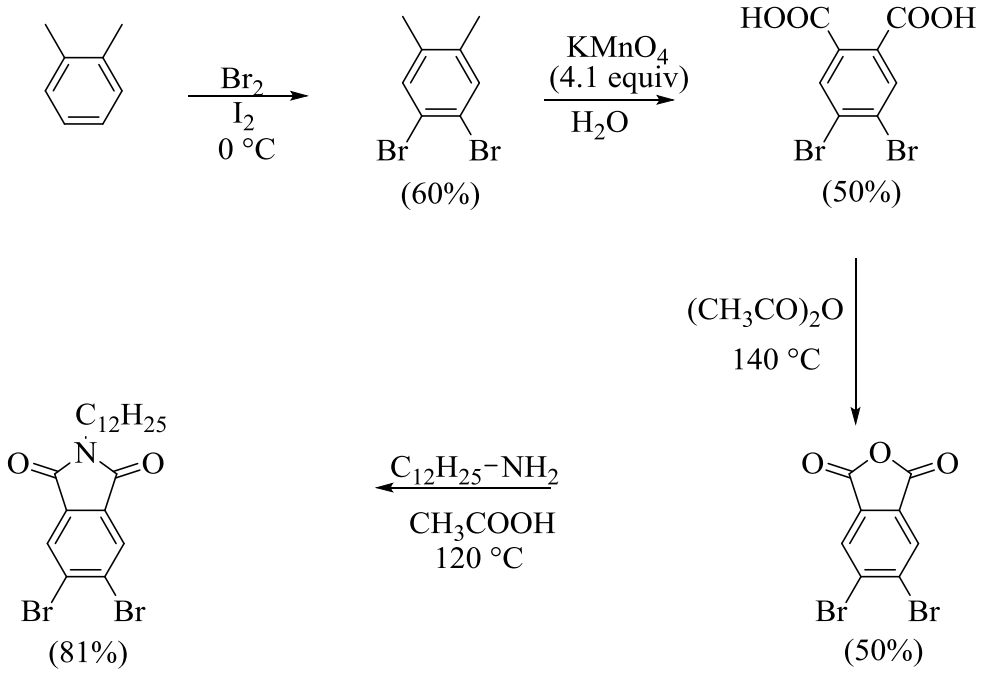

Scheme 1: Synthesis of N-dodecylaminne-4,5-dibromophthalimide.

^{1}HNMR spectrum of compound **13** in $CDCl_3$ showed well-resolved sharp signals in the aromatic region and other peaks due to dodecyl aliphatic chain in the aliphatic region as assigned in Figure **23**.

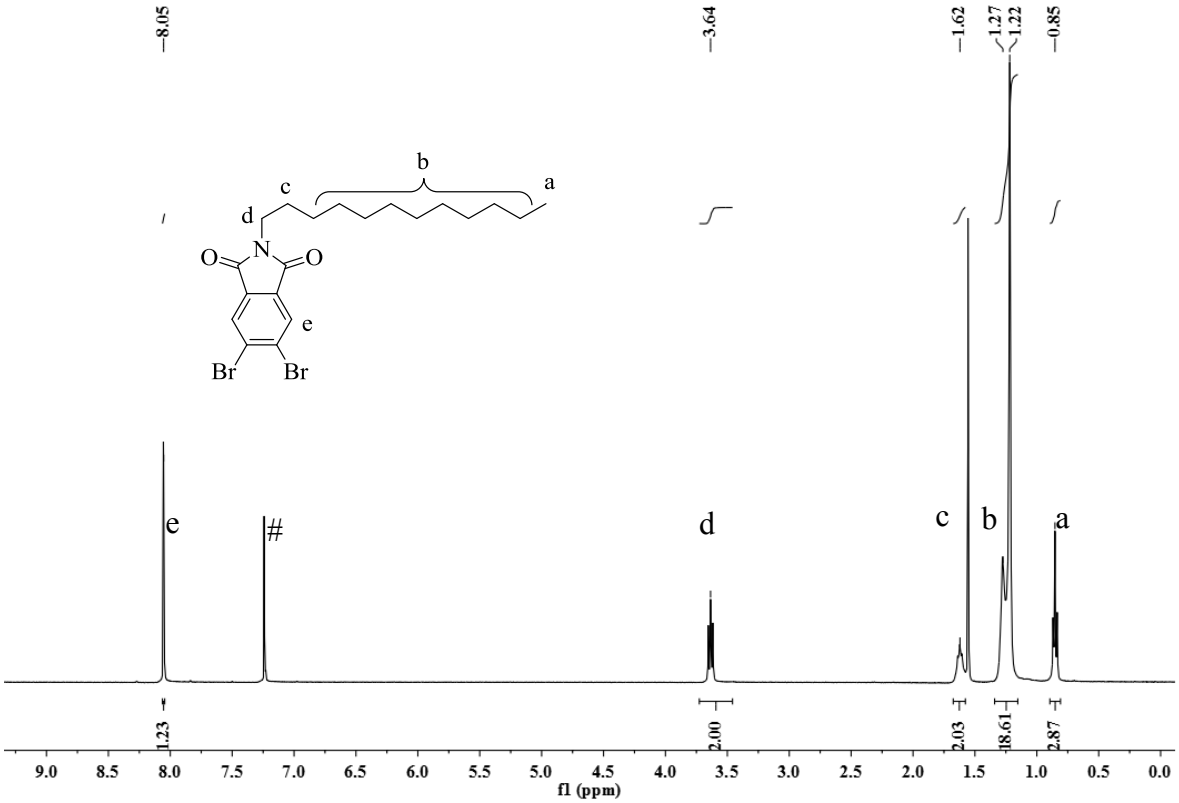

Figure 23: ^{1}HNMR spectrum of *N*-dodecylaminne-4,5-dibromophthalimide.

The imide-functionalized triphenylene-based acceptor monomers were synthesized using the modified published procedure as shown in Scheme **2**.[127] N-dodecylamine-4,5-dibromophthalimide **13** was used a starting material for the synthesis of these monomers.

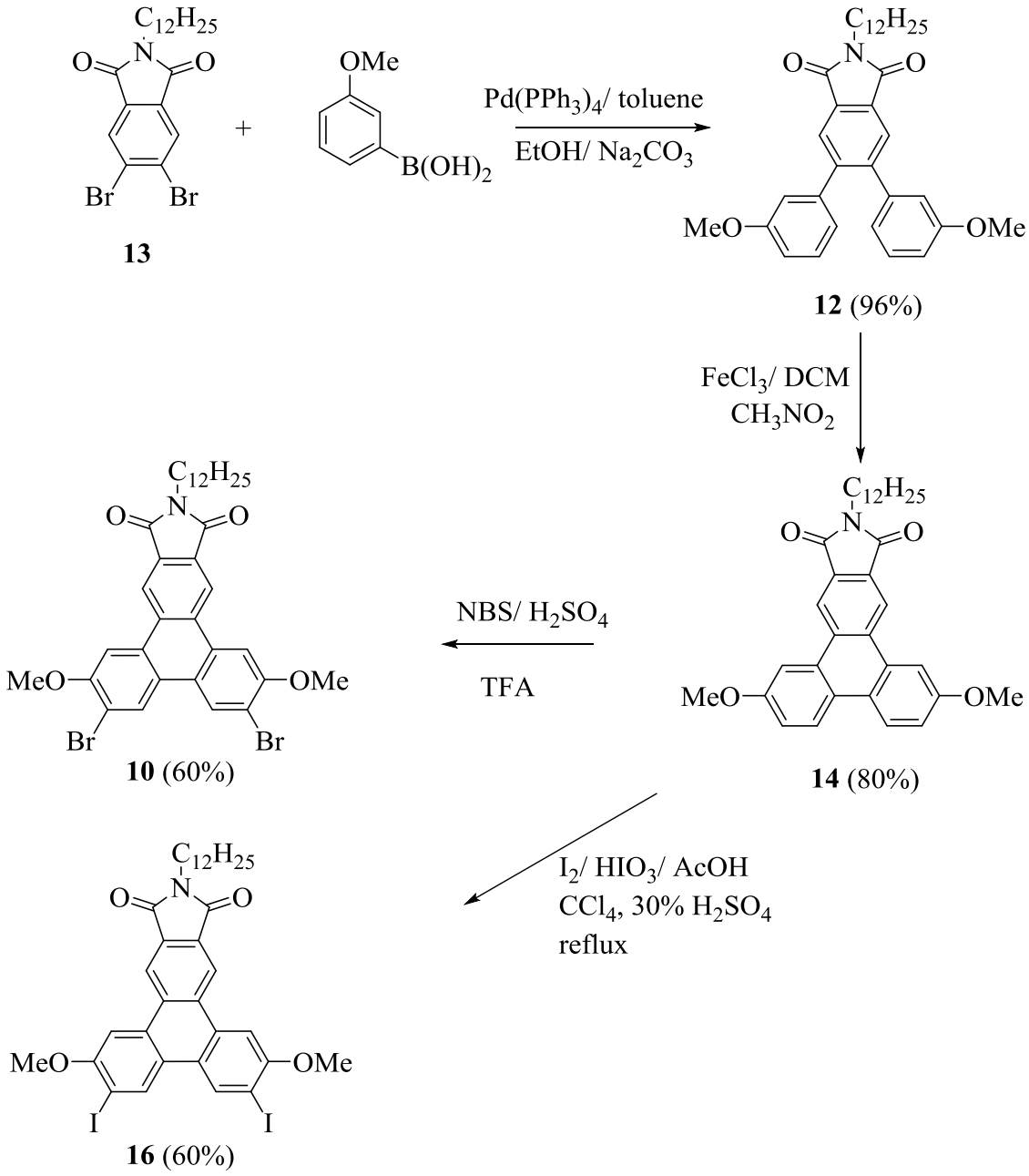

Scheme 2: Synthesis of triphenylene based acceptor monomer

The conventional Suzuki coupling of phthalimide derivative **13** with (3-methoxyphenyl) boronic acid gave compound **12** in excellent yields. Compound **12** in $CDCl_3$ gave appropriate spectrum (Figure **24**) indicating the presence of dodecyl chain in between 0.84- 1.73 ppm, -N-CH_2 and –OCH_3 protons at 3.77 and 4.05, respectively. Also, the aromatic

protons due to the addition of methoxyphenyl ring were well separated from each other from 7.35 to 9.02 ppm.

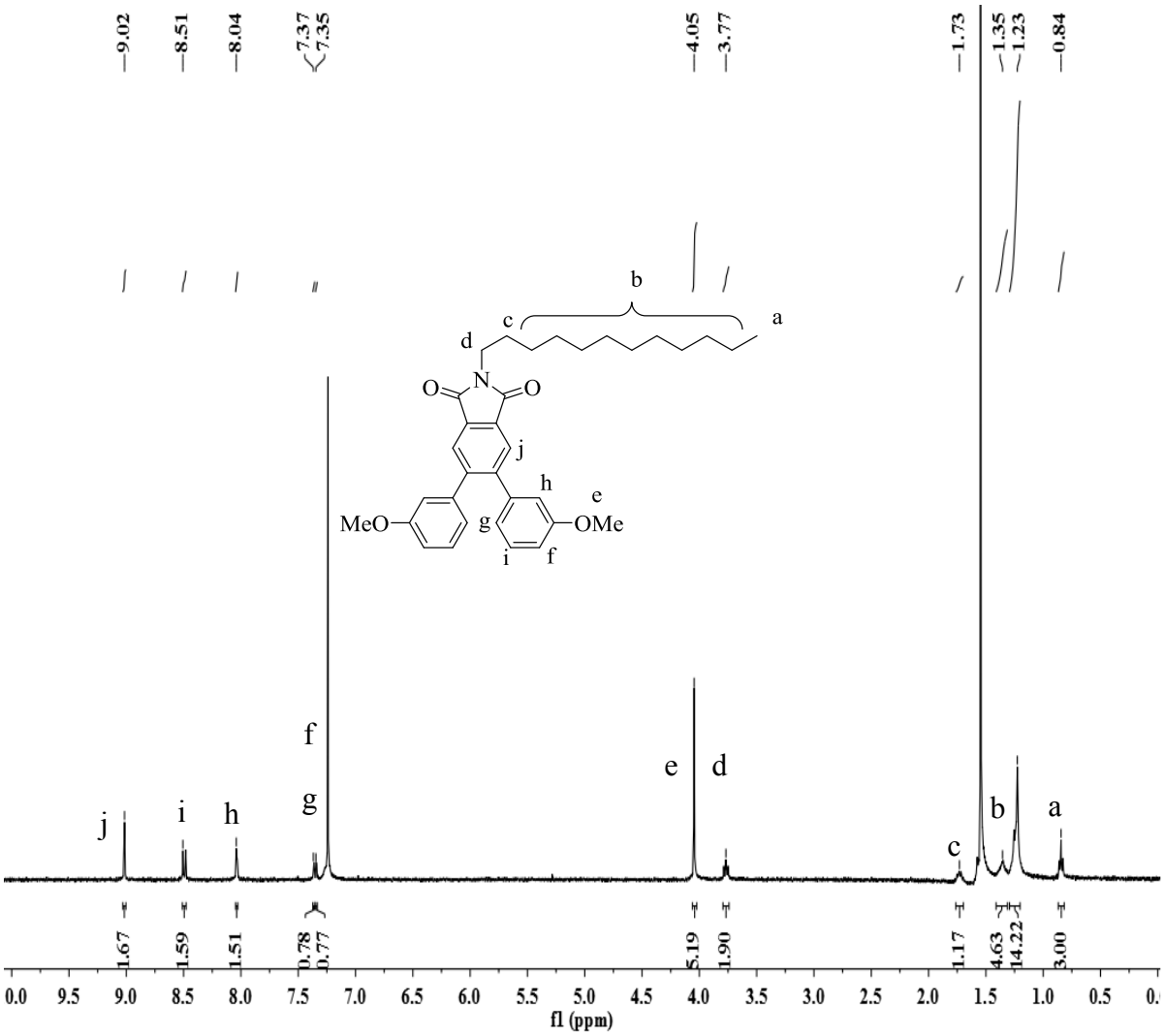

Figure 24: [1]HNMR spectrum of compound **12**.

A Scholl oxidation reaction was later used to aromatize the triphenylene system using Lewis acid, such as $FeCl_3$. The oxidation reaction here is believed to proceed via radical-ion (cation) mechanism.[128] The electron withdrawing imide group destabilizes some of the intermediate resonance structures, but it is compensated by the presence of electron donating methoxy groups at the *para* positions and drove the reaction forward to give compound **14**.

The structure was confirmed by the shift of the aromatic protons from 9.02 to 9.46 ppm in the aromatic region, as well as the absence of any new major peak as shown by the ^{1}HNMR spectrum of **14** in $CDCl_3$ (Figure **25**).

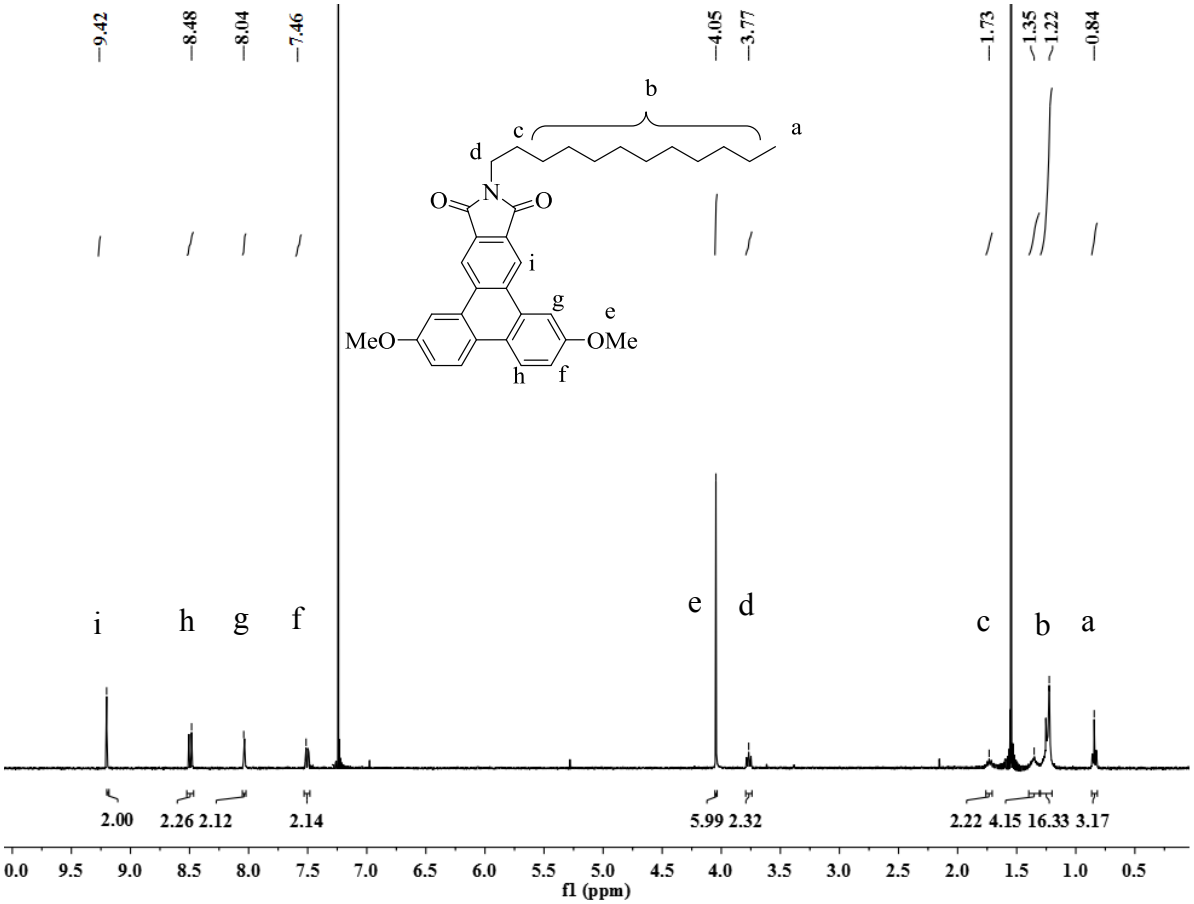

Figure 25: ^{1}H-NMR spectrum of compound **14**.

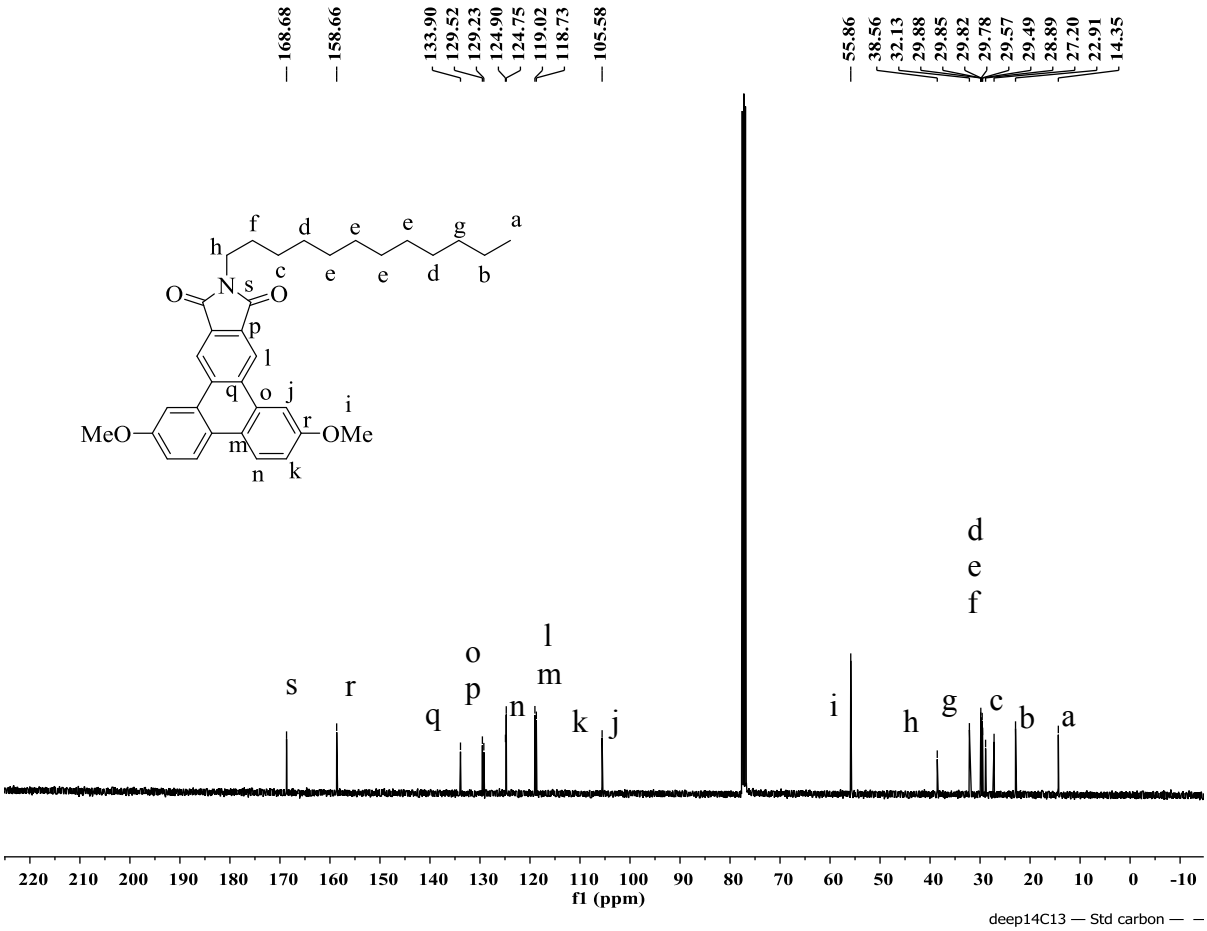

Figure 26: ^{13}CNMR spectrum of compound **14**

Additionally, a ^{13}CNMR spectrum also supported the identity of compound **14**, wherein all the carbons in the molecule are accounted for as depicted in the Figure **26**. This was followed by bromination of **14** using more severe conditions (NBS/H_2SO_4/TFA) as compared to normal triphenylene (Br_2/ DCM) because of the electron deficient nature of the system. The bromination occurs regiospecifically at 3 and 6 positions in good yields (60%) to obtain final triphenylene-based acceptor monomer **10**. The ^{1}HNMR spectrum of **10** showed three singlets in the aromatic region at 7.98, 8.66, and 8.97 ppm for three separated aromatic protons in the molecule (Figure **27**).

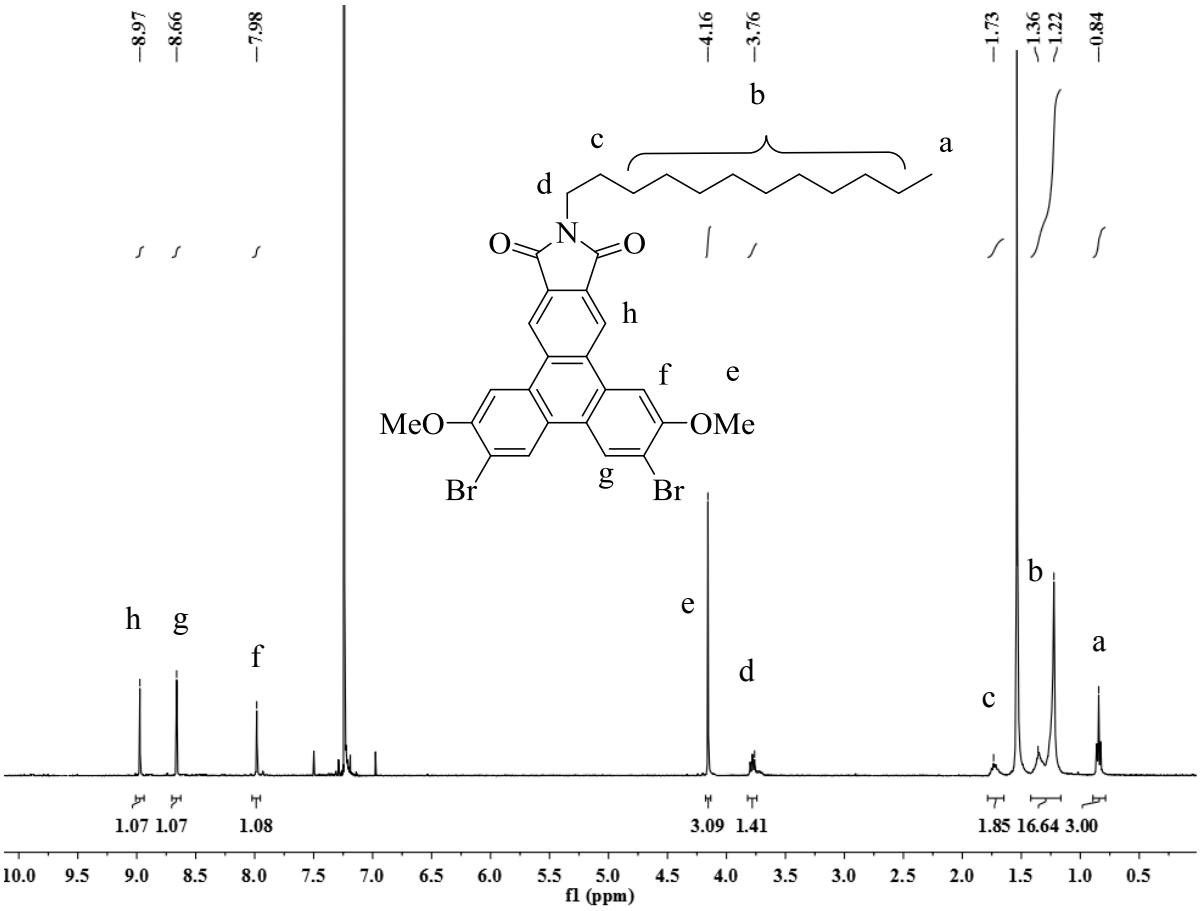

Figure 27: [1]HNMR spectrum of compound **10**

Compound **14** was also subjected to iodination using iodine and periodic acid to give another triphenylene-based monomer **16**. The [1]HNMR spectrum of **16** also gave three signals in the aromatic region due to the three unique aromatic protons in its structure (Figure **28**). All the synthetic steps involved in this scheme **2** can be isolated via simple work up followed by simple purification techniques such as recrystallization and can be easily scaled up to multigram scale.

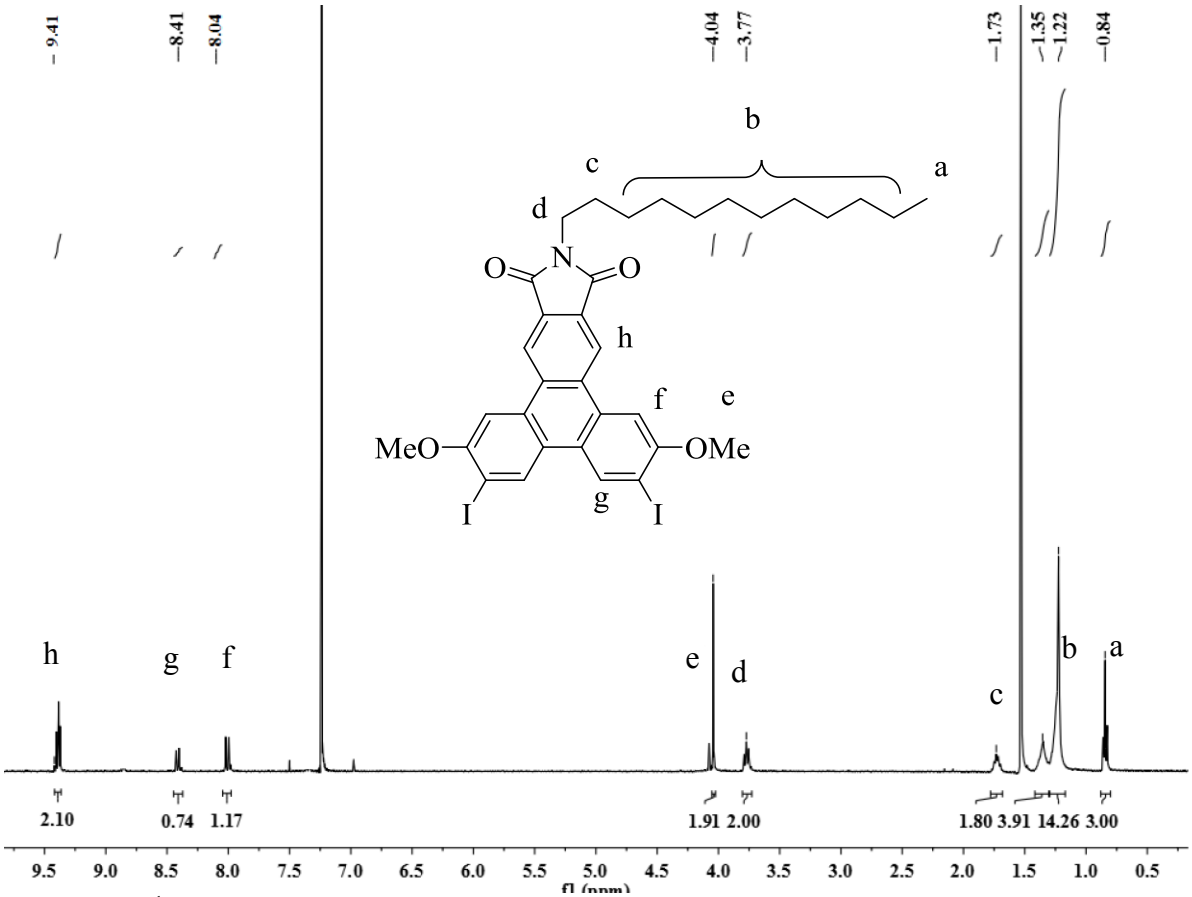

Figure 28: ^{1}H-NMR spectrum of compound **16**

We have also synthesized compound **11** the acceptor unit with triphenylene core without any imide functionalization using the reported literature procedure in our group. The precursor **TR-18** synthesized previously was subjected to iodination reaction using iodine and periodic acid to give compound **11** in yields of about 65% (Scheme **3**). The purity of the compound was checked by the ^{1}HNMR and ^{13}CNMR spectroscopy. In the ^{1}HNMR spectrum of **11** there were three well-resolved, separated sharp signals in the aromatic region for the aromatic protons. Also, the triplet at 4.15 ppm and the singlet at 4.06 ppm due to the –OCH_2- and –OCH_3 protons respectively assisted to confirm the identity of the product. In addition, the ^{13}CNMR spectrum was in agreement with all the ^{13}C signals as seen in the spectrum.

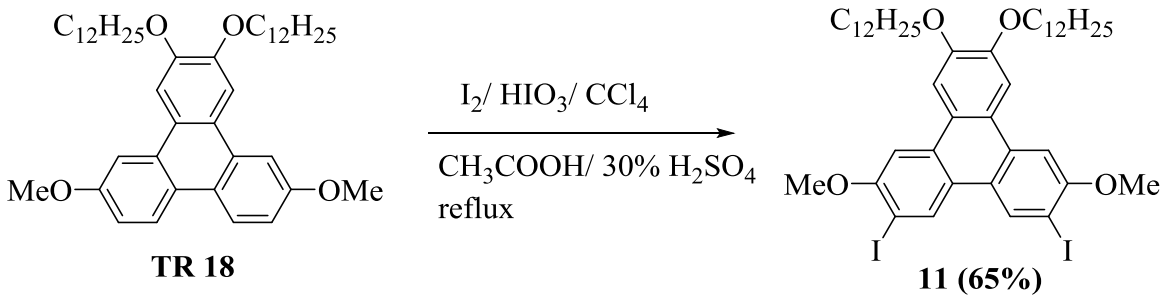

TR 18

11 (65%)

Scheme 3: Synthesis of compound **11**.

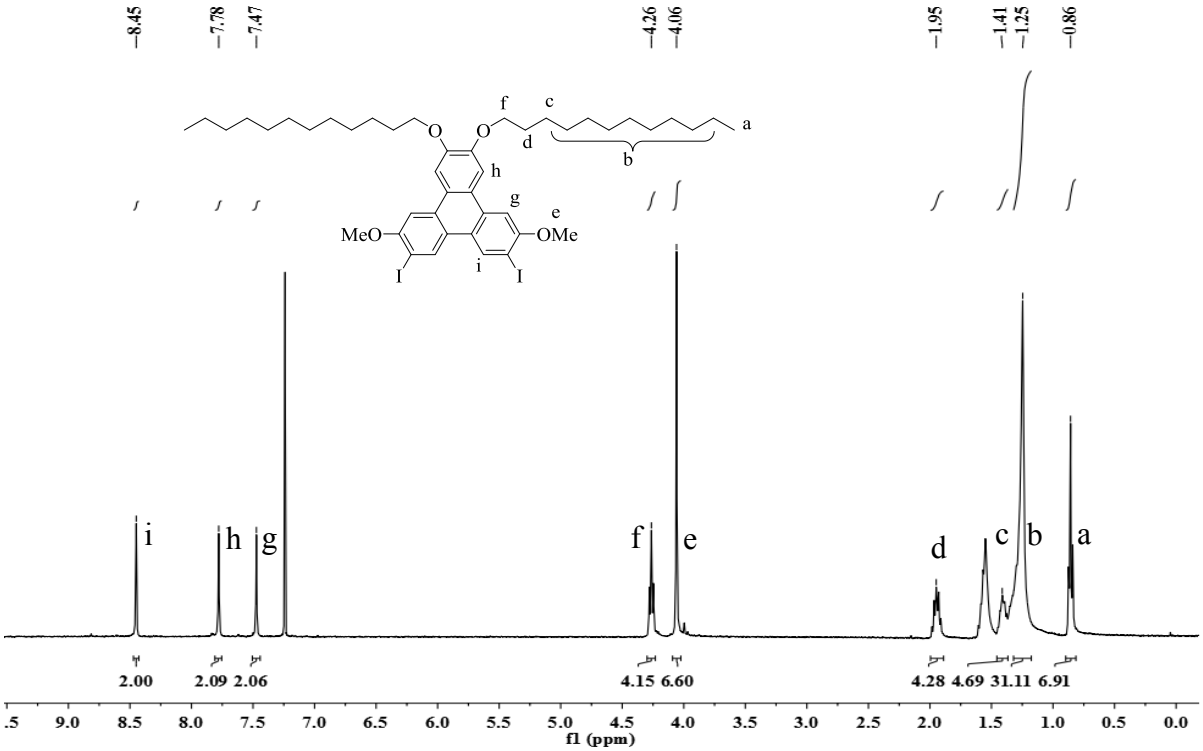

Figure 29: [1]HNMR spectrum of compound **11**.

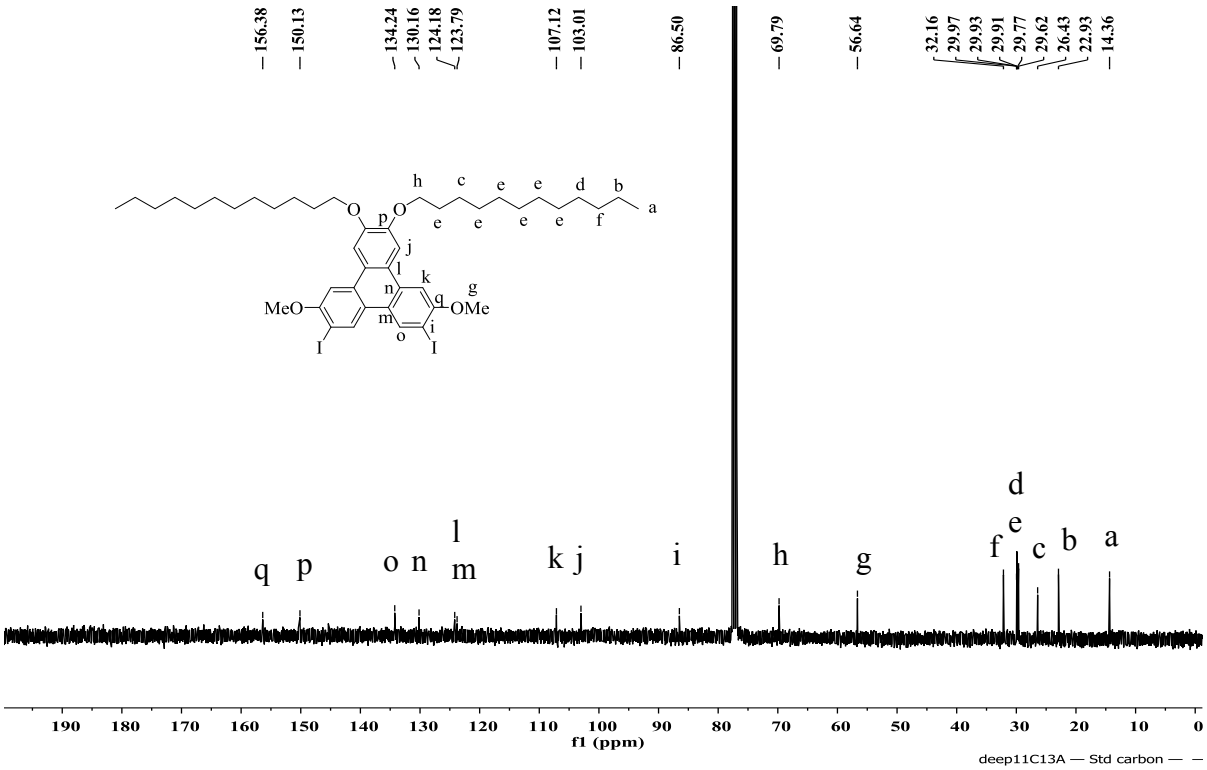

Figure 30: [13]CNMR spectrum of compound **11**.

The donor monomer was synthesized using modified published procedure[129] as depicted in Scheme **4**. The synthesis of 3,3'-dialkoxy-2,2'-bithiophene monomer was performed using commercially available 3-methoxythiophene. It was reacted with dodecylalcohol, and the methyl group was substituted with dodecyl group. Then, bromination reaction was carried out using NBS in DMF to synthesize 2-bromo-3-dodecyloxy thiophene in 84% yields. Homocoupling at the 2 positions of the bromoderivative was performed using $Ni(COD)_2$/COD/2,2'-bipyridine to give 3,3'-didodecyloxy-2,2'-bithiophene. It was finally converted to the tributyltin substituted 3,3'-didoceyloxy-2,2'-bithiophene monomer (**44**) in 83% yields.

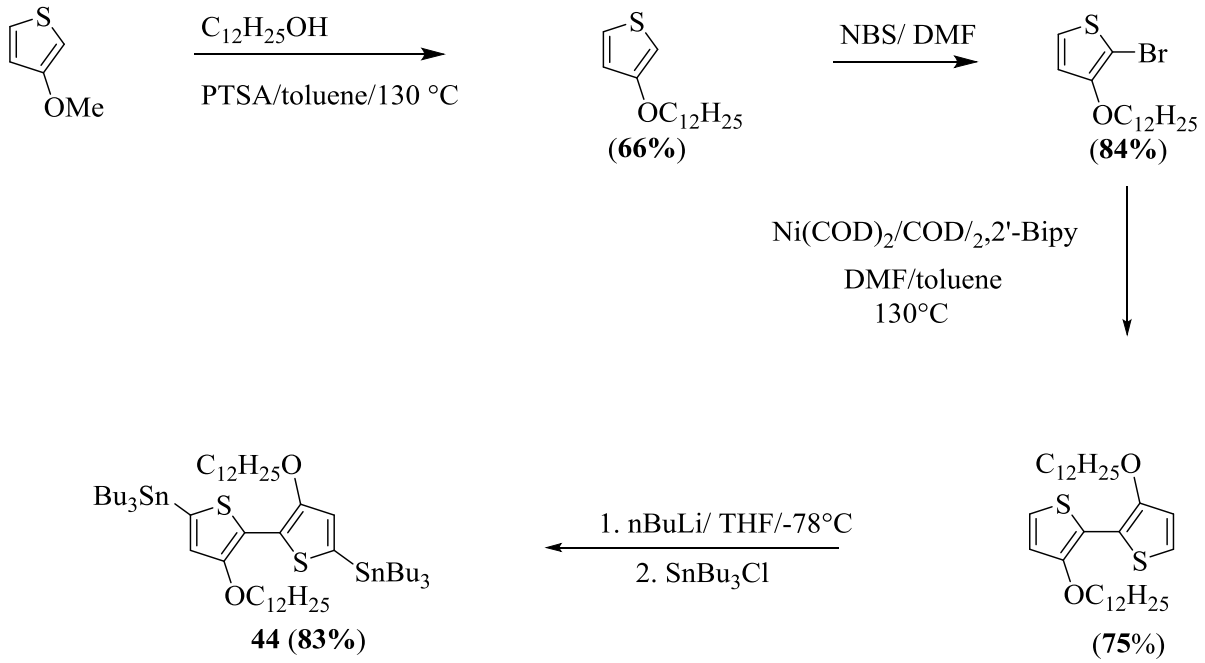

Scheme 4: Synthesis of bithiophene donor monomer

The ^{1}H-NMR spectrum of **44** showed the splitting pattern between 0.87-1.83 ppm for the tributyl and the dodecyl chains, and triplet at 4.08 ppm for $-OCH_2$ protons, as well as the

aromatic signal at 6.81 ppm confirmed the presence of aromatic protons on the thiophene ring (Figure **31**).

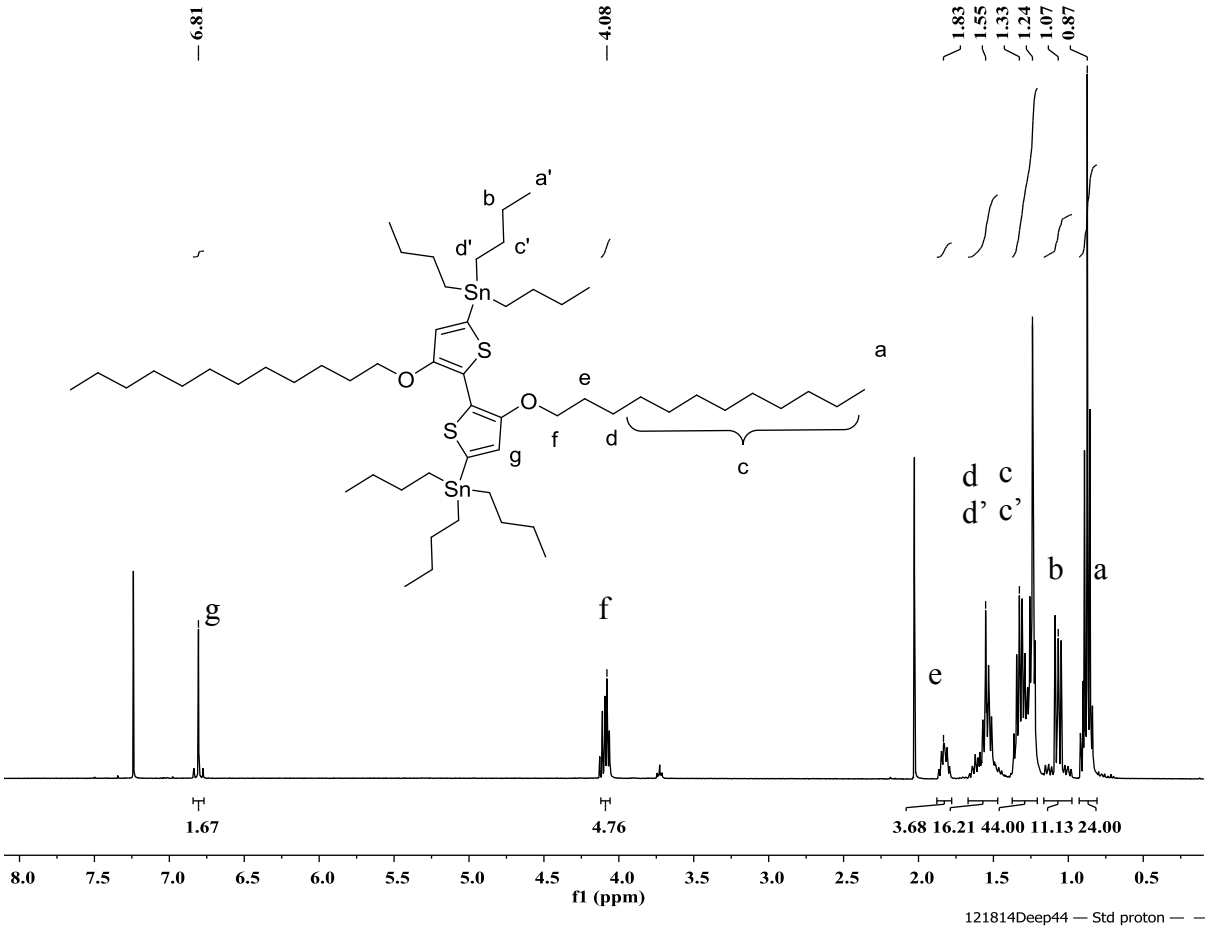

Figure 31: [1]HNMR spectrum of compound **44**.

The polymerization reaction was carried out using Stille cross-coupling polymerization and gave the polymer **58** as a dark orange solid in excellent yields. The polymer was purified by dissolving in minimum amount of good solvent like $CHCl_3$ and then precipitation in MeOH, where it had poor solubility. The reaction scheme for this polymerization is given in Scheme **5**.

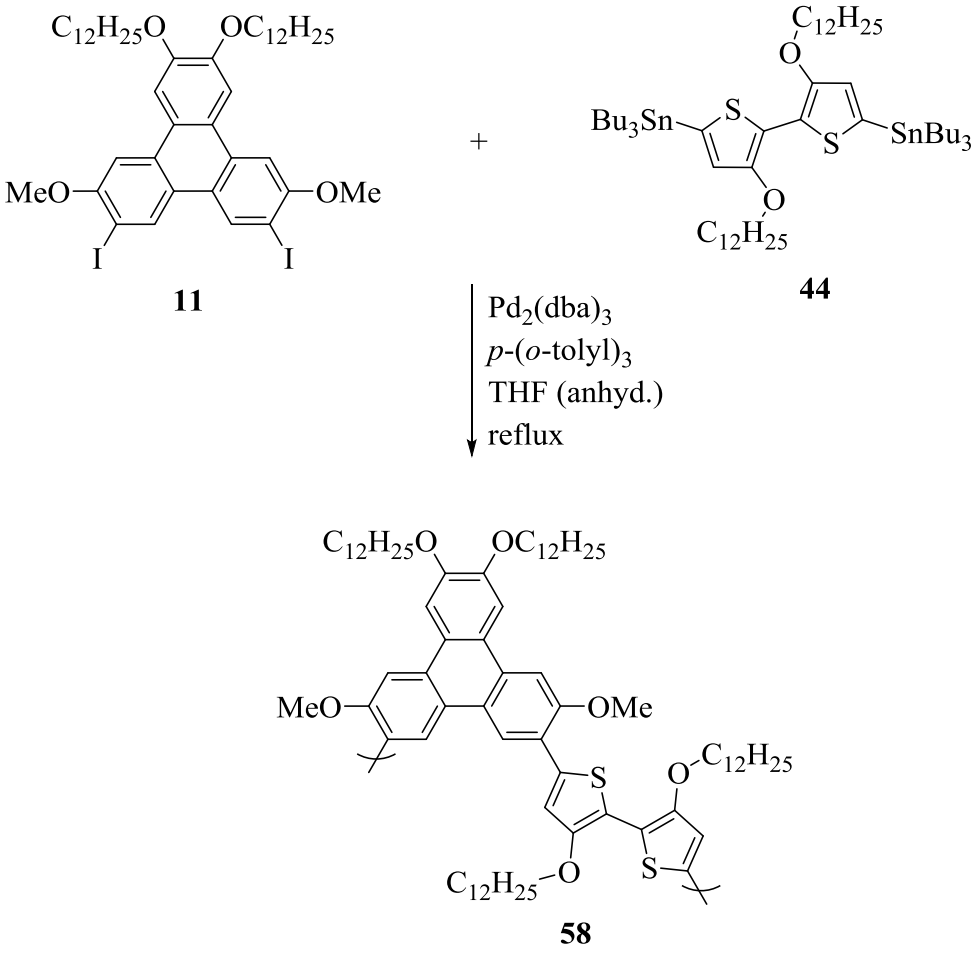

Scheme 5: Synthesis of polymer **58** using Stille cross-coupling reaction.

Similarly, the polymerization of compounds **10** and **44** was carried out following Stille coupling reaction using THF as a solvent for about 40 h to yield polymer **59** in excellent yields (Scheme **6**). The synthesized polymer **59** was isolated by repeated precipitation in solvent like MeOH where it had poor solubility gave compound **59** as a dark red solid.

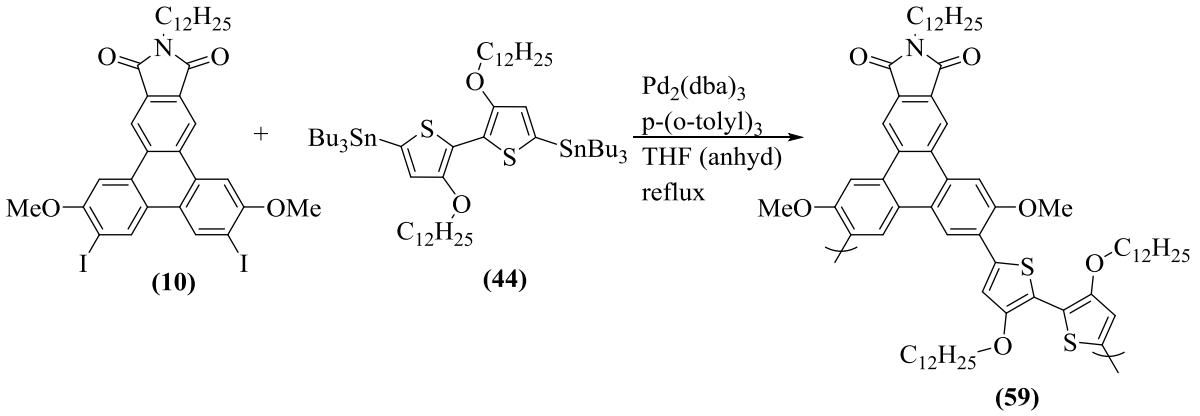

Scheme 6: Synthesis of polymer **59** using Stille coupling reaction

All the Stille coupling reactions were carried out using $Pd_2(dba)_3$/p-(o-tolyl)$_3$ catalyst systems and are known to be producing high molecular weight polymers with lower backbone defects.[130,131] Although **58** has limited solubility in nonpolar solvent like hexane, it has good solubility in solvents like chloroform, THF, DCM at room temperature and, the solubility of polymer **59** was good in $CHCl_3$, THF, acetone, DCM, DMF, and DMSO at room temperature, and it was partially soluble in solvents like hexane and acetonitrile at elevated temperatures. The four long dodecyloxy chains improve the solubility of the polymer **58** and **59** in most of the organic solvents.

Polymer **58** was characterized by ^{1}HNMR spectroscopy in $CDCl_3$, which is shown in the Figure **32**. The sharp signals in the aromatic region, the methoxy and –O-CH_2- protons around 4.00 ppm as well as the –CH_2 protons, due to the dodecyloxy protons in the monomer are all replaced by broad signals in the case of polymer **58**. The broadening is caused by the interpolymer aggregation. All these broad signals in the proton spectrum clearly suggests that there is much stronger interchain aggregation in case of triphenylene based D-A conjugated polymer **58**.

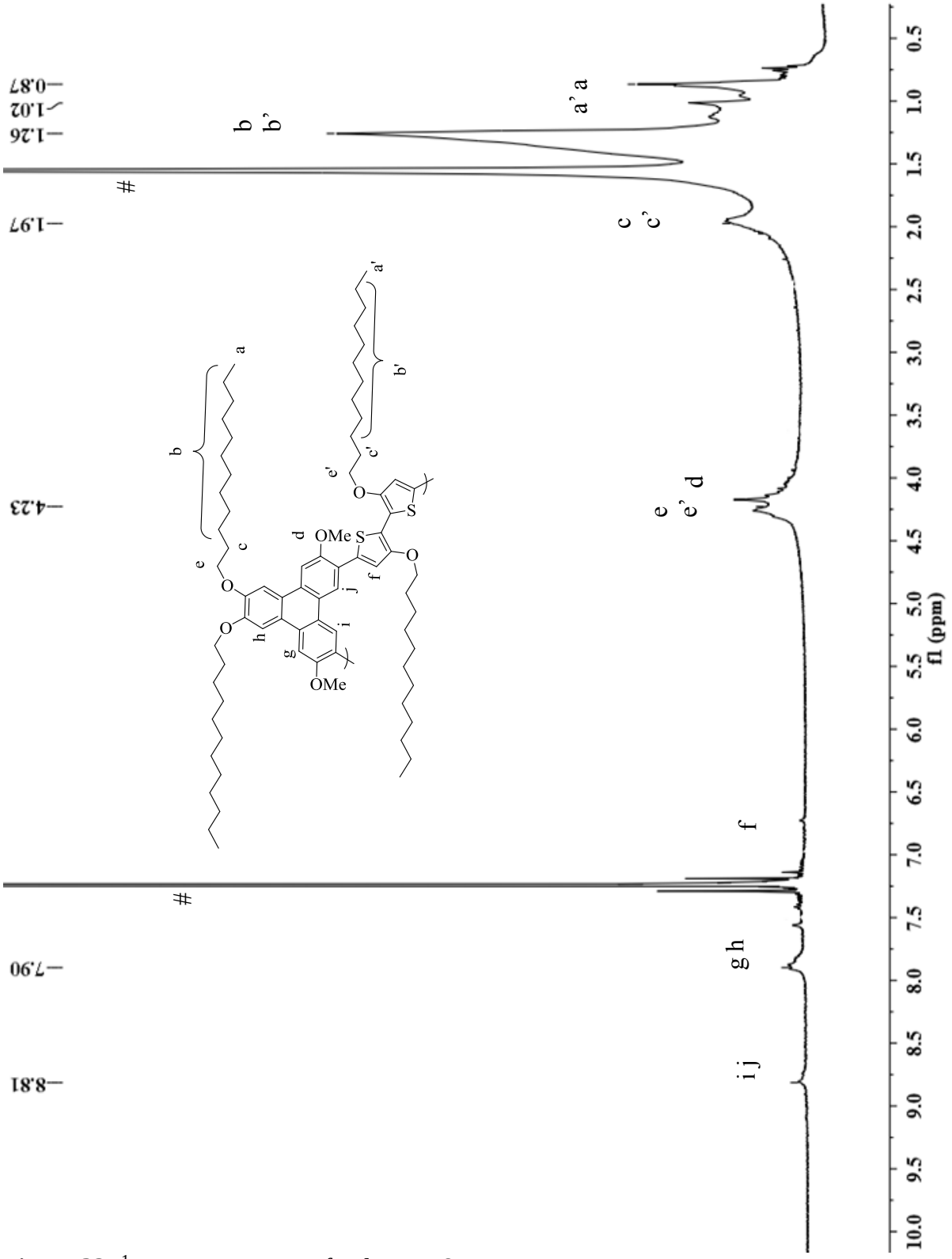

Figure 32: [1]HNMR spectrum of polymer **58**.

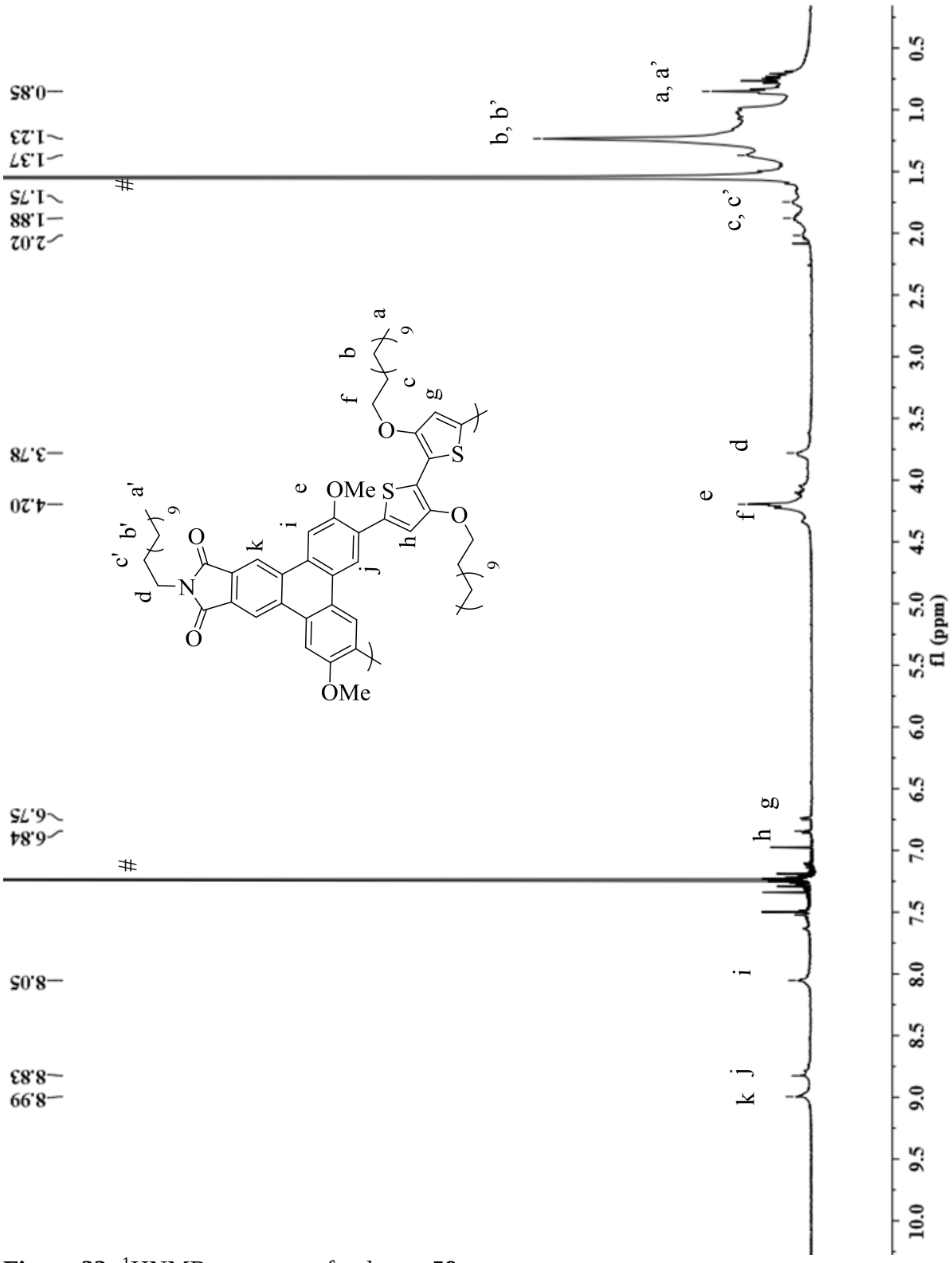

Figure 33: [1]HNMR spectrum of polymer **59**.

The ^{1}H-NMR spectrum of polymer **59** is shown in Figure **33**. The spectrum showed broadening of the aromatic signals, as well as, the signals due to protons in the N-dodecyl and dodecyloxy chains on the comonomer around 4.00 ppm and metheylene protons of the side chains around 0.80- 2.00 ppm. The broadening of the peaks is usually seen in case of polymers due to π-π stacking of the neighboring protons and the interchain aggregation. The broadening of the peaks in both polymers **58** and **59** indicate the clear distinction from their monomers and suggest there is much stronger interchain aggregation.

Polymers **58** and **59** were characterized by gel permeation chromatography to determine the molecular weights using THF as an eluent and polystyrene as the standard. The number average molecular weight (M_n) of polymer **58** was found to be 4.06 kDa, while the weight average molecular weight (M_w) was 4.83 kDa. For polymer **59,** the Mn and Mw were estimated to be 2.91 kDa and 3.42 kDa, respectively. Both polymers have narrow polydispersity indices (PDI) (1.19 and 1.18 for **58** and **59**, respectively). The results of polymerization for **58** and **59** are summarized in the Table **2**.

Table 2: Polymerization data for polymers **58** and **59**

Polymer	Mn (kDa)	Mw (kDa)	PDI	Yield (%)
58	4.06	4.82	1.19	95
59	2.91	3.42	1.18	86

2.6 Density functional theory (DFT) calculations

Theoretical calculations were carried out to predict the backbone geometries and the electronic structures of the trimers of **58** and **59**. These calculations were carried out using Gaussian03 program[132] using DFT with a B3LYP functional and a polarized 6-31G(d) basis set. This method has generally proved to be viable for structural optimizations and energy level calculations for various molecular systems.[133-137] The dodecyloxy side chains on the bithiophene units and dodecyl chain on the triphenylene acceptor units were truncated to methoxy and methyl groups respectively to reduce the computational efforts in **58** and dodecyloxy side chain on the imide groups to methoxy group in **59**. The Figures **34** and **35** below gives different orientations of the minimized energy conformers of the trimers of **58** and **59** to understand the backbone geometry and their dihedral angles are summarized in the Table **3**. The twist between the monomers for polymers **58** and **59** is approximately the same around 20°. However, as seen from Table **3**, the values for comonomer twist are very different, 4.93° for trimers of **58** while -82.07° for trimers of **59**. Based on these theoretical calculations, **59** seems to adopt C_{2V} symmetry at the bithiophenes and have a better chance to fold as seen from the Figure **35**. Hence, **59** have a better chance to fold as compared to **58**, which seems to be having more planar backbone geometry and less twisting was observed in their trimers.

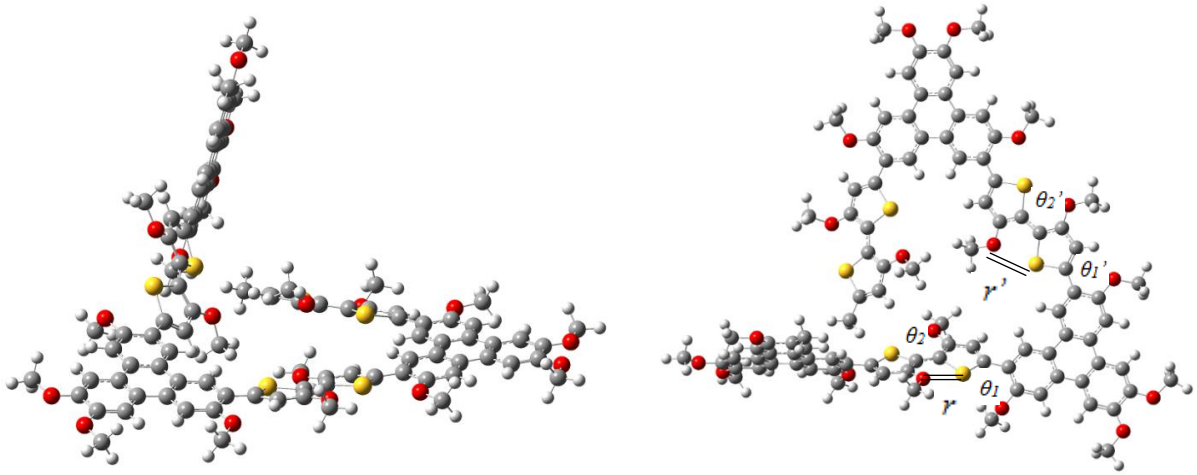

Figure 34: Energy minimized geometries of trimers of **58** in different positions; side (left), top view (right).

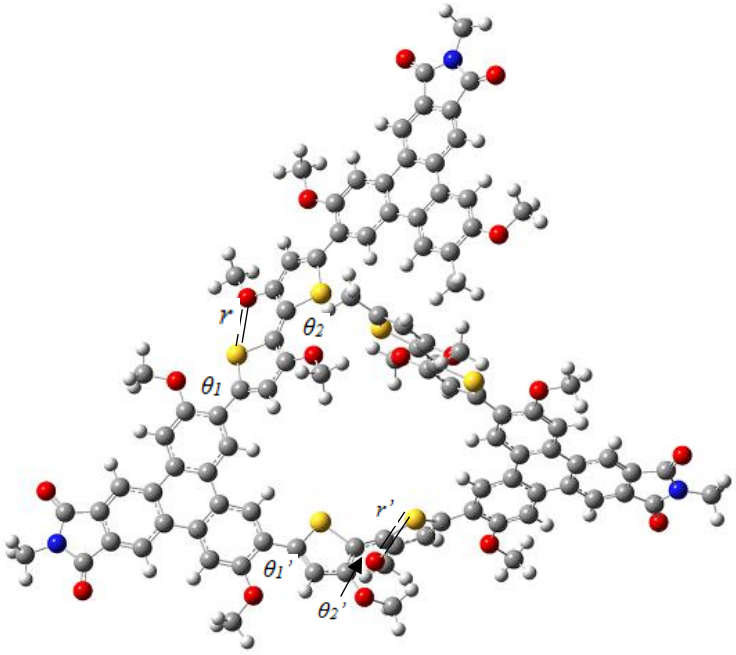

Figure 35: Energy minimized conformer of trimers for **59**.

The HOMO and LUMO energy levels of these polymers were estimated from the energy minimized structures of their trimers described above using DFT calculations at the B3LYP/6-31G(d) level. The HOMO/ LUMO distributions of the energy minimized structures are shown in the Figures **36** and **37**. The HOMO/ LUMO energy levels are calculated to be -4.14/ -1.54 eV and -4.57/ -2.51 eV, and the band gaps are 2.60 and 2.06 for trimers of polymers

58 and **59**, respectively. It is evident from Figure **50** that in the LUMO distribution of trimers for **59**, the node passes through the imide nitrogen atom.

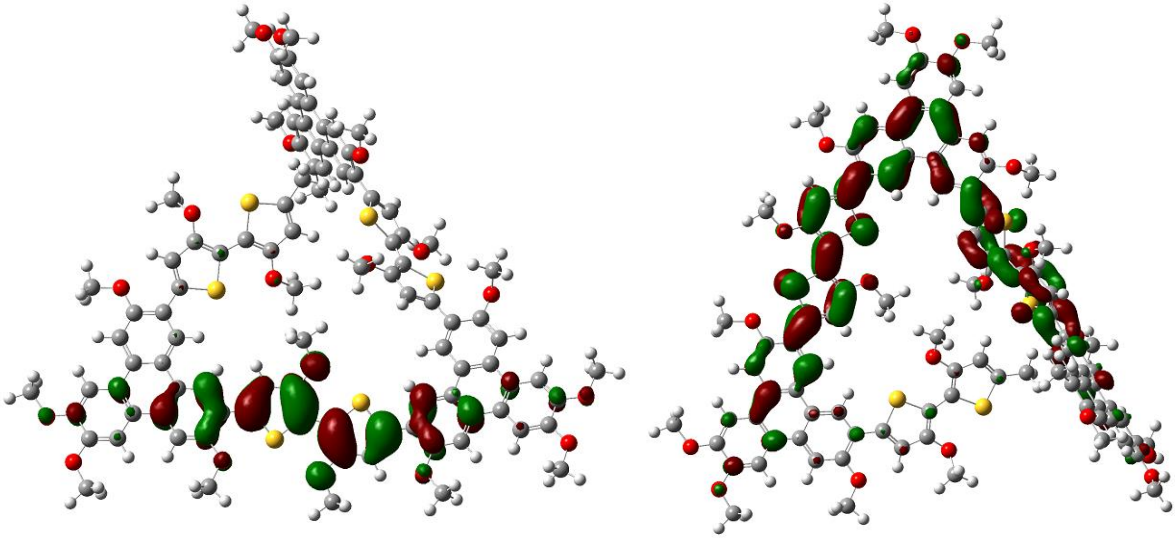

Figure 36: HOMO (left) and LUMO (right) distributions of energy minimized structures of trimers of **58**.

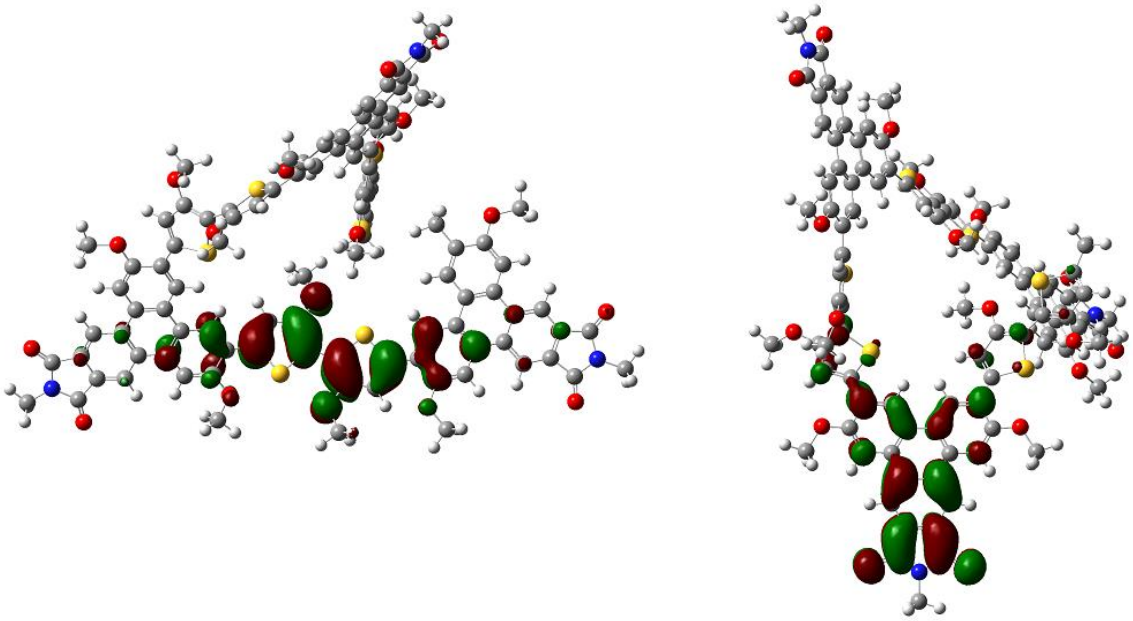

Figure 37: HOMO and LUMO distributions of energy minimized structures of **59** trimers.

The HOMO distributions in both the polymers are concentrated on the bithiophene unit which acts as a donor whereas the LUMO distributions are concentrated more on the triphenylene unit in **59**, which acts as an acceptor unit. Also, the LUMO energy levels are lowered for **59** as compared to **58** due to the presence of imide functionality. Hence, there would be an advantage of the use of imide functionalization in lowering the LUMO energy, and thereby, reducing the band gap as seen from the theoretical calculations.

Table 3: The dihedral angles and the S--O short contact distances for polymers **58** and **59** using DFT calculations.

Polymer	**Intermonomer twist**		**Comonomer twist**		**S—O short contact (Å)**	
	θ_1	**θ_1'**	**θ_2**	**θ_2'**	**r**	**r'**
58	14.87	20.43	4.93	-3.39	2.86	2.98
59	-22.05	-34.16	-82.07	-2.48	2.82	3.82

2.7 Electrochemical studies of triphenylene-based conjugated polymers

The electrochemical properties of the two triphenylene-containing conjugated polymers were studied as thin films using cyclic voltammetry (CV) measurements. For polymer **58**, one irreversible reduction wave was observed during the cathodic scan, and the irreversible oxidation wave was shown during the anodic scan as seen in Figure **38**. In case of polymer **59**, two reversible reduction waves were observed during the cathodic scan, and two semi-reversible oxidation waves were seen during the anodic scan. By making use of the first onset oxidation potential during the anodic scan and the first reduction potential in the cathodic scan, the HOMO and LUMO energy levels of the polymers **58** and **59** were estimated to be -5.24/ -2.98 and -5.20/ -4.05, respectively. As discussed previously, in D-A conjugated polymers, the HOMO energy levels are controlled by the D units, while the LUMO energy levels are controlled by A units. Since, in the cases of both polymers **58** and **59**, the donor comonomer are the same, and the HOMO levels are very close to each other, while the LUMO levels are different. The LUMO energy levels in case of polymer **59** was lowered substantially due to the presence of imide functionalization and that in turn lowered the effective band gap. The bandgaps of polymers **58** and **59** were found to be 2.26 and 1.15 eV respectively. Thus, the CV measurements were in agreement with the theoretical calculations and showed the lowering of the energy gap in the imide functionalized triphenylene-based conjugated foldamers.

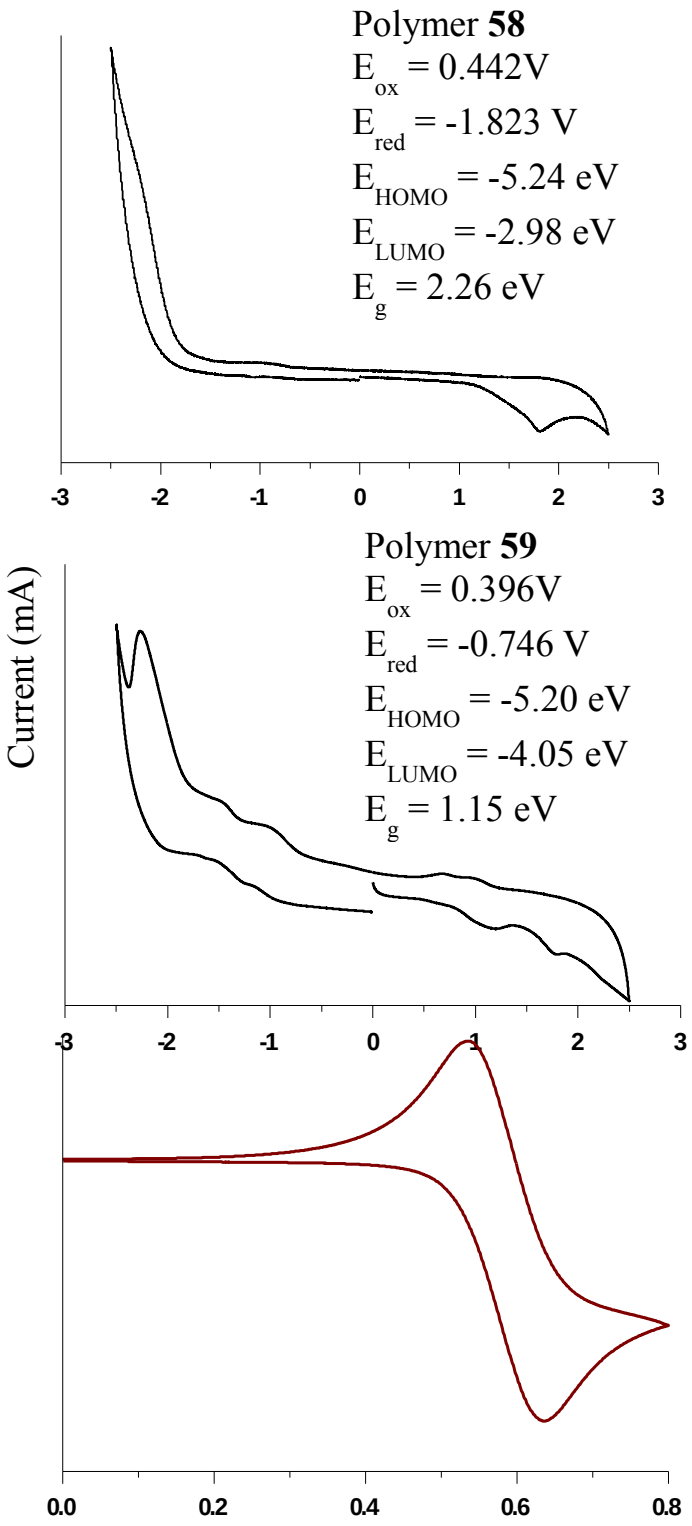

Figure 38: Cyclic voltammograms of polymer thin films of **58** and **59**, and the Fc/Fc^{+} redox couple used as a reference.

2.8 Optical studies of triphenylene based conjugated polymers

Polymer **58** showed good solubility in acetone, chloroform, DCM, *o*-dichlorobenzene, DMF, DMSO, and THF but poor solubility in methanol, acetonitrile and hexane. Their absorption spectra in chloroform, THF, acetonitrile, and hexane are shown in Figure **39**. The solutions of polymer **58** in solvents e.g. CH_3CN and hexane were prepared by adding a drop of its concentrated chloroform solution into acetonitrile or hexane having poor solubility in them.

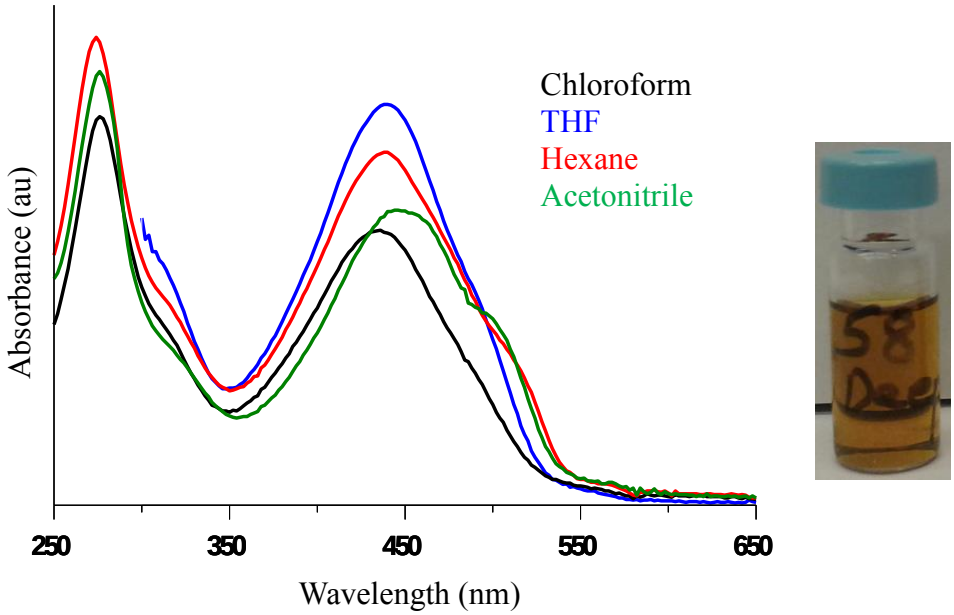

Figure 39: Absorption spectra of polymer **58** in different solvents

As shown in Figure **39**, polymer **58** showed two absorption maxima at approximately 276 and 440 nm in good solvents. In acetonitrile and hexane, a prominent shoulder peak around 500 nm appeared. A red shift of about 8 nm is also observed for the absorption λ_{max} in the visible range when the solvent is changed from chloroform to acetonitrile. The slight red shift

in the band edge from chloroform to acetonitrile may be due to the polarity differences between the solvents, while the shoulder peak is likely due to polymer aggregation.

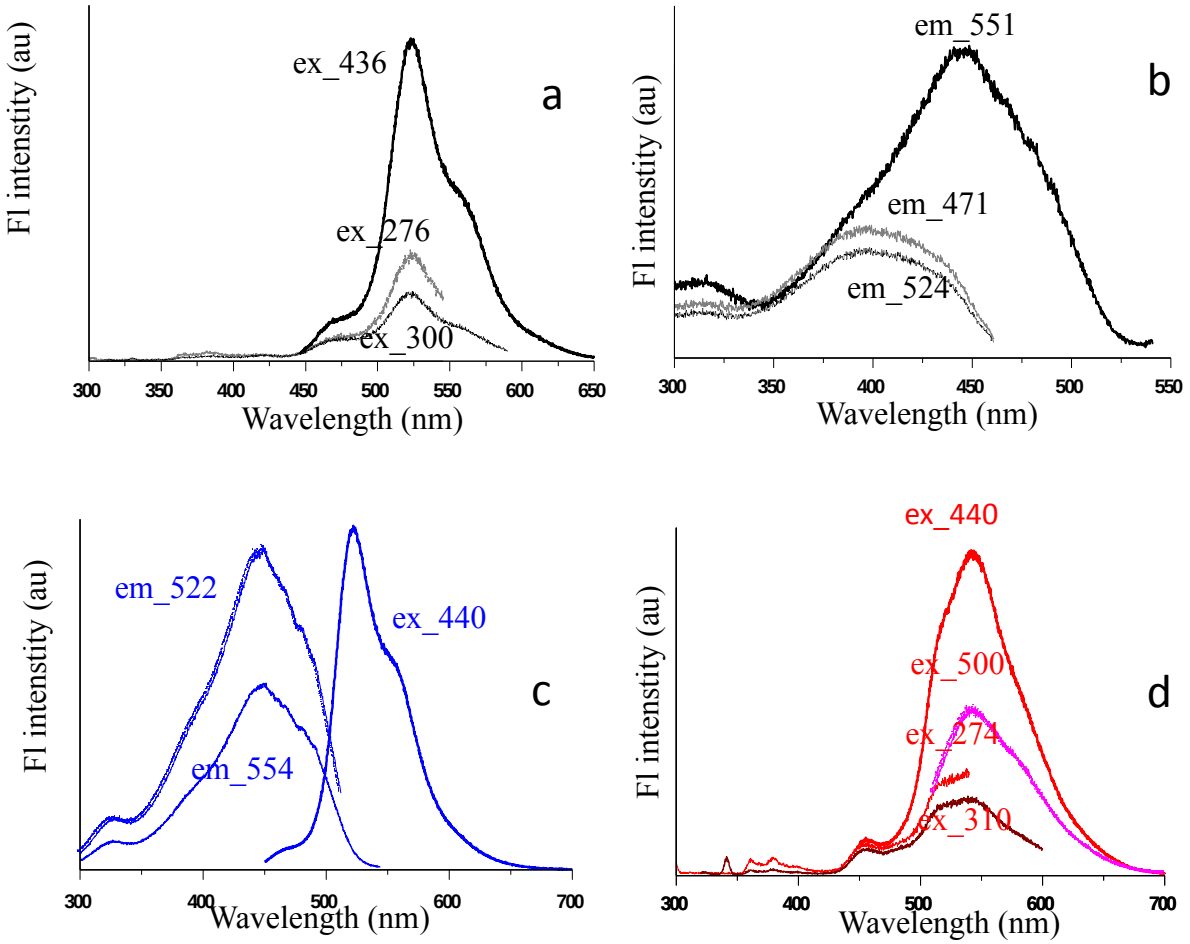

Figure 40: a) Emission spectra in chloroform, b) Excitation spectra in chloroform, c) Emission and excitation spectra in THF, d) Emission spectra in Hexane for polymer **58**.

The emission and excitation spectra of polymer **58** in chloroform, THF, and hexane were shown in Figure **40**. In chloroform solution, it was excited at 276 and at 436 nm, it gave the broad emission peak around 524 nm with the shoulder peak around 551 nm. Similar emissions were observed in THF. However in hexane the emission λ_{max} is at 550 nm. In all these solvents, when the excitation spectra at different emission wavelengths were taken, they

gave the same excitation spectra indicating the presence of only one type of conformer predominant in these solvents for polymer **58**. The emission spectra of **58** in acetonitrile (Figure **41**) was different from its emission in other solvents, as it had very poor solubility in acetonitrile and showed weak emissions around 500 nm.

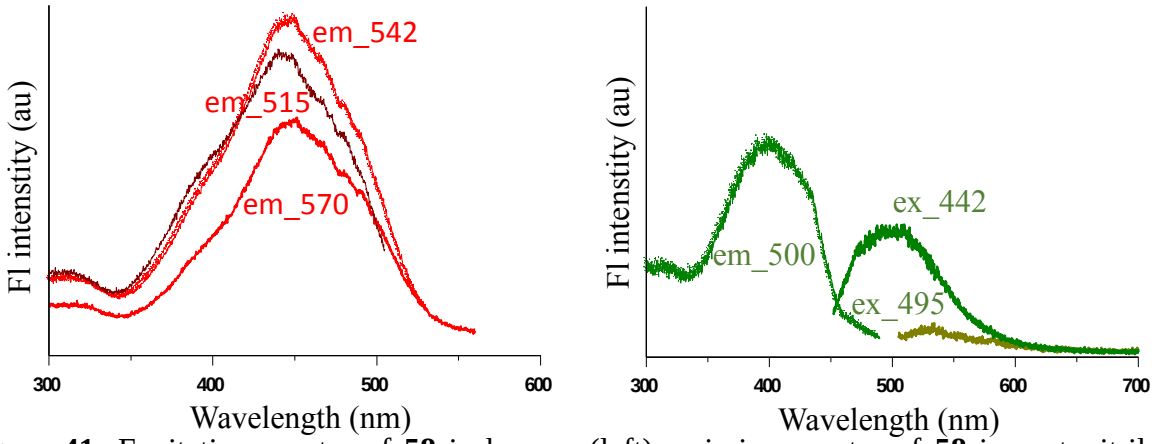

Figure 41: Excitation spectra of **58** in hexane (left) emission spectra of **58** in acetonitrile (right).

In order to understand the effect of solvent composition on the emissions of the polymer, an acetonitrile solution of **58** was prepared and continuously diluted with THF (Figure **42**) and vice versa. As shown previously, polymer **58** in 100% acetonitrile showed very weak emission around 500 nm. As the THF content increases upon continuous dilution with THF, the fluorescence quantum yield increases, and there is a red shift in the emission wavelength and the emission at 522 nm becomes dominant. Also, the reverse trend can be seen in Figure **43** where the solution of **58** in THF was continuously diluted with acetonitrile: the emission wavelength are blue shifted from 522 to 500 nm and emission intensity decreases as the amount of acetonitrile increased.

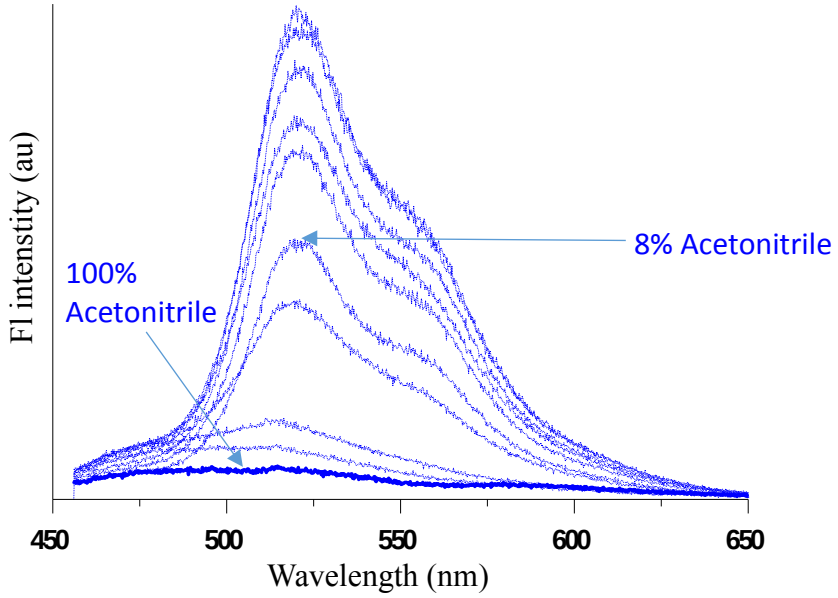

Figure 42: Emission spectra of **58** in acetonitrile by dilution with THF.

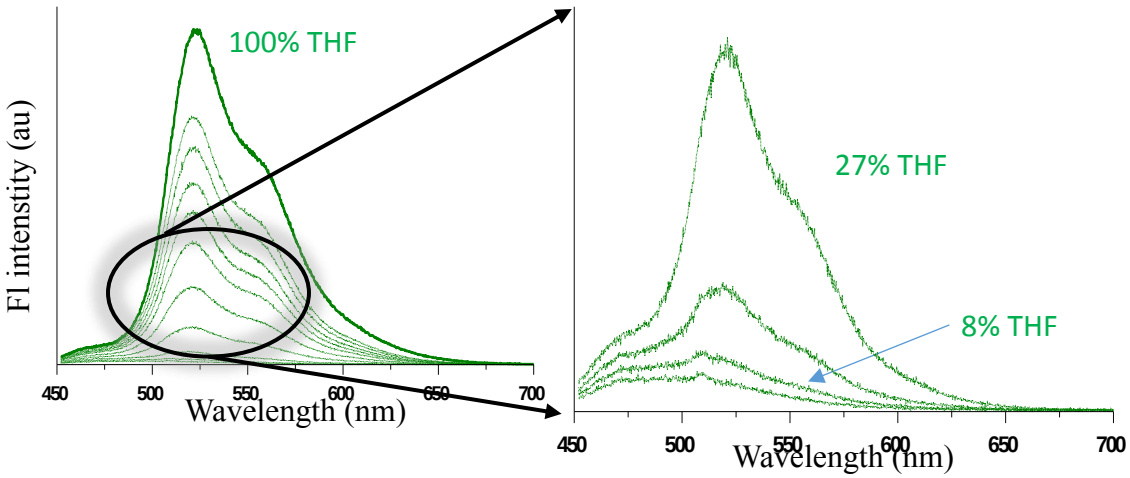

Figure 43: Emission spectra of **58** in THF by dilution with acetonitrile.

Also, the solvent dependence study for the emission of polymer **58** in $CHCl_3$ was studied by continuous dilution with hexane in which it had partial solubility. As it can be observed (Figure **44**), there was a decrease in the fluorescence quantum yield/fluorescence quenching effect was seen as the chloroform content decreases but there was not much shift in the emission wavelength between the two solvents.

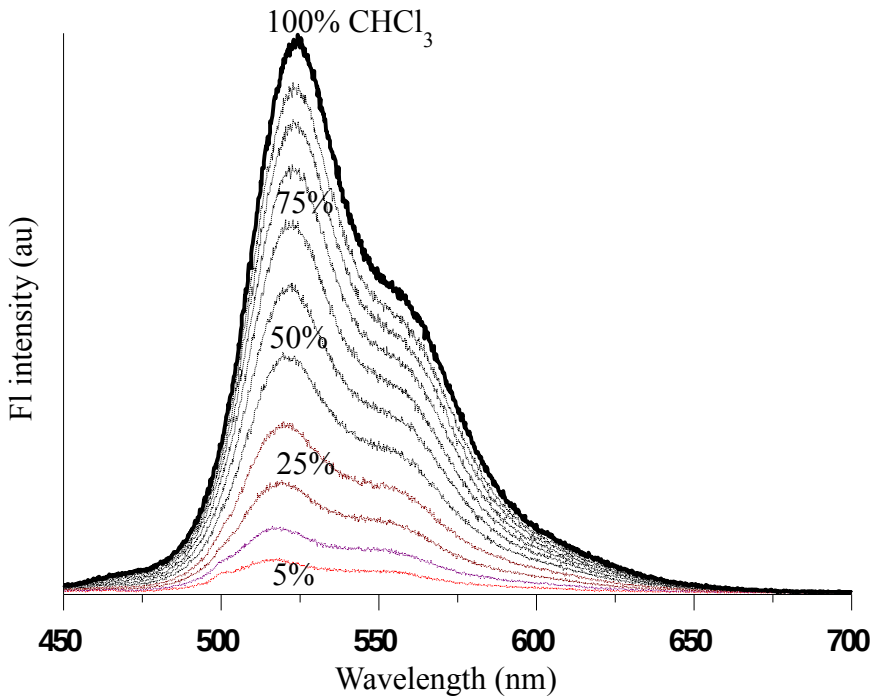

Figure 44: Emission data of polymer 58 in chloroform dilution by hexane.

Polymer **59** exhibits good solubility in solvents like $CHCl_3$, THF, DCM, DMF, and acetone at room temperature but is only partially soluble in solvents like hexane and has poor solubility in acetonitrile/methanol. The absorption spectra of polymer **59** in a solvents like $CHCl_3$, THF, (good solubility) and hexane, acetonitrile (poor solubility) are shown in Figure **45**.

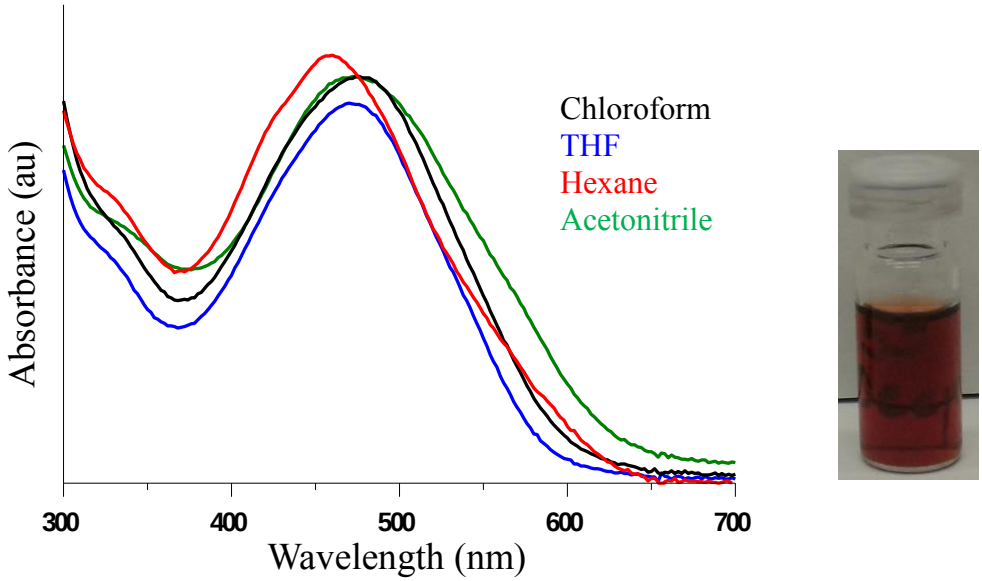

Figure 45: Absorption spectra of polymer **59** in different solvents.

The absorption maxima in hexane was 458 nm, while it was 478 nm in chloroform, hence there was about 20 nm red shift in the band edge for polymer **59** as the polarity of the solvent was increased. The emission and excitation spectra of polymer in hexane as well as chloroform can be seen in Figure **46**. Polymer **59** showed very weak, broad and featureless emissions in chloroform but showed much stronger, blue-shifted emissions with vibrionic bands in hexane. The maximum emission wavelength (λ_{max}) in chloroform was 618 nm, while the λ_{max} in hexane was 518 nm along with a shoulder peak at about 550 nm. The excitation spectra of **59** in hexane which was monitored at these two emission wavelengths are similar (Figure **46**).

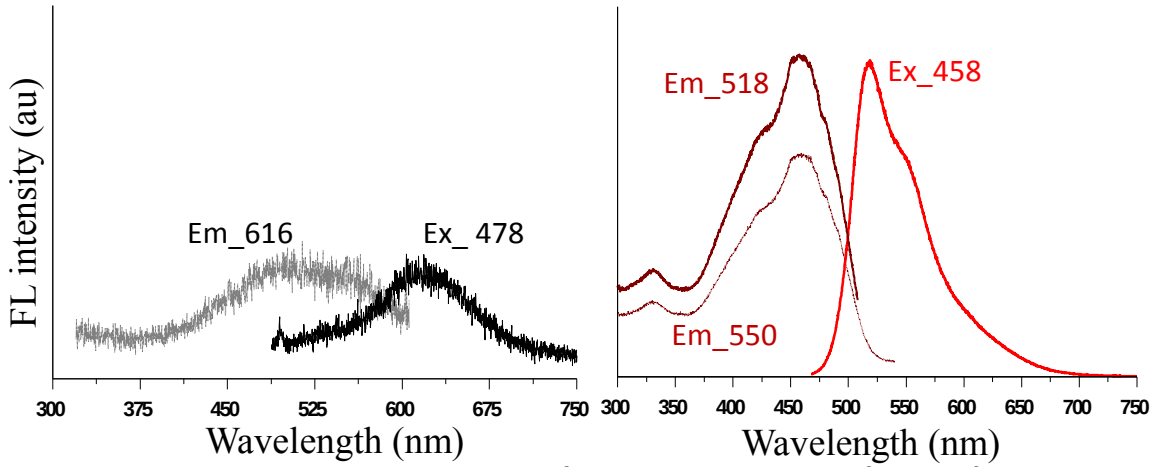

Figure 46: Emission and excitation spectra of polymer **59** in chloroform (left) and hexane (right).

The polymer solution of **59** in hexane was subjected to continuous dilution as shown in the figure **47**. As the concentration of polymer decreases, one sees no change in emission λ_{max} and spectral profile. To further understand the emission changes in different solvents, the polymer was dissolved in hexane first and then continuously diluted with $CHCl_3$ and vice versa. The emission spectra of polymer **59** in hexane/ $CHCl_3$ mixtures is depicted in Figure **48**. As the $CHCl_3$ volume increased, there was clear red shift in the emission wavelength and decrease in the intensity of the emission. The drastic changes in the emission wavelengths indicate that the polymer adopts different conformations in solvents with varying solubility.

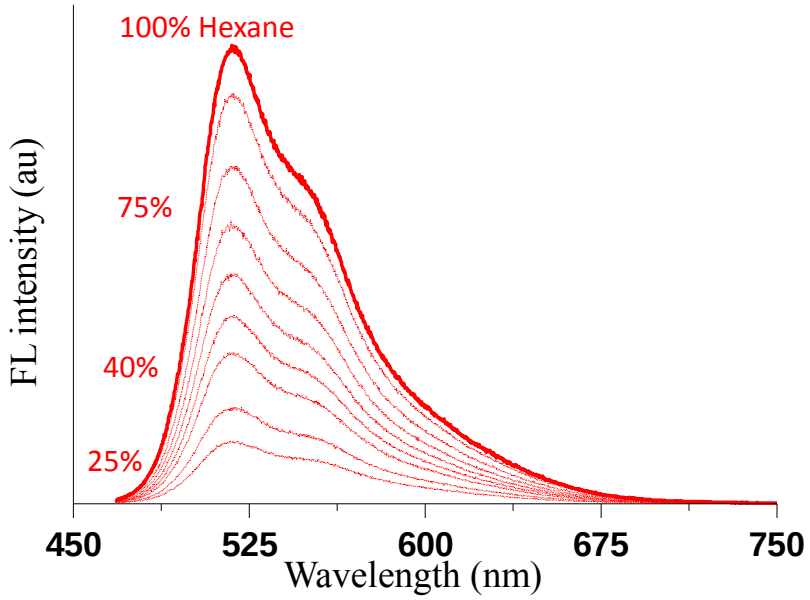

Figure 47: Dilution effects on the emission spectra of **59** in hexane.

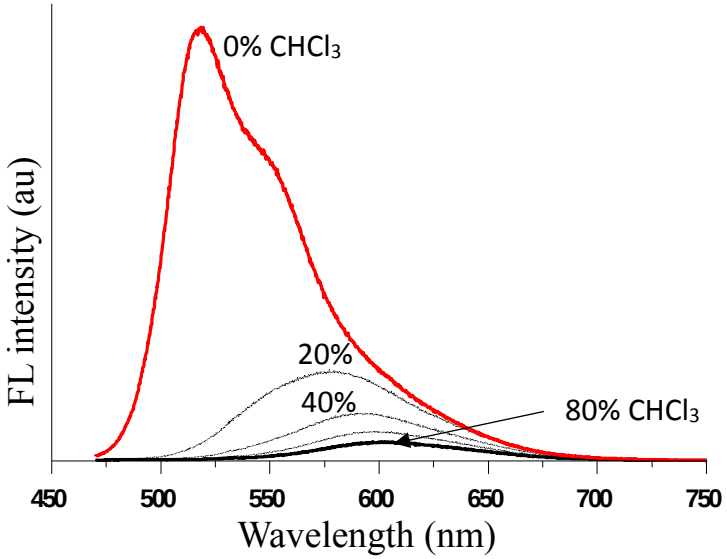

Figure 48: Emission spectra of **59** in different solvents (hexane solution diluted with $CHCl_3$).

It is interesting to note the significant differences in the solvent dependent emission properties of polymers **58** and **59** in chloroform and hexane. For **58**, the polymer is more fluorescent in a good solvent $CHCl_3$ and the emission λ_{max} is blue shifted. For **59**, the observation is exactly opposite: polymer **59** has significantly less fluorescence in the good solvent chloroform and the emission λ_{max} in chloroform is significantly red-shifted by about 100 nm compared to that in hexane.

In case of polymer **59**, aggregation is caused possibly due to the folding-induced emission in hexane while in chloroform CT transition dominates. In hexane having poor solubility of **59**, emissions are possibly from π*-π transition. While the labile side chains are favored in non-polar solvents like hexane, and the side chains interactions with solvent would cause the polymer to fold. However, in polymer **58**, there are no CT in either solvent. In good solvent, there is less aggregation.

2.9 Conclusion and future directions

To summarize, we have successfully synthesized D-A conjugated polymers with triphenylene backbone and have studied their optical, electrochemical properties. This have been compared with the theoretical energy calculations obtained by using the Gaussian 03 program. According to the hypothesis, the energy gap for the polymers should be lowered by the inclusion of imide group which was supported by both the theoretical calculations (DFT) and the experimental results (optical and CV measurements). The results are summarized in the following Table **4**.

Table 4: Optoelectronic properties of the polymers **58** and **59**.

Polymer	λ_{max}^{abs} **(nm)**	E_g^{opt} **(eV)**	**Experimental (eV) CV**			**Calculated (eV) DFT**		
			E_{HOMO}	E_{LUMO}	**Eg**	E_{HOMO}	E_{LUMO}	**Eg**
58	436	2.16	-5.24	-2.98	2.26	-4.14	-1.54	2.60
59	478	2.06	-5.20	-4.05	1.15	-4.57	-2.51	2.06

The optical data for polymers **58** and **59** suggests that these polymers exhibited different conformers in different solvents. For example polymer **58** showed weak fluorescence in hexane (poor solubility) and was more blue shifted whereas it showed broad and structureless fluorescence in $CHCl_3$ (good solubility). This result suggests the presence of different conformers in different solvents. Whereas, for polymer **59**, broad and structureless emission was observed in hexane (poor solubility), while weak and red shifted emission by 100 nm was observed in $CHCl_3$ (good solubility).

Thus, optical data suggests that **59** is present as folding conformer in hexane, whereas interchain aggregation is seen in polymer **58** in good solvent like $CHCl_3$. Although, further studies need to be completed in this regard, as well as to explore the device properties of these polymers especially for imide functionalization of polymer **59**. In addition, theoretical studies showed that the bithiophene donor monomer would be less planar due to the comonomer twisting, and hence the use of alternate donor monomers would be preferred. Also, the pitch angle for the polymers with triphenylene core would be much smaller due to the structural constraints. Therefore, we would focus our attention to the synthesis and characterization of polymers with NDT and INDT based D-A conjugated polymers in order to provide much larger pitch radius and easier folding of the polymers with fewer structural constraints.

2.10 Experimental section

Solvents were distilled from appropriate drying agents under inert conditions prior to use. Unless otherwise stated, all other chemicals were purchased from commercial sources and used without further purification. All reactions were carried out under nitrogen using standard Schlenk techniques. ^{1}HNMR and ^{13}CNMR spectra were collected using a Varian INOVA 400 MHz NMR spectrometer. All samples were referenced to the deuterated solvents. Polymer molecular weights were determined at 30 ^{o}C on a Tossoh EcoSec HLC 8320GPC system equipped with a differential refractometer, UV detector, and styragel column with THF as the eluent versus polystyrene standards. UV-Vis absorption spectra were measured using a Hewlett-Packard 8452A diode array spectrophotometer. Cyclic voltammetry (CV) studies were carried out under argon atmosphere using BAS Epsilon EC electrochemical station employing a Pt working electrode, a silver wire reference electrode and a Pt wire as the counter electrode. A 0.1 M tetra-n-butylammonium hexafluorophosphate solution in acetonitrile as supporting electrolyte and the scan rate was 20 mVs^{-1}. Fc/Fc^{+} was used as reference for all measurements and assigned an absolute energy of -4.8 eV versus vacuum.

Compound 13

In a 100 mL two-neck RBF, 4,5-dibromophthalic anhydride (1.00 g, 3.26 mmol) was added. The flask was subjected to three cycles of vacuum drying and N_2 purging. N-dodecyl amine (0.91 g, 4.90 mmol) was then added, followed by the addition of acetic acid (50 mL). The resulting reaction mixture was stirred at 120 °C for 2 h. The excess acetic acid was removed by rotavapor to give crude product as yellowish brown solid, which was purified by passing through a silica column with the mobile phase of ethyl acetate: hexane (30:70). After performing the column chromatography, **13** was obtained as a yellowish-orange solid (1.25 g,

2.64 mmol, 81%). H^1NMR (400 MHz, $CDCl_3$): δ 8.05 (s, 2H, Ar-H), 3.64 (t, J = 8 Hz, 2H, -N-CH_2-), 1.62 (m, 2H, -CH_2-), 1.22 (m, 18H, -CH_2-), 0.85 (t, J = 8 Hz, 3H, -CH_3) ppm.

Compound 12

Compound **13** (0.50 g, 1.06 mmol) and (3-methoxyphenyl) boronic acid (0.39 g, 2.53 mmol) were added in a schlenk flask and the mixture was subjected to three cycles of pumping and purging with N_2. Toluene (50 mL) and ethanol (20 mL) were then added to the flask, and N_2 was bubbled into the reaction mixture for 20 min. Tetrakis(triphenylphosphine)palladium(0) (0.06 g, 0.05 mmol) and sodium bicarbonate (0.67 g, 6.33 mmol) were subsequently added to the flask, and N_2 was bubbled into the reaction mixture for an additional 10 min. The reaction mixture was stirred under reflux for 16 h. It was then cooled to room temperature and neutralized with 10% HCl. It was then washed with deionized (DI) water, and the aqueous layer was extracted with dichloromethane (DCM) (3x 30 mL). The organic layers were combined, and dried over magnesium sulfate. The solvent was removed to give thick yellow liquid as the crude product. It was purified by column chromatography on a silica gel with ethyl acetate: hexane (30:70) as the eluent, affording **12** as a yellow solid (0.54 g, 1.02 mmol, 96%). H^1NMR (400 MHz, $CDCl_3$): δ 9.02 (s, 2H, Ar-H), 8.51 (dd, J= 8 Hz, 2H, Ar-H), 8.04 (s, 2H, Ar-H), 7.37 (d, J= 4 Hz, 2H, Ar-H), 7.35 (d, 2H, Ar-H), 4.05 (s, 6H, -O-CH_3), 3.77 (t, J = 8 Hz, 2H, -N-CH_2-), 1.73 (m, 2H, -CH_2-), 1.23 (m, 18H, -CH_2-), 0.84 (t, J = 6 Hz, 3H, -CH_3) ppm.

Compound 14

In a schlenk flask, compound **12** (0.90 g, 1.71 mmol) was added, and the flask was subjected to three cycles of pumping and purging with N_2. To this flask under N_2, freshly distilled DCM (90 mL) was added, followed by the addition of Iron (III) chloride (1.38 g, 8.55 mmol). The

resulting reaction mixture was stirred at room temperature for approximately 20 min. Methanol (60 mL) was then added, and the mixture was stirred for another one h. It was then poured into DI water and was extracted with DCM. The organic layers were combined and dried over $MgSO_4$. It was passed through a 2" filtration column, and the solvent was evaporated to give the orange crude product. It was then recrystallized from DCM: methanol to give compound **14** (0.72 g, 1.37 mmol, 80%) as a yellow solid. H^1NMR (400 MHz, $CDCl_3$): δ 9.42 (s, 2H, Ar-H), 8.48 (d, J = 12 Hz, 2H, Ar-H), 8.04 (s, 2H, Ar-H), 7.46 (dd, J = 8 Hz, 2H, Ar-H), 4.05 (s, 6H, -O-CH_3), 3.77 (t, J = 8 Hz, 2H, -N-CH_2-), 1.73 (m, 2H, -CH_2-), 1.22 (m, 18H, -CH_2-), 0.84 (t, J = 6 Hz, 3H, -CH_3) ppm. C^{13}NMR (400 MHz, $CDCl_3$): δ 168.7, 158.7, 133.9, 129.5, 129.2, 124.9, 124.8, 119.0, 118.7, 105.6, 55.9, 38.6, 32.1, 29.9, 29.8, 29.6, 29.5, 28.9, 27.2, 22.9, 14.4 ppm.

Compound 10

In a 100 mL RBF was added compound **14** (0.50 g, 0.95 mmol). To the same flask, trifluoroacetic acid (22.5 mL) was added, followed by the addition of con. H_2SO_4 (5 mL) dropwise to obtain a reddish solution. N-bromosuccinamide (0.42 g, 2.38 mmol) was then added to the above solution to yield a dark red colored soln. It was stirred at room temperature overnight. The reaction mixture was diluted with DI water, extracted with DCM. The organic layers were collected and dried over $MgSO_4$. The solvent was evaporated to give reddish solid as the crude product. It was then recrystallized from DCM: CH_3OH to yield compound **10** as a pale yellow solid. (0.36 g, 0.53 mmol, 56%). H^1NMR (400 MHz, $CDCl_3$): δ 8.97 (s, 2H, Ar-H), 8.66 (s, 2H, Ar-H), 7.98 (s, 2H, Ar-H), 4.16 (s, 6H, -O-CH_3), 3.76 (t, J = 8 Hz, 2H, -N-CH_2-), 1.73 (m, 2H, -CH_2-), 1.22 (m, 18H, -CH_2-), 0.84 (t, J = 8 Hz, 3H, -CH_3) ppm.

Compound 11

In a 100 mL RBF, 2,3-bis(dodecyloxy)-6,11-dimethhoxytriphenylene (1.00 g, 1.52 mmol), iodine (0.42 g, 1.67 mmol), periodic acid (0.16g, 0.91 mmol), CCl_4 (9 mL), acetic acid (24 mL), and H_2SO_4 (30%, 10 mL) were added. The resulting mixture was stirred under reflux at 80 °C overnight. The reaction was cooled to room temperature. It was neutralized with sodium bicarbonate solution and then extracted three times with DCM. The organic layers were combined, washed with sat. $NaHSO_3$ soln., and with DI water. The organic layer was then dried over MgSO4, filtered, and concentrated to give dark brownish crude solid. It was recrystallized from methanol to give compound **11** as a grey solid (0.89 g, 0.98 mmol, 65%). H^1NMR (400MHz, $CDCl_3$): δ 8.45 (s, 2H, Ar-H), 7.78 (s, 2H, Ar-H), 7.47 (s, 2H, Ar-H), 4.26 (t, J = 8 Hz, 4H, -O-CH_2-), 4.06 (s, 6H, -O-CH_3-), 1.95 (p, J = 6 Hz, 4H, -CH_2-), 1.41 (m, 4H, -CH_2-), 1.25 (m, 32H, -CH_2-), 0.86 (t, J = 6 Hz, 6H, -CH_3) ppm. C^{13}NMR (400 MHz, $CDCl_3$): δ 156.4, 150.1, 134.2, 130.1, 124.2, 123.8, 107.1, 103.0, 86.5, 69.8, 56.6, 32.2, 30.0, 29.9, 26.4, 22.9, 14.4 ppm.

Compound 16

In a schlenk flask, compound **14** (1.00 g, 1.90 mmol) was added, and the flask was subjected to the three cycles of pumping and purging with N_2. To the flask, acetic acid (25 mL), 30% H_2SO_4 (10 mL), and CCl_4 (10 mL) were added. This addition was followed by the addition of iodine (0.43 g, 1.71 mmol) and iodic acid (0.20 g, 1.14 mmol). The reaction mixture was stirred at 80 °C for approximately 20 h. The reaction progress was monitored by TLC in ethyl acetate: hexane (20:80), once the starting material has been consumed, it was stopped. The reaction mixture was poured into DI water and was neutralized with saturated sodium bicarbonate soln. It was then extracted with DCM. The organic layers were collected, combined, and dried over $MgSO_4$. The organic solvent was stripped to give the crude product as brownish solid. It was

purified by column chromatography on a silica gel with ethyl acetate: hexane (20:80) as the eluent, affording **16** as a grey solid (0.98 g, 1.26 mmol, 66%).): H^1NMR (400 MHz, $CDCl_3$): δ 9.41 (s, 2H, Ar-H), 8.41 (s, 2H, Ar-H), 8.04 (s, 2H, Ar-H), 4.04 (s, 6H, -O-CH_3), 3.77 (t, J = 6 Hz, 2H, -N-CH_2-), 1.73 (m, 2H, -CH_2-), 1.22 (m, 18H, -CH_2-), 0.84 (t, J = 6 Hz, 3H, -CH_3) ppm.

Compound 44

3,3'-Di(dodecyloxy)-2,2'-bithiophene (0.4 g, 0.74 mmol) was added to a schlenk flask. The flask was subjected to three pump/ purging cycles with N_2. To this flask, freshly distilled anhydrous THF (25 mL) was added, and the flask was cooled down to -78 °C. n-BuLi (2.5 M in hexane), (0.66 mL, 1.65 mmol) was added dropwise to the solution. The resulting solution was stirred at -78 °C for 1 h and at room temperature for another hour. It was again cooled to -78 °C, and tri(n-butyl)tin chloride (0.61 g, 1.87 mmol) was added dropwise. After the addition was complete, the reaction mixture was brought to room temperature, and stirred for another h (monitored by TLC). The reaction was then diluted with ethyl acetate (50 mL) (checked by TLC), washed with DI water (2 x 20 mL), and brine (2 x 20 mL). The organic layer was dried over $MgSO_4$. After removal of solvent from the organic layer, the residue was purified using alumina column using hexane: triethyl amine (95: 5) as the eluent to afford compound **44** as pale yellow oil. (0.71 g, 0.64 mmol, 86%). H^1NMR (400 MHz, $CDCl_3$): δ 6.81 (s, 2H, Ar-H), 4.08 (t, J = 6 Hz, 4H, -O-CH_2-), 1.83 (p, J = 8 Hz, 4 H, -CH_2-), 1.55 (m, 16H, -CH_2-), 1.33 (m, 12H, -CH_2-), 1.24 (m, 32H, -CH_2-), 1.07 (m, J = 8 Hz, 12H, -CH_2-), 0.87 (t, J = 6 Hz, 24H, -CH_3) ppm.

Polymer 58

In an two-neck schlenk flask under argon protection was added compound **11** (85.7 mg, 0.09 mmol), compound **44** (105 mg, 0.09 mmol), tris(dibenzylideneacetone)dipalladium(0) (4.3 mg, 0.005 mmol), and tri(o-tolyl)phosphine (11.5 mg, 0.04 mmol). The flask was subjected to three cycles of pump and purge with argon. To this flask, oxygen-free THF (5 mL) was added, and the reaction mixture was refluxed at 80 °C for 60 h. It was then cooled to room temperature, and the reaction mixture was poured into a solvent mixture containing methanol (45 mL) and 12 N HCl (5 mL). It was stirred for an additional 3 h. The precipitate was collected by centrifugation and was poured into solvent mixture containing methanol (45 mL) and chloroform (5 mL). It was again stirred for 3 h, and precipitate was collected by centrifugation and dried under reduced pressure to give the polymer as reddish brown solid (109 mg, 0.09 mmol, 94.6%). H^1NMR (400 MHz, $CDCl_3$): δ 8.81 (br, 2H, Ar-H), 7.90 (br, 2H, Ar-H), 6.75 (br, 2H, thiophene H's), 4.0- 4.4 (br, 14H, -OCH_2-, -OCH_2- [on thiophene], -OCH_3), 1.97 (br, 8H, -CH_2-), 1.26 (br, 72H, -CH_2-), 1.10- 0.99 (br, 6H, -CH_3), 0.93- 0.82 (br, 6H, -CH_3) ppm. Molecular weights from GPC measurements: Mn 3.63 kDa, Mw 4.66 kDa, PDI 1.28.

Polymer 59

Polymer **59** was synthesized following the same procedure as that of polymer **58**. The reaction time was approximately 40 h. Yield: (0.14 g, 0.13 mmol, 86%). H^1NMR (400 MHz, $CDCl_3$): δ 8.99 (br, 2H, Ar-H), 8.83 (br, 2H, Ar-H), 8.05 (br, 2H, Ar-H), 6.84 (1H, thiophene H), 6.75 (1H, thiophene H), 4.20 (br, 4H, -O-CH_2-), 4.20 (br, 6H, -OCH_3), 3.82-3.73 (br, 2H, -N-CH_2-), 1.75-2.02 (br, 6H, -CH_2-), 1.0-1.40 (br, 54H, -CH_2-), 0.70-0.85 (br, 9H, -CH_3) ppm.

CHAPTER 3

SYNTHESES AND OPTICAL STUDIES OF IMIDE FUNCTIONALIZED NAPHTHALENE DITHIOPHENE BASED CONJUGATED FOLDAMERS

After the discovery of conducting polymers, such as polyacetylene in 1977,[138-140] there has been continuous interest in this area. Conducting polymers are used as organic light-emitting diodes (OLEDs),[10] organic field-effect transistors (OFETs),[11] organic photovoltaic devices (OPVDs),[12] sensors,[141] radio-frequency identification (RFID) tags,[140] and electrochromic devices[142]. An organic photovoltaic device is usually comprised of one or more photoactive layers present between two electrodes. This photoactive layer is important since the processes, such as absorption of light from the sun and generation of charge, mainly take place in this layer. It is usually compromised of layers of donor and acceptor layers stacked one over another in a heterojunction structure or a blended mixture of donor and acceptor layers in a bulk heterojunction structure. Further, more the charge carrier injection buffer layers are used to enhance the performance of the device.[143] One of the electrodes needs to be transparent in order to allow transmission of light to the active layer, and the most commonly used transparent electrode is indium tin oxide (ITO). Based on the molecular composition of the photoactive layer, there are two main categories, small molecule solar cells and polymer solar cells.[144]

3.1 Physics of organic solar cells

The device performance of an OSC is generally characterized by the current-voltage (I-V) measurements both in dark and under illumination. The typical current-voltage curve of common OSC in dark and under illumination is shown in the Figure **49**. The upper curve is normal diode corresponding to a photovoltaic in the dark, and the lower curve is the photovoltaic response when light is shined. In the dark, there is almost no current flowing until the contact starts to inject heavily at forward bias larger than the built-in potential. While under illumination, the current flows in the opposite direction to the injected currents. This current that is raised at reverse bias under illumination is called photocurrent. The most important parameters on this cell are V_{OC} (voltage at open circuit); J_{SC} (current density at short circuit); the fill factor (*FF*) that is a measure of the quality of the cell [if it is closer to 1 that is better], and the P_{max} that is the maximum power, which can be obtained from this cell.

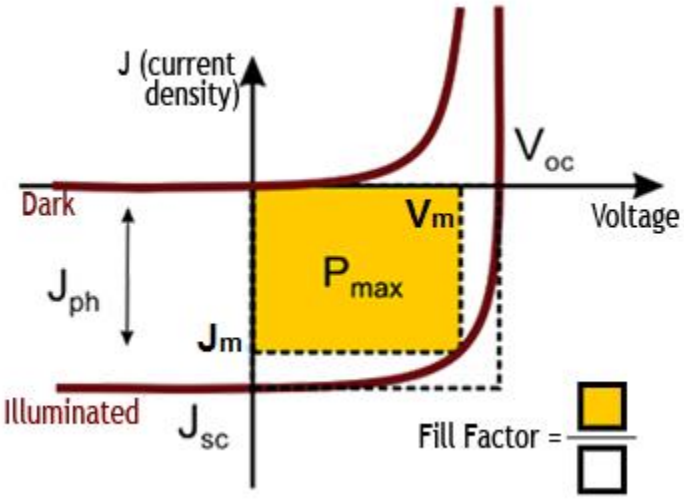

Figure 49: Current-voltage (I-V) curves of a common organic solar cell.

The photocurrent is also known as the short circuit photocurrent, J_{SC}, since there is current flowing without any external voltage applied, like a short circuit in the system. In a

reverse bias current, electrons flow toward the cathode, and holes migrate to the anode. When the voltage is applied in a forward bias, the system compensates for the reverse photocurrent until the current goes to zero. This is called as open-circuit voltage, V_{OC}, since there is no current even after applying voltage, as if electric circuit is open. The lower quadrant of the I-V curve shows a forward bias with positive voltage and negative current, as the photocurrents are reverse. The product of the current and voltage gives the power; and the maximum power that can be obtained from the cell will be the product of J_m (current density) and V_m (voltage). On the I-V curve, this maximum power point can be obtained by looking at the dashed backward L-line. The fill factor, *FF*, which gives the comparison for the performance of the cell against the theoretical maximum, is calculated by

$$FF = \frac{JmVm}{JscVoc} \quad \ldots\ldots\ldots\ldots\ldots\ldots (1)$$

And the power conversion efficiency (η_p) of the cell is calculated using the equation

$$np = \frac{JmVm}{Po} = \frac{JscVocFF}{Po} \quad \ldots\ldots\ldots\ldots\ldots\ldots (2)$$

Where P_0 is the incident light intensity, which is usually standardized to AM 1.5G spectrum.

Thus, the three key parameters that determine the efficiency of the solar cell are J_{SC}, V_{OC} and *FF*. V_{OC} is directly dependent upon the offset or energy difference between the highest occupied molecular orbital energy level of the donor (E^{D}_{HOMO}) and the lowest unoccupied molecular orbital energy level of the acceptor (E^{A}_{LUMO}), where the contacts are assumed to be ohmic. Whereas, in case of non-ohmic contacts, V_{OC} depends upon the work functions of the electrodes. Thus, the simple equation used to represent the open circuit voltage is as follows:

$$Voc = \frac{1}{e} \text{ x } (E^{D}_{HOMO} - E^{A}_{LUMO}) - 0.3 \quad \ldots\ldots\ldots\ldots\ldots\ldots (3)$$

Where e is the elementary charge and 0.3 is an empirical factor.[145] Hence, to increase the V_{OC}, the effective band gap (E_g), difference between E^{D}_{HOMO} and E^{A}_{LUMO} must be increased.

3.2 Operations involved in the OPVDs

The simple structural geometry of an organic photovoltaic device (PVD) is schematically shown in the Figure **50**. The active layer consists of the semiconducting organic compound either small molecule or polymer, which is used as a donor material combined with an electron accepting material (acceptor, usually buckminsterfullerene C_{60} or C_{70} derivatives, e.g., $PC_{61}BM$ or $PC_{71}BM$). The active layer containing donor material absorbs the light and that generates an electron-hole pair or exciton. The energy differences between the LUMOs of the donor and acceptor materials provide the driving force for the dissociation of excitons at the donor-acceptor interface. The exciton being neutral diffuses in the active layer and at the donor-acceptor interface; exciton dissociates to form electron and hole, the process being energetically favorable. Then finally, the separated holes are transported to the anode by the donor matrix, and electrons are transported to the cathode by the acceptor matrix, and electricity is thus produced.

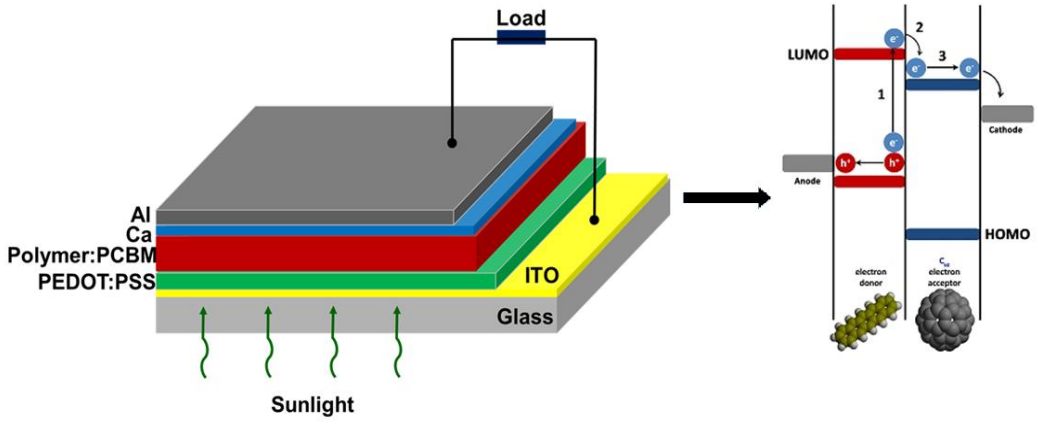

Figure 50: Structure of a bulk heterojunction solar cells (left) and working principle (right).

The elaborate process of mechanisms of organic photovoltaic devices can be explained for the generation of photocurrent in D/A OPV cells as depicted in Figure **51**.[146] The electric current that is generated by a device depends on the number of charge carriers generated which are collected at the electrodes, and this number depends upon the fraction of photons absorbed (η_A), the fraction of electron-hole pairs which can reach the D/A interface (η_{ED}), the fraction of these electron-hole pairs that dissociate at the D/A interface by charge transfer (η_{CT}), and the faction of separated charge carriers that reach the electrodes (η_{CC}).[146] Hence, the overall quantum efficiency (η_{EQE}) is:

$$\eta EQE = \eta A.\eta ED.\eta CT.\eta CC \quad \ldots\ldots\ldots\ldots\ldots (4)$$

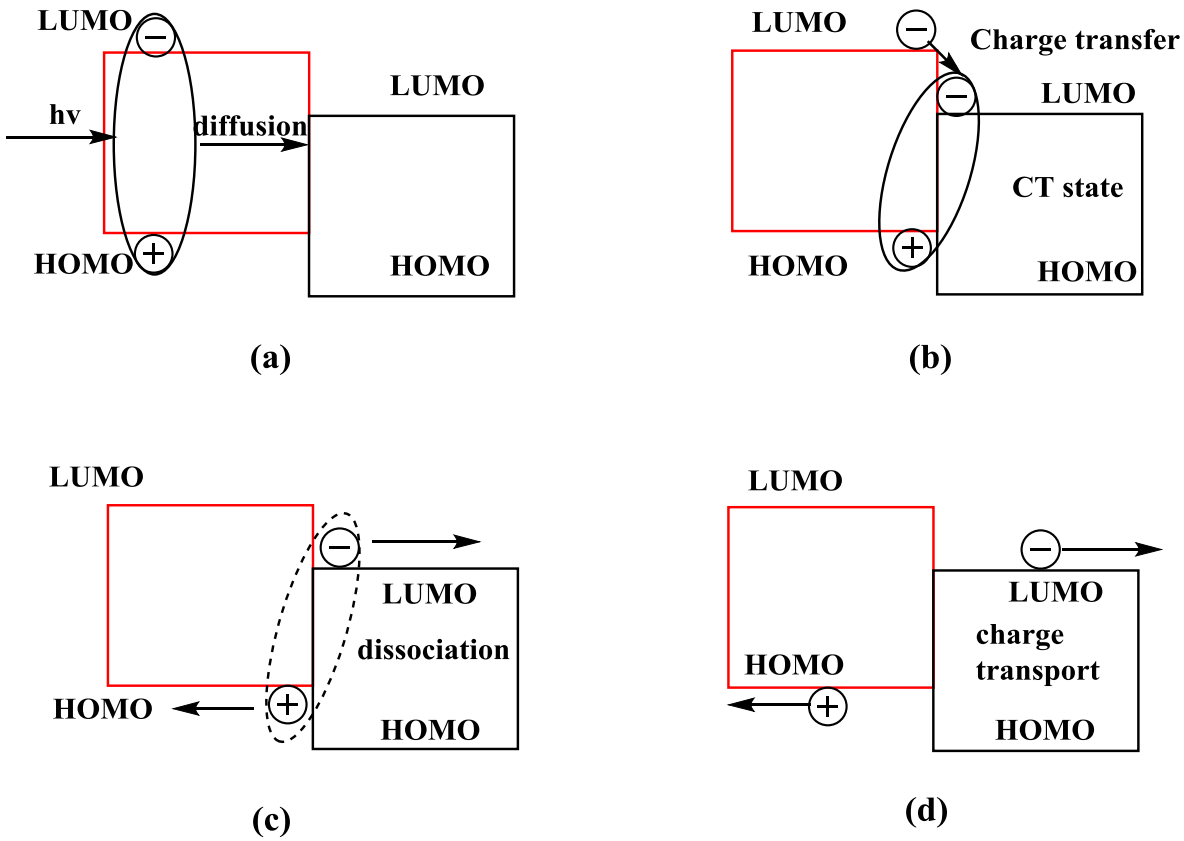

Figure 51: Mechanistic pathway for the electricity generation in an OPV cell. (a) exciton generation by light absorption, (b) electron-hole pair of a CT state is formed, (c) exciton dissociation, and (d) charge transport to electrodes.

3.3 Significance of band-gap control and factors affecting the band gap

In order to develop efficient organic electronic devices, it is important to understand the structure-property relationship. The literature survey reveals that most of the highly conducting organic materials are π-conjugated molecules and polymers. By modulating the π-conjugated skeleton, the device performance could be further enhanced since properties such as conjugation length, exciton dynamics, band gap, absorption of light, crystallinity, and/or intermolecular interactions, can all be varied.

Band gap control is crucial for solar cell performance. The difference between the lowest band energy in the conduction band and the highest band energy in the valence band is known as the band gap (E_g) of the system. Conjugated polymers are semiconductors with a finite band gap.

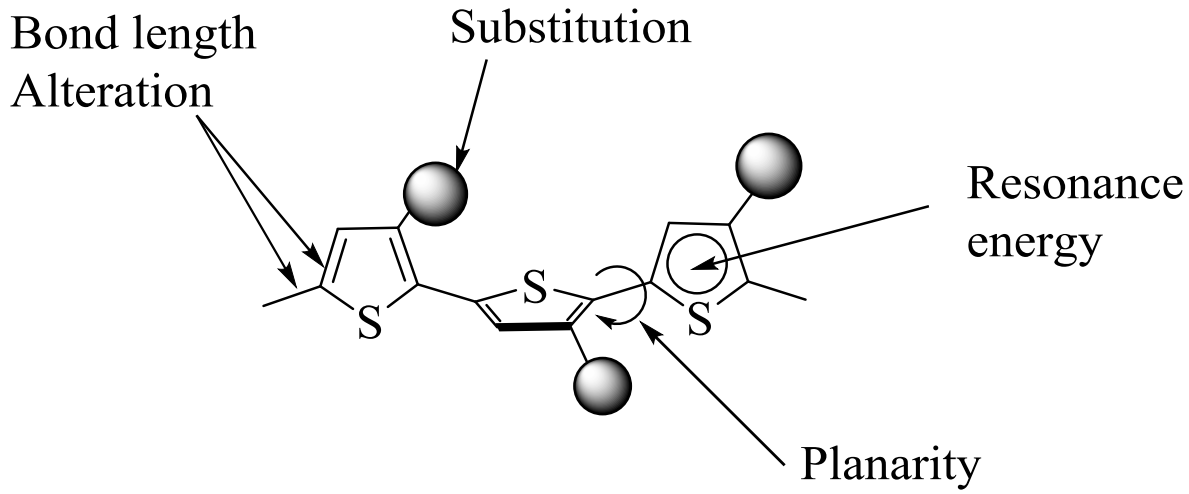

Figure 52: Factors affecting band gap of a conjugated polymer

The band gap (**E_g**) of a conjugated polymer depends on the following factors[147] (Figure **52**) as given in the equation (5);

$$\mathbf{E_g = E^{\delta r} + E^{\theta} + E^{Res} + E^{Sub} + E^{int}} \quad \ldots\ldots (5)$$

Where $\mathbf{E^{\delta r}}$ is the energy related to the degree of bond length alterations, $\mathbf{E^{\theta}}$ is the energy depending on the mean deviation from the planarity of the successive units in the polymer

backbone, $\mathbf{E^{Res}}$ is the aromatic resonance energy, $\mathbf{E^{Sub}}$ is the electronic (mesomeric/ inductive) effect of substituents, and $\mathbf{E^{int}}$ is the intermolecular coupling in the solid state.

In aromatic systems, there is large change in the bond lengths during transition from the benzoid form to the quinoid form. Due to the loss of aromaticity, large energy cost is required to go from the benzoid to the quinoid form, resulting in a large band gap [3.2 eV for polyparapheneylene (PPP)] (Figure **53**).

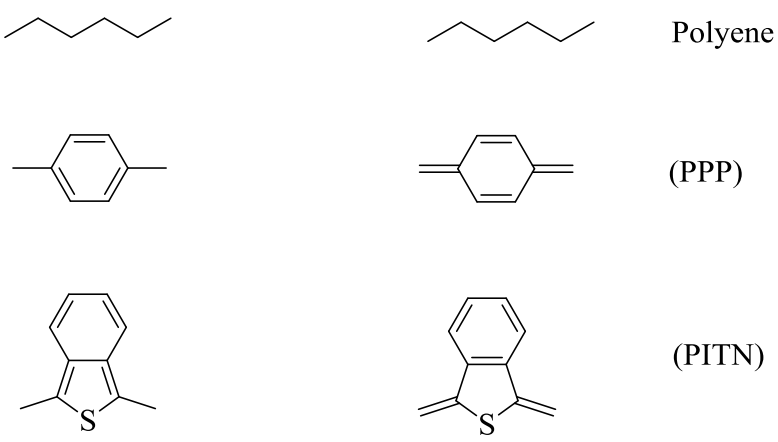

Figure 53: The two band length alternate forms of polyacetylene, polyparaphenylene and polyisothianapthene.

In order to maintain the aromaticity, Wudl[148,149] fabricated a polymer, polysisothianapthene (PITN, see Figure **53**), where bond-length alteration (BLA) was reduced as both forms have aromatic stabilization, and reducing the polymer bandgap to approximately 1 eV. The enhancement of the quinoid contribution to the conjugated chain with respect to the aromatic character is apparently an effective approach to lower the band gap E_g.[150, 151] This strategy has led to the design of many low band gap polymers (< 1.5 eV). Since quinoid and aromatic polymers have their positions of single and double bonds reversed, copolymerization of quinoid and aromatic units tend to reduce BLA. Because BLA is one of the factors to influence the band gaps,[152] reduction of L_{AB} would contribute to the band-gap reductions

observed for copolymers.[153] Ou *et. al.* reported the structures and electronic properties of furo[3,4-b] pyridine (FPD)-based alternating donor and acceptor conjugated oligomers.[154] Based on their study, BLA, bond critical point (BCP) properties, nucleus-independent chemical shift (NICS), and Wiberg bond index (WBI) all showed that degree of conjugation increased with main chain extension.[154]

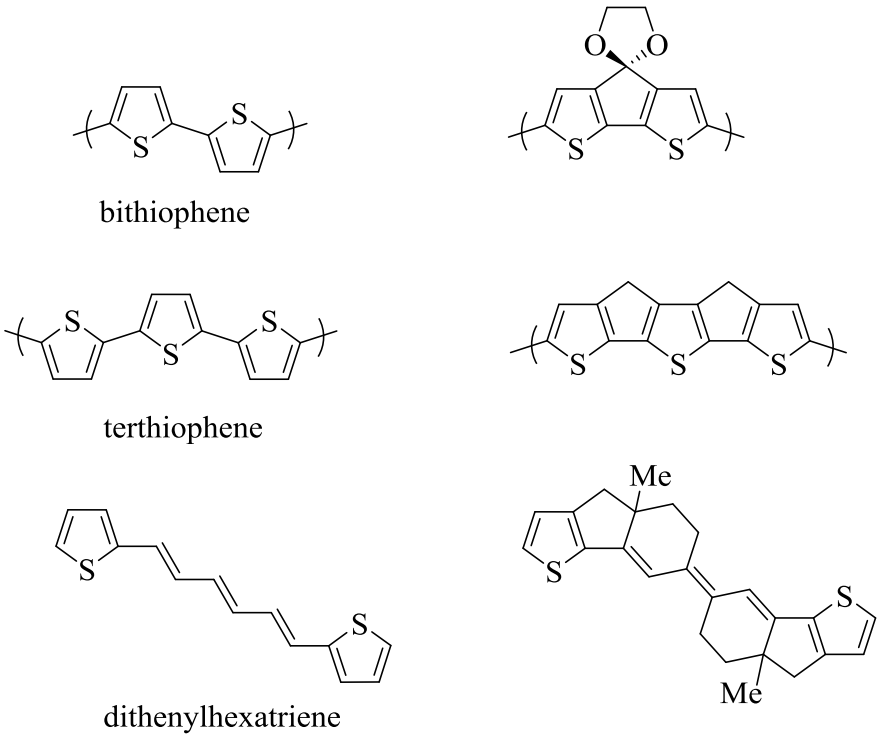

Figure 54: Rigidification of thiophenic systems to fully planar structures.

The co-planarity by means of covalent rigidification represents an efficient strategy for band gap control (Figure **54**). Application of this approach to bithiophene,[155] terthiophene,[156] or dithienylhexatriene[157] leads to fully planar structures with respect to their parent compounds. This results in lowering of ΔE and considerable increase in the photoluminescence efficiency.[158]

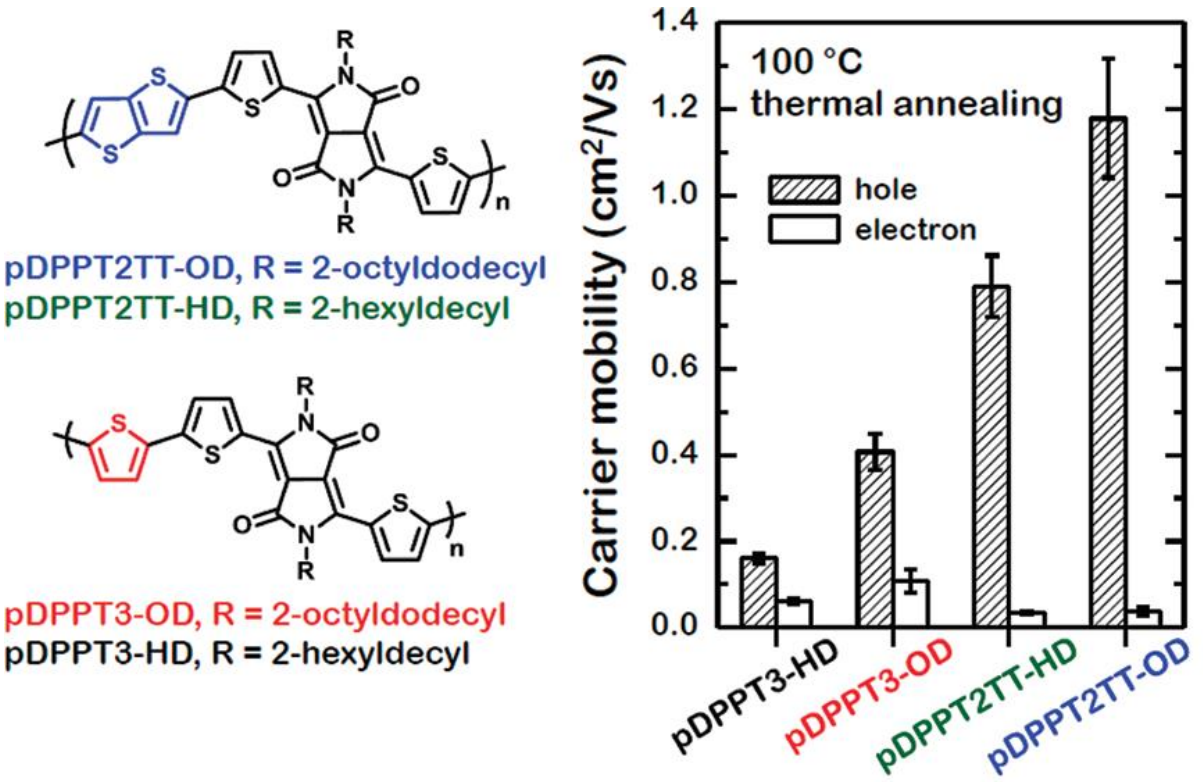

Figure 55: Structures of oligothiophene-alt-DPP polymers and their hole and electron mobilities.

Recently, Joong Suk Lee and co-workers synthesized low-band polymers based on oligothiophene-alt-diketopyrrolopyrrole (DPP) units by varying oligthiophene units, such as terthiophene [T3], thiophene-thienothiophene-thiophene [T2TT], and branched alkyl side chain lengths of 2-hexyldecyl [HD] or 2-octyldecyl [OD] (Figure **55**).[159] They observed that longer branched alkyl side chains, i.e. OD, and longer and more planar oligothiophene, i.e., T2TT, generated more crystalline structures. The highest hole mobility of 2.2 $cm^2V^{-1}s^{-1}$ was achieved for p-DPPT2TT-OD which is more planar.

The energy required to switch from the aromatic form to quinoid form depends on the aromatic stabilization resonance energy of aromatic unit. This resonance effect confine the π electron to the aromatic ring and prevent the delocalization along the entire conjugated chain. This resonance effect E_{Res} thus contributes to the magnitude of ΔE.[147]

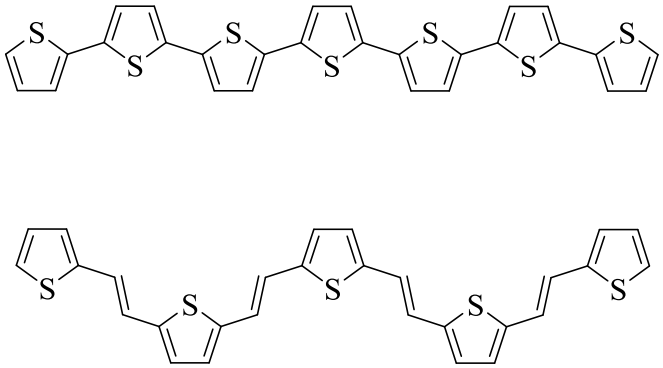

λ_{max} = 440 nm

λ_{max} = 490 nm

Figure 56: Effect of conjugation (double bonds) to thiophene system.

As seen in the Figure **56**, the insertion of ethylenic linkages between the thiophene rings leads to a decrease in the band-gap, due to the red shift by 50 nm of λ_{max} from 440 to 490 nm. This structural modification of poly(thienylene-vinylene) (PTV) has several consequences. The insertion of double bonds not only limits the rotational freedom around the thiophene-thiophene single bonds but also decreases the overall aromaticity of the system, which eventually reduces the ΔE, precisely, from 2.00 eV to 1.70 eV.[160]

Another way of reducing the band gap is to introduce electron withdrawing or electron releasing groups in the conjugated system (Figure **57**). The attachment of acceptor groups like cyano, carboxy, or nitro at the 3rd position of the thiophene ring induces large increase in the oxidation potential.[161] In 1991 Ferraris and Lambert reported poly(cyclopentabithiophene)s with keto (E_g = 1.20 eV) and dicyano (E_g = 0.80 eV) at the bridging carbon, which are electron-withdrawing groups.[162, 163] The advantage of this approach lies in the simple and straight forward synthesis of these cyano compounds by using methods such as Knoevenagel condensation. The cyano groups are electron-withdrawing and render a decrease in the HOMO level, which causes stabilization of the neutral state of the system. However, cyano groups

generally decrease solubility of the compounds, hence correct balance of substituents need to be maintained while synthesizing these target molecules.

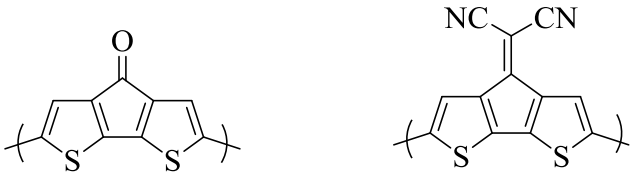

Electron-withdrawing groups

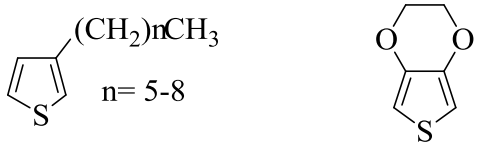

Electron-releasing groups

Figure 57: Electron donating/ withdrawing groups reduces the band-gap.

Even electron donating groups like long alkyl chains or electron rich elements like oxygen would result in the increase of HOMO level in turn reducing the band gap. Thus, alkyl chains having inductive effect decreases oxidation potential of thiophene ring by approximately 0.20 eV.[164] 3,4-Ethylenedioxythiophene (EDOT) can be easily polymerized with lower band gap than polythiophene PT and generates non-covalent, intramolecular, sulfur-oxygen interactions which provides self-rigidification to the conjugated structure and gives a planar form (Figure **58**).[165,166]

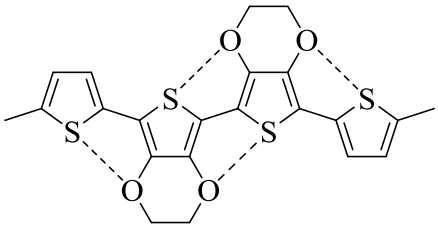

Figure 58: Sulfur-oxygen interactions present in the EDOT structure

For example, Hendriks *et. al.* studied the opto-electronic and photovoltaic properties of the diketopyrrolopyrrole (DPP) based semiconducting polymers where DPP unit is in conjugation with alternating conjugated bis(dithienyl)phenylene (4TP) unit (Figure **59**).[167] Electron donating groups, such as an alkoxy group provided additional electron density to the main chain without changing the overall chemical structure of the main polymer backbone.[168] The authors found that optical band gap of PDPP4TP was 1.54 eV, which has alkyl side chains while PDPP4TOP that has alkoxy side chain substitution had lower band gap of 1.45 eV, which ultimately resulted in higher photocurrents.

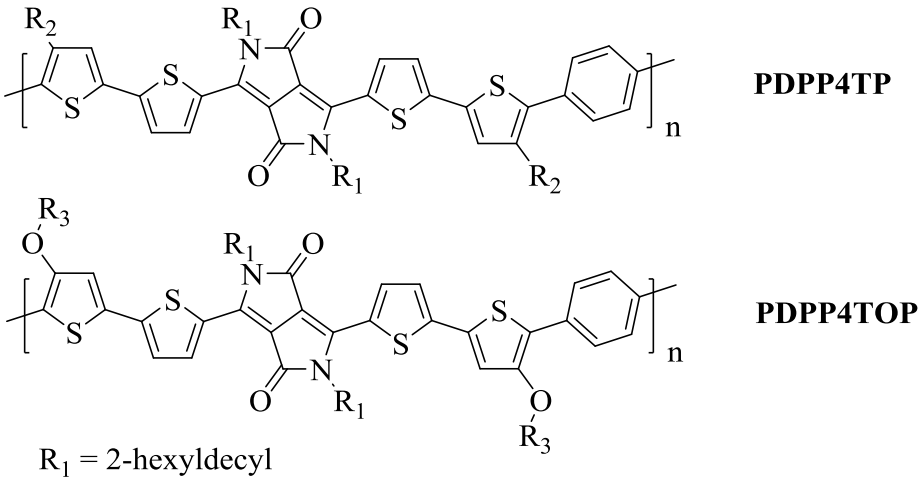

PDPP4TP

PDPP4TOP

R_1 = 2-hexyldecyl
R_2 = dodecyl
R_3 = decyl

Figure 59: Chemical structures of PDPP4TP and PDPP4TOP with differing substituents.

The interchain couplings have a considerable effect on the HOMO-LUMO energy gap of the polymers. As the effect of interchain coupling in the solid-state increases, the band gap E_g becomes narrower. These interactions arise due to packing of individual molecules or polymer chains in a material such as non-covalent interactions like H-bonding, van der Waals interactions or π- π stacking.[147]

One of the widely used and most important factors in this "band-gap engineering" is the use of **Donor-Acceptor (D-A) approach**, which makes use of alternating electron donating and electron accepting units in the polymer backbone. The resultant HOMO energy level of the D-A polymers depend upon HOMO energy level of the electron donating nature of the donor monomer while LUMO energy level of the D-A polymer is largely dependent on the LUMO energy level of the electron accepting nature of the acceptor monomer as shown in the Figure **60**. Hence, as demonstrated by the energy diagram in the adjoining figure, donor b with higher donating strength would increase the HOMO level of the resultant D-A polymer as compared to donor a. However, it will not affect the LUMO energy level of the resultant D-A polymer. Thus, by cleverly choosing the appropriate donor and acceptor monomers and tuning the HOMO-LUMO levels, polymers with a lower band gap can be achieved.

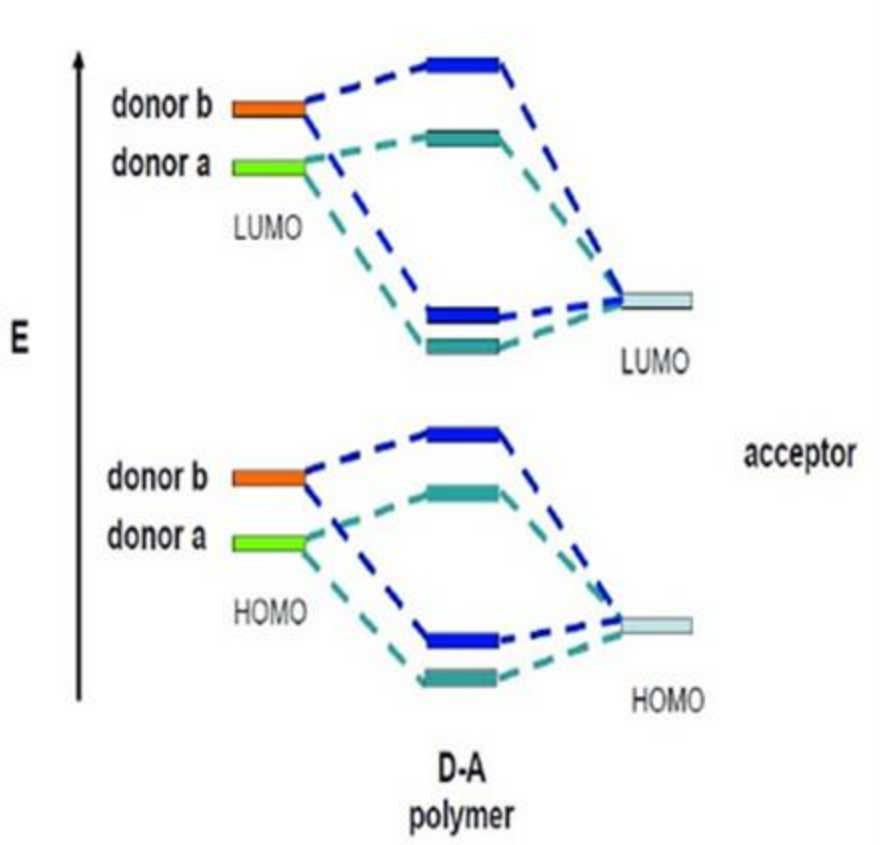

Figure 60: Donor- Acceptor approach for band-gap engineering.

Zhang and Tour[169] have demonstrated the advantage of synthesizing [AB] systems, where the A units have strong electron donating moieties and B units have strong electron withdrawing moieties, since it helps to minimize twisted arrangements in conjugated polymers.[170] They also showed that these alternating donor and acceptor moieties in the repeating units helps to maximize the extended π-conjugation, lower the band gap, induce the intermolecular charge transfer (ICT), and significant zwitterionic character in the polymers which was evident from their optical and solubility data.

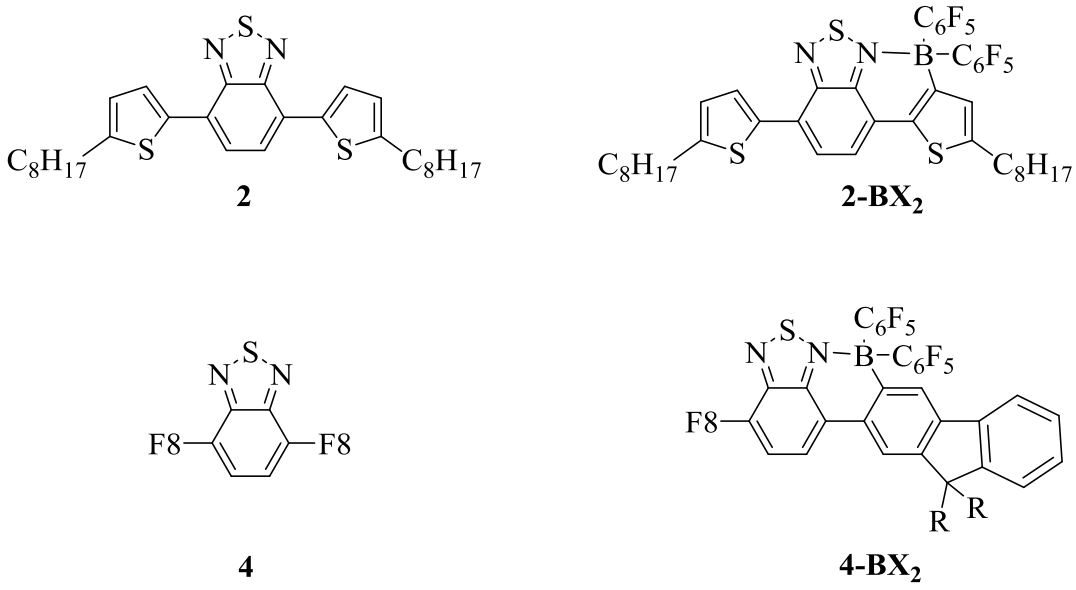

Figure 61: D-A-D structures prepared by borylation for reduction of LUMO energy level.

Recently, Crossley and co-workers synthesized a series of compounds by using electrophilic borylation to afford alternating D-A systems that minimally changed the HOMO energy levels but significantly reduced the LUMO energy levels.[171] Borylative fusion dramatically lowered the LUMO energy of these materials, particularly with exocyclic C_6F_5 substituents on boron. In Figure **61**, the results and structures are given. (**2**, λ_{max}= 471 nm, E_g= 2.29 eV; **2-BX2**, λ_{max}= 641 nm, E_g= 1.60 eV and **4**, λ_{max}= 419 nm, E_g= 2.59 eV; **4-BX2**, λ_{max}= 579 nm, E_g= 1.83 eV).

In conclusion, the power conversion efficiency (PCE) of an organic solar cell depends directly on the open circuit voltage (V_{OC}), the short circuit current (I_{SC}) and the fill factor (*FF*). To have maximum PCE, it is important to have optimized band gap, appropriate HOMO and LUMO energy levels, high charge mobility, percolating morphology, good solubility, and high stability.

3.4 Objective

Amongst the various conjugated polymers, those containing discotic nature have drawn particular attention due to the high charge carrier mobilities and the high organic solar cell perform ances.[165- 172] As discussed in the previous chapter, the introduction of planar or near planar PACs in the backbone resulted in an extended π-conjugated system where the planarity would ensure stronger interactions due to the π-π stacking as well as that induces higher charge carrier mobilities along the stacked columns.[180, 181] In our laboratory, Tanmoy Dutta and coworkers have recently shown that a PAH based imide functionalized naphtha[1,2-b:4,3-b']dithiophene (INDT) building block can be used to prepare low bandgap D-A conjugated polymers using substituted bithiophenes as D unit.[182] By the alteration of the backbone geometry via the selection of the D unit would make it possible to synthesize conjugated polymers with favorable bending angles that allow the formation of helical foldamers. It is also envisioned that with INDT (or other PAH building blocks) in the polymer backbone, the polymer would not only have stronger propensity for folding due to the stronger stacking interactions but also would possess higher high charge transporting properties.

Thus, foldamers based on polycyclic aromatic heterocycles containing conjugated polymers may form stacked columns and these stacked columns may form folding structures that enable efficient charge transporting. A potential function for helical foldamers is the exploitation of the inner void to host a guest. Depending on the design, helical foldamers may possess an inner void of sufficient size to accommodate ions or small molecules. The polymer will be forced to fold due to structural constraints, and further π-π interactions are capable of stabilizing the architecture. We have been studying conjugated foldamers in the past few years. We envision that in a composite containing a conjugated foldamer and doped electron

acceptors (such as PCBM) the dopants may be encapsulated inside the folded polymers (Figure **62**), which would lead to improved morphological stability and thus device stability.

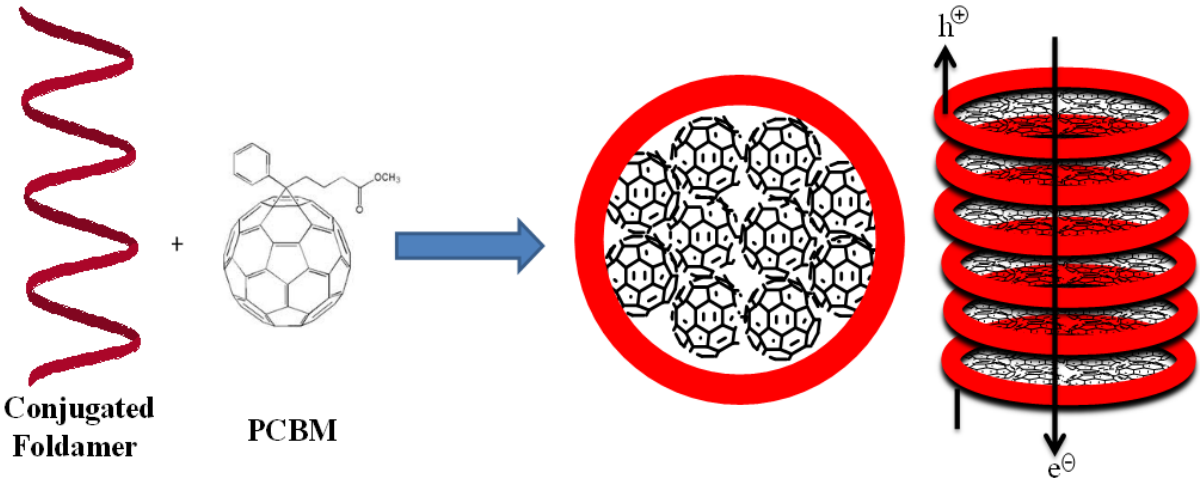

Figure 62: Conceptual assembly of foldamers and PCBM dopant.

3.5 Target molecules of NDT based copolymers

The polymers with nonimide-based NDT copolymers were synthesized for comparison purposes with INDT based copolymers. The main purpose of this chapter was to synthesize low bandgap D/A conjugated polymers for solar cell applications. The polymers with donor-acceptor alternating copolymers were our target compounds (Figure **63**) that could be made using few steps involved in the previous chapter. The polymers with naphthalene dithiophene core would be synthesized from the target acceptor monomers with diester and dicarboxylic side chains and their polymerization were carried out which was not attempted before (Stille cross coupling polymerization with dicarboxylic acid sides), which could lead to some interesting properties.

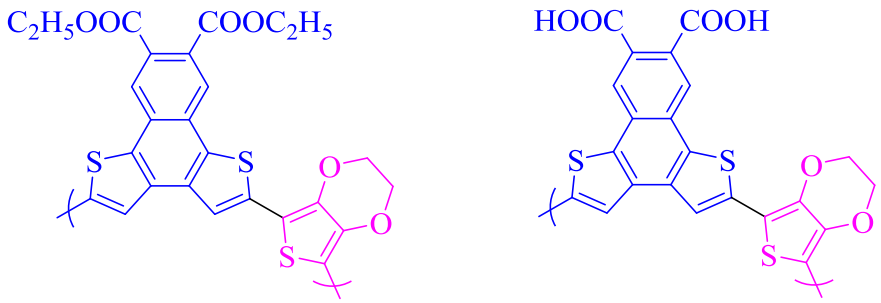

Figure 63: Chemical structures of NDT based D-A copolymers.

3.5.1 Syntheses and characterization of NDT based copolymers

The naphthalenedithiophene (**NDT**) based acceptor monomers were synthesized using previously published and modified reaction scheme as shown in Scheme **7**. 4,5-dibromophthalic acid synthesized earlier was used as the starting material for this scheme. It was initially subjected to acid catalyzed esterification[183] using sulfuric acid as a catalyst to furnish compound **23**.

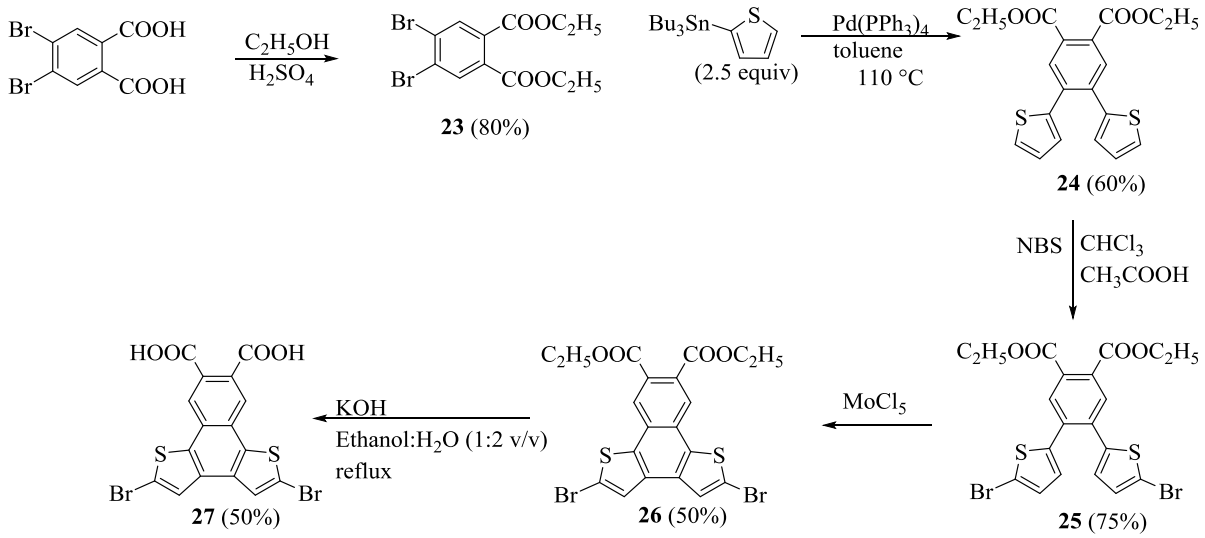

Scheme 7: Synthetic route for preparation NDT based acceptor monomer.

The triplet and quartet typical of a $–CH_3$ and $–OCH_2$ at 1.34 and 4.33 ppm respectively, followed by sharp singlet at 7.93 ppm for the aromatic protons, comprise of and confirm the identity of compound **23** in the ^{1}HNMR spectrum (Figure **64**). When compound **23** was treated with 2-(tributylstannyl) thiophene, it underwent Stille coupling to fuse thiophene rings in the system to give compound **24**. The ^{1}HNMR spectrum for compound **24** in $CDCl_3$ (Figure **65**) showed clear aromatic signals for four aromatic protons from 6.96-7.83 ppm.

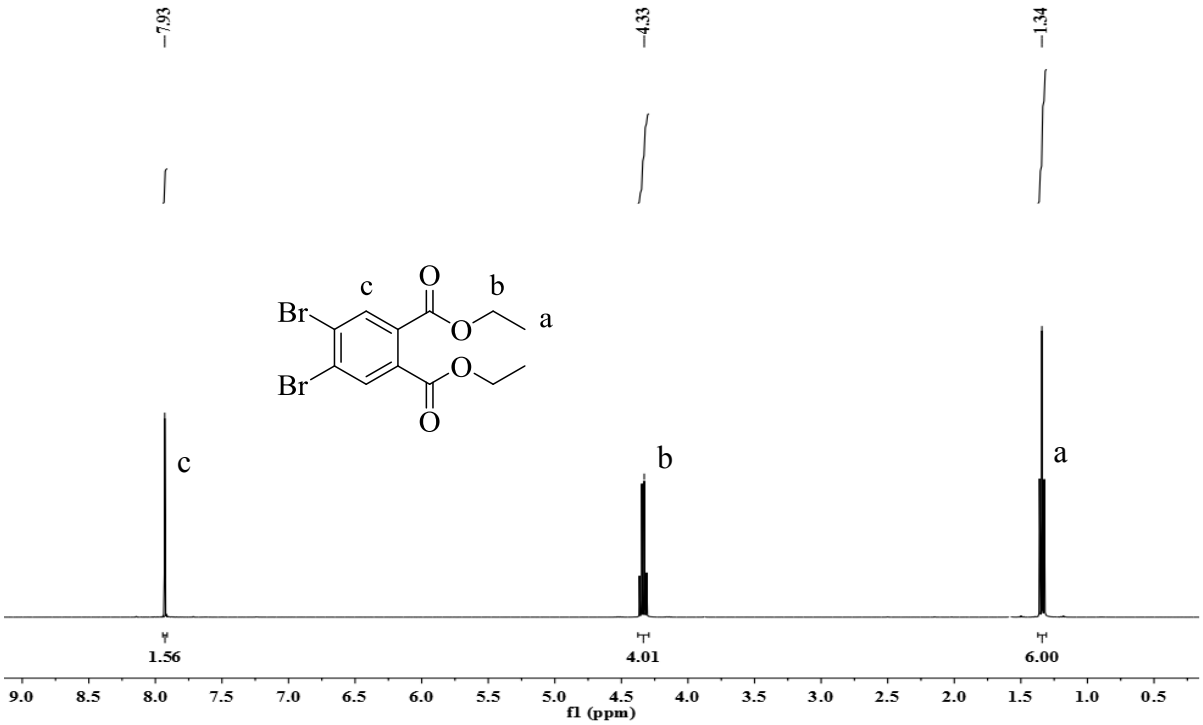

Figure 64: [1]HNMR spectrum of compound **23**.

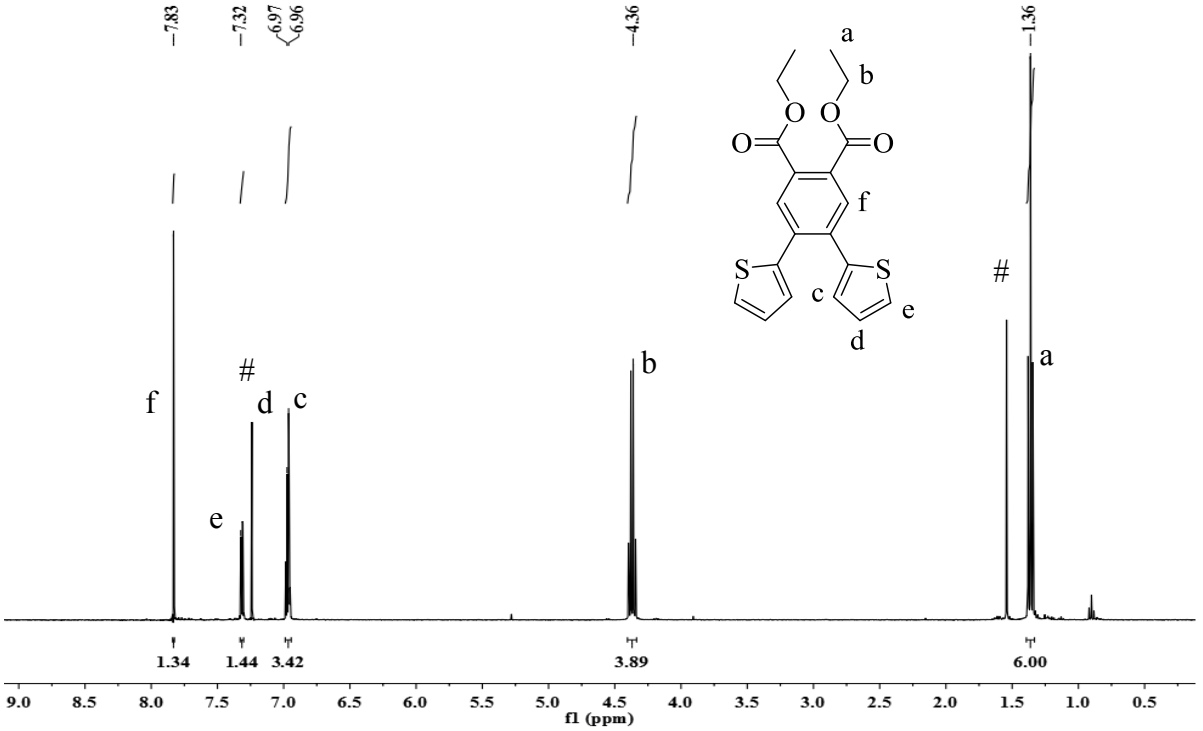

Figure 65: [1]HNMR spectrum of compound **24**.

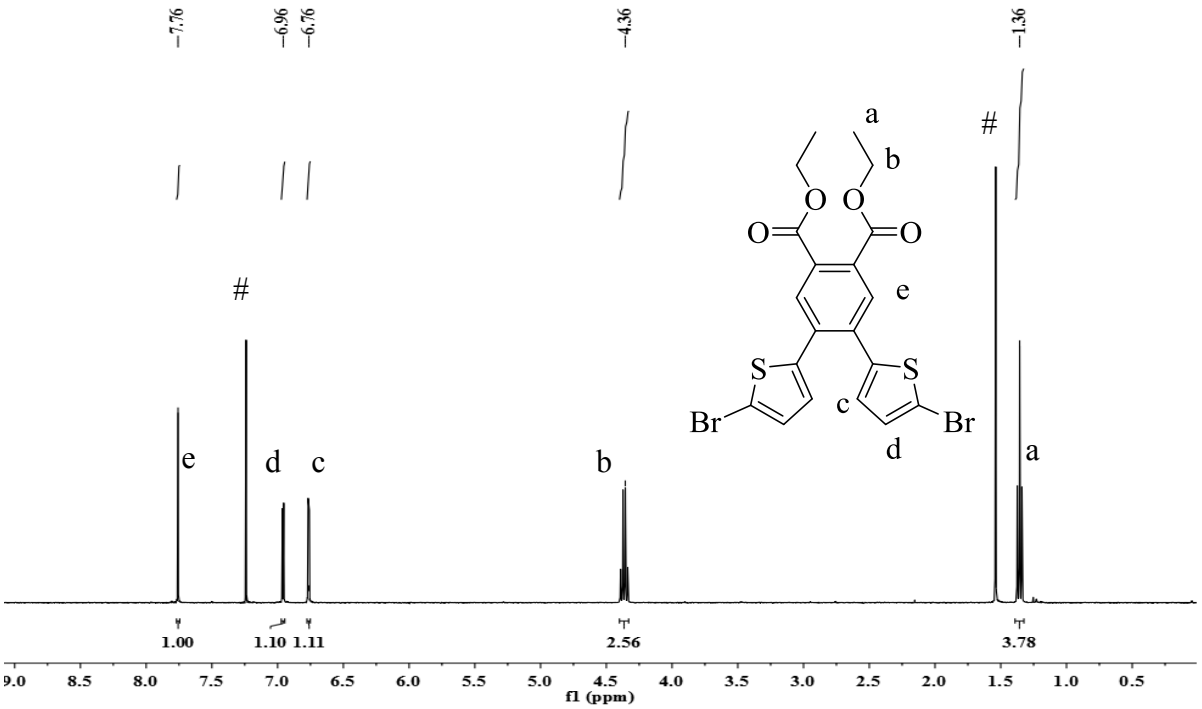

Figure 66: [1]HNMR spectrum of compound **25**.

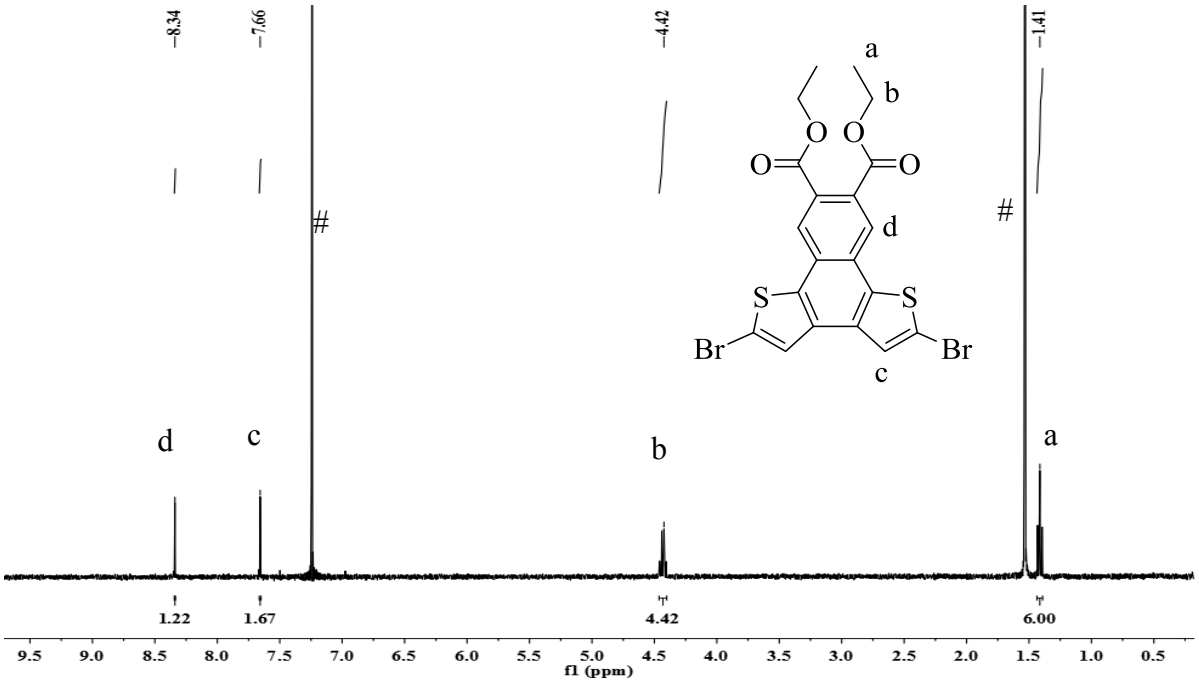

Figure 67: [1]H-NMR spectrum of compound **26**.

Unlike triphenylene derivatives, when Scholl-type reaction was carried out with electron rich thiophenes, they tend to polymerize via intermolecular coupling through *α*-positions under oxidative conditions (Figure **68**). Hence, the α-positions on the thiophene rings in compound **24** was blocked with bromine before the ring fusion reaction.[184] It was achieved by reaction with *N*-bromosuccinamide using more severe reaction conditions of NBS/$CHCl_3$/CH_3COOH due to the electron-deficient nature of the ring to yield compound **25**. Furthermore, ^{1}HNMR spectrum of compound **25** was in agreement showing doublets at 6.76 and 6.96 ppm due to aromatic protons on thiophene ring and another singlet in the aromatic region downfield at 7.76 ppm accounting for total six aromatic protons in the molecule (Figure **66**).

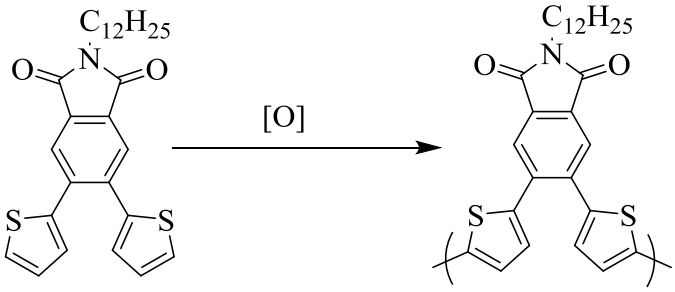

Figure 68: Polymerization of thiophene rings at the *α*-positions.

As mentioned previously, the oxidation reaction was believed to proceed via arenium cation mechanism.[128] The electron withdrawing imide groups present in compound **24** tend to destabilize some of the intermediate resonance structures. Although lone pairs on the sulphur in thiophene adds to stabilization, it was not sufficient. Hence, the use of $FeCl_3$ as an oxidizing agent was unsuccessful in these oxidative cyclization reactions. Watson *et al* have used Mallory type cyclization (Figure **69**) to overcome difficulties in oxidative cyclization with

electron deficient systems.[185] It was a photo-oxidative process but the disadvantage was it can be used in extremely low concentrations.[186, 187]

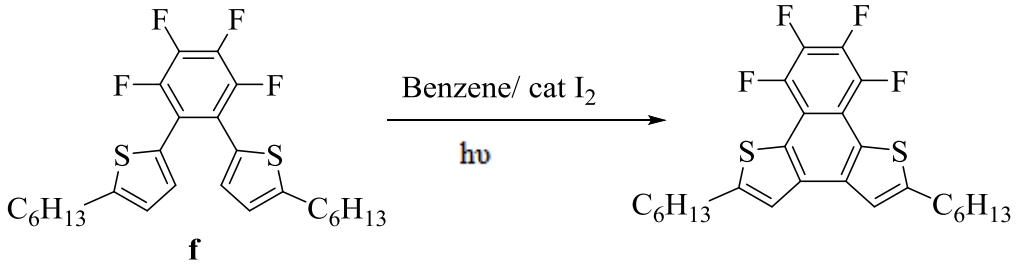

Figure 69: Mallory-type oxidative cyclization by Watson *et al*[185]

Due to these limitations in Mallory type cyclization, we used strong oxidative conditions to ensure the formation of relatively unstable arenium cation (with no significant resonance stabilization) by using molybdenum pentachloride ($MoCl_5$). $MoCl_5$ is known for its strong oxidative ability (stronger than $FeCl_3$) and Lewis acidity.[188] This modified Scholl conditions using $MoCl_5$ yielded successful formation of compound **26** in approximately 50% yields. The ^{1}HNMR spectrum (Figure **67**) gave clear evidence for the formation of **26** wherein, there are two well separated sharp singlets downfield at 7.66 and 8.34 ppm, respectively, due to the aromatic protons, and the ethoxy protons were observed at 1.41 and 4.42 ppm. Compound **26** was then subjected to base hydrolysis to undergo oxidation and formed another NDT based acceptor monomer, compound **27** with dicarboxylic acid side chains. Compound **26** was insoluble in aqueous medium therefore the reaction mixture was insoluble initially. Since compound **27** was soluble in water, the product became soluble at the end of the reaction, which also make it easier to monitor the progress of the reaction. The ^{1}HNMR spectrum (Figure **70**) of compound **27** clearly indicate the presence of only two aromatic protons close to each

other at around 8.24 and 8.32 ppm, and the broad featureless hump at about 13.50 ppm was due to the proton of the carboxylic acid groups.

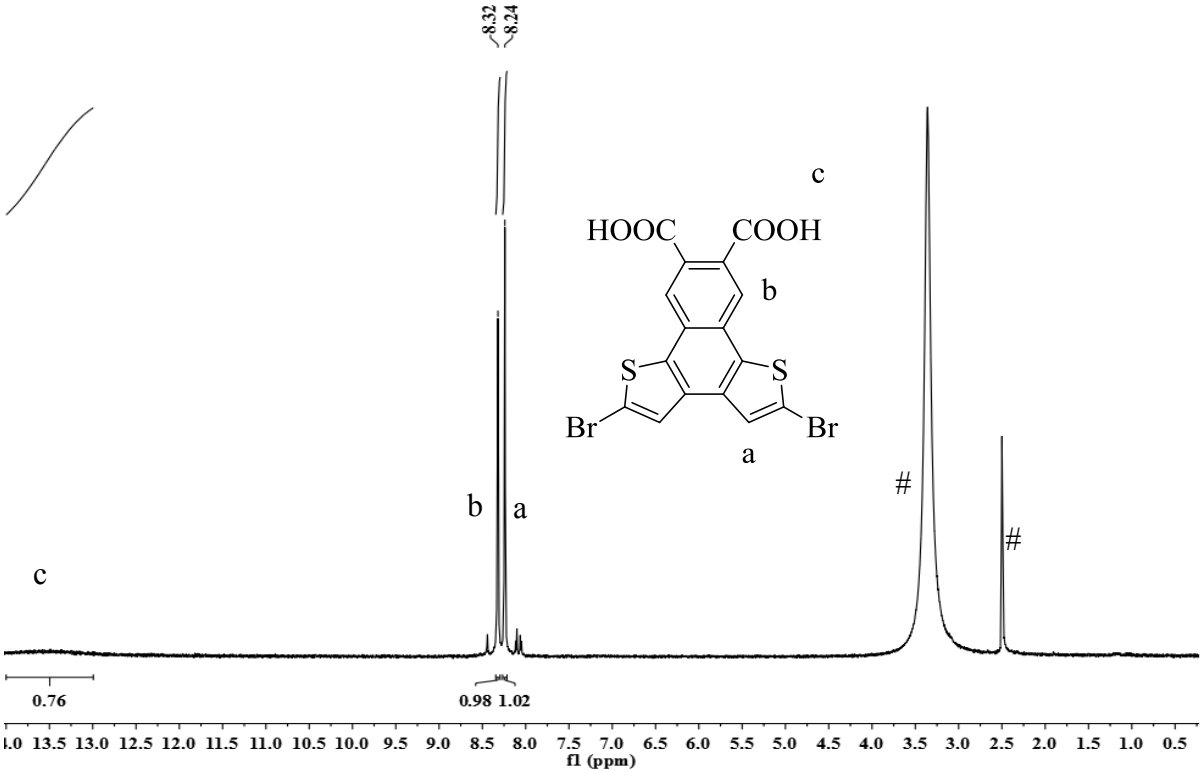

Figure 70: [1]HNMR spectrum of compound **27**.

The synthesis of donor monomers was carried out from commercially available 3,4-ethylenedioxythiophene in good yields following a procedure published previously as depicted in Scheme **8**.[189] The [1]HNMR spectrum, for compound **6** in $CDCl_3$ gave a sharp signal at 4.10 ppm due to ethylene protons, and the signals between 0.87-1.55 ppm were due to protons on butyl chains (Figure **71**).

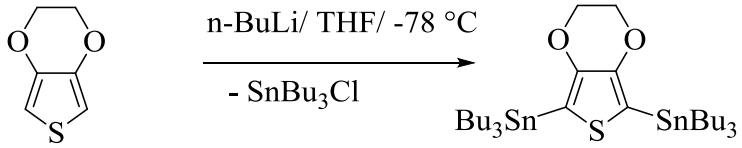

Scheme 8: Synthesis of donor monomer from EDOT.

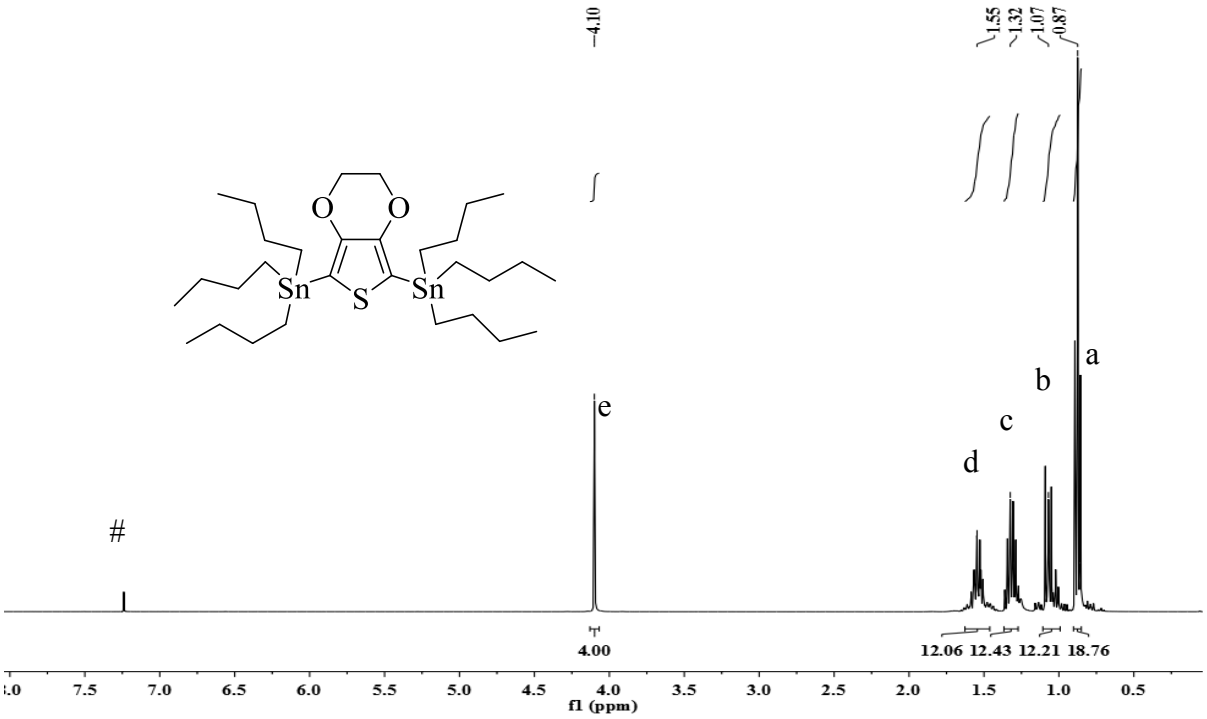

Figure 71: ^{1}HNMR spectrum of compound **30**.

The synthesis of NDT-based D-A alternating copolymers was represented in following Scheme **9**. These polymers were synthesized to compare with INDT-based polymers. The polymerization was carried out using similar Stille cross-coupling polymerization techniques. $Pd_2(dba)_3$/*p*-(*o*-tolyl)$_3$ was used as a catalyst for the coupling reaction, and toluene was used as a solvent for the synthesis of polymer **36**, in which it was refluxed for 48 h. While, for the synthesis of polymer **31**, *N*,*N*-dimethylformamide was used as a solvent because comonomer **27** was insoluble in other organic solvents. Both the polymers were purified by repetitive precipitation with methanol.

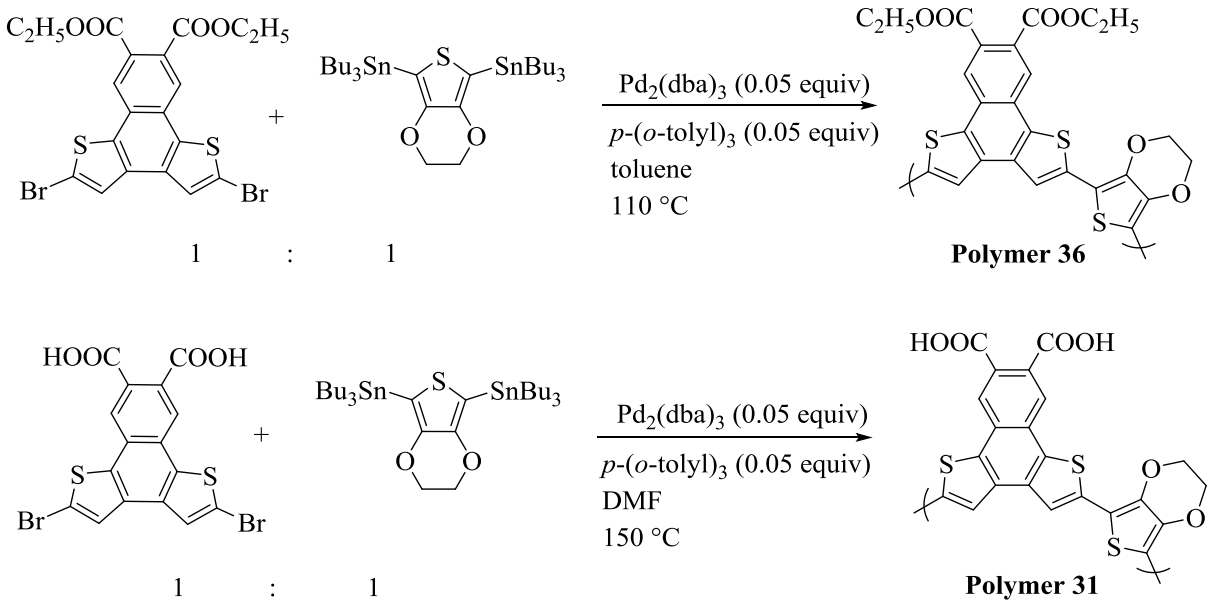

Scheme 9: Polymerization of NDT based D-A alternating copolymers.

The ^{1}H-NMR spectrum (Figure **72**) of polymer **36** gave broad featureless peak from 3.50-4.70 ppm which could be due to the ethylene protons on the donor molecule, and the other broad peak at 1.30 ppm could be assigned to the diester side chains on the acceptor monomer. However, the sharp singlets observed in the monomer were absent in this spectrum for the polymer. This broadening observed in the spectrum was attributed to the interchain aggregation of the successive repeating units.

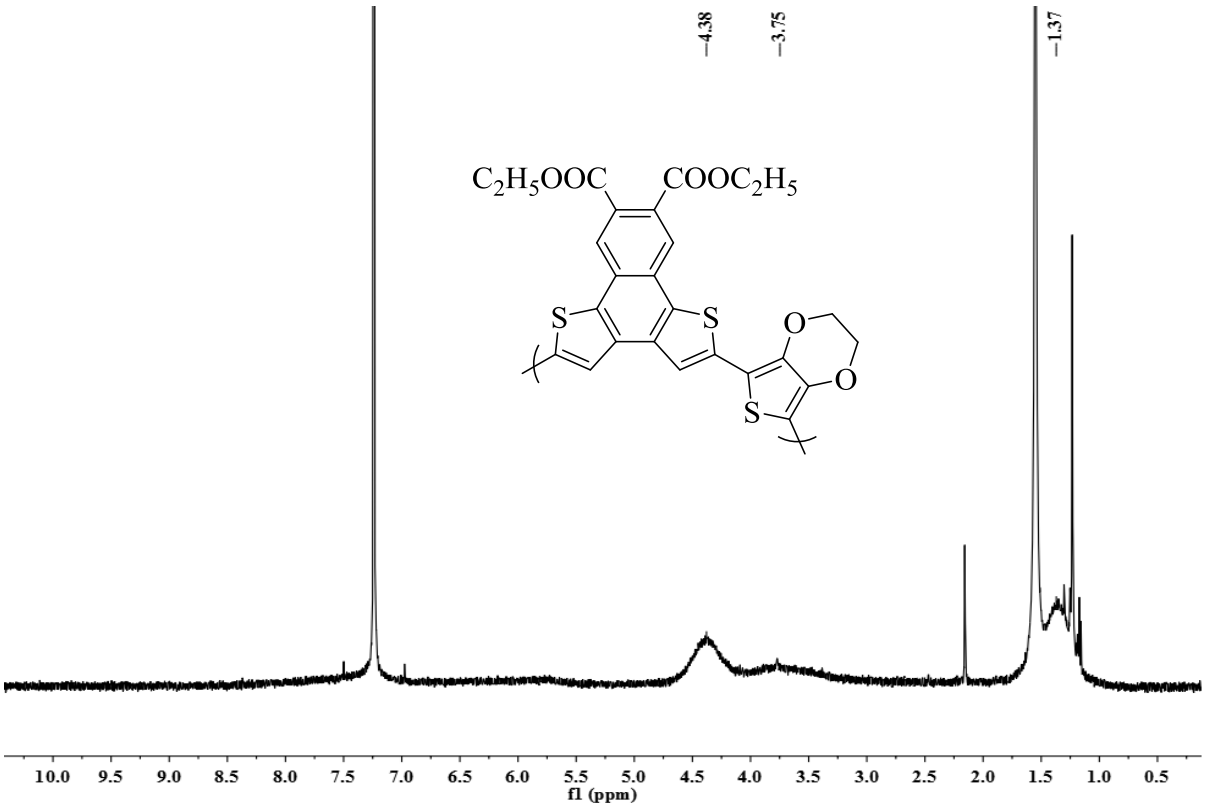

Figure 72: [1]HNMR spectrum of polymer **36**.

Also, the [1]HNMR spectrum (Figure **73**) of polymer **31** is in accordance with the structure of the molecule where it shows broad peaks around ~ 4.00- 4.50 ppm for the ethylene protons and 8.00- 8.50 ppm for the aromatic protons. In addition to those peaks, there are also broad peaks around 13.50 ppm, which was assigned to the carboxylic acid protons expected to be in the far downfield region.

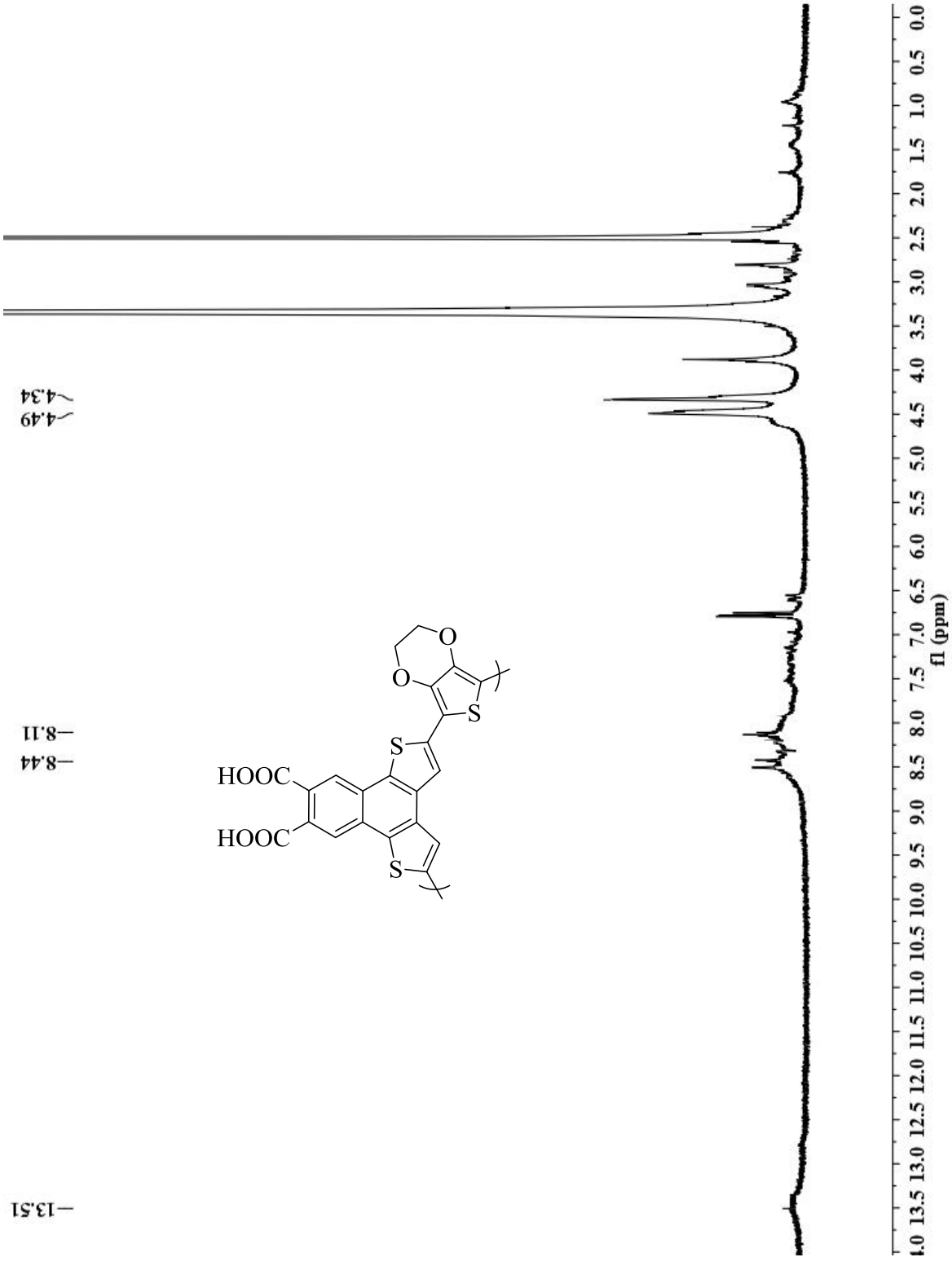

Figure 73: ^{1}H-NMR spectrum of polymer **31**.

The molecular weights of the polymers **31** and **36** were determined by the GPC data using THF as an eluent. Polymer **31** was not completely dissolved in THF, whereas **36** had good solubility. The characterization data of these polymers are summarized in Table **5**. Due to the limited solubility of **31**, the soluble part was analyzed by GPC and the number average molecular weight and PDI were found to be 42.0 kDa and 1.64, respectively. For polymer **36** with ethoxy side chains, M_n was found to be 2.46 kDa with PDI of 1.21.

Table 5: Polymerization data for polymers **31** and **36**.

Polymer	**Yield (%)**	**Mn (kDa)**	**Mw (kDa)**	**PDI**
31	90	42.0	69.0	1.64
36	88	2.46	2.97	1.21

3.5.2 Density functional theory (DFT) calculations for NDT based polymers

The backbone geometries and the electronic structures of the polymers can be predicted by performing DFT calculations of the trimers of polymers **31** and **36**. The theoretical calculation was carried out with the Gaussian-03 program using DFT with a B3LYP functional and the basis set of 6-31G(d). In the Figures **74** and **75**, different orientations of the energy minimized conformers of trimers **36** and **31** were showed to understand the geometry of their backbone and dihedral angle between them.

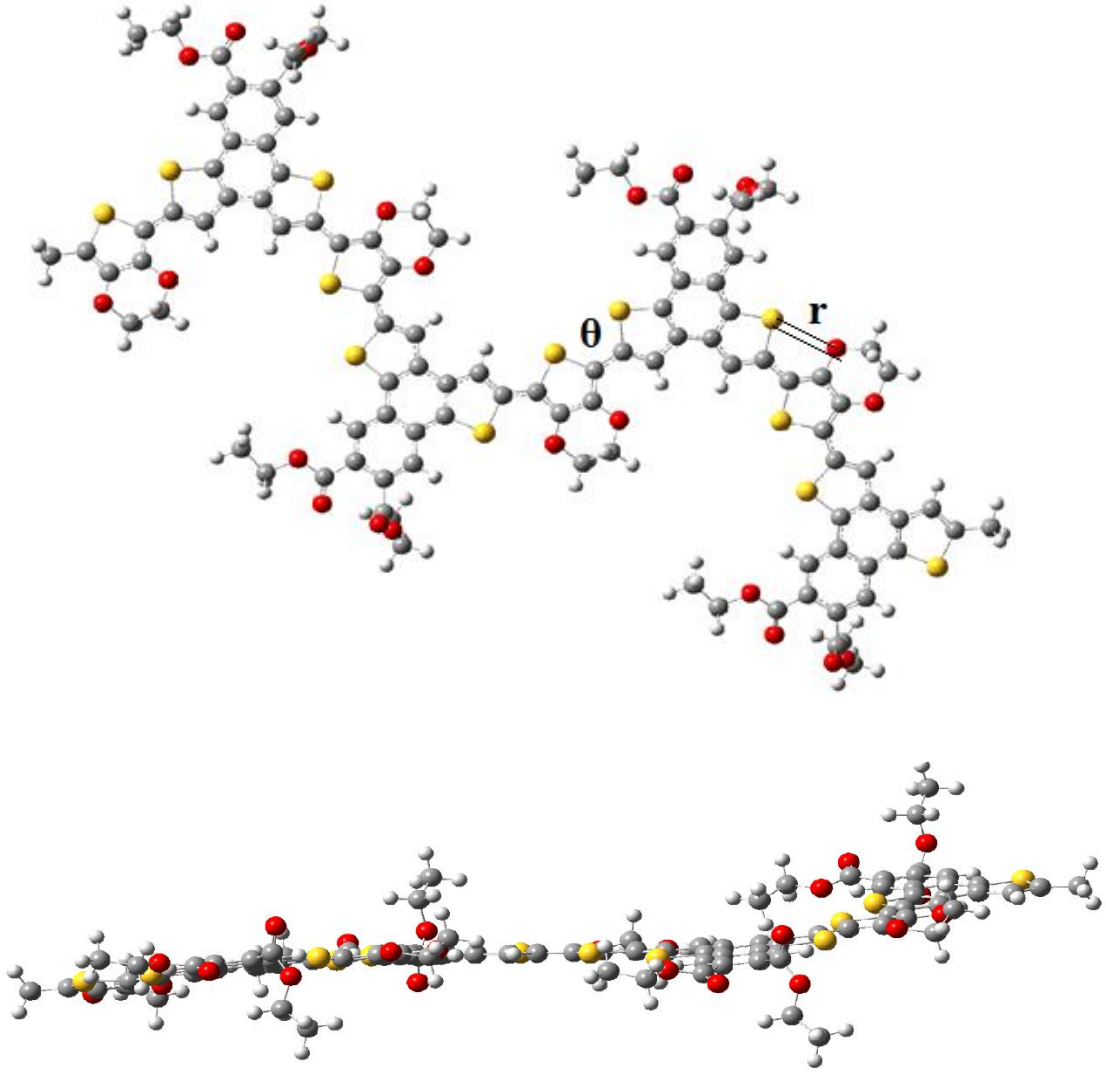

Figure 74: Energy minimized geometries of **36** (trimer) with different views.

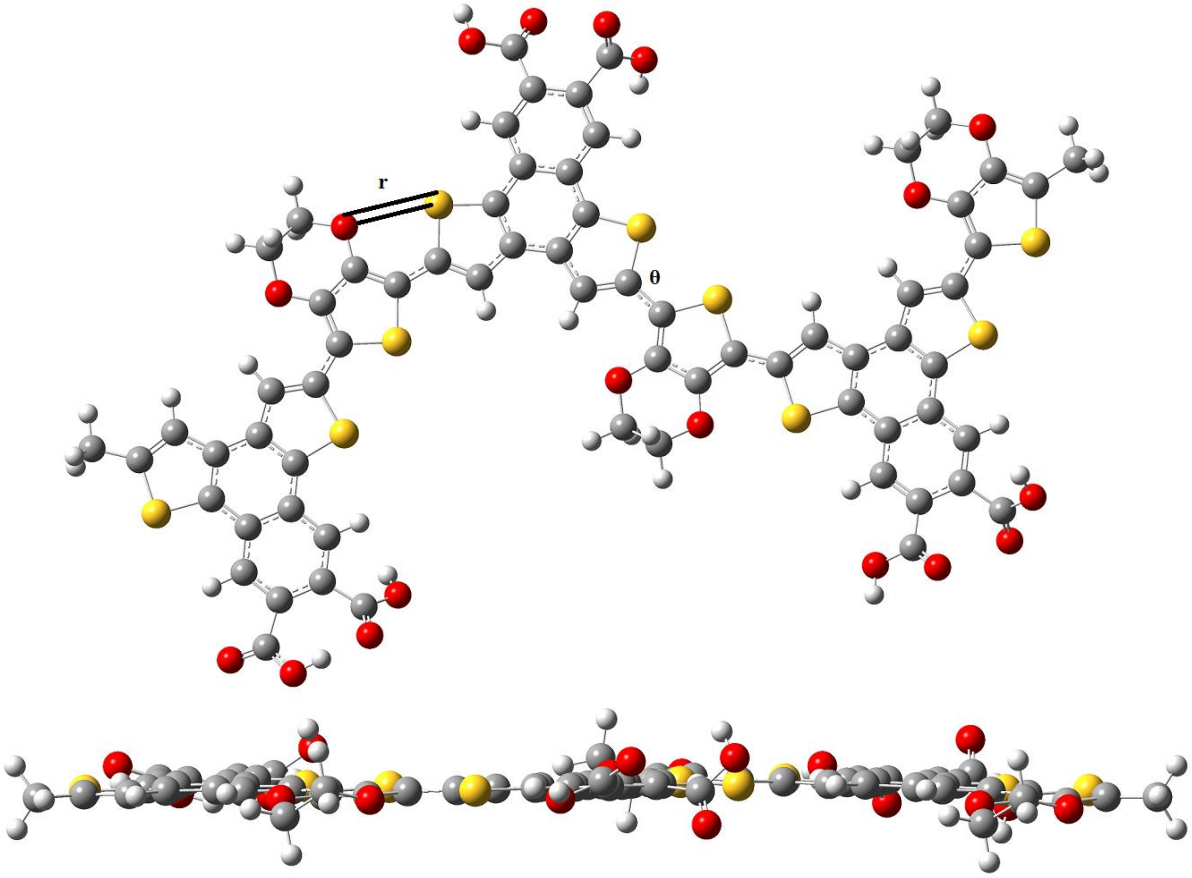

Figure 75: Energy minimized geometries of **31** (trimer) with different views.

As seen from the geometries of the trimers for both the polymers and the dihedral angles between the comonomer, they have nearly planar structures and minimal twisting between the comonomers. The dihedral angle was 6.52° and 6.23° in case of polymers **36** and **31**, respectively (Table **6**). This near planar orientation in their structures was attributed to the presence of only one thiophene unit in the donor unit as opposed to bithiophene units in case of polymers **58** and **59**. In addition, there is also S--O short contact between them that prevents the backbone twisting. The computed S--O distance in the energy minimized structure was found to be 2.96 Å, smaller than the sum of their van der Waals radii (3.32 Å).[190]

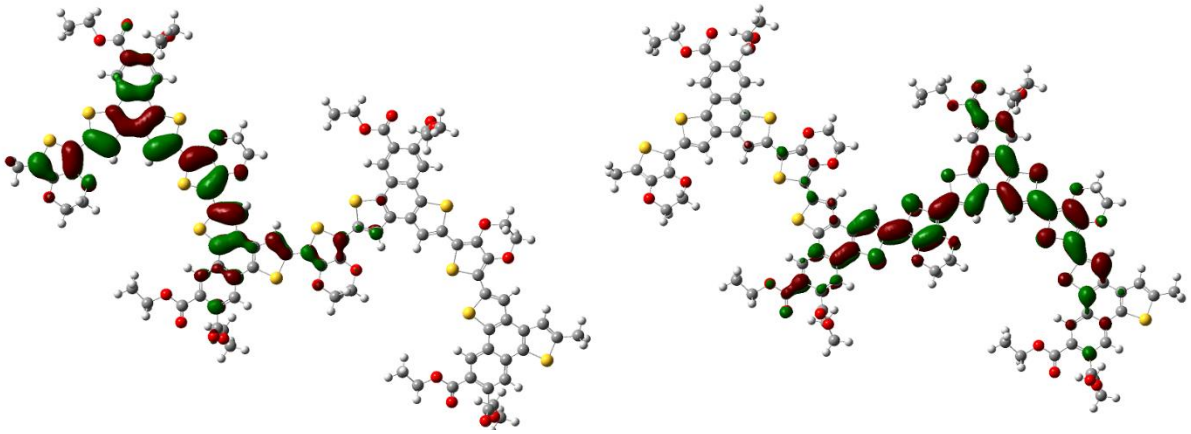

Figure 76: Energy minimized HOMO and LUMO energy conformers for trimer **36**.

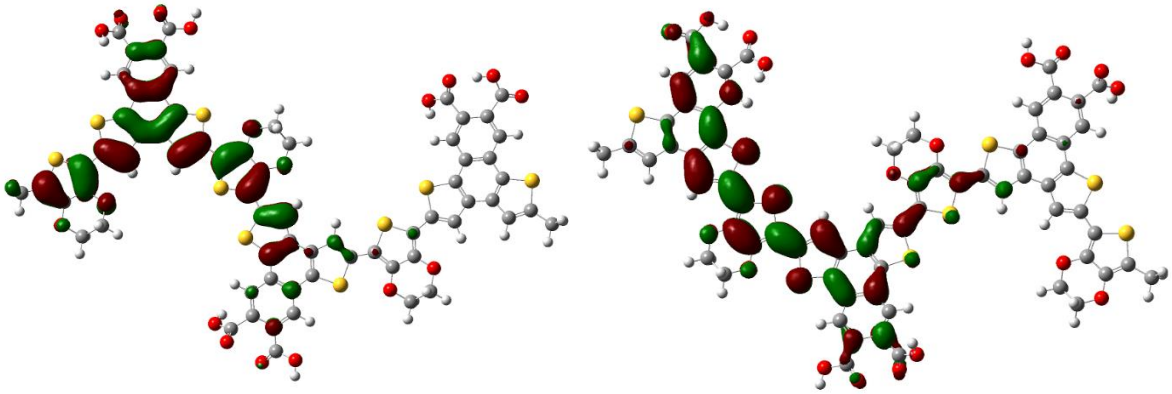

Figure 77: Energy minimized HOMO and LUMO energy conformers for trimer **31**.

Although none of these conformations exhibited folded backbone structure in these DFT calculations, various external factors such as solvent polarity or internal factors like π-π stacking interactions were not considered. Hence, it does not represent the actual scenarios as to how the polymer would rearrange in presence of various solvents, and it only correspond to a single molecule in vacuum.[191]

The HOMO and LUMO energy levels of these polymers were estimated from the energy minimized structures of their trimers described above using DFT calculations at the B3LYP/6-31G(d) level. The HOMO/ LUMO distributions of the energy minimized structures

for their trimers are shown in the Figures **76** and **77**. The HOMO/ LUMO energy levels are calculated to be -5.28/ -2.72 eV and -5.27/ -2.65 eV, and the band gaps are 2.56 and 2.62 for trimers of polymers **36** and **31**, respectively. As expected, there was very little difference between the HOMO and LUMO distributions and the energy gap for both these polymers since they have same ethylenedioxythiophene donor unit and the NDT based acceptor units.

Table 6: The dihedral angle between the monomers and the S--O short contact distance for polymers **31** and **36** using DFT calculations.

Polymer	**Intermonomer twist**	**S—O short contact (Å)**
	Θ	**R**
31	6.23	2.96
36	6.52	2.96

3.5.3 Electrochemical properties for NDT based polymers

The electrochemical properties of the naphthalene dithiophene-based, conjugated polymers were calculated by preparing thin films of polymer solutions of **31** and **36** in $CHCl_3$ by cyclic voltammetry (CV) measurements. In case of polymer **31**, there were two irreversible oxidation waves in the anodic scan, and one irreversible reduction wave observed in the cathodic scan as shown in Figure **78**. Whereas, for polymer **36**, there were three irreversible oxidation waves in the anodic scan and one semi reversible reduction wave in the cathodic scan. The HOMO and LUMO energy levels of the polymers were calculated using the first onset oxidation potential in the anodic scan and the first onset reduction potential in the cathodic scan. The HOMO and LUMO energy levels for polymers **31** and **36** were calculated to be -5.38/-3.64 and -5.24/-3.45 respectively. The HOMO and LUMO energy levels for both these polymers are not too different due to the same comonomer D units used for their synthesis. Although these polymers only have naphthalene dithophene based unit in the acceptor (no imide functionalization), the effective band gap may be lowered due to the presence of heteroatoms in their backbone that lead to the S--O short contacts present among the neighboring comonomer units thereby improving the planarity of the backbone in their structures. The effective band gap energy for these polymers **31** and **36** were calculated to be 1.74 and 1.79 eV, respectively. The calculated values for these polymers were lower as compared to their theoretical energy calculations.

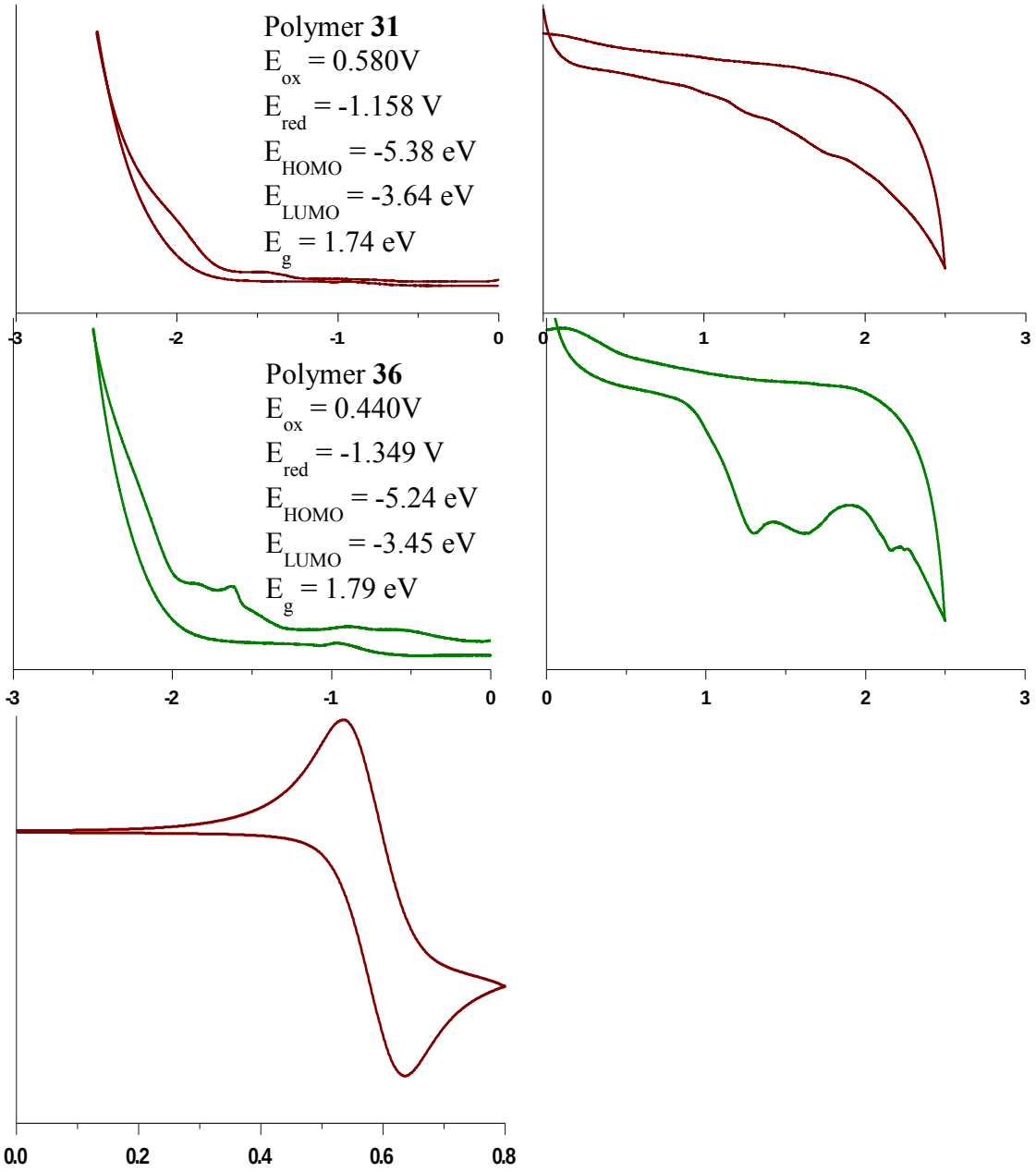

Figure 78: Cyclic voltammograms of polymers **31** and **36**, scale referenced to Fc/ Fc^{+} redox couple.

3.5.4 Optical properties of NDT based D-A alternating copolymers

Polymer **36** was soluble in organic solvents like chloroform, acetone, DMF, DMSO and DCM. It exhibited poor solubility in solvents like acetonitrile, hexane, and methanol. In case of polymer **31**, however the solubility was poor in most of the organic solvents with the exception of DMF and DMSO and showed moderate solubility in aqueous medium. The solutions of these polymers were prepared in good solvents and solvents having poor solubility and their absorbance data was obtained. The absorption spectra of polymer **36** is shown in Figure **79**.

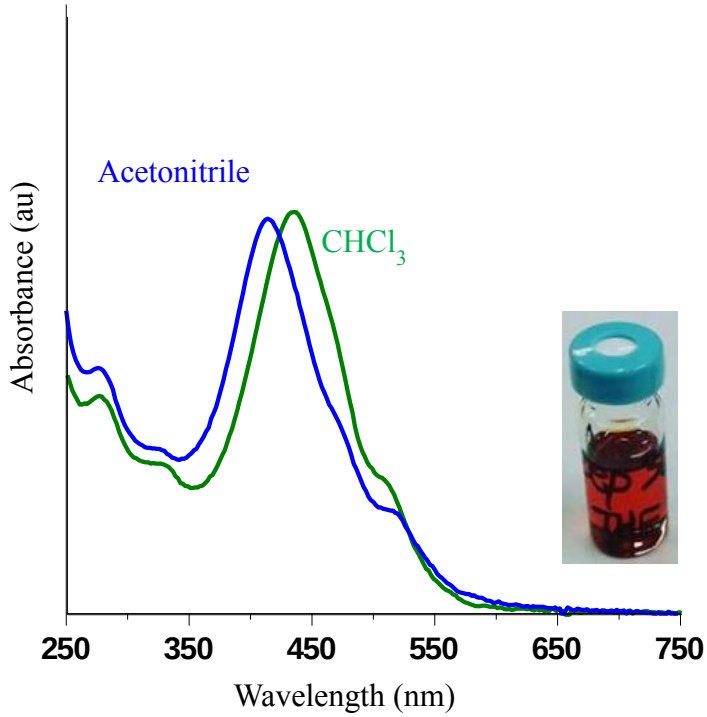

Figure 79: Absorption spectra of polymer **36** in different solvents.

The absorption spectra of polymer **36** in acetonitrile (poor solubility) exhibited an absorption maxima at 414 nm with the shoulder peak at about 515 nm. Whereas in good solvent, like chloroform also there was red shift in the λ_{max}^{abs} by 22 nm, and giving absorption

maxima at 436 nm and shoulder peak at 515 nm. Other than those minor shift in the band edge that may be due to differences in solvent polarity or inter-ring π-π stacking, the absorption spectra of **36** is consistent in both solvents.

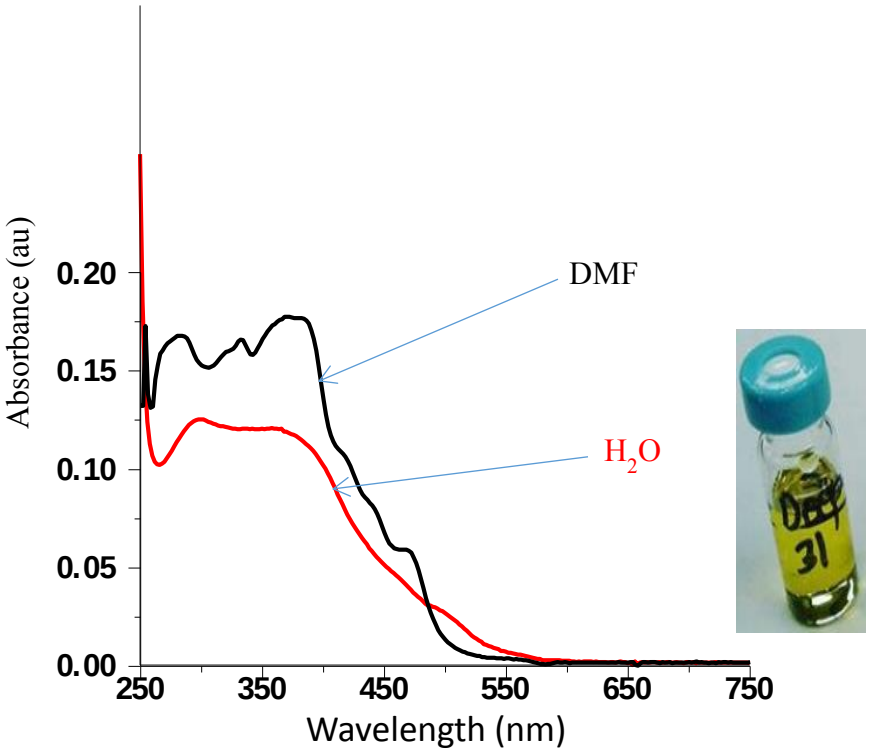

Figure 80: Absorption spectra of polymer **31** in different solvents.

The absorption spectra of polymer **31** were taken in DMF and water (Figure **80**). It was moderately soluble in water but readily soluble in DMF. Polymer **31** showed a broad unresolved absorption band in the range of 350- 450 nm with the shoulder peak at around 470 nm in DMF which could be due the presence of various states causing the spectral broadness. Also, the absorption spectra of **31** in water gave a broad featureless absorption in the region from 320-400 nm.

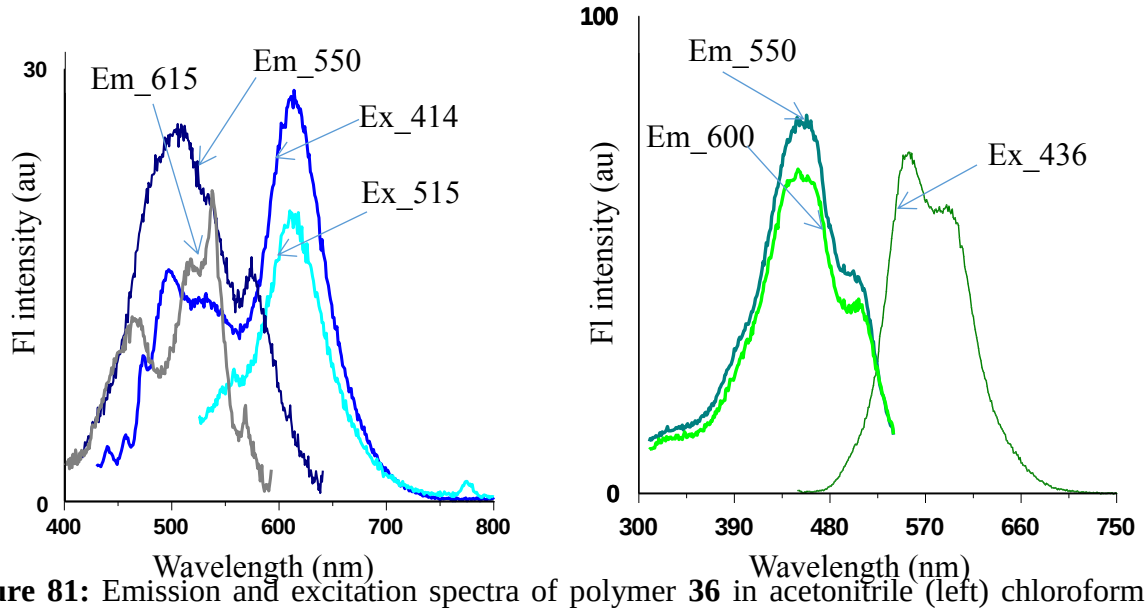

Figure 81: Emission and excitation spectra of polymer **36** in acetonitrile (left) chloroform (right).

When excited at the absorption maxima in the absorption spectra at 414 nm in acetonitrile the fluorescence emission spectra of polymer **36** gives two emission bands at 500 nm (minor) and at 615 nm (major) (Figure **81**) . The emission spectra from excitation at 515 nm (shoulder peak in the absorption spectra) results in the emission band at 615 nm. In acetonitrile, **36** has very low emissions. In solvents like acetonitrile (poor solubility), the excitation spectra at emission wavelength of 615 nm showed two peak at around 410 nm and 540 nm that resembles the absorption spectra. The excitation spectra when emitted at lower wavelength of 550 nm shows major peak at about 510 nm and a shoulder around 575 nm. The fluorescence emission spectra of **36** in chloroform when excited at absorption maxima of 436 nm yields two emission bands at 550 nm and at 600 nm. However, the excitation spectra of **36** at different emission wavelengths results in the similar excitation spectra.

When excited at different excitation wavelengths starting from 370, 420, 440 and 470 nm the fluorescence emission spectra (Figure **82**) of **31** in DMF gives two emission bands at

about 470 nm and 520 nm with the shoulder peak at 450 nm. These two major emission bands are more prevalent at higher excitation wavelengths (440 and 470 nm). While at lower excitation wavelengths (370 and 420 nm), there is only one major emission observed around 470 nm. The excitation spectra of **31** in DMF at the emission wavelength of 450 nm shows a major peak at about 390 nm that may be due to the monomer. The excitation spectra in DMF at emission wavelength of 520 nm yields three peaks similar to that of the absorption spectra.

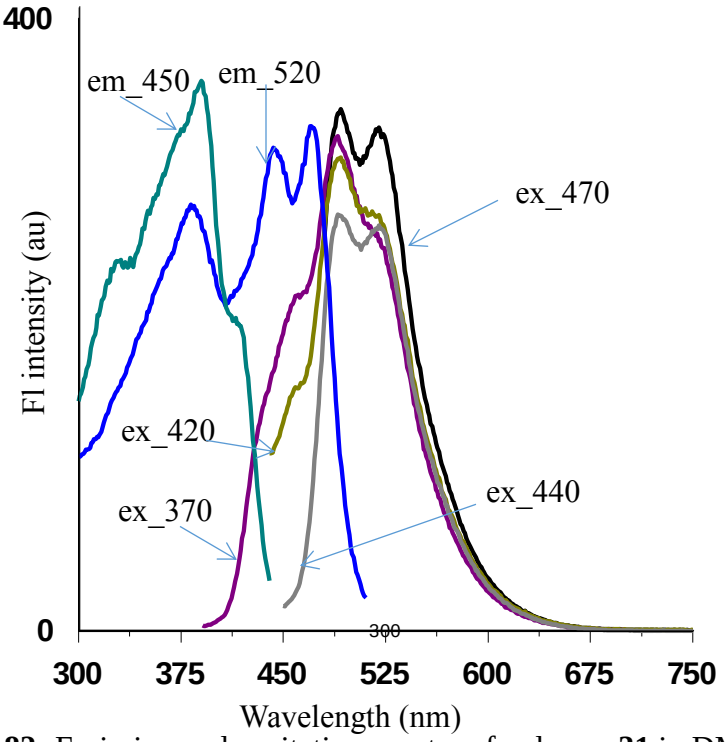

Figure 82: Emission and excitation spectra of polymer **31** in DMF.

Thus, it can be assumed that both polymers **36** and **31** maintain only one type of conformation (possibly folding) in good solvents like $CHCl_3$/ DMF but in solvents with poor solubility, there are more than one conformation (nonaggregated polymers). Further studies exploring different solvents and mixtures of solvents are in progress to provide more direct evidence for the possible folding conformations.

3.6 Target molecules for INDT-based copolymers

In addition to the NDT-based copolymers INDT-based copolymers were also synthesized (Figure **83**) owing to the advantages of imide functionalization, similar to what we observed in case of triphenylene-containing conjugated polymers. Different side chains could be attached to the imide nitrogen to improve the solubility, and their results would be compared with NDT based polymers to study the effect on the HOMO, LUMO energy levels, band gap and PCE.

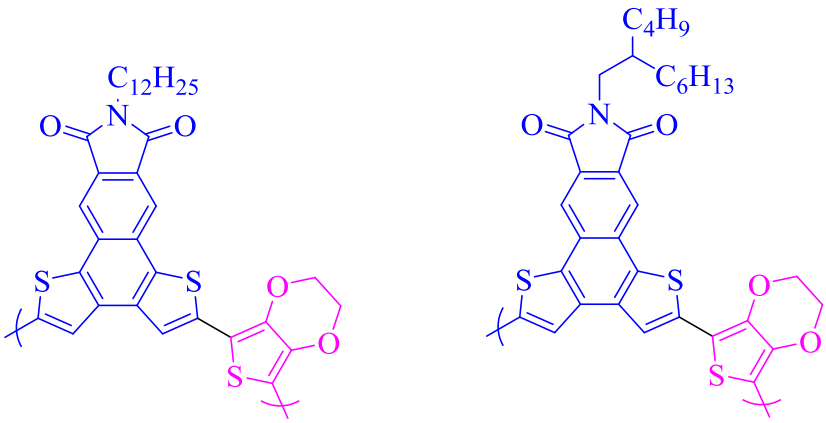

Figure 83: Chemical structures of INDT-based D-A polymers.

The retrosynthetic route for the synthesis of INDT-based D-A alternating copolymer with straight or branched alkyl side chain was shown in Scheme **10**.

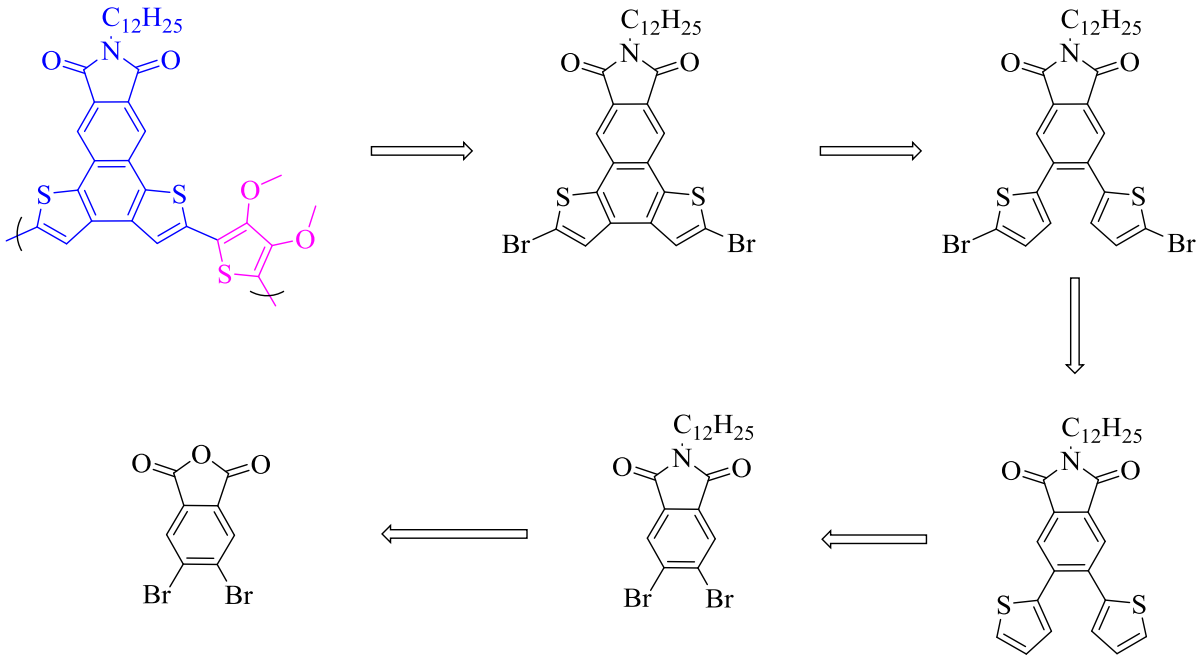

Scheme 10: Retrosynthetic pathway for the synthesis of INDT based D-A copolymer.

3.6.1 Synthesis and characterization of INDT-based copolymers

In this scheme of reactions to synthesize donor-acceptor based conjugated foldamers, *N*-dodecylamine-4,5-dibromo-phthalimide, compound **13** was utilized as the starting material that was synthesized in the previous chapter. The modified scheme (Scheme **11**) was used to prepare INDT-based acceptor monomer containing the heteroatoms like S introduced in the polymer backbone.

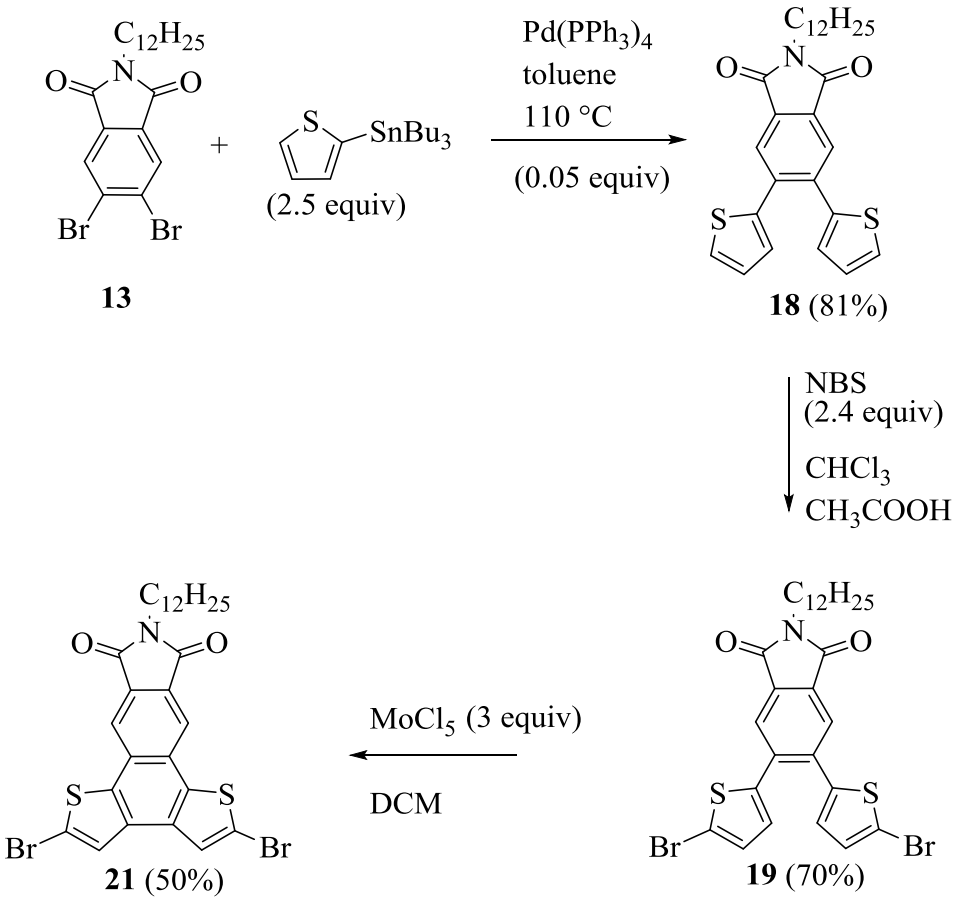

Scheme 11: Synthesis of INDT based acceptor monomer.

Coupling reactions, like Stille coupling, produced compound **18** introducing thiophene rings to the system in excellent yield. The formation of **18** was confirmed by ^{1}HNMR spectrum in $CDCl_3$, which gives new aromatic protons at 6.98 and 7.35 ppm because of the coupling of thiophene rings to the system (Figure **84**).

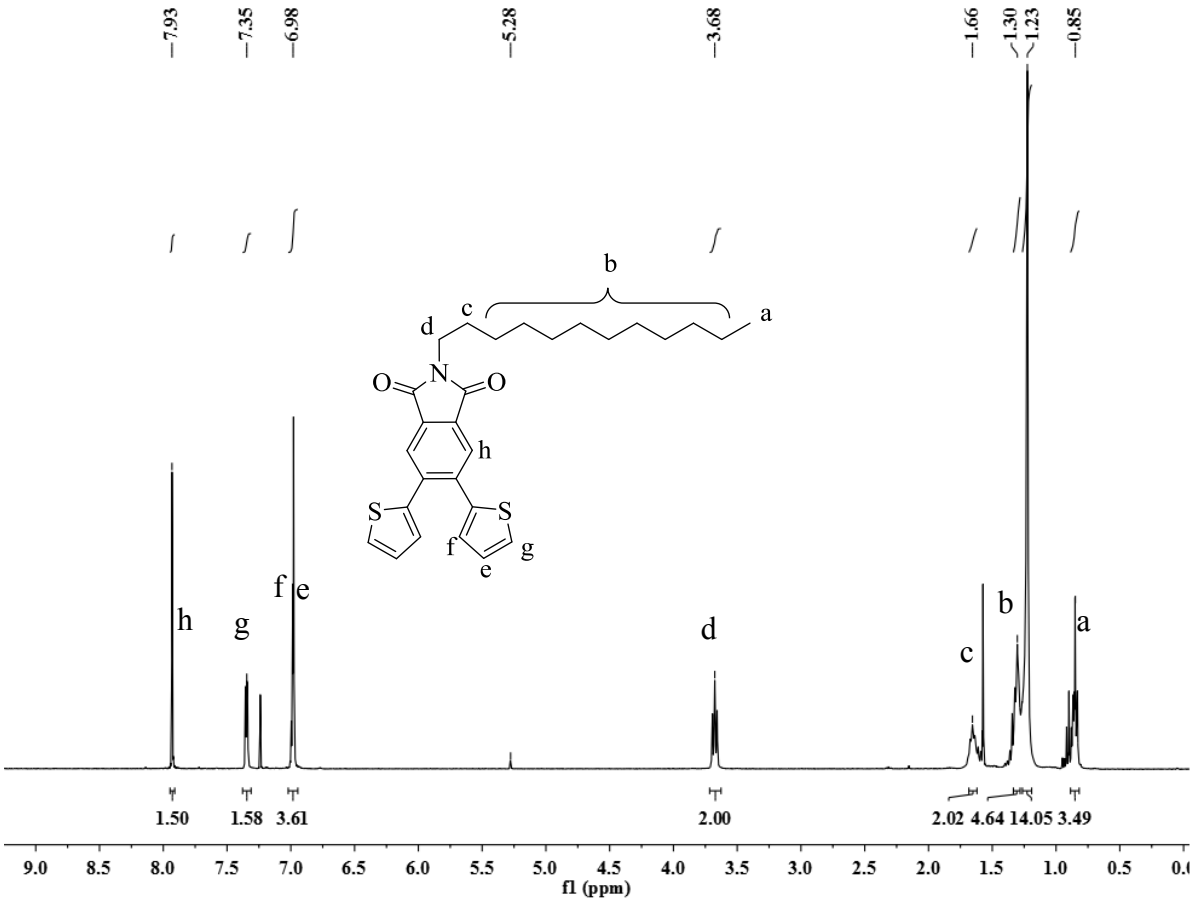

Figure 84: ^{1}HNMR spectrum of compound **18**.

The α-positions on the thiophene rings in compound **18** was then blocked by reaction with *N*-bromosuccinamide using severe conditions of NBS/AcOH/$CHCl_3$ to afford compound **19**. The formation of compound **19** was confirmed by the ^{1}HNMR spectrum that showed two new well-resolved aromatic signals at 6.80 and 9.98 ppm (Figure **85**). Another challenge of this route was the ring closure of two thiophene rings to form imide functionalized naphthalene dithiophene based acceptor monomer.

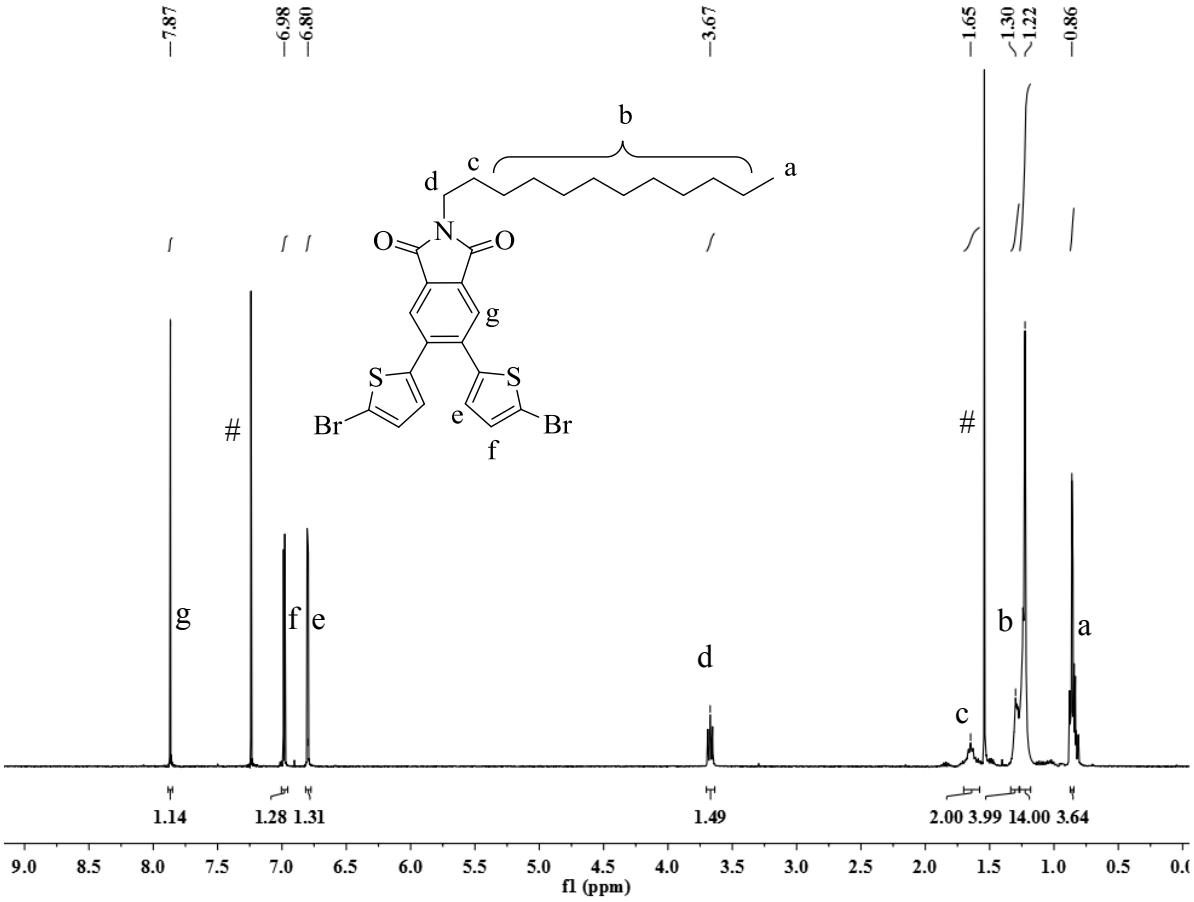

Figure 85: H[1]NMR spectrum of compound **19**.

Compound **19** was then successfully cyclized via oxidative cyclization using strong oxidizing agents like $MoCl_5$ to give INDT-based acceptor monomer **21** with dodecyl side chain in good yields. [1]HNMR spectrum showed the confirmation for the formation compound **21** (Figure **86**). Two well separated and well resolved sharp singlets at 7.68 and 8.45 ppm due to different neighboring environments and the absence of any other major new peak in the aromatic region established the formation of our desired monomer.

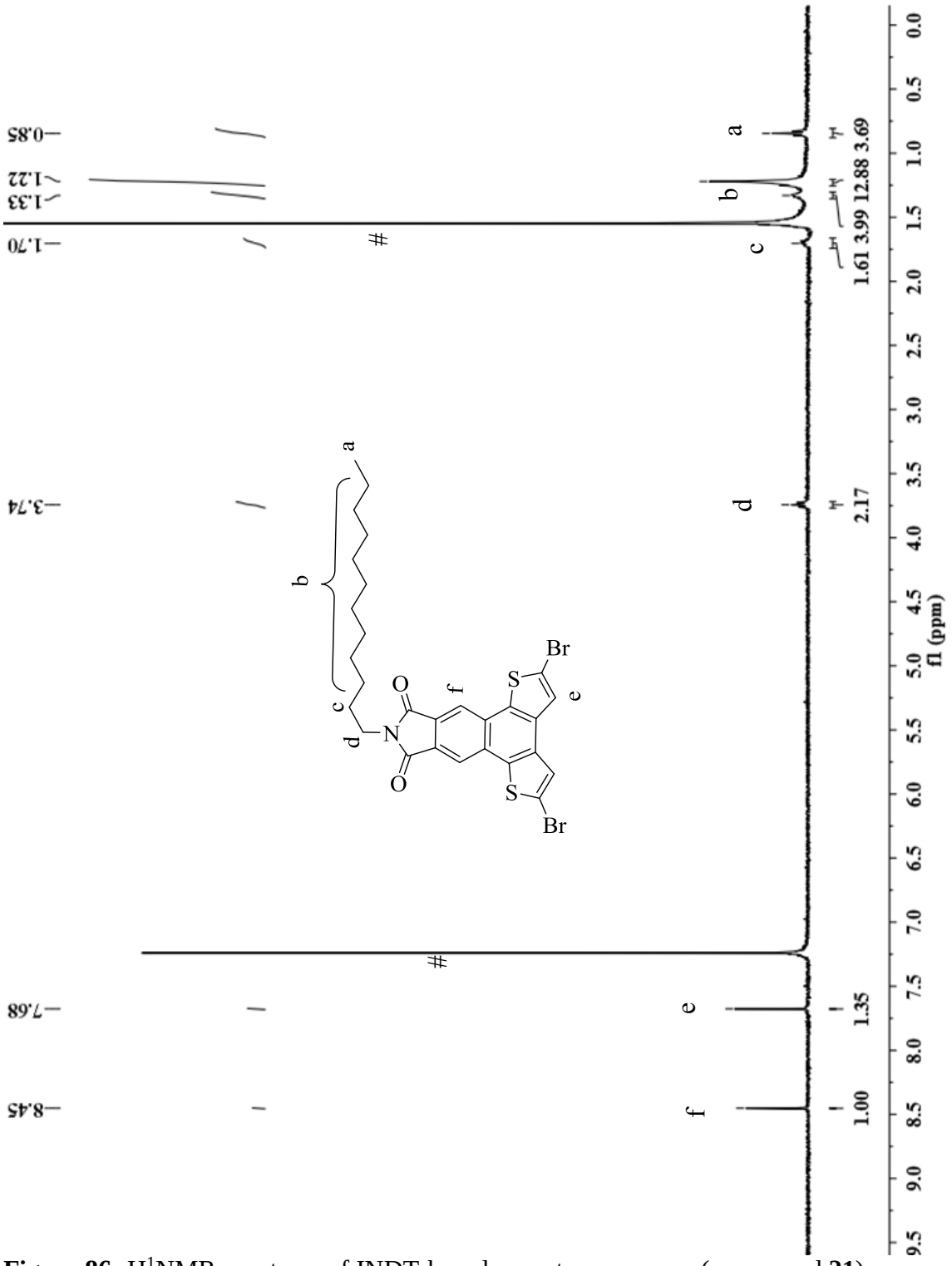

Figure 86: H^1NMR spectrum of INDT-based acceptor monomer (compound **21**).

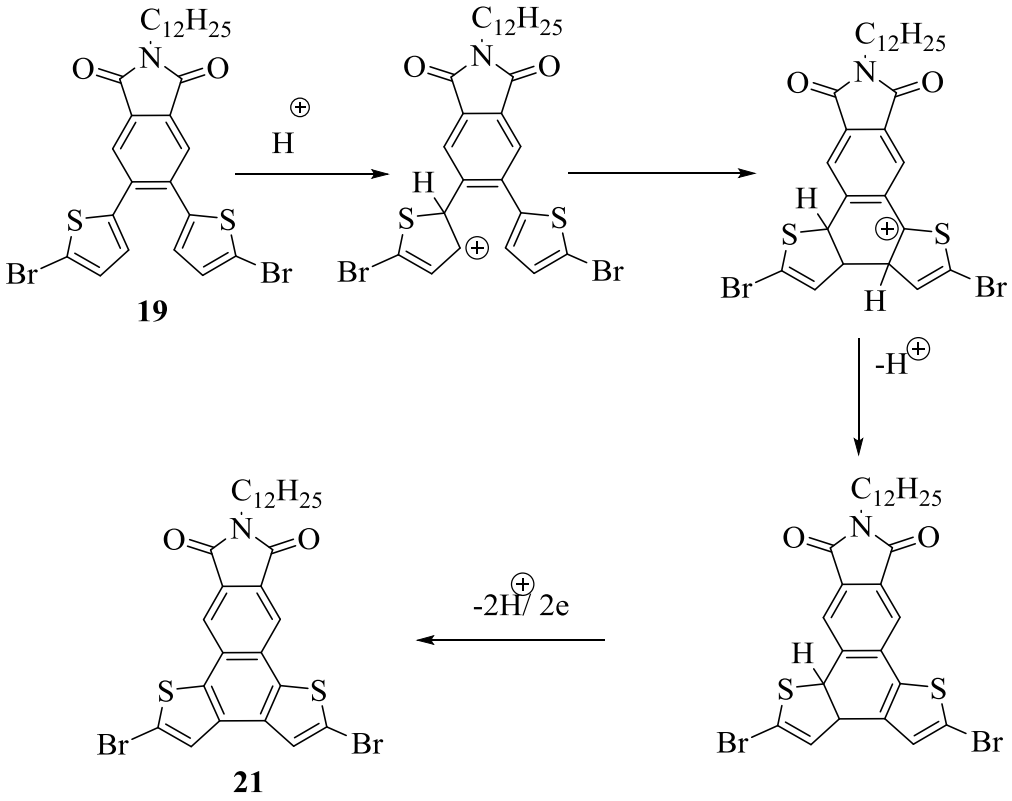

Scheme 12: Modified Scholl oxidation using strong oxidizing agent.

In the Scheme **12**, the mechanistic pathway of the oxidative cyclization of compound **19** to synthesize INDT-based acceptor monomer **21** was given. The synthesis of donor monomers was carried out from commercially available 3,4-dimethoxythiophene in good yields following a procedure[189] published previously as depicted in Scheme **13**. In the ^{1}H-NMR spectrum for compound **6** in $CDCl_3$, the sharp singlet at 3.76 ppm due to methoxy protons and the signals between 0.89- 1.54 ppm due to protons on butyl chains confirmed the identity of the comonomer (Figure **87**). Further, the ^{13}CNMR spectrum for the comonomer gave five signals for the methoxy and butyl carbons and two signals for the aromatic carbons on the thiophene ring as assigned in Figure **88**.

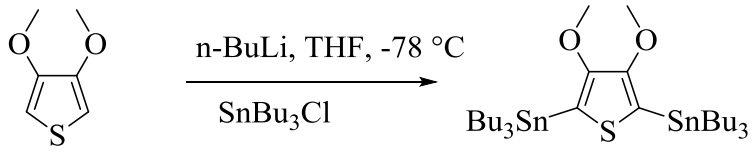

6

Scheme 13: Synthesis of compound **6**.

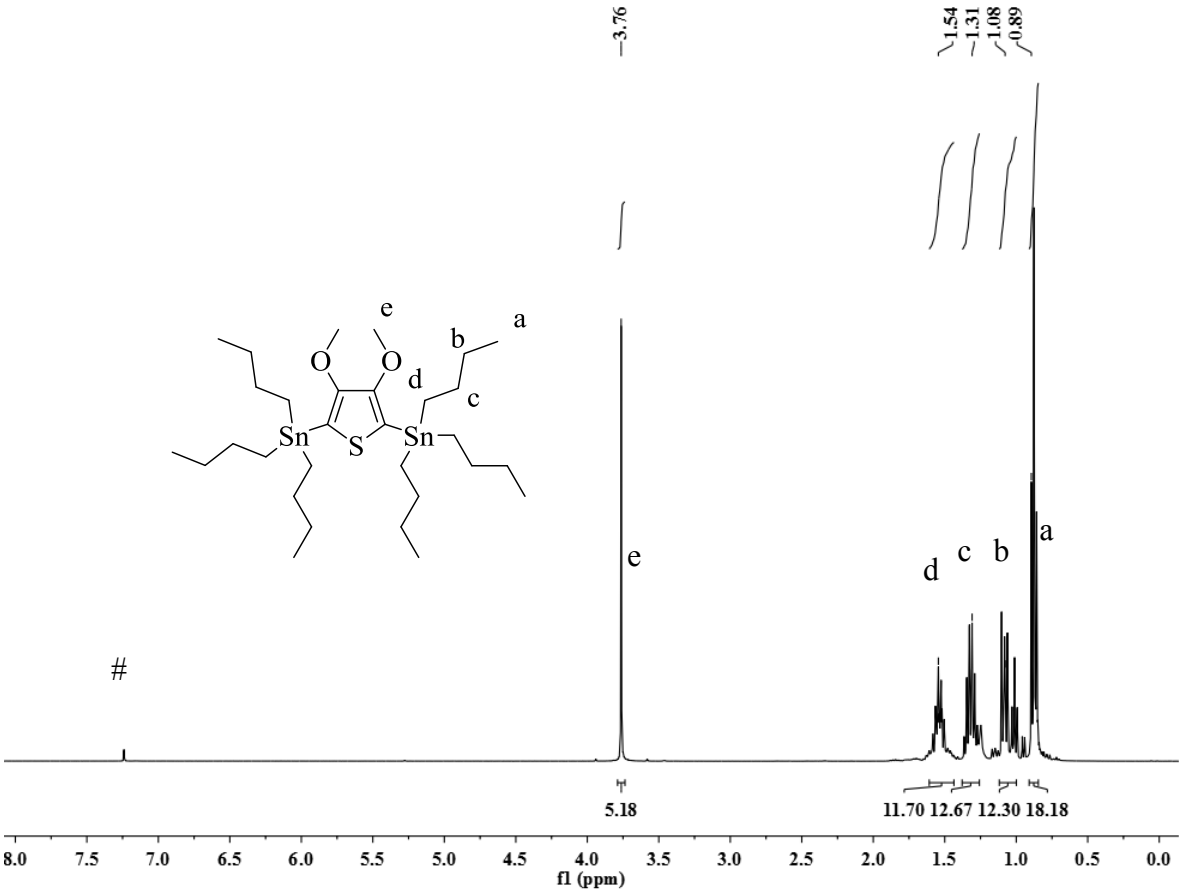

Figure 87: [1]HNMR spectrum of compound **6**.

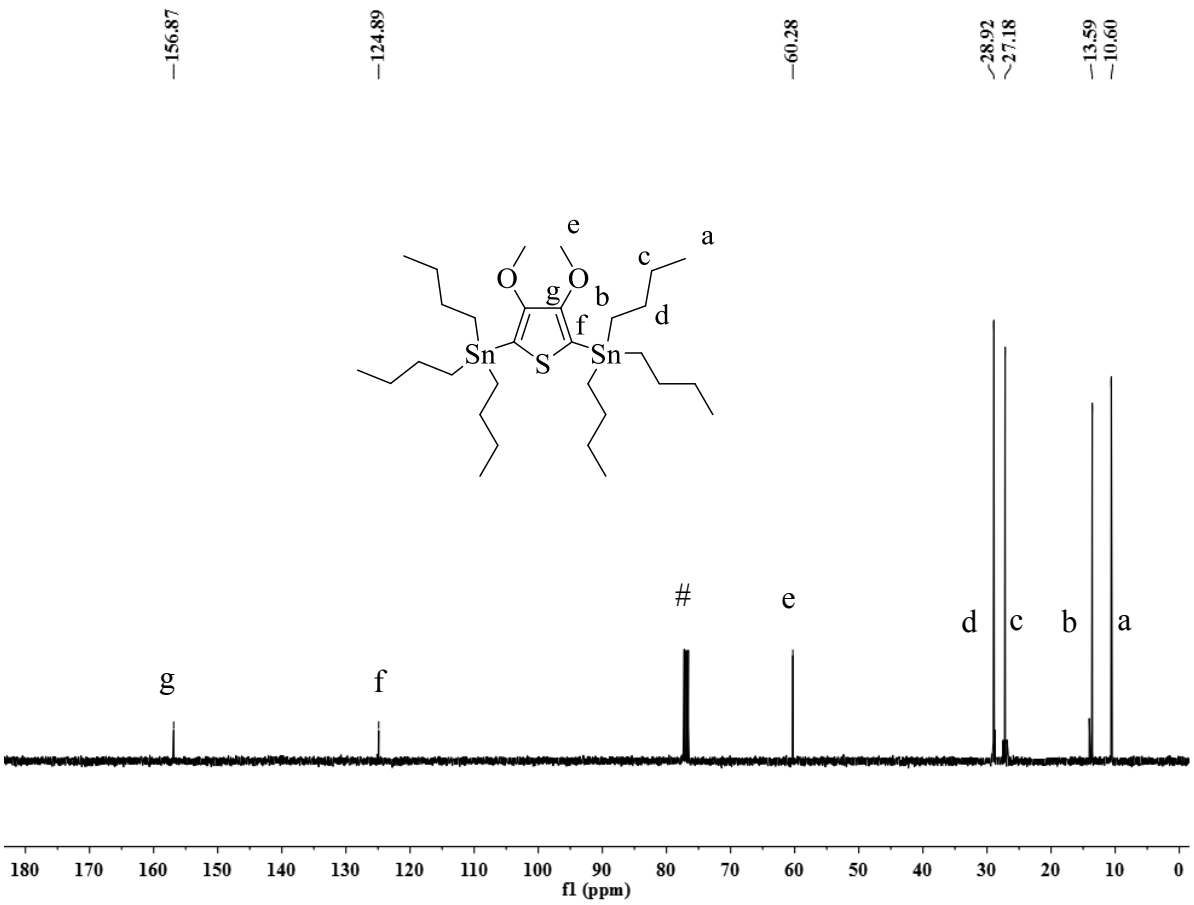

Figure 88: ^{13}CNMR spectrum of compound **6**.

The synthesis of D-A alternating copolymers was achieved by Stille cross-coupling polymerizations that gave high molecular weight polymers with lower backbone defects and excellent yields (scheme **14**). The polymerization reactions were carried out using $Pd_2(dba)_3$/ *p*-(*o*-tolyl)$_3$ catalyst system and refluxing in minimal solvent for approximately 48 h. The synthesized polymers were purified using successive precipitation with methanol and followed by sequential soxhalation with a series of solvents like acetone, methanol or hexane.

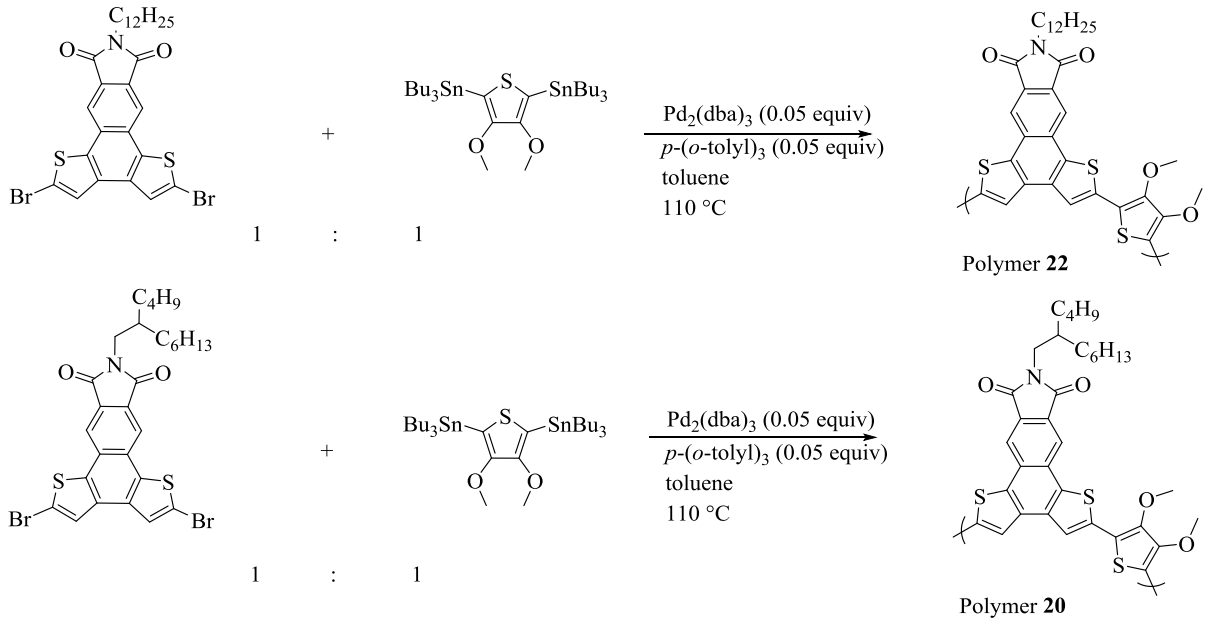

1 : 1

1 : 1

Scheme 14: Polymerization of INDT-based D-A alternating copolymers.

The polymers with long dodecyl chain and branched chain at the imide position give good solubility to theses polymers in most of the organic solvents like THF, chloroform, acetone or DCM. The molecular weights of these polymers were determined by gel permeation chromatography using THF as the eluent and polystyrene as the standard. The weight average molecular weight for polymers **20** and **22** were found to be 9.27 and 9.70 kDa, respectively. Also, the polydispersity indices for both the polymers **20** and **22** were relatively narrow 1.48 and 1.94, respectively. The results are summarized in following Table **7**.

Table 7: Polymerization data for polymers **20** and **22**.

Polymer	**Yield (%)**	**Mn (kDa)**	**Mw (kDa)**	**PDI**
20	84	6.26	9.27	1.48
22	68	5.00	9.70	1.94

The ^{1}H-NMR spectrum of polymer **20** was measured in 1,1,2,2-tetrachloroethane (Figure **89**). The sharp singlets in the aromatic region and the peaks due to methylene on the imide nitrogen and methoxy protons around 4 ppm for the monomer become broader after polymerization. This is usually observed in case of polymers because of interchain aggregation. The intermolecular interactions (π-π stacking) between neighboring polymer chains are responsible for broadening of aromatic proton signals. The broadening of signal between 3.20-4.50 ppm could be due to the high aggregation tendency of the polymer backbone due to higher PAH- unit density in the polymer backbone.

Polymer **22** also showed similar trend when the ^{1}HNMR spectrum was taken using $CDCl_3$ (Figure **90**). The broadening of peaks was observed for the region between 0.80-1.50 ppm, 3.50-4.50 ppm, and around 8.50 ppm, which earlier showed signals for dodecyl chains, methylene on imide, and methoxy protons on the donor units as well as the aromatic protons respectively. As mentioned previously, the interchain aggregation and π-π stacking between the neighboring polymer chains after folding would be responsible for these broad signals observed in case of ^{1}HNMR spectra of polymers.

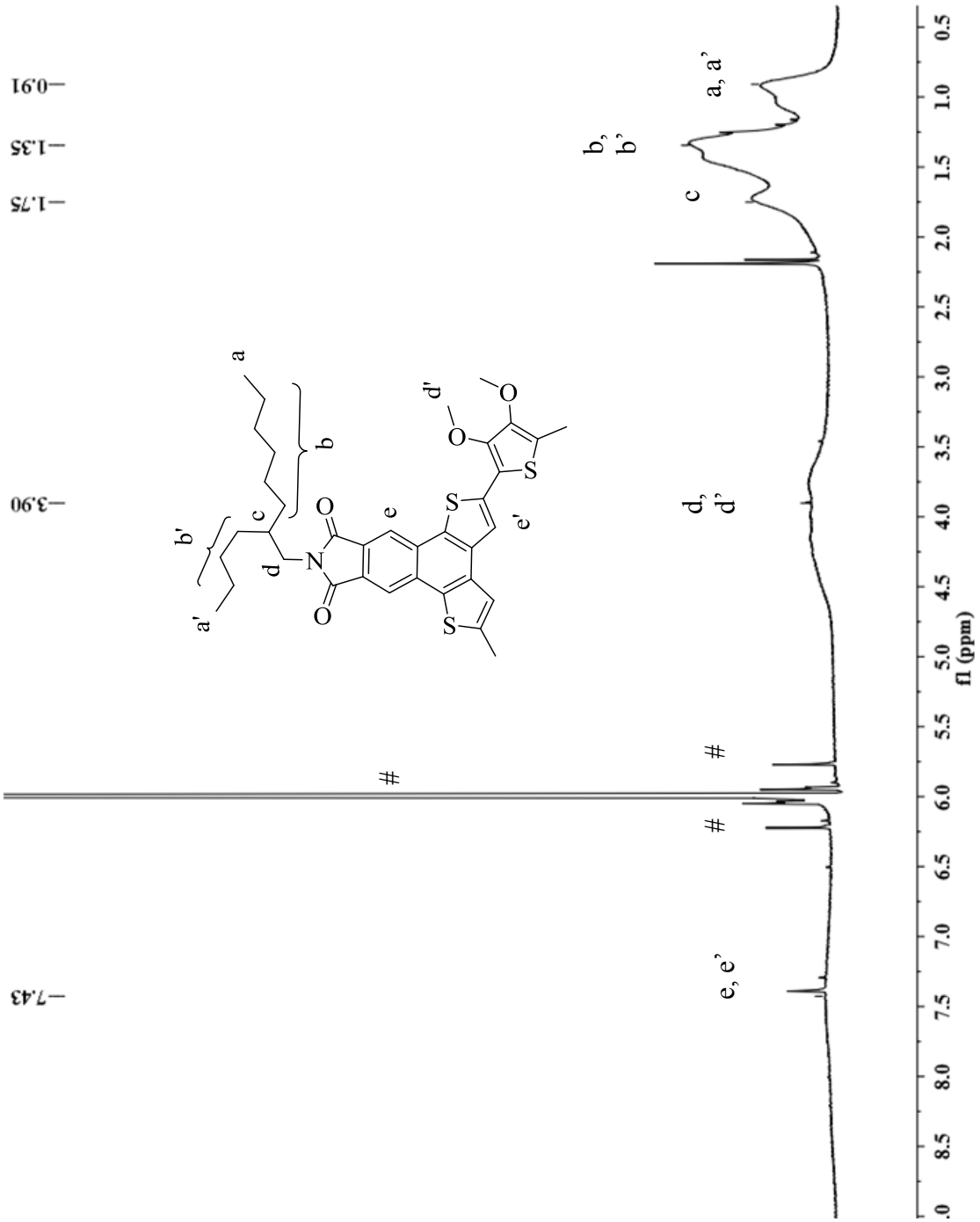

Figure 89: [1]HNMR spectrum of polymer **20**.

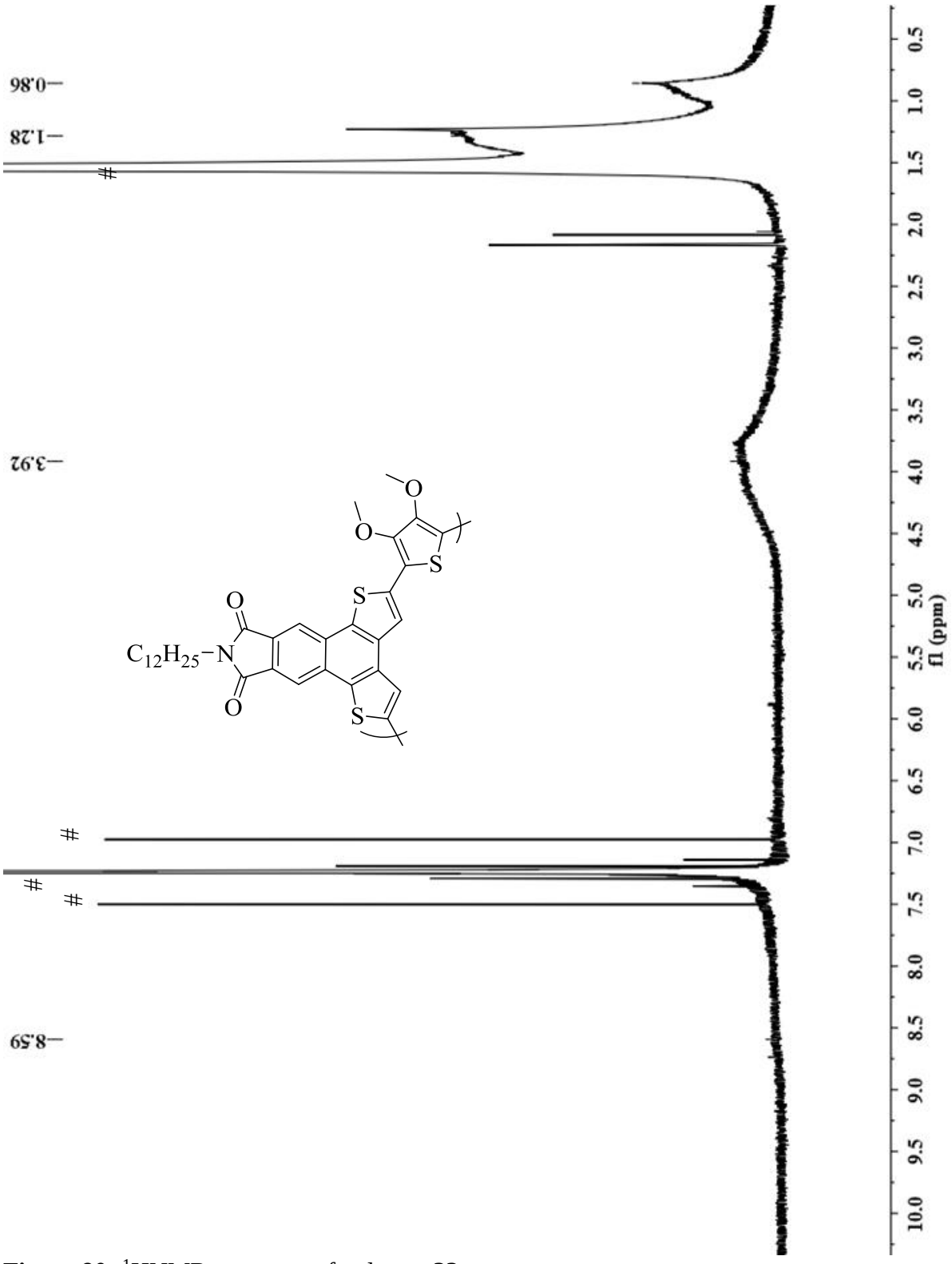

Figure 90: [1]HNMR spectrum of polymer **22**.

3.6.2 Density functional theory (DFT) calculations of INDT based polymers

To understand the backbone geometries and the energy levels of the polymers, theoretical calculations were performed on their corresponding dimers using the density functional theory (DFT) with the Gaussian03 program[132] at the B3LYP level with the polarized 6-31G(d) basis set,[192-194] a method shown to be a viable for structural optimizations and energy calculations for various molecular systems.[133-137] In order to minimize the computational efforts, the dodecyl and branched chains at the imide position of INDT backbone for polymers **22** and **20** were truncated to methyl groups, respectively. The energy minimized conformer of dimer for **20** and **22** with selected dihedral angles is depicted in Figure **91**. The dihedral angle between the donor and monomer units was found to be approximately 3.50°. Hence the absence of any comonomer twist and very small intermonomer twist makes the backbone of these polymers with imide functionality relatively planar. In addition, there were also S--O short contacts present between the co-monomers as seen in the figure. The computed S--O distance in the energy minimized structure was found to be 2.81 Å on an average, which is smaller than the sum of their van der Waals radii (3.32 Å). From these computational studies, it can be assumed that these polymers with INDT-based conjugated polymers have planar backbone structures and as shown in the Figure **91** are likely to arrange in the folded conformations.

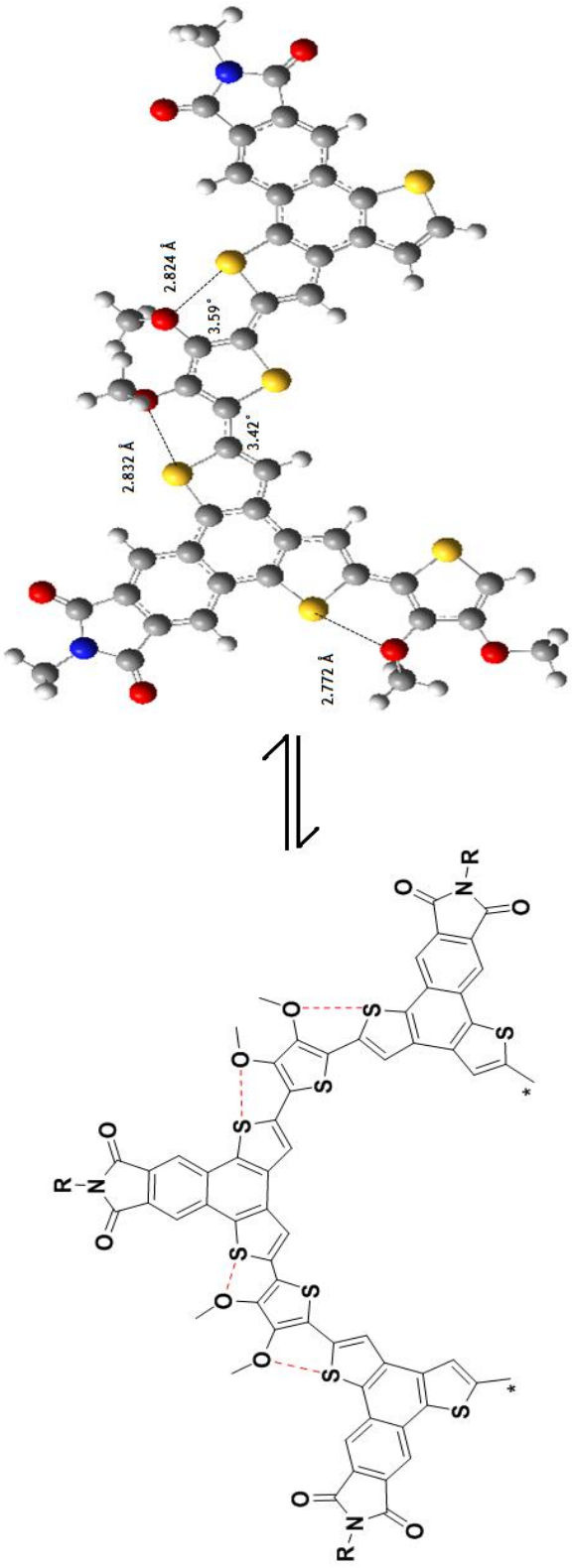

Figure 91: Energy minimized geometries of dimers of **20** and **22** using DFT calculations at the B3LYP/6-31G(d) level.

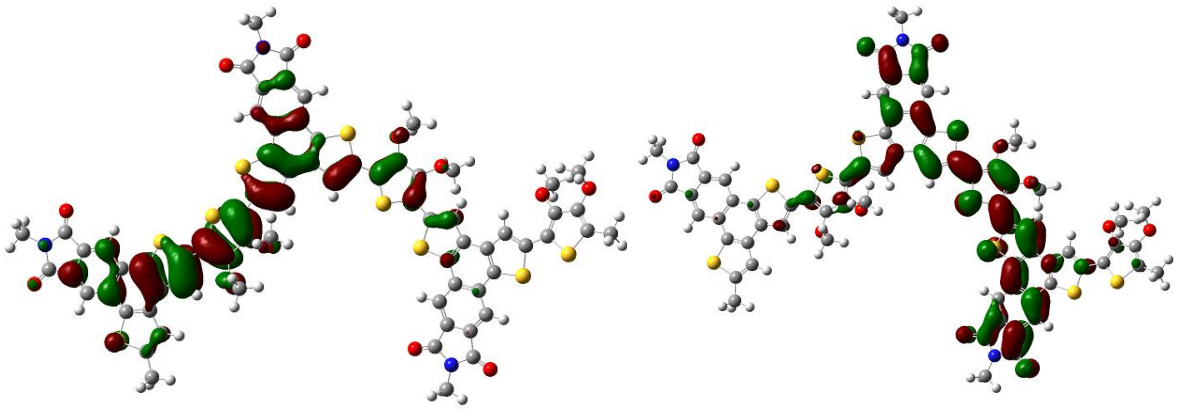

Figure 92: HOMO/ LUMO distributions of energy minimized structures of **20** and **22** dimers.

The HOMO and LUMO energy levels of the INDT-based copolymers were estimated from the energy minimized structures of their dimers using DFT calculations at the B3LYP/6-31G(d) level. The energy levels are -5.29/-2.55 eV for dimers of polymers **20** and **22**. The bandgap from this calculated HOMO/ LUMO energy level was 2.74 since both contained donor units with electron donating alkoxy side chains whereas the acceptor unit affects the LUMO energy levels. The HOMO energy levels are similar to those calculated for the trimers of NDT-based polymers. It can be also observed in Figure **92** that in the LUMO distribution of dimers of **20** and **22** the node passes through the imide nitrogen.

3.6.3 Electrochemical properties for INDT based D-A alternating copolymers

The electrochemical properties of the two INDT based polymers **20** and **22** were studied as thin films using cyclic voltammetry (CV), and the results are shown in Figure **93**.

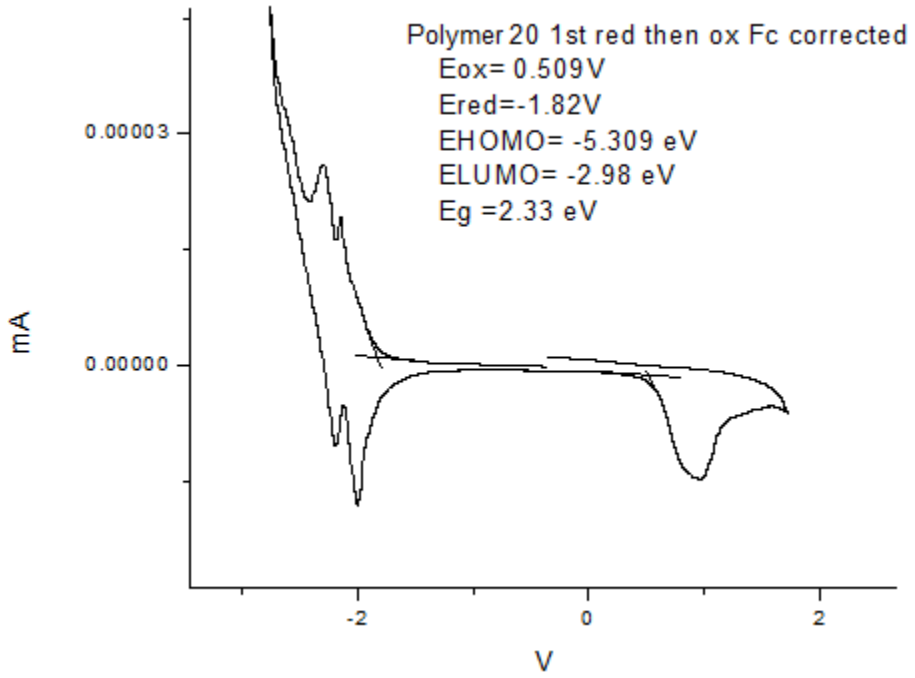

Figure 93: Cyclic voltammogram for INDT based copolymer **20** thin film. Scale referenced to Fc/Fc^{+} redox couple.

Since the polymers **20** and **22**, are having similar INDT backbone, and the donor units except the imide substitution being straight chained in **22** and branched chain in **20**, their electronic levels would be similar. Also, the node passing through the imide nitrogen, as seen previously would not affect which side chain is incorporated at the imide nitrogen. As seen in the CV measurements, the polymer showed two reversible reduction waves in the cathodic scan and one irreversible oxidation wave in the anodic scan. Using the first oxidation onset potential in the anodic scan and the first reduction potential in the cathodic scan, the HOMO and LUMO energy levels of the polymer **20** was estimated to be -5.31/-2.98. The bandgap measurement estimated from these values was found to be 2.33 eV. The experimental results for the energy

gap difference was found to be slightly lower than theoretical values obtained from the DFT calculations.

3.6.4 Optical properties for INDT based D-A alternating copolymers

Polymers **20** and **22** are both soluble in common organic solvents, such as chloroform, methylene chloride, acetone, tetrahydrofuran, acetone, dimethyl sulfoxide and *N*,*N*-dimethyl formamide. This is due to the imide substituted side chains, branched and long side chain respectively, however, they have poor solubility in solvents like methanol, acetonitrile and hexane. Their absorption spectra in chloroform, THF (good solubility) and hexane, acetonitrile (poor solubility) are shown in the Figures **94** and **95**.

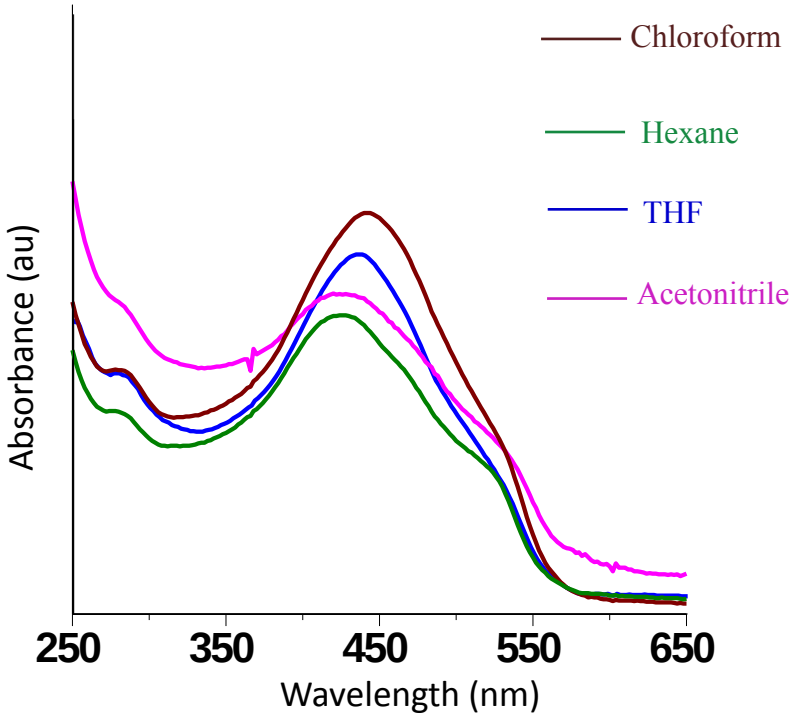

Figure 94: Absorption spectra of polymer **20** in different solvents.

The solutions of polymer **20** and **22** were prepared in acetonitrile and hexane (poor solubility) by adding a drop of their concentrated solutions in good solvents like chloroform. In acetonitrile and hexane polymer **20** shows a clear peak at about 424 and 432 nm and a shoulder peak at about 530 and 520 nm, respectively. While in solvents, such as chloroform

and THF, there is slight red shift in the band edge at 442 and 436 nm, and the shoulder peak remains at 520 nm. Apart from these minor differences, the absorption spectra of polymer **20** is consistent in all the solvents studied. The red shift in the band edge is attributed to inter-ring π-π stacking or the solvent polarity.

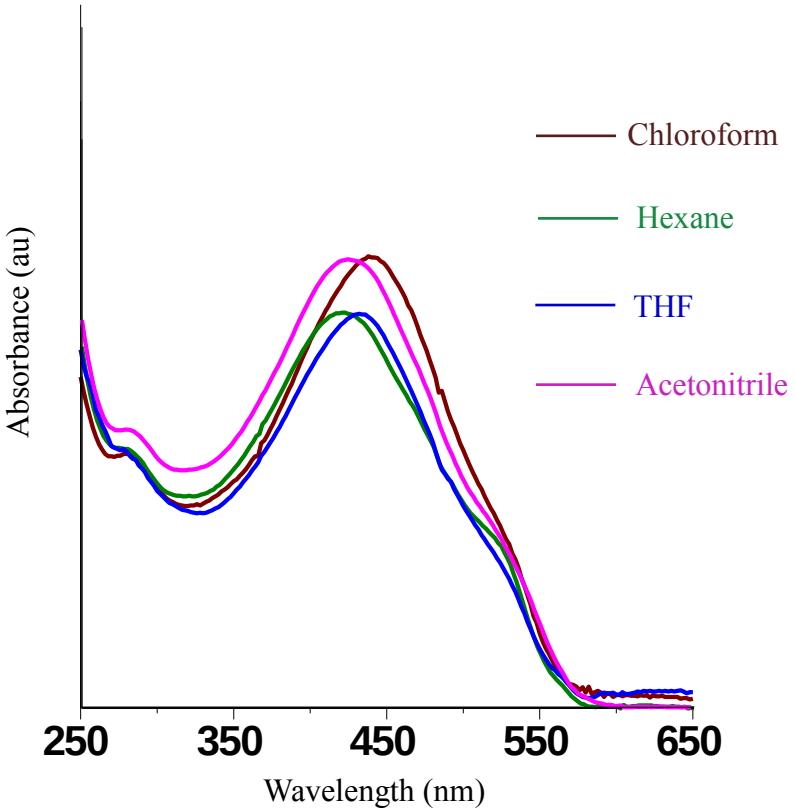

Figure 95: Absorption spectra of polymer **22** in different solvents.

For polymer **22**, the absorption spectra are shown to have similar trend as expected since both **20** and **22** have same INDT-backbone present in their structure, except for the different side chains in the imide position. In hexane and acetonitrile, there are absorption peaks at about 420 and 424 nm with a shoulder peak around 520 nm. With the good solvent like chloroform, there is a red shift in the band edge of about 18 nm.

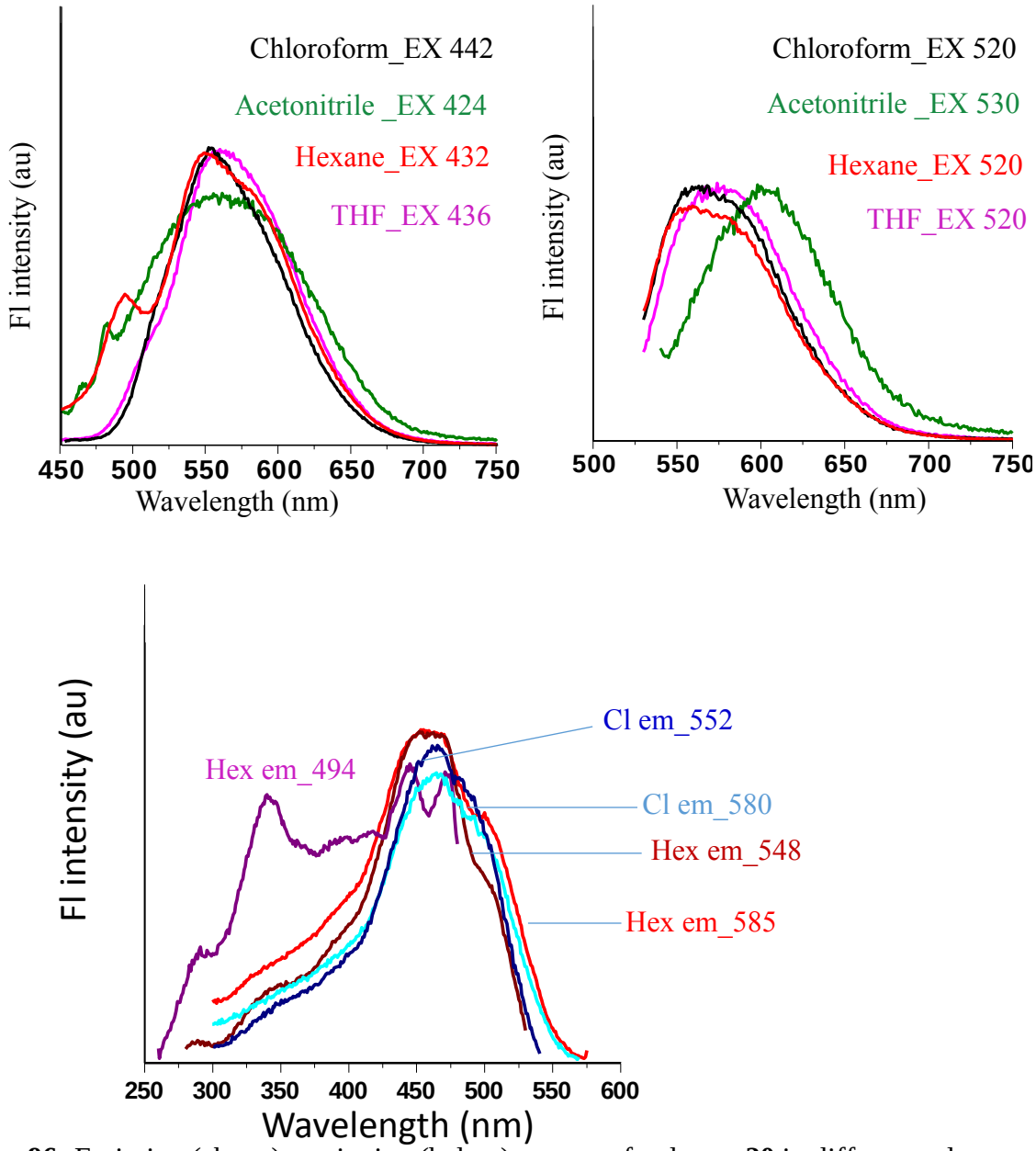

Figure 96: Emission (above), excitation (below) spectra of polymer **20** in different solvents.

The fluorescence emission spectra for polymer **20** when excited at 442 nm for chloroform or at 424 for acetonitrile gave similar emission spectra as shown in the above Figure **96**. Except a shoulder emission at about 475 nm for solvents with poor solubility could be due to monomeric emissions. When it is excited at 520 nm, which is the shoulder band in

the absorption spectra, it gives only one major peak at 560 nm but its slightly red shifted in case of acetonitrile at about 600 nm that may be due to aggregation or internal charge transfer (ICT) emission. Hence, in good solvents, the emission is due to only one kind of emitting excitons for polymer **20**, which may be due to folded conformations present among this polymer. Also, the excitation spectra in different solvents were measured to shed more light on the photophysical properties of the polymer. The excitation spectra in chloroform at different wavelengths 552 and 580 nm and in hexane at 548 and 585 nm showed identical features to that of absorption spectra and similar shapes. Whereas when hexane is excited at 494, the emission wavelengths results in a different excitation spectrum.

In the case of polymer **22**, the fluorescence emission spectra when excited at their absorption maxima 438 nm for chloroform and 420 nm for hexane produced a broad peak centered at 560 nm in good solvents and at 600 nm in solvents with poor solubility (Figure **97**). Furthermore, when the solutions of polymer **22** were excited at 510 nm (shoulder peak in the absorption spectra) in different solvents, there was continuous red shift from chloroform to THF to hexane and acetonitrile, i.e. around 50 nm red shift between good solvent to solvents with poor solubility. Even after changing different excitation wavelengths, no particular change was observed in the positions of the peak; hence, it may be because one type of conformation predominates in good solvents while a different conformation is adopted in solvents such as hexane with poor solubility. Similar observations were obtained for measurements of their excitation spectra in different solvents. As depicted in the Figure **97** below, the excitation spectra of **22** in THF at different emission wavelengths of 515, 560, and 580 nm showed major peak around 450 nm with a shoulder around 400 nm, whereas the excitation spectra in hexane at emission wavelength of 603 nm resulted in major peak at 450

nm with a shoulder peak about 520 nm. Hence, for polymer **22** it gives indirect indication that it adopts different conformations in solvents with good (folding) and poor solubility (interchain aggregation).

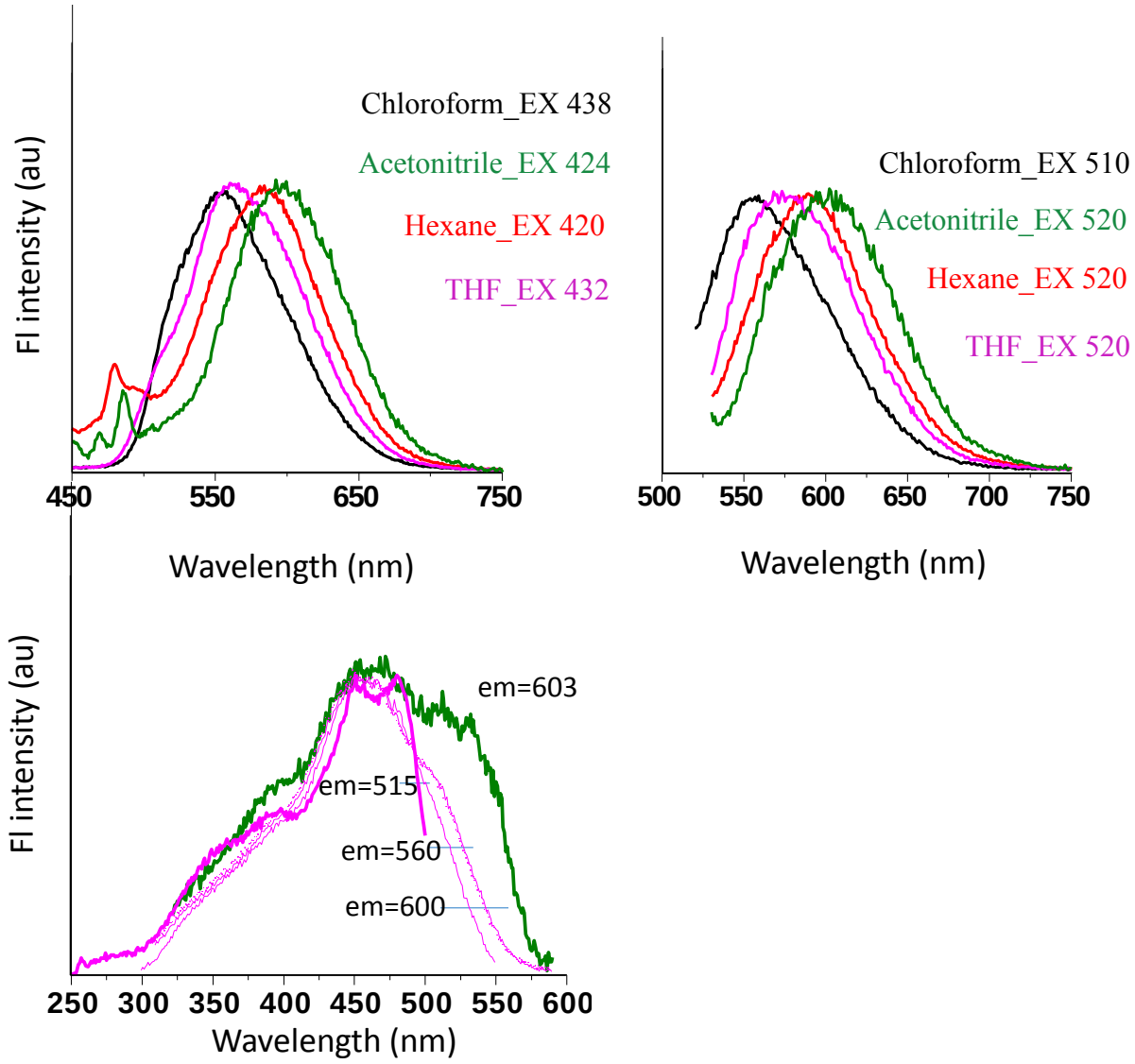

Figure 97: Emission (above) and excitation (below) spectra of polymer **22** in different solvents.

3.6.5 Photovoltaic properties of INDT-based D-A alternating copolymers

The polymers were tested for the photovoltaic properties by fabricating devices (BHJSCs). The general structure of the solar cells was ITO/PEDOT: PSS/polymer: $PC_{71}BM$/Ca/Al where the active layer was prepared by blending a mixture of synthesized polymers as donors and $PC_{71}BM$ as the acceptors (Figure **98**). Polymers were dissolved in *o*-dichlorobenzene with the concentration of 20 mg/mL and mixed with $PC_{71}BM$ in 1:1 weight ratio. This blended mixture was spincast on to an ITO slide coated with PEDOT: PSS. After solvent annealing for 1 h, the top Ca/Al electrode was sequentially deposited using high vacuum thermal evaporation. These fabricated devices were measured in air initially and later measured after thermal annealing. They were measured under 1-sun air mass 1.5 global illumination. In the table below, for the solar cells fabricated from polymers **20** and **22**, their *J-V* characteristics, including J_{SC}, V_{OC}, *FF* and PCE are given. Under the same conditions, and devices fabricated with same configuration, polymers **20** and **22** showed PCEs of 0.026 and 0.18 before annealing and 0.0011 and 0.08 after annealing respectively (Table **8**). The performance of these solar cells were not satisfactory, polymer **22** has a better PCE as compared to polymer **20**. Polymer **20** has higher V_{OC} value of 1.55; however, due to lower J_{SC} values, the performance was poor. These lower values of J_{SC} arise due to larger bandgaps of the polymers. Also, moderate solubility in common organic solvents would affect the morphology of the polymers and lead to lower *FF* values. Hence, we need polymers with lower bandgaps and improved solubility in most of the organic solvents.

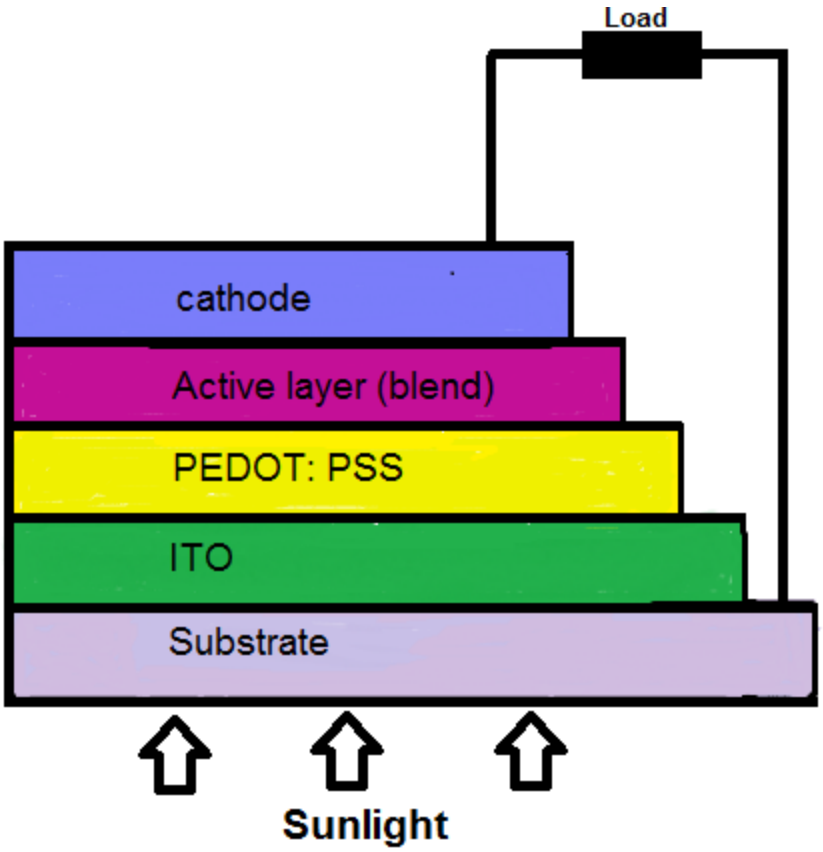

Figure 98: Design of photovoltaic device structure.

Table 8: Photovoltaic properties of the polymers ([a] Polymer: $PC_{71}BM$, 1:1 wt ratio).

Polymer: acceptor[a]	**V_{OC} (V)**	**J_{SC} (mA/cm^2)**	**FF**	**η (%)**
20:$PC_{71}BM$	1.55	0.088	0.19	0.026
20:$PC_{71}BM$ (annealed)	0.79	0.011	0.12	0.0011
22:$PC_{71}BM$	0.81	0.88	0.26	0.18
22:$PC_{71}BM$ (annealed)	0.62	0.48	0.27	0.08

3.7 Circular dichroism studies of polymers

The optical studies performed for INDT and NDT-based polymers **20**, **22**, **31**, and **36** suggest that there is folding conformations present in good solvents. However, it does not give direct evidence of folding nature for these polymers. Hence, CD studies of these polymers were carried out (Figure **99**). When these structures fold into a helical conformation, and if there is a preference for one handedness over another, then a CD signal would be detected to show the direct evidence of folding. All the polymers were dissolved in THF (good solubility) and THF: water mixture (60:40) (poor solubility).

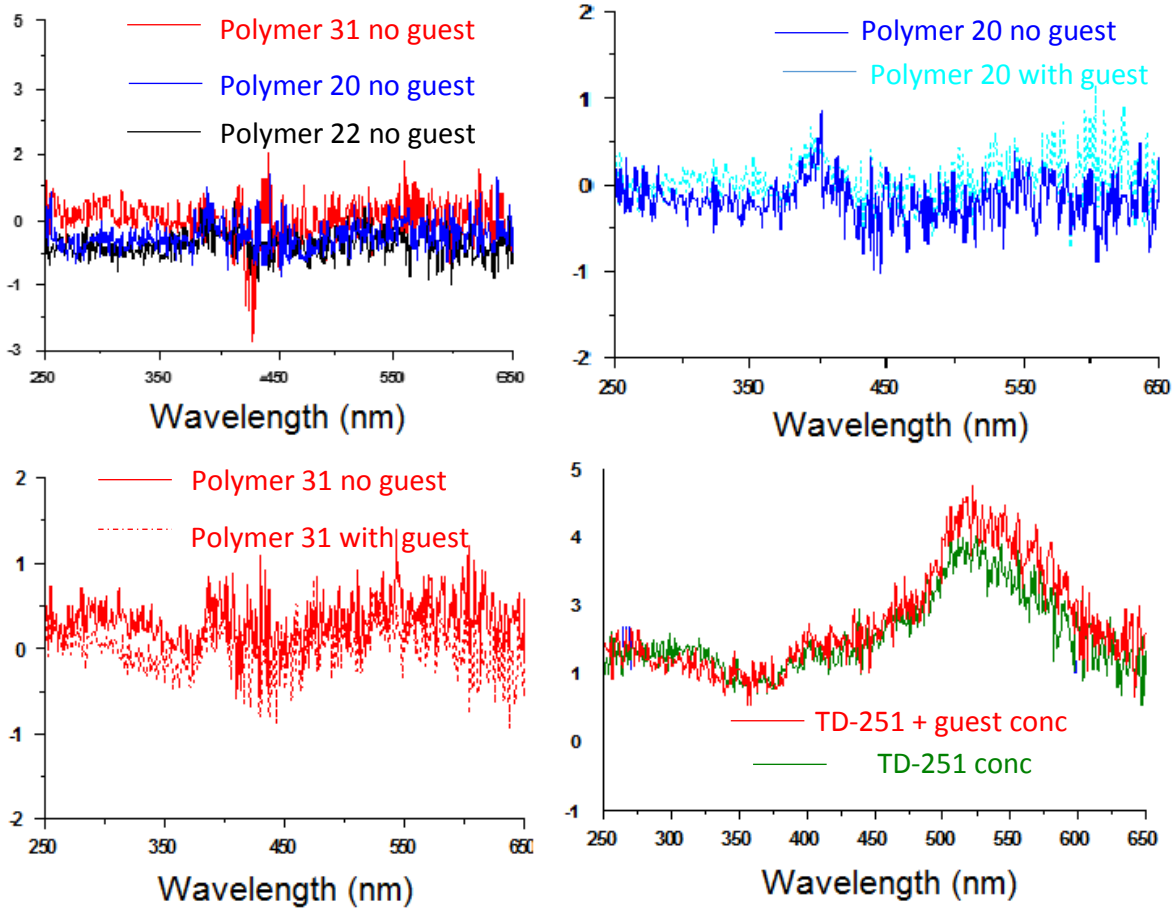

Figure 99: CD spectra of INDT and NDT-based polymers.

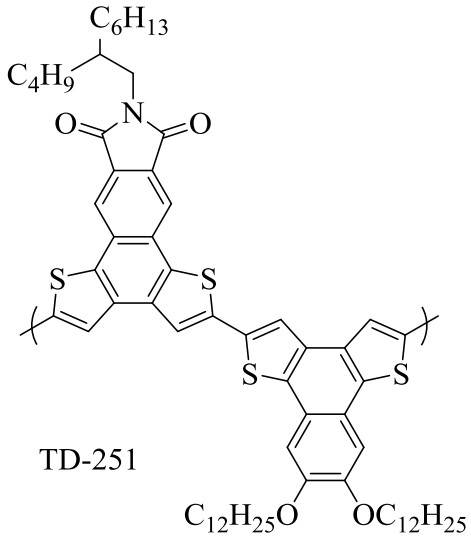

Figure 100: INDT based D-A alternating copolymers used for comparative study

We have also compared some of the previously synthesized polymers **TD-251** in our group for the comparative study (Figure **100**) due to the similarities of the polymer backbone (INDT).[195] As expected for an achiral molecule or for a racemic mixture, none of these polymers show discernable signals in the CD spectra. Amongst all the polymers tested for the CD spectroscopy, **TD-251** exhibited clear CD signals in the wavelength range of 550 nm. Although the alkylating agents used for the synthesis of monomers are racemic and alkyl chains have no absorption, the CD signal suggests that there is a dominance of one helix (*P* or *M*) over another. Also, the highly crystalline nature of **TD-251** was seen after precipitation, and is possible that **TD-251** foldamers with same handedness are aggregated during solution concentration making one handedness dominant. Such solution with dominant handedness would yield a signal in CD spectra. This phenomenon was not observed in other polymers. We have also explored using chiral guest molecules such as (*α*- pinene) to bias the folded helices. However it did not resulted in any major changes in the CD signals, also in case of **TD-251** guest-induced changes were small and slow, and since the strong intra-chain π-π stacking interactions would make the folded helices very stable and difficult to unfold. Additional

studies are required to perform these CD studies for other polymers and choice of appropriate guest molecule that would induce the folding would help to create the helical bias and in turn give the CD signals in them.

3.8 Conclusion and future directions

We have synthesized the naphthalene dithiophene and imide functionalized naphthalene dithiophene based D-A alternating copolymers and have studied their optical, electrochemical, and photovoltaic properties. We also compared them with the theoretical energy calculations obtained by using the Gaussian03 program. The results of their optical and electrical properties are summarized in Table **9**. The optical data suggests the lowering of the energy band gap for INDT-polymers compared to NDT-polymers which is in accordance with the hypothesis of introduction of imide moiety in the system. The CV measurements however showed increase in energy gap for INDT-polymers, which was also in agreement with the DFT calculations.

Table 9: Optoelectronic properties of the polymers **31, 36, 20**, and **22**.

Polymer	λ_{max}^{abs} **(nm)**	E_g^{opt} **(eV)**	**Experimental (eV) CV**			**Calculated (eV) DFT**		
			E_{HOMO}	E_{LUMO}	**Eg**	E_{HOMO}	E_{LUMO}	**Eg**
31	370	2.81	-5.38	-3.64	1.74	-5.27	-2.65	2.62
36	436	2.34	-5.24	-3.45	1.79	-5.28	-2.72	2.56
20	520	2.19	-5.31	-2.98	2.33	-5.29	-2.55	2.74
22	520	2.17	-5.31	-2.98	2.33	-5.29	-2.55	2.74

The optical data of polymers in the NDT and INDT-polymers showed that these polymers adopt different conformations (folding in good solvents) and interchain aggregation in solvents with poor solubility. Although, these are no direct evidences and hence CD studies were carried out to confirm the presence of helical folding in these structures. The absence of any clear signals in the CD spectra indicates that these conjugated polymers may be simultaneously distributed and introduction of a specific guest to induce preferential handedness of one over another may be needed to observe any real change in these spectra. Further studies are required in this regard.

We have also studied the photovoltaic properties of these polymers and polymer **22** showed one of the highest PCE amongst the INDT-based D-A alternating copolymers[195] under ambient conditions. Although these solar cell results are not exceptional, there may be several factors affecting them such as wider bandgap, lower solubility, and the pitch radius of these polymers may be too small for the encapsulation of any guest within the folded helices. Hence, we designed the polymers with hydrophilic side chain which would have the solvophobic interactions and π-π stacking which are essential factors for the non-covalent interactions in folding.

In addition, we are also exploring the possibilities of introducing new heterocycles in the polymer backbone such as fluorine. Fluorination was found to have achieved modulation in HOMO and LUMO energy levels and optical properties to some extent.[196] Moreover, intermolecular interactions involving fluorine atoms have significant influence on blend film morphology as well as resulting organic photovoltaic solar cells showed some of the highest PCE values reported.[197] With this in mind, we have also proposed to synthesize polymers with

fluorine heteroatoms in the donor units as shown in Figure **101** and study their effect on the solar cell performance.

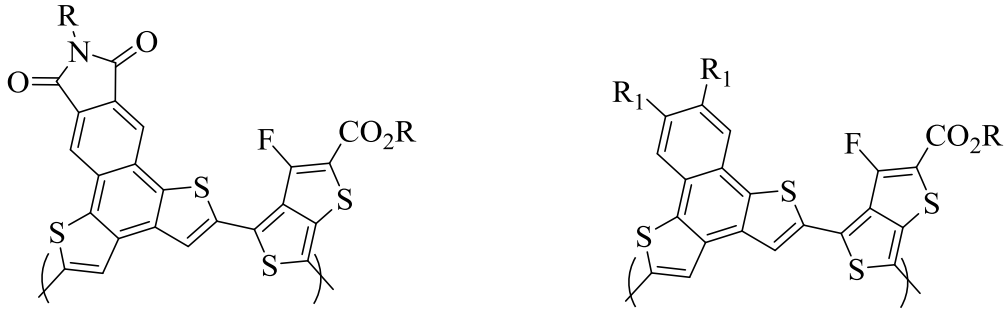

Figure 101: Proposed D-A alternating polymers with F heteroatoms in the system.

3.9 Experimental section

Solvents were distilled from appropriate drying agents under inert conditions prior to use. Unless otherwise stated, all other chemicals were purchased from commercial sources and used without further purification. All reactions were carried out under nitrogen using standard Schlenk apparatus. [6,6]-phenyl-C_{71}-butyric acid methyl ester ($PC_{71}BM$) was purchased form Nano-C, Inc. Highly conductive poly(3,4-ethylenedioxythiophene):poly(styrenesulfonate) (PEDOT:PSS) (Clevios P VP AI4083) was purchased from Heraeus Precious Metals. Indium tin oxide (ITO)-coated glass was purchased from Delta Technologies. ^{1}HNMR and ^{13}CNMR spectra were collected using a Varian INOVA 400 MHz NMR spectrometer. Polymer molecular weights were determined at 30^{0}C on a Tossoh EcoSec HLC 8320GPC system equipped with a differential refractometer, UV detector, and styragel column with THF as the eluent versus polystyrene standard. UV-Vis absorption spectra were measured using a Hewlett-Packard 8452A diode array spectrophotometer. Cyclic voltammetry (CV) studies were carried out under argon atmosphere using BAS Epsilon EC electrochemical station employing a Pt working electrode, a silver wire reference electrode and a Pt wire as the counter electrode. A 0.1 M tetra-n-butylammonium hexafluorophosphate solution in acetonitrile as supporting electrolyte and the scan rate was 20 mVs^{-1}. Fc/Fc^{+} was used as reference for all measurements and assigned an absolute energy of -4.8 eV versus vacuum.

Compound 23

In a 100 mL RBF, compound **2** (1.00 g, 3.09 mmol) was added and dissolved in ethanol (20 mL). It was followed by the dropwise addition of a catalytic amount of con. H_2SO_4 (0.2 mL). The reaction mixture was then refluxed at 80 °C for about 18 h. It was then neutralized by addition of sat. $NaHCO_3$, washed with DI water, and extracted with DCM. The organic layers

were combined. It was dried over $MgSO_4$, filtered. The solvent was evaporated to give compound **23** as a white solid (0.94 g, 2.47 mmol, 80%). ^{1}HNMR (400 MHz, $CDCl_3$): δ 7.93 (s, 2H, Ar-H), 4.33 (q, *J*= 6 Hz, 4H, -OCH_2-), 1.34 (t, *J*= 8 Hz, 6H, -CH_3) ppm.

Compound 24

In a schlenk flask, compound **23** (2.00 g, 5.26 mmol) was added. The flask was subjected to three cycles of pump/ purging with N_2 gas. To this flask, 2-tributylstannous thiophene (4.91 g, 13.1 mmol), tetrakis(triphenylphosphine)palladium(0) (0.31 g, 0.26 mmol) catalyst and anhydrous toluene (100 mL) were added. The resulting reaction mixture was refluxed at 110 °C for 16 h. The solvent was evaporated and the remaining reaction mixture was poured into DI water and extracted with DCM. The organic layers were combined, dried with $MgSO_4$, filtered. The solvent was removed to yield yellow crude product. It was then recrystallized using methanol to give **24** as pure pale yellow solid (1.22 g, 3.16 mmol, 60%). ^{1}HNMR (400 MHz, $CDCl_3$): δ 7.83 (s, 2H, Ar-H), 7.32 (d, *J*= 4 Hz, 2H, Ar-H), 6.97 (dd, *J*= 4 Hz, 2H, Ar-H), 6.96 (d, *J*= 4 Hz, 2H, Ar-H), 4.36 (q, *J*= 8 Hz, 4H, -OCH_2-), 1.36 (t, *J*= 8 Hz, 6H, -CH_3) ppm.

Compound 25

In a RBF, compound **24** (1.00 g, 2.59 mmol) was added and dissolved in chloroform (30 mL) followed by addition of acetic acid (30 mL). To this flask, *N*-bromosuccinamide (2.49 g, 14.0 mmol) was added, and the resulting reaction mixture was stirred at room temperature overnight. The reaction mixture was then diluted with DI water and extracted with DCM. The organic layers were combined and dried with $MgSO_4$, filtered. The solvent was concentrated to give crude product. It was then recrystallized from DCM: methanol to give shiny white crystals of compound **25** (1.06 g, 1.94 mmol, 75%). ^{1}HNMR (400 MHz, $CDCl_3$): δ 7.76 (s,

2H, Ar-H), 6.96 (d, *J* = 4 Hz, 2H, Ar-H), 6.76 (d, *J* = 4 Hz, 2H, Ar-H), 4.36 (q, *J* = 8 Hz, 4H, -OCH_2-), 1.36 (t, *J* = 6 Hz, 6H, -CH_3) ppm.

Compound 26

In a schlenk flask, compound **25** (1.00 g, 1.83 mmol) was added, and the flask was subjected to three cycles of pumping and purging with N_2 gas. To this flask under N_2, freshly distilled anhydrous DCM (120 mL) was added, followed by the addition of $MoCl_5$ (1.51 g, 5.51 mmol). The resulting reaction mixture was stirred at room temperature for one h. Methanol (150 mL) was then added and stirred for an additional one h. It was poured into DI water and was extracted with DCM. The organic washes were combined and dried over $MgSO_4$. The solution was passed through a 2" filtration column, and the solvent was then evaporated to give yellow crude product. It was recrystallized from DCM: MeOH to afford compound **26** as white crystals (0.50 g, 0.92 mmol, 50%). ^{1}HNMR (400 MHz, $CDCl_3$): δ 8.34 (s, 2H, Ar-H), 7.66 (s, 2H, Ar-H), 4.42 (q, *J* = 8 Hz, 4H, -OCH_2-), 1.41 (t, *J* = 6 Hz, 6H, -CH_3) ppm.

Compound 27

In a 250 mL RBF, compound **26** (0.20 g, 0.37 mmol) was added, followed by the addition of a solvent mixture of ethanol: DI water (1:2 v/v) (60 mL). To this flask, potassium hydroxide (2.07 g, 36.9 mmol) was added, and the reaction mixture was refluxed overnight at 80 °C. It was then neutralized with dil. HCl until the pH was 2. The white solid was precipitated, filtered, washed with DI water and dried to give compound **27** (0.09 g, 0.19 mmol, 50%). ^{1}HNMR (400 MHz, DMSO-d_6): δ 13.5 (br, 2H, -COOH), 8.32 (s, 2H, Ar-H), 8.24 (s, 2H, Ar-H) ppm.

Compound 30

Ethylenedioxythiophene (0.50 g, 3.52 mmol) was added to a schlenk flask. The flask was subjected to pump/ purging cycle with N_2 gas three times. To this flask, freshly distilled

anhydrous THF (30 mL) was added, and the flask was cooled to -78 °C. n-Butyl lithium (2.5 M in hexane) (3.10 mL, 7.74 mmol) was added dropwise to the solution. The resulting solution was stirred at -78 °C for 1 h and at room temperature for an additional 1 h. It was again cooled to -78 °C, and tri(n-butyl)tin chloride (2.87 g, 8.79 mmol) was added dropwise. After the addition was complete, the reaction mixture was stirred at room temperature for another one h. The reaction mixture was diluted with DCM and washed with DI water. The organic layers were combined, dried over $MgSO_4$ and filtered. The solvent was evaporated to give dark colored crude product. It was then purified using alumina column with hexane: triethyl amine (95:5) as the eluent to give compound **30** as a thick pale yellow liquid (1.90 g, 2.64 mmol, 75%). ^{1}HNMR (400 MHz, $CDCl_3$): δ 4.10 (s, 4H, -OCH_2), 1.55 (m, 12H, -Sn-CH_2-), 1.32 (m, 12H, -CH_2-), 1.07 (m, 12H, -CH_2-), 0.87 (*t*, *J* = 8 Hz, 18H, -CH_3) ppm.

Polymer 31

In an two neck schlenk flask under argon protection, compound **27** (100 mg, 0.21 mmol), compound **30** (151 mg, 0.21 mmol), tris(dibenzylideneacetone)dipalladium(0) (9.16 mg, 0.01 mmol) and tri(o-tolyl)phosphine (24 mg, 0.08 mmol) were added. The flask was subjected to three cycles of pump and purge with argon. To this flask, oxygen free *N*,*N*-dimethylformamide (5 mL) was added, and the reaction mixture was refluxed at 150 °C for 48 h. It was then cooled to room temperature, and the reaction mixture was poured to the solvent mixture containing methanol (45 mL) and 12 N HCl (5 mL). It was stirred for an additional three h. The precipitate was collected by centrifugation and poured into solvent mixture containing methanol (45 mL) and chloroform (5 mL). It was again stirred for three h and precipitate was collected by centrifugation. The collected crude precipitate was dried under reduced pressure to give polymer **31** as a dark brown solid (94 mg, 0.19 mmol, 90%). ^{1}HNMR (400 MHz, DMSO-d_6):

δ 13.5 (br, 2H, -COOH), 8.4 (br, 2H, Ar-H), 8.1 (br, 2H, Ar-H), 4.3- 4.9 (br, 4H, -OCH_2) ppm. Molecular weights from GPC measurements: Mn= 42 kDa, Mw= 69 kDa, PDI= 1.64.

Polymer 36

Polymer **36** was synthesized following the same procedure that was used for the synthesis of Polymer **31**. Yield: (0.09 g, 0.16 mmol, 88%). ^{1}HNMR (400 MHz, $CDCl_3$): δ 4.2- 4.7 (br, 4H, -OCH_2-), 3.2- 3.8 (br, 4H, -OCH_2 on co-monomer), 1.1- 1.4 (br, 6H, -CH_3) ppm. Molecular weights from GPC measurements: Mn= 2.46 kDa, Mw= 2.97 kDa, PDI= 1.21.

Compound 18

In a schlenk flask, compound **13** (1.00 g, 2.11 mmol) was added. The flask was subjected to three cycles of vacuum drying and N_2 purging. To this flask, 2-tributylstannous thiophene (1.97 g, 5.28 mmol) was added followed by addition of tetrakis(triphenylphosphine)palladium(0) (0.12 g, 0.11 mmol) catalyst and anhydrous toluene (50 mL). The resulting reaction mixture was stirred at 110 °C for 16 h. The solvent was evaporated and the remaining reaction mixture was poured over DI water and extracted with DCM. The organic layers were combined, dried with $MgSO_4$ and filtered. The solvent was removed to yield dark yellow crude product. It was then purified by passing over a silica gel column using DCM: hexane (50:50) as the eluent to give pure product **18** as a yellow solid (0.82 g, 1.71 mmol, 81%). ^{1}HNMR (400MHz, $CDCl_3$): δ 7.93 (s, 2H, Ar-H), 7.35 (d, *J*= 4 Hz, 2H), 6.98 (d, *J*= 4 Hz, 2H), 6.98 (m, 2H), 3.68 (t, *J*= 8 Hz, 2H, -N-CH_2-), 1.66 (m, 2H, -CH_2-), 1.23 (m, 18H, -CH_2-), 0.85 (t, *J*= 8 Hz, 3H, -CH_3) ppm.

Compound 19

In a RBF, compound **18** (1.00 g, 2.08 mmol) was added and was dissolved in chloroform (30 mL); followed by addition of acetic acid (30 mL). To this flask, *N*-bromosuccinamide (0.89 g,

5.00 mmol) was added, and the resulting reaction mixture was stirred at room temperature for about 18 h. The reaction mixture was diluted with DI water, and extracted with DCM. The organic layers were collected and dried over $MgSO_4$. The solvent was removed to give crude product. It was purified by column chromatography on a silica gel with DCM: hexane (40: 60) as the eluent, affording **19** as a yellow solid (0.92 g, 1.46 mmol, 70%). ^{1}HNMR (400MHz, $CDCl_3$): δ 7.87 (s, 2H, Ar-H), 6.98 (d, J = 4 Hz, 2H), 6.80 (d, J = 4 Hz, 2H), 3.67 (t, J = 8 Hz, 2H, -N-CH_2-), 1.65 (m, 2H, -CH_2-), 1.22 (m, 18H, -CH_2-), 0.86 (t, J = 8 Hz, 3H, -CH_3) ppm.

Compound 21

In a schlenk flask, compound **19** (1.00 g, 1.56 mmol) was added, and the flask was subjected to three cycles of pumping and purging with N_2. To this flask under N_2, freshly distilled DCM (60 mL) was added followed by addition of $MoCl_5$ (1.28 g, 4.71 mmol). The resulting reaction mixture was stirred for one h at room temperature. Methanol (100 mL) was then added and stirred for another one h to give buff colored solid. It was poured into DI water and extracted with DCM. The organic washes were combined and dried over $MgSO_4$. This was passed through a 2" filtration column, and the solvent was then evaporated to give yellow crude product. It was then recrystallized from DCM: MeOH to afford pale yellow crystals of compound **21** (0.50 g, 0.78 mmol, 50%). ^{1}HNMR (400 MHz, $CDCl_3$): δ 8.45 (s, 2H, Ar-H), 7.68 (s, 2H), 3.74 (t, J = 8 Hz, 2H, -N-CH_2-), 1.70 (m, 2H, -CH_2-), 1.22 (m, 18H, -CH_2-), 0.85 (t, J = 8 Hz, 3H, -CH_3) ppm.

Compound 6

3,4-Dimethyoxythiophene (0.50 g, 3.46 mmol) was added in a schlenk flask. The flask was subjected to pump/ purging cycle with N_2 gas three times. To this flask, freshly distilled anhydrous THF (30 mL) was added, and the flask was cooled to -78 °C. n-Butyl lithium (2.5

M in hexane) (3.05 mL, 7.62 mmol) was added dropwise to the solution. The resulting solution was stirred at -78 °C for one h and at room temperature for another one h. It was again cooled to -78 ^{0}C and tri(n-butyl)tin chloride (2.82 g, 8.67 mmol) was added dropwise. After the addition was complete, the reaction mixture was stirred at room temperature for another one h. The reaction mixture was diluted with DCM and washed with DI water. The organic layers were combined, dried over $MgSO_4$, filtered. The solvent was evaporated to give the dark brown crude product. The crude product was purified using basic alumina column using hexane: triethyl amine (95:5) as the eluent to give compound **6** as a thick yellow liquid. (2.00 g, 2.77 mmol, 80%). ^{1}HNMR (400 MHz, $CDCl_3$): δ 3.76 (s, 6H, -O-CH_3), 1.54 (t, J = 8 Hz, 12H, -Sn-CH_2-), 1.31 (m, 12H, -CH_2-), 1.08 (m, 12H, -CH_2-), 0.89 (t, J = 8 Hz, 18H, -CH_3) ppm. C^{13}NMR (100 MHz, $CDCl_3$): δ 156.9, 124.9, 60.3, 28.9, 27.2, 13.6, 10.6 ppm.

Polymer 20

In an two neck schlenk flask under argon protection compound **6** (113 mg, 0.15 mmol), compound **TD-246** (100 mg, 0.15 mmol), tris(dibenzylideneacetone)dipalladium(0) (7.2 mg, 0.007 mmol) and tri(o-tolyl)phosphine (19 mg, 0.06 mmol) were added. The flask was subjected to three cycles of pump and purge with argon. To this flask, oxygen free toluene (5 mL) was added, and the reaction mixture was refluxed at 110 °C for 60 h. It was then cooled to room temperature, and the reaction mixture was poured into a solvent mixture containing methanol (45 mL) and 12 N HCl (5 mL). It was stirred for an additional three h. The precipitate was collected by centrifugation and poured into solvent mixture containing methanol (45 mL) and chloroform (5 mL). It was again stirred for three h, and precipitate was collected by centrifugation. The collected crude precipitate of polymer was dried under reduced pressure and then purified by sequential Soxhlet extraction with methanol and acetone. The residual

polymer was finally extracted with chloroform. The chloroform solution was concentrated and poured into methanol to precipitate the polymer. It was then isolated by centrifugation and dried under reduced pressure to give polymer as a reddish brown solid (82 mg, 0.13 mmol, 84%). ^{1}HNMR (400 MHz, $C_2D_2Cl_4$): δ 7.0-8.0 (br, 4H, Ar-H), 3.2-4.5 (br, 8H, -N-CH_2-, –O-CH_3), 1.75 (br, 1H, -CH-), 1.35 (br, 16 H, -CH_2-), 0.91 (br, 6H, -CH_3) ppm. Molecular weights from GPC measurements: Mn 6.26 kDa, Mw 9.27 kDa, PDI 1.48.

Polymer 22

Polymer **22** was synthesized following the same procedure to that of polymer **20**. Yield: (0.07 g, 0.11 mmol, 68%). ^{1}HNMR (400 MHz, $CDCl_3$): δ 8.59 (br, 4H, Ar-H), 3.5-4.5 (br, 8H, -N-CH_2-, -O-CH_3), 1.2- 1.7 (br, 20H, -CH_2-), 0.86 (br, 3H, -CH_3) ppm. Molecular weights from GPC measurements: Mn 5.0 kDa, Mw 9.7 kDa, PDI 1.94.

CHAPTER 4

IMIDE FUNCTIONALIZED NAPHTHALENE DITHIOPHENE BASED CONJUGATED POLYMERS WITH HYDROPHILIC SIDE CHAINS

4.1 Objective of the hydrophilic side chains

We have discussed in the previous chapter the photovoltaic properties of INDT, NDT-based acceptor monomers, advantages of using them in synthesizing polymers. The mechanism of conversion of photon energy to electrical energy was also explained in detail in the first chapter. The acceptor monomers that have imide functionalization have an added advantage since the substitution on the imide nitrogen does not affect the electronic nature of the molecules. Therefore, solubilizing alkyl side chains can be attached and help to improve the solubility, morphology of the film, and PCE for the performance of the solar cells. The polymers that tend to arrange themselves in a helical conformation in suitable solvents, foldamers, and their folding properties will depend on various non-covalent interactions such as solvophobic interactions, H- bonding, π-π interactions, and Van der Waal's interactions. With this in mind, those compounds that have heteroatoms such as O, N, or S with lone pair of electrons that are capable of forming H-bonding in the solution state are preferable. We have synthesized INDT based polymers with straight (polymer **22**) or branched alkyl chains (polymer **20**) previously. However, the inclusion of e thylene oxide or triethylene glycol would be expected to improve the device performance of these polymers as it would help to prevent steric twisting of the polymer as well as it would improve the solubility of those polymers in number of non-aromatic or non-chlorinated solvents. In addition, these triethylene glycol (TEG) side chains would also have solvophobic interactions in suitable solvents and would

help to arrange these conjugated polymers in the folded conformations and retain these conformations.

4.2 Target molecules

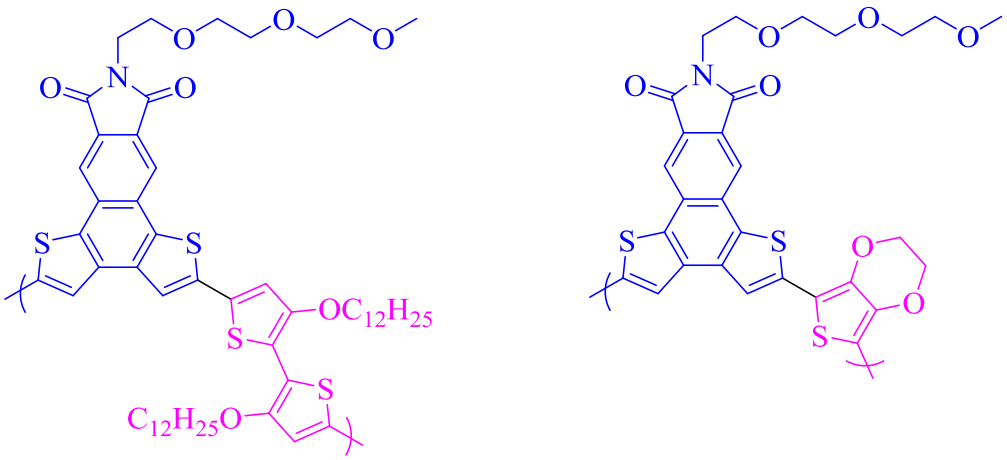

Figure 102: Chemical structures of INDT-based D-A copolymers with TEG side chain.

4.3 Results and discussion

In order to prepare INDT-based conjugated polymers with hydrophilic side chain, the hydrophilic side chain was synthesized initially following the modified literature[198,199] starting from commercially available triethyleneglycol monomethyl ether. The synthetic route for the synthesis of compound **5** is shown in Scheme **15**.

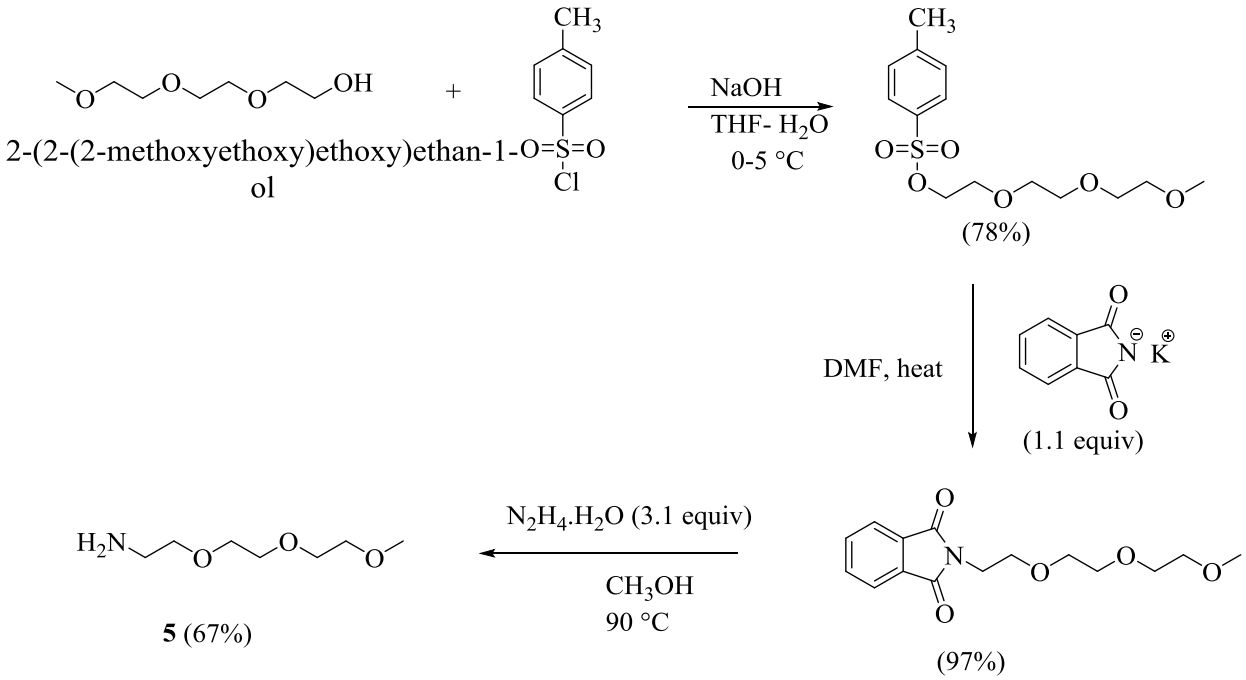

Scheme 15: Synthesis of tri(ethylene glycol) methyl ether amine.

The synthesized compound **5** can be confirmed by the ^{1}HNMR analysis that showed (Figure **103**) no aromatic signal as opposed to its precursor and the broad peak at 2.02 ppm and other peaks from 3.05-3.31 ppm verified the formation of **5**. It was further confirmed by ^{13}CNMR, where all the carbon atoms present in compound **5** were accounted for (Figure **104**).

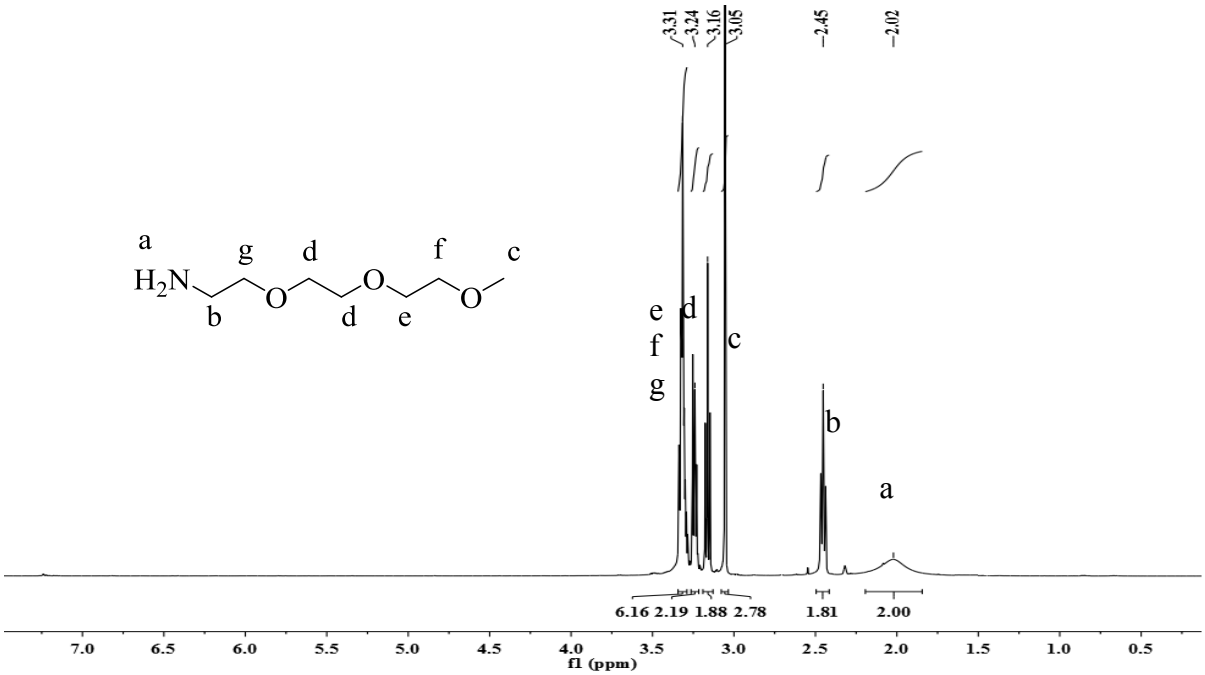

Figure 103*:* [1]HNMR spectrum of compound **5**.

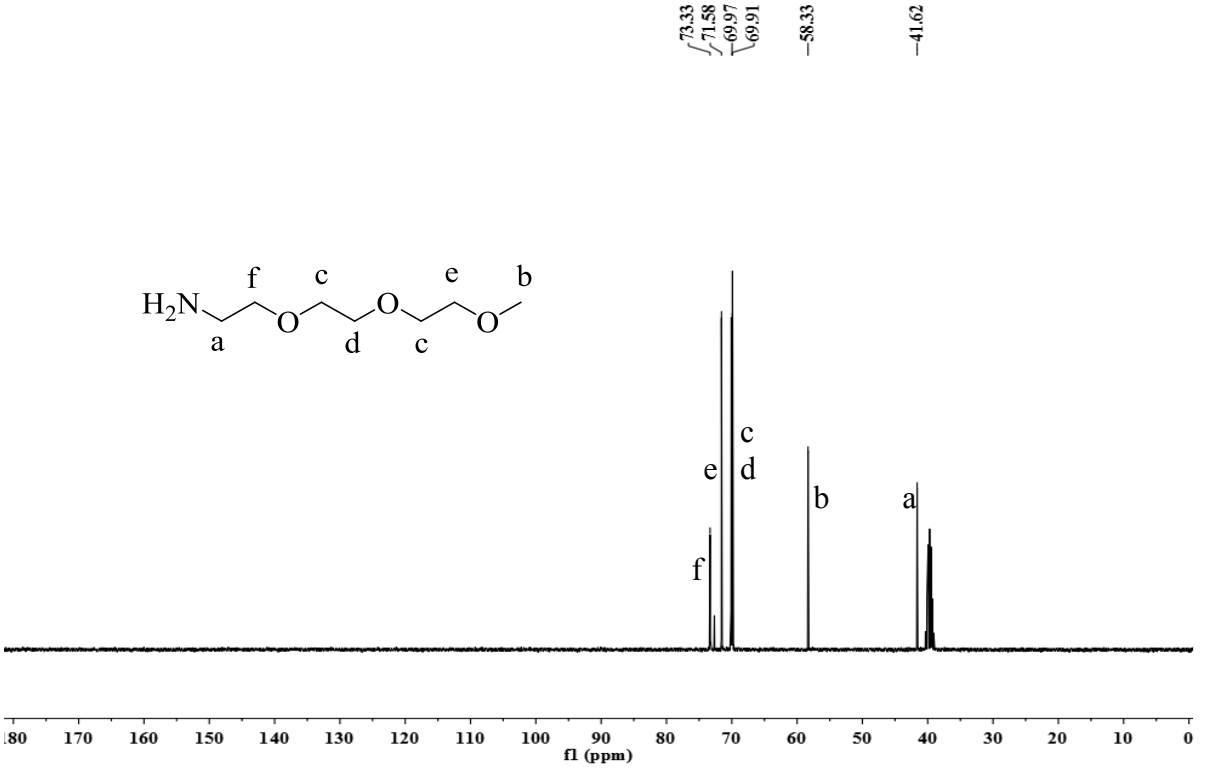

Figure 104: [13]CNMR spectrum of compound **5**.

The NDT-based acceptor monomer was synthesized earlier (**27**) and used as a precursor for the preparation of our target molecule in this Scheme **16**. Upon treatment with acetic anhydride for about 12 h compound **27** gave the corresponding anhydride **32**.

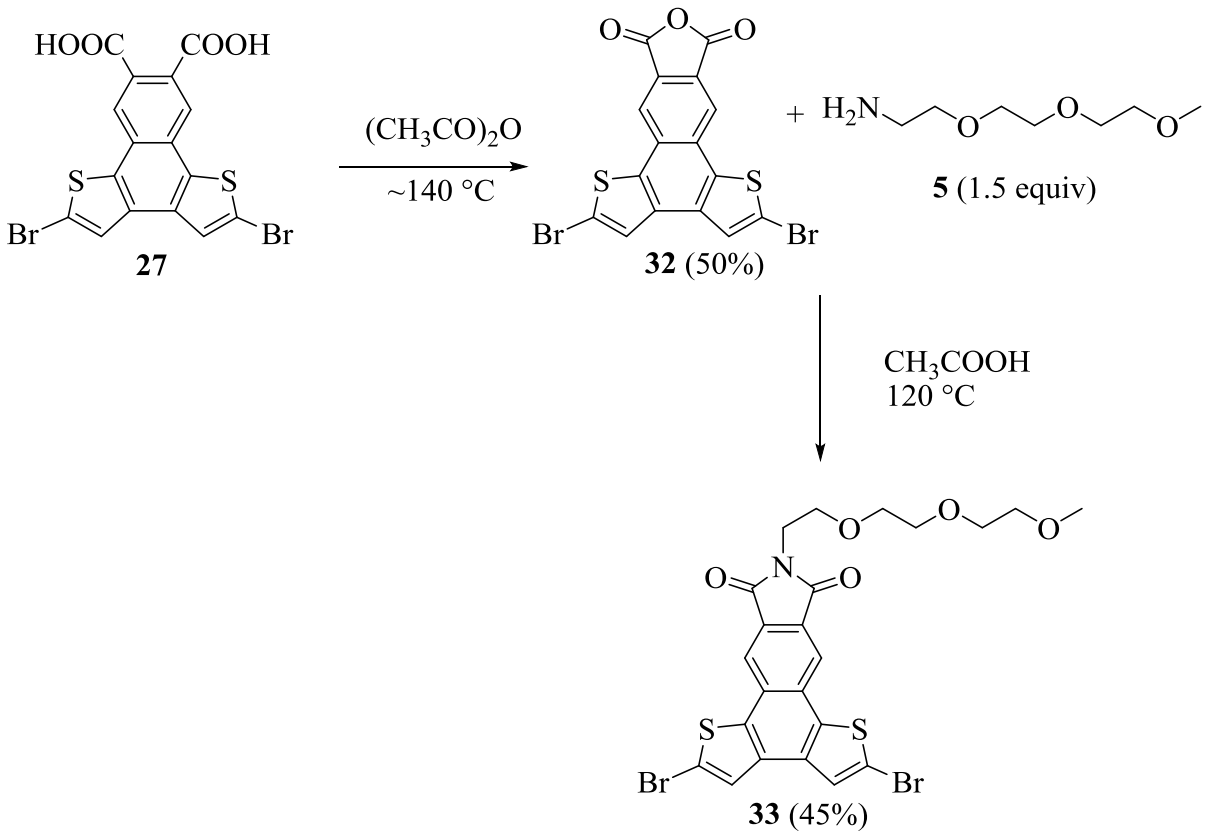

Scheme 16: Synthesis of INDT based acceptor monomer with ethylene oxide side chain

The ^{1}HNMR spectral analysis of compound **32** in DMSO-d_6 showed only two aromatic protons downfield in the aromatic region at 8.35 and 8.85 ppm due to the lack of any other protons in its structure (Figure **105**). Additionally, the IR spectrum of compound **32** also confirmed the completion of the reaction and distinguish it from the starting dicarboxylic acid **27** (Figure **106**). The IR spectrum of compound **27** showed a broad stretch around 2800-3200 cm^{-1} due to the hydroxyl group of the carboxylic acid present in the structure. It also showed a

sharp and strong carbonyl stretch around 1710 cm^{-1} of the carboxylic acid groups. The IR spectrum of compound **32** showed two sharp carbonyl stretches around 1780 and 1820 cm^{-1} due to the anhydride group and the absence of broad stretch around 2800-3200 cm^{-1} confirmed presence of anhydride group in the synthesized molecule.

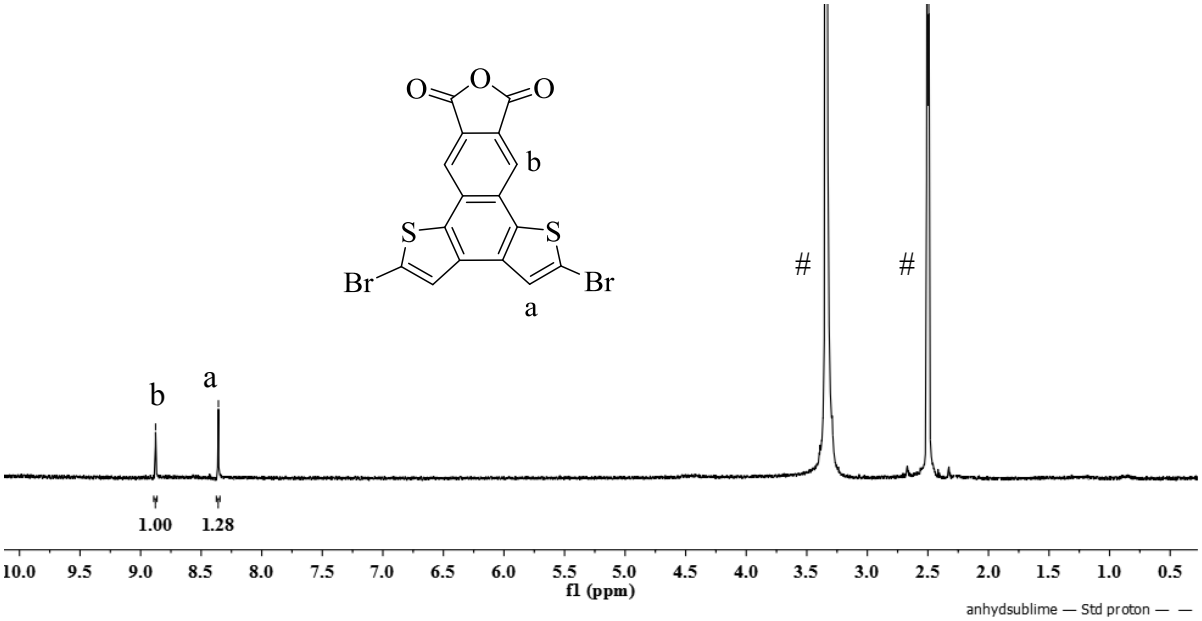

Figure 105: ^{1}HNMR spectrum of compound **32**.

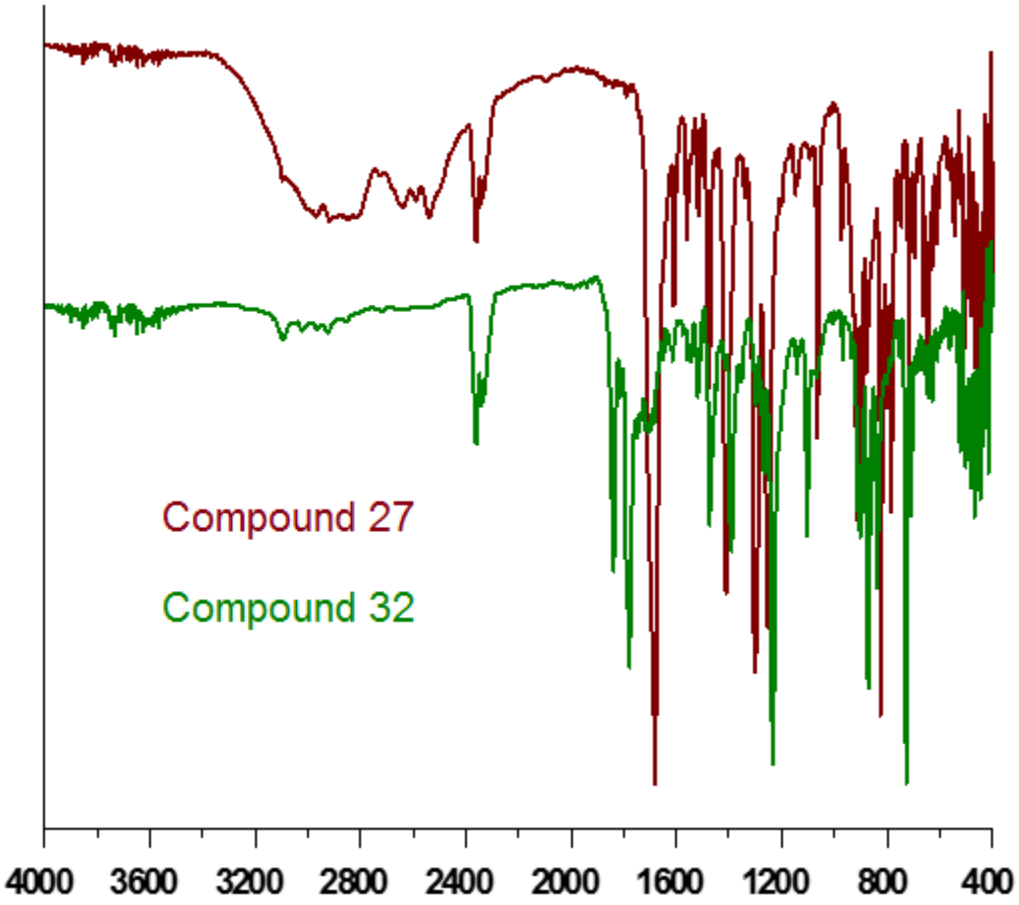

Figure 106: IR spectra of compounds **27** and **32**.

Compound **32** was then treated with compound **5** in the presence of acetic acid to yield compound **33**, INDT-based acceptor monomer. The ^{1}HNMR spectrum of **33** showed two aromatic protons with clear upfield shift in their positions as well as the peaks from 3.11-3.84 ppm for the ethylene oxide side chain confirmed the formation of compound **33** (Figure **107**).

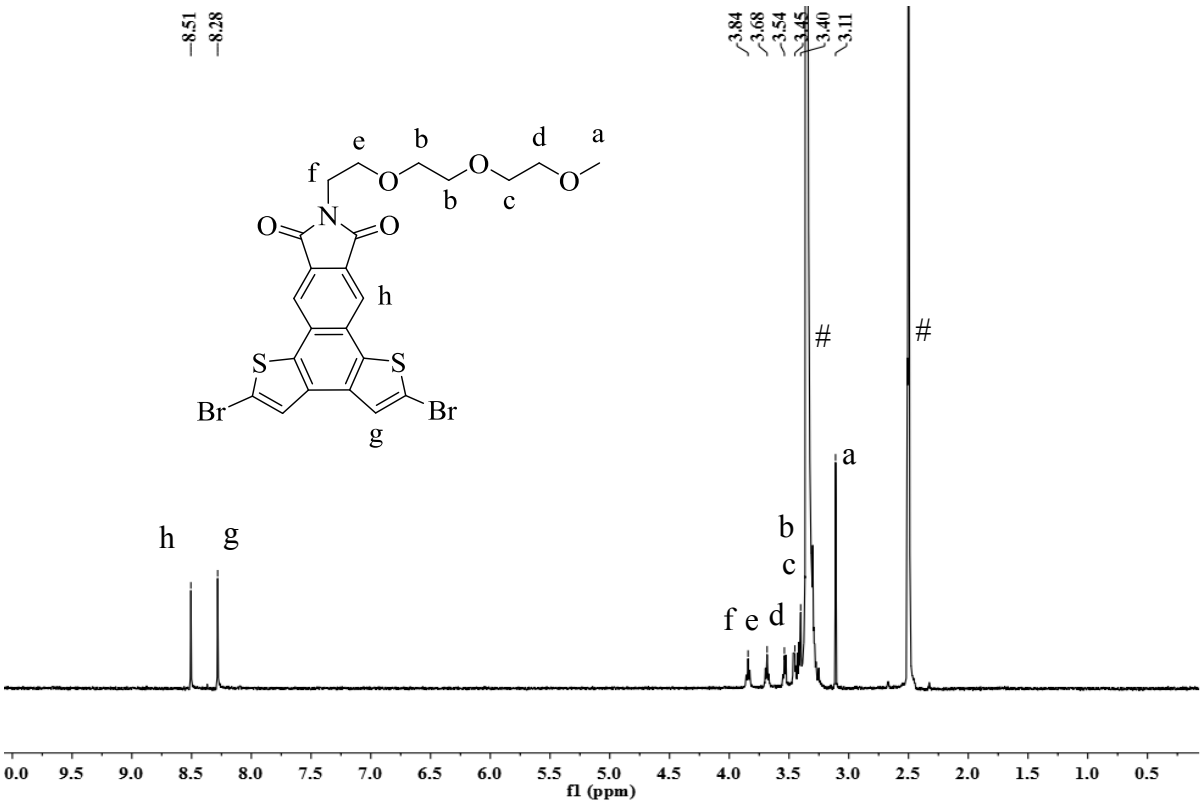

Figure 107: [1]HNMR spectrum of compound **33**.

The polymerization reactions were carried out using Stille cross-coupling reactions to synthesize D-A alternating copolymers with INDT backbone and hydrophilic ethylene oxide side chain at the imide position. (Scheme **17**). DMF was used as a solvent of choice in lower concentrations to perform these polymerizations and refluxed for approximately 48 h.

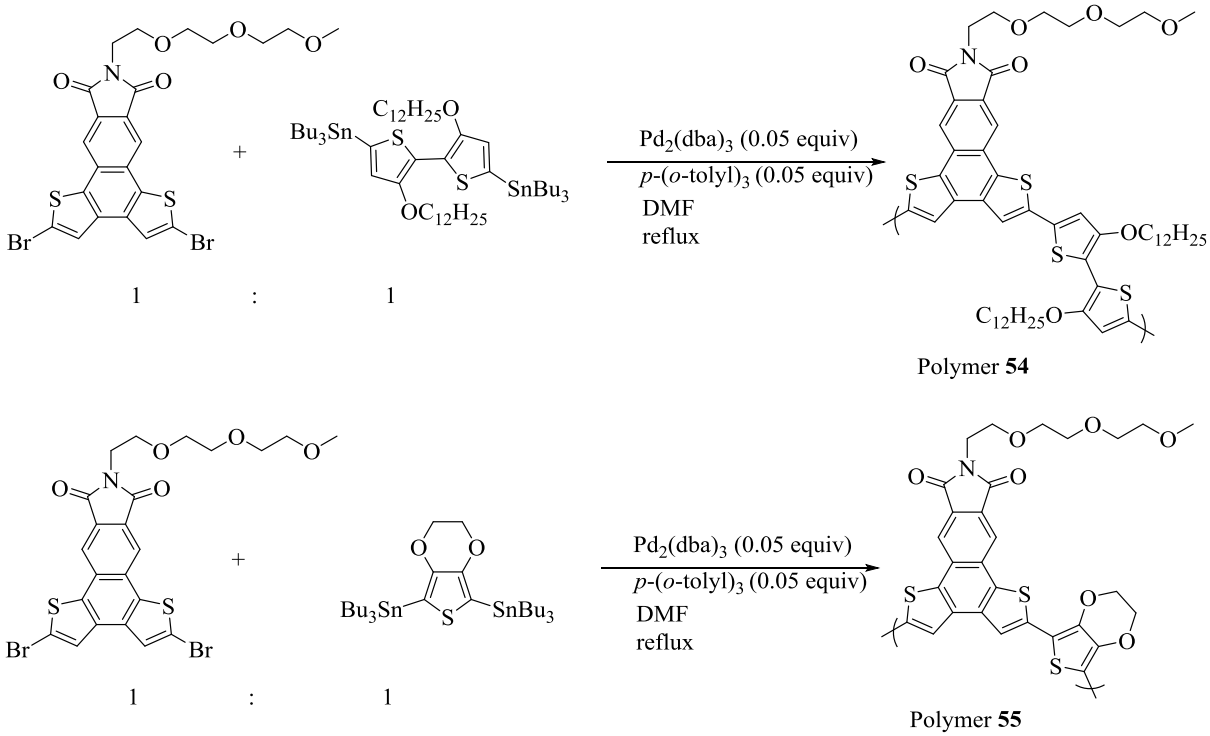

Scheme 17: Synthesis of INDT based D-A alternating copolymers with TEG side chain.

The ^{1}H-NMR spectra of polymers **54** and **55** were taken in $CDCl_3$. In case of both these polymers, the acceptor monomers were identical. For polymer **54**, the ^{1}HNMR spectrum showed broad signals (Figure **108**) for the protons in the region from 0.80-1.40 ppm and from 3.50-4.50 ppm, that are typical of the -$C_{12}H_{25}$ chains and -OCH_2 protons present in the starting monomer. However, due to the π-π stacking between the neighboring repeating units such broadening of peaks could be observed. The aromatic protons were also hidden in case of the polymer.

In the ^{1}H-NMR spectrum (Figure **109**) of polymer **55**, in $CDCl_3$, the broadening of peaks is seen in the region between 3.50 to 4.00 ppm due to the -OCH_2 protons and broad peaks around 4.50 ppm due to the ethylene protons in the donor unit, as well as a broad peak around 9.50 ppm in the aromatic region for aromatic protons was also seen.

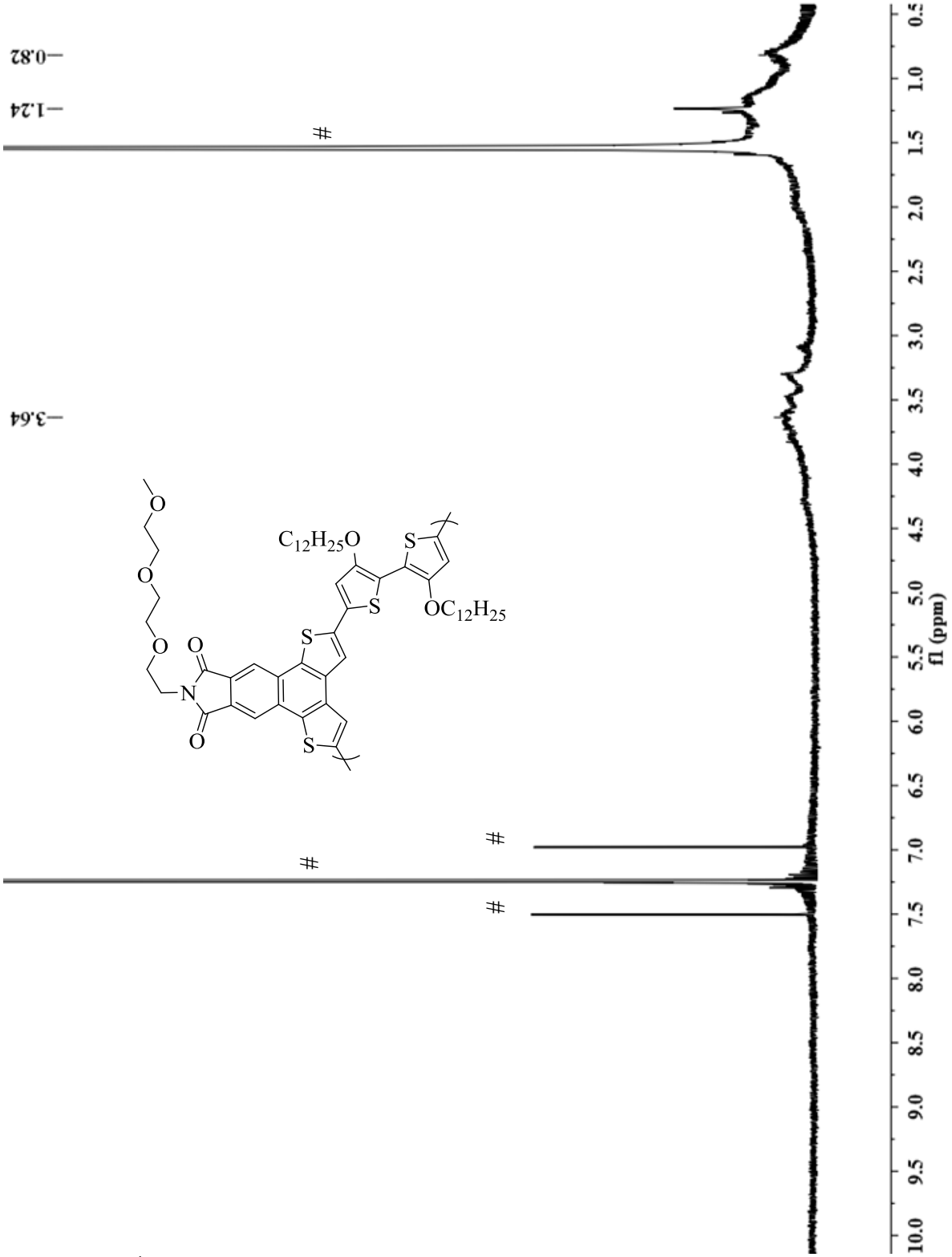

Figure 108: ^{1}HNMR spectrum of polymer **54**.

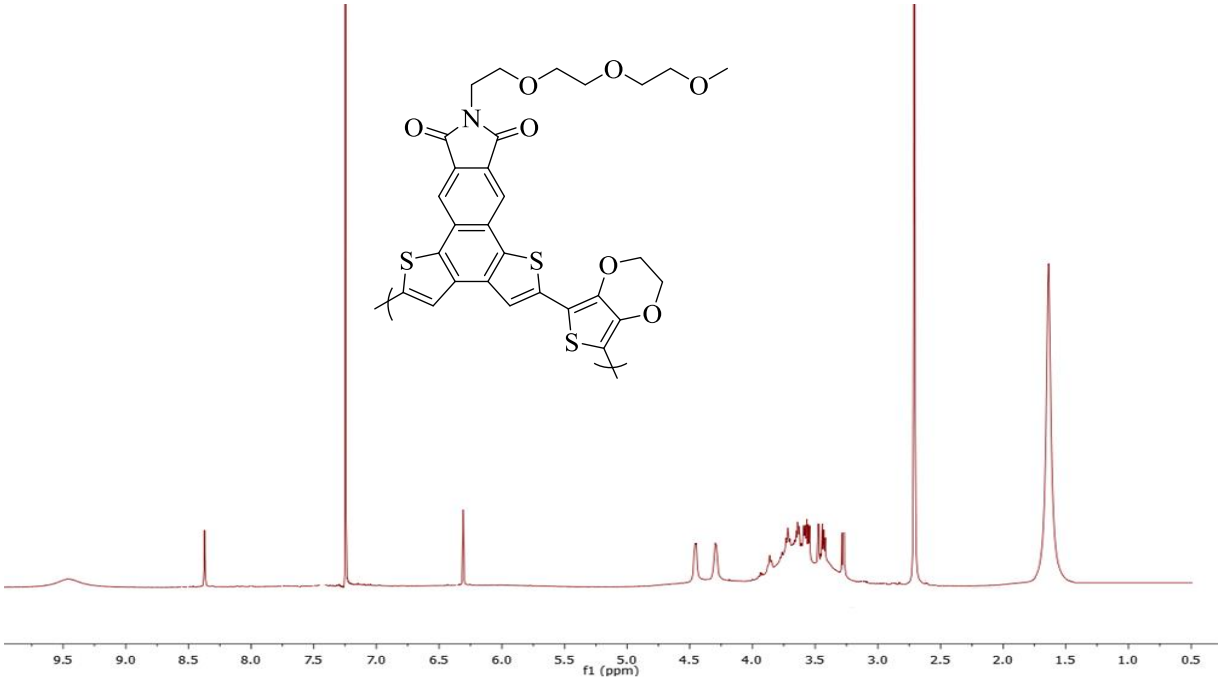

Figure 109: H^1NMR spectrum of polymer **55**.

The molecular weights of polymer **54** and **55** were characterized by GPC analysis using THF as an eluent. The polymers were dissolved in THF, and polymer **55** was readily soluble in THF. However, polymer **54** was only partially soluble in it, hence it was passed through the 0.45 µm filter and the GPC analysis for the soluble component in **54** was recorded. The characterization data for the INDT based polymers **54** and **55** are summarized in Table **10** along with their percentage yields.

Table 10: Polymerization data of polymers **54** and **55**.

Polymer	Yield (%)	Mn (kDa)	Mw (kDa)	PDI
54	88	9.8	21.5	2.19
55	90	29.0	52.0	1.79

4.4 DFT calculations for INDT based copolymers

In order to predict the backbone geometries, folding tendencies and the electronic structures of the polymers, theoretical calculations were carried out on the trimers and tetramers of polymers **54** and **55**. DFT calculations were performed by means of Gaussian03 program using DFT with a B3LYP functional and a 6-31G(d) basis set. For reducing the computational efforts, the triethylene oxide side chain on the INDT unit and the dodecyloxy side chain on the bithiophene unit were truncated to monoethylene oxide and methoxy groups respectively. The different orientations and HOMO/ LUMO energy distributions of energy minimized conformers of the trimer of polymer **54** are shown in Figure **110**.

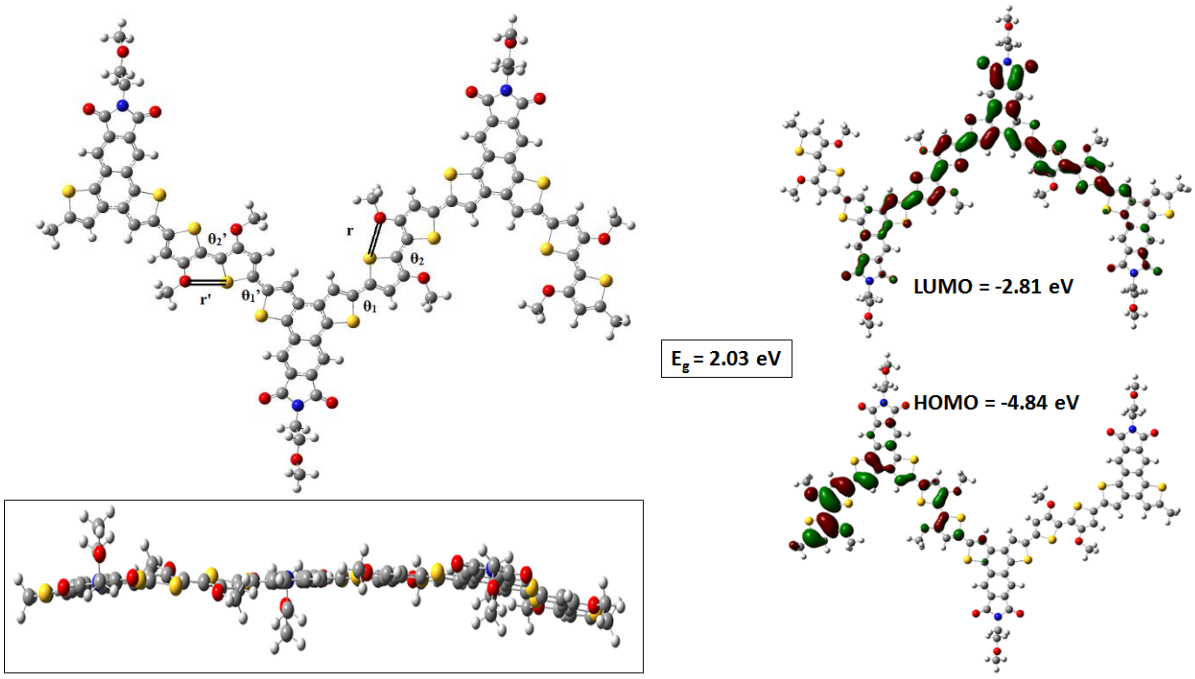

Figure 110: Energy minimized geometries of polymer **54** (trimer) in different views (left) HOMO/ LUMO distributions of energy minimized structures (right).

In the following Figure **111**, different orientations of energy minimized conformers of the trimers of polymer **55** are shown.

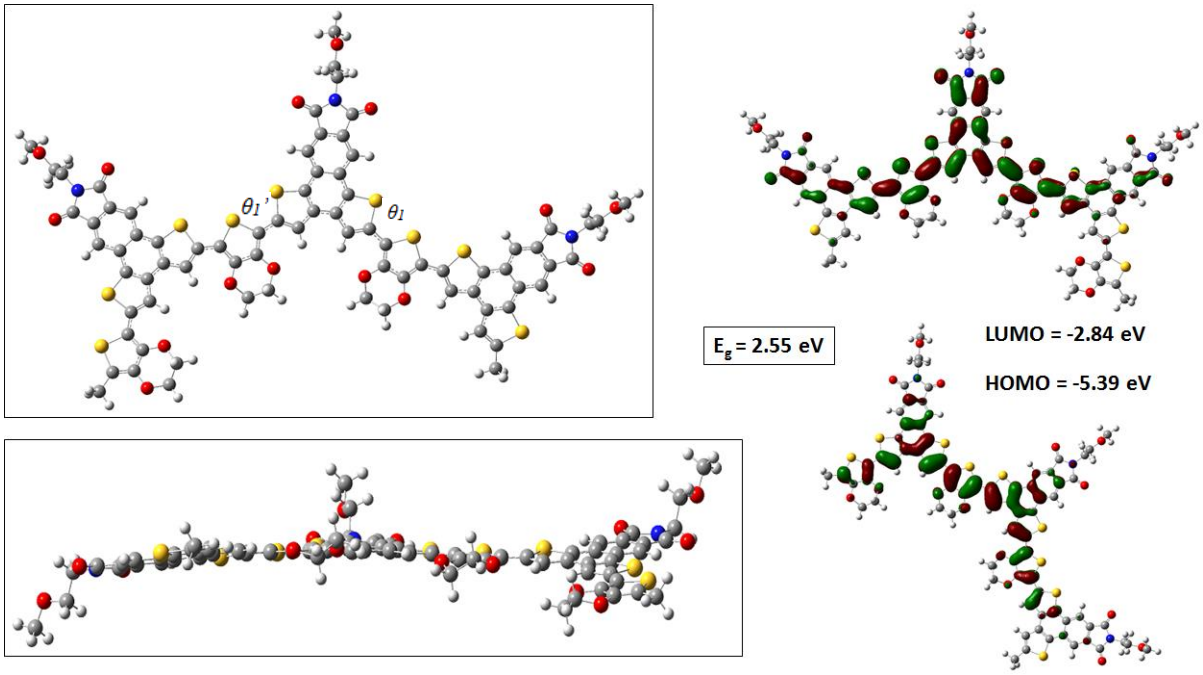

Figure 111: Energy minimized geometries of polymer **55** (trimer) with different views (left) HOMO/ LUMO energy levels for energy minimized structures (right).

Polymers **54** and **55** were also subjected to perform DFT calculations on the tetramer units following the same methods as used for the trimer units (Figures **112**, **113**). From these theoretical calculations (Table **11**), it can be observed that polymer **54** has higher intermonomer twist (13.3° for trimer and 24.6° for tetramers) as compared to polymer **55** (5.3° for trimer and 0.7° for tetramers). Thus, polymer **54** seems to be adopting a slightly more twisted structure due to less short contacts like S-O/ S-N between the comonomer units. In **54**, there was higher comonomer twisting due to the presence of those bithiophene units (56° for tetramers) are thereby it seems to adopt more of a zigzag structure (Figure **125**). While for **55** since the comonomer used contained only single thiophene unit with ethylenedioxy substitution, there was not any twisting present in their conformers. Hence, to have more planar backbone, it will be advantageous to use the polymers like **55** (single thiophene unit) over **54** (bithiophne unit).

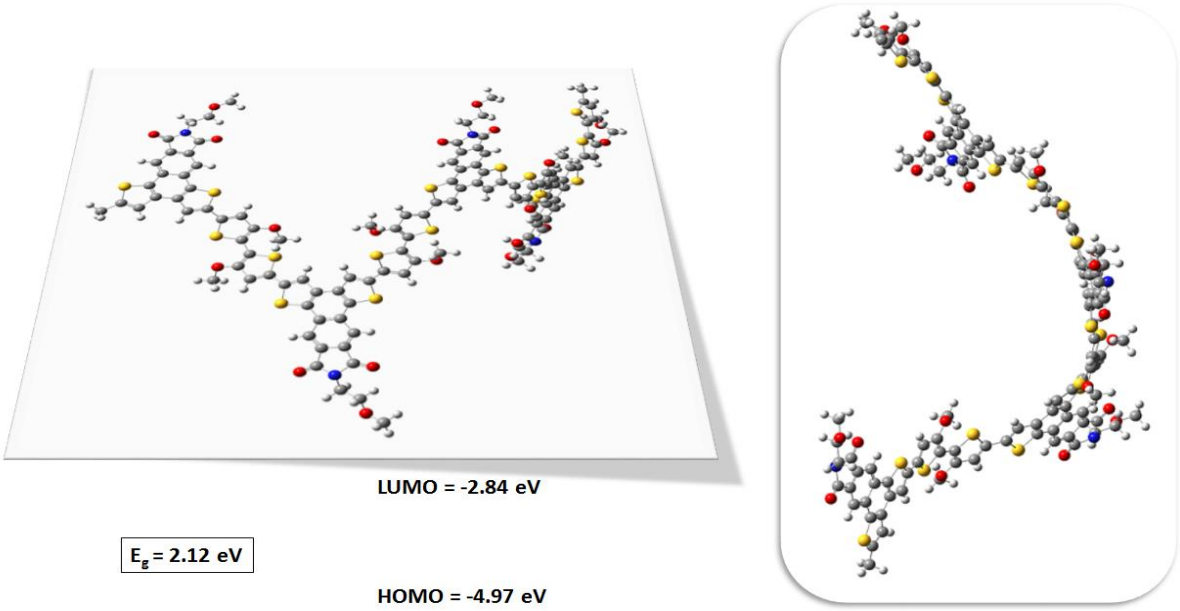

Figure 112: Energy minimized geometries of polymer **54** (tetramer) with different views.

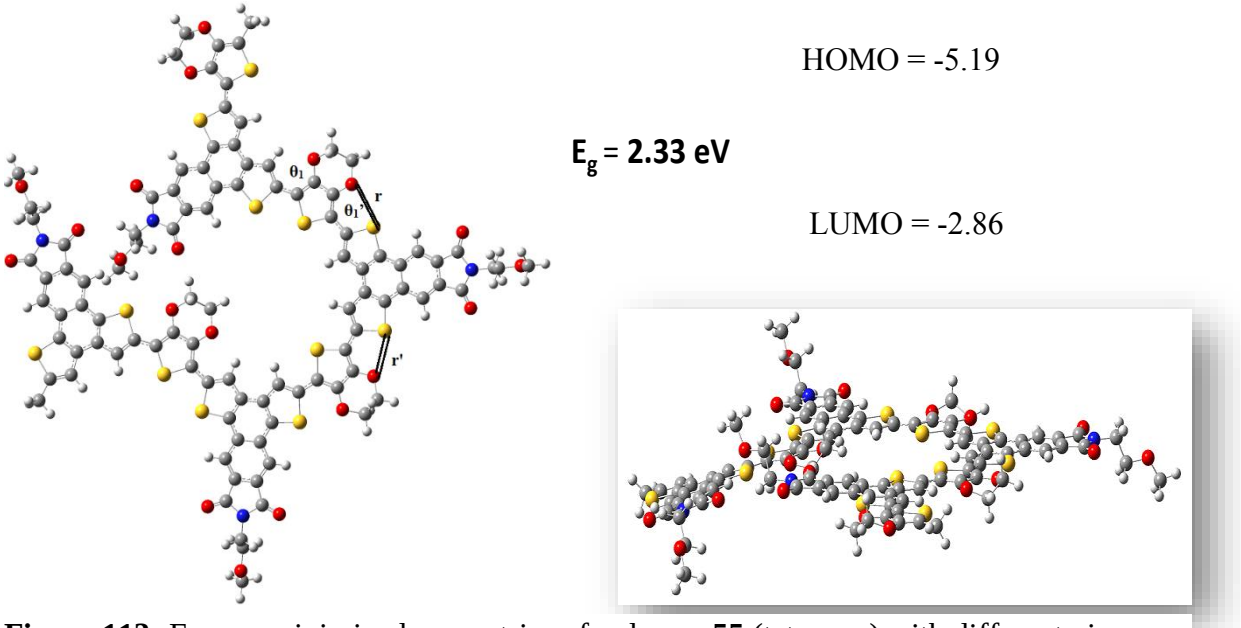

Figure 113: Energy minimized geometries of polymer **55** (tetramer) with different views.

The HOMO and LUMO energy levels and the band gap of the INDT-based polymers were estimated from the energy minimized structures of their trimers and tetramers using DFT calculations at the B3LYP/6-31G(d) level. The HOMO/ LUMO energy levels are -4.84/-2.81

and -5.39/-2.84 for trimers of **54** and **55**, respectively. The band gaps from the calculated HOMO/ LUMO energy levels are 2.03 and 2.55 for trimers of **54** and **55**, respectively. Similar trend was observed in case of tetramer units of both the polymers (-4.97/ -2.84 eV and E_g= 2.12 for **54**; -5.19/ -2.86 eV and E_g= 2.33 for **55**)**.** The LUMO level of both the polymer were similar since both **54** and **55** contain same acceptor units (INDT). However, HOMO level of **54** was increased as compared to **55** since the donor units are different for both the polymers. Polymer **54** containing dodecyloxy side chains and two thiophene units would have additive effect on their donating strength and in turn would increase the HOMO energy level. The effective band gap of **54** (E_g≈ 2.03 eV) was less as compared to that of **55** (E_g≈ 2.55 eV) based on theoretical calculations.

Table 11: Dihedral angles and S--O short contacts for polymers **54** and **55** using DFT calculations.

Polymer	**Intermonomer twist**		**Comonomer twist**		**S—O short contact (Å)**	
	θ_1	**θ_1'**	**θ_2**	**θ_2'**	**r**	**r'**
54 (trimer)	-4.16	-13.26	-1.36	-0.13	2.84	2.84
54 (tetramer)	0.66	-24.63	0.07	-56.29	2.84	NA
55 (trimer)	6.43	5.28	NA	NA	NA	NA
55 (tetramer)	0.08	-0.77	NA	NA	2.88	2.89

4.5 Electrochemical properties of INDT-based D/A alternating copolymers with hydrophilic side chains

The electrochemical properties of the INDT based D/A alternating copolymers with hydrophilic side chains were studied using thin films of polymers **54** and **55** in $CHCl_3$ solution by CV measurements (Figure **114**). The CV spectrum of **54** showed two semireversible oxidation waves in the anodic scan and three irreversible reduction waves in the cathodic scan. For polymer **55**, one reversible oxidation and reduction wave was observed in anodic and cathodic scan, respectively. By using the first onset oxidation potential in the anodic scan and first onset reduction potential in the cathodic scan the HOMO and LUMO energy levels for polymers **54** and **55** were estimated. The HOMO and LUMO energy levels for **54** and **55** were -4.99/-3.51 and -5.74/-4.15 eV, respectively. The effective band gap for these polymers obtained from CV measurements were 1.48 eV (**54**) and 1.59 eV (**55**). Both of these polymers have the same acceptor units. Since the LUMO energies are more dependent on the acceptor units as compared to the donor units, they were expected to be similar. However, the spatial arrangement of these polymers would be different as seen in the theoretical calculations and hence, the backbone planarity of these polymers would be also different (**55** being more planar compared to **54**). The effective band gap of both these polymers are close to each other due to both of them having similar INDT-based acceptor units with hydrophilic side chain and the donor units with heteroatoms that would create S--O short contacts between the comonomers and copolymers.

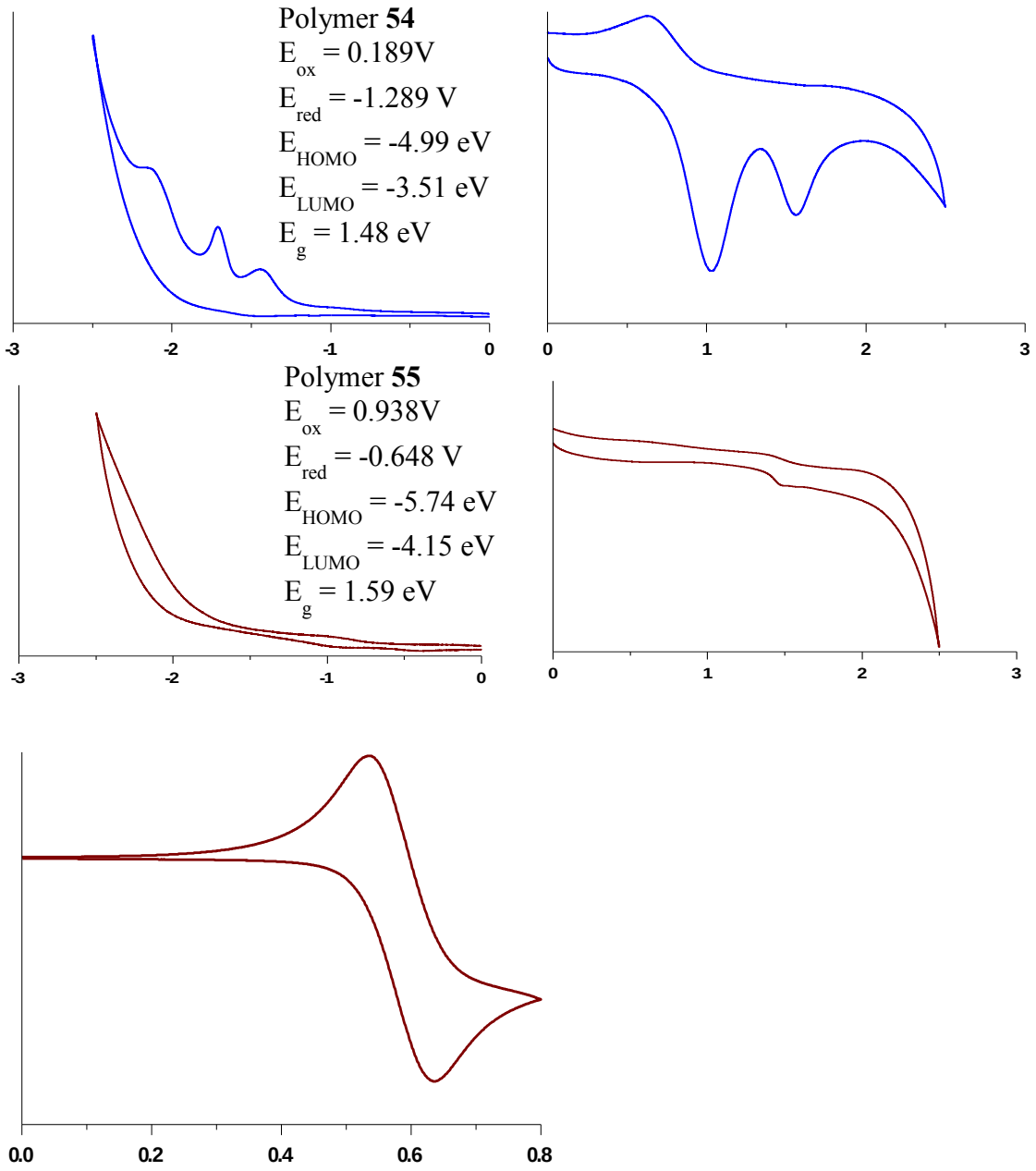

Figure 114: Cyclic voltammograms of polymer **54** and **55** thin films, scale referenced to Fc/ Fc^{+} redox couple.

4.6 Optical properties of INDT-based D-A alternating copolymers with hydrophilic side chains

Both the polymers synthesized with triethylene oxide substitution on the imide nitrogen were synthesized from the same acceptor monomer having INDT-backbone in their unit. The solubility of both these polymers **54** and **55** as expected was good in most of the common organic solvents like *o*-DCB, acetone, DCM, DMF, DMSO, and ethyl acetate. The absorption spectra of polymer **54** was studied in $CHCl_3$ and shown in the Figure **115**. In $CHCl_3$, however, **54** was mostly soluble, but some of the solid remained undissolved in it, and hence, filtered and then used for the optical measurements.

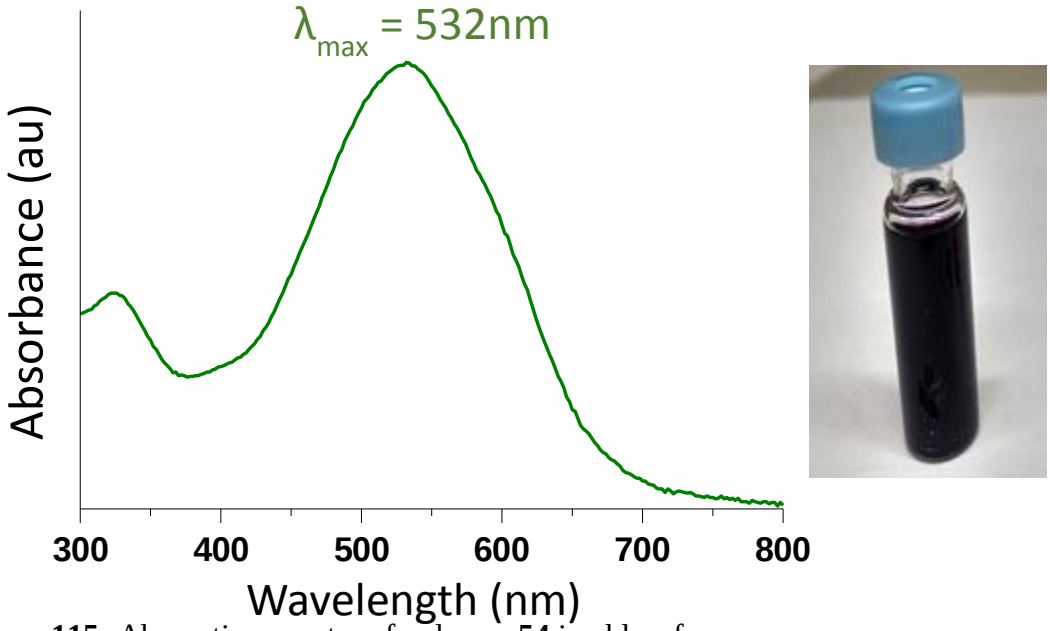

Figure 115: Absorption spectra of polymer **54** in chloroform.

The absorption spectra of polymer **54** produced a strong and sharp absorption with the absorption maxima at 532 nm with no other shoulder or minor peaks in the absorption region. The absorbance peak around 320 nm would be due to the monomer. Polymer **54** has a weak fluorescence and also a maximum red shift as compared to other polymers with INDT-based

units studied thus far previously. When excited at 532 nm the fluorescence emission spectra of polymer **54** resulted in emission band at 600 nm. Also, the excitation spectra at the emission wavelength of 600 nm gave only one major peak 570 nm similar to the absorption spectra. This suggests, that only one type of conformation would be present in chloroform (Figure **116**).

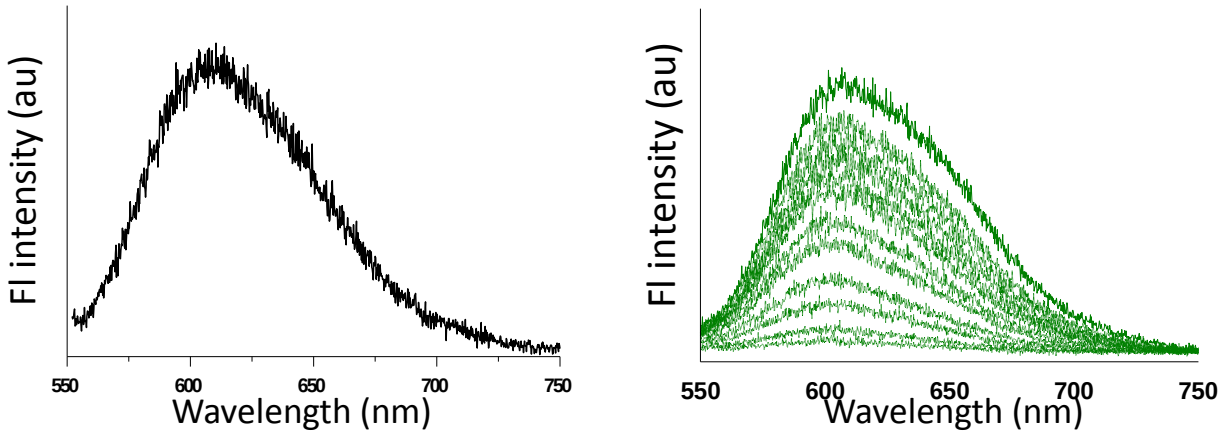

Figure 116: Emission spectrum of polymer **54** in chloroform (left) dilution effect (right).

Additionally, the dilution experiment of **54** in chloroform also validated that there were no other major peaks present in the emission spectra as depicted in the following figure. The solution of **54** in chloroform showed emission band at 600 nm and this solution was continuously diluted by adding more chloroform into it. Upon continuous dilution, it was observed that there was no significant change in the position or the pattern of the fluorescence emission for **54** in chloroform. This again suggests that there is only one type of conformer prevalent for **54** in chloroform. The intensity ratio of emissions at 600 nm decreases when the solution is further diluted, indicating that the emission is likely due to polymer aggregation (intramolecular excimer emission) and the aggregation likely account for weaker fluorescence.

The absorption spectrum (Figure **117**) of polymer **55** in chloroform, which has good solubility, showed the absorption maxima at 382 nm and 410 nm along with a shoulder peak observed at 495 nm.

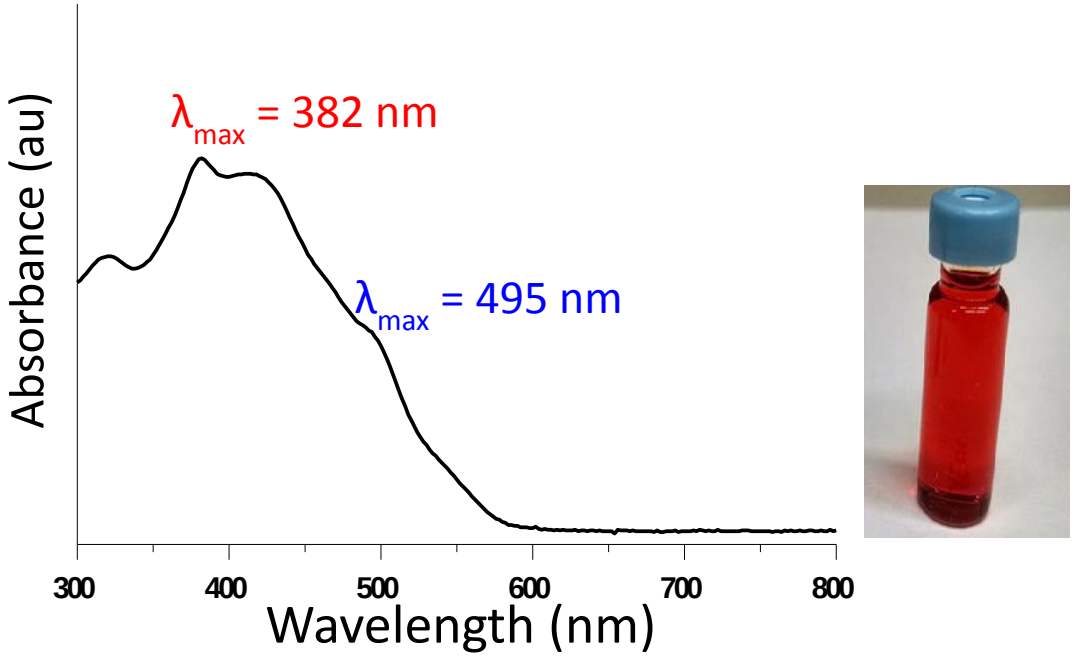

Figure 117: Absorption spectrum of polymer **55** in chloroform.

Polymer **55** is highly fluorescent in chloroform solution. When it is excited at different wavelengths corresponding to absorption maxima in the absorption spectra namely at 320, 425, 382, and 495 nm, it produced only one strong emission band at 520 nm. The excitation at 495 nm resulted in emission that had slight shoulder around 553 nm (Figure **118**). The excitation spectra of **55** in chloroform gives pattern similar to that of the absorption spectra. The absence of any other fluorescence emission for **55** in good solvent suggests the presence of only one type of conformations and such strong emissions are typically due to foldamer conformers. Upon further investigation, dilution experiments were carried out using solution of **55** in chloroform (Figure **119**).

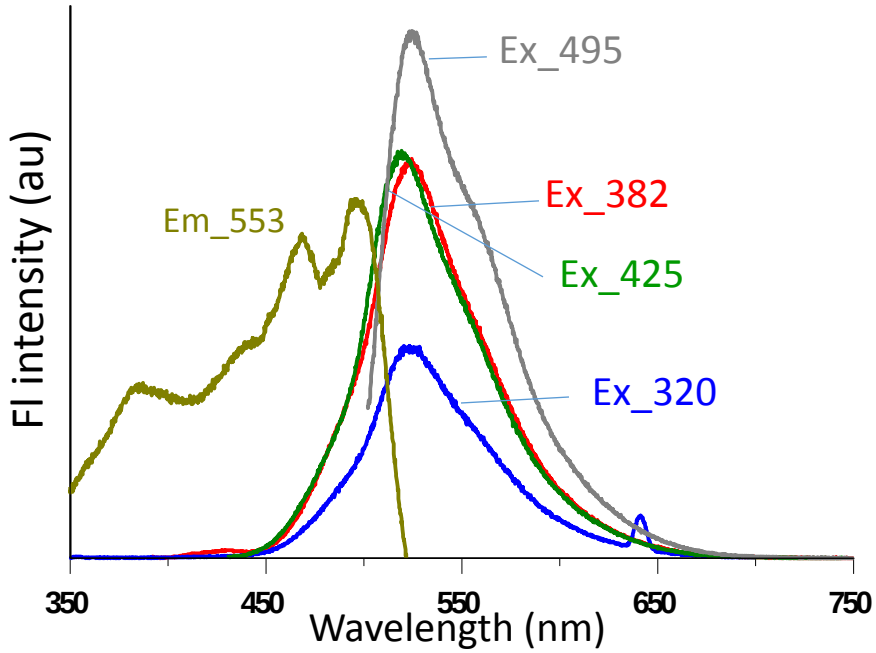

Figure 118: Emission and excitation spectra of polymer **55** in chloroform.

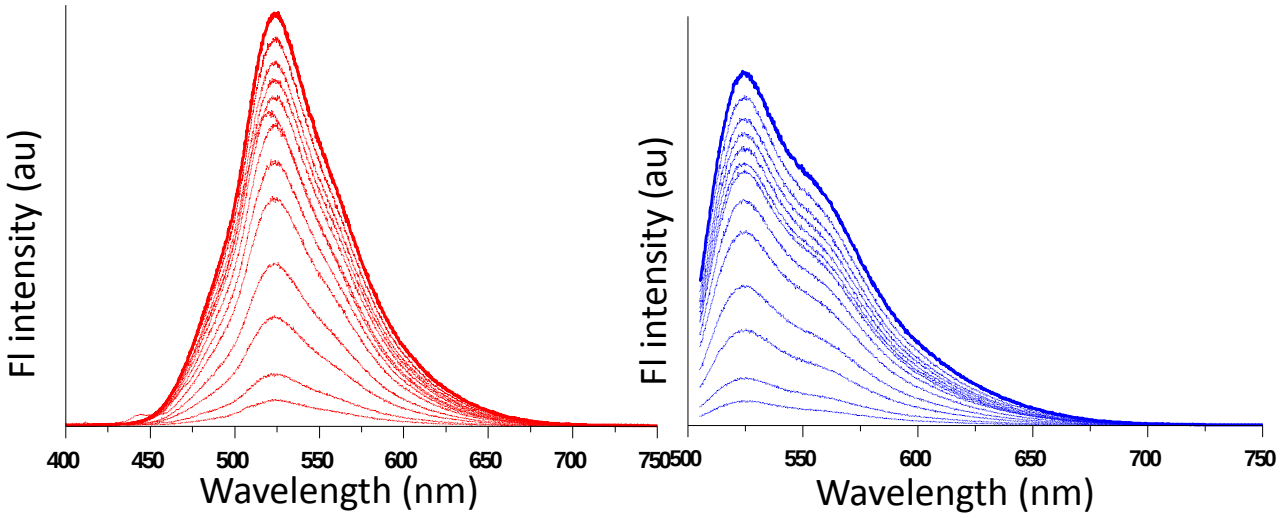

Figure 119: Dilution effect of chloroform in polymer **55** at 382 nm (left) and 495 nm (right).

The solution of polymer **55** was subjected to concentration dependence study in in good solvent like chloroform (Figure **119**). The solution [1 mg of **55** in 2 mL $CHCl_3$] was then subjected to continuous dilution, and the subsequent fluorescence emission spectra excited at 382 and 495 nm were recorded as shown in Figure **133**. There was no shift in the broad featureless emission spectra at both wavelengths that would be due to the folding and suggests that polymer **55** maintain its folding conformation at all concentrations in a good solvent. This effect was also seen in polymer **54** when dilution experiment was carried out.

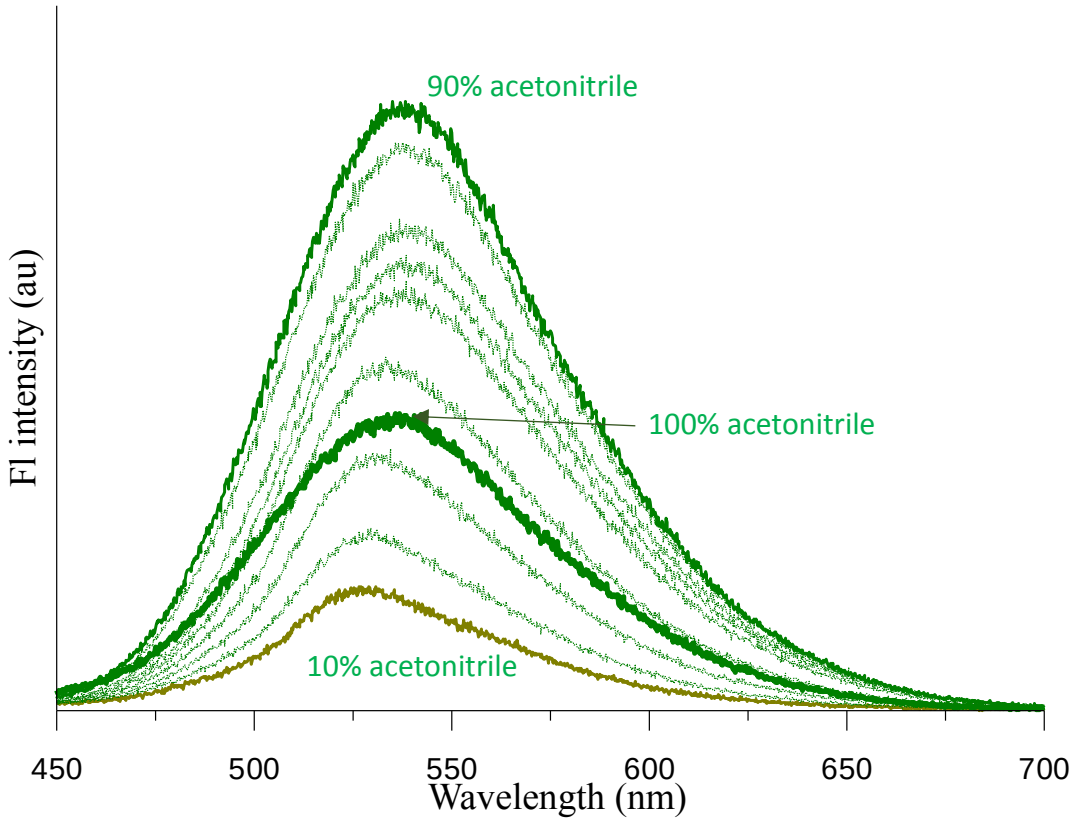

Figure 120: Emission spectra of polymer **55** (chloroform in acetonitrile).

In addition, the solution of **55** in acetonitrile was subjected to continuous dilution with chloroform to study the behavior of their emissions in different solvents (Figure **120**). It was observed that there was slight blue shift in their emission wavelengths as the chloroform content increased, however the shape of the emission peaks remained unchanged. Further, the solvent dependence study for **54** is in progress to see if the folding emissions are consistent in different solvents. Hence, it is likely that polymer **54** seems to be forming random aggregates in good solvents while polymer **55** seems to be forming folding conformers in solvents with good and poor solubility.

4.7 Conclusion and future directions

We have successfully synthesized imide functionalized naphthalene dithiophene based D-A alternating copolymers with trietheylene glycol as the hydrophilic side chain and using bithiophene units as the donor monomers in polymer **54** and and ethylene dioxy thiophene units as donor units in polymer **55**. We also tested the polymers for their theoretical energy values (trimers as well as tetramers) using DFT calculations and measured their electrical and optical properties and the summary of their optoelectronic properties are given in the following Table **12**.

Table 12: Optoelectronic data for polymers **54** and **55**,[a] energy values for trimer conformers.

Polymer	λ_{max}^{abs} **(nm)**	E_g^{opt} **(eV)**	**Experimental (eV) CV**			**Calculated (eV) DFT[a]**		
			E_{HOMO}	E_{LUMO}	**Eg**	E_{HOMO}	E_{LUMO}	**Eg**
54	532	1.82	-4.99	-3.51	1.48	-4.97	-2.84	2.13
55	382	2.16	-5.74	-4.15	1.59	-5.19	-2.86	2.33

Both these polymers showed lower energy gap for the experimental results using the optical data as well as the CV measurements, also the theoretical values showed the similar trend wherein, **54** had lower energy gap as compared to **55**. The theoretical data using DFT calculations predicted the nearly planar backbone for both these polymers with less twisting due to the presence of S--O short contacts present between the comonomers and the copolymer units. Also, the spatial arrangement for tetramer of polymer **55** showed the helical structures formed due the structural constrains.

The optical data for polymers **54** and **55** also showed broad and featureless emissions for **54** in good solvents. This result correspond to the folding structures and for polymer **55**

further dilution, and concentration dependent studies showed presence of predominantly strong emissions without much shift in the wavelength or shape which is typical of folding conformations. Further studies have to be performed such as 2D-NMR and CD analysis to confirm the presence of folding in these polymers. Also, the photovoltaic studies of these polymers are in progress and showed the promise to further improve the solar cell performance for these INDT-based D-A alternating copolymers.

In addition, we have also started towards synthesizing new polymers with addition of copolymers to increase the pitch radius of the folded helices and increase the length of conjugation and π-π interactions. Hence, as shown in Figure **121**, inclusion of NDT units in the polymers would allow to expand the pitch angle and would be easier for the encapsulation of guests to improve the host-guest chemistry.

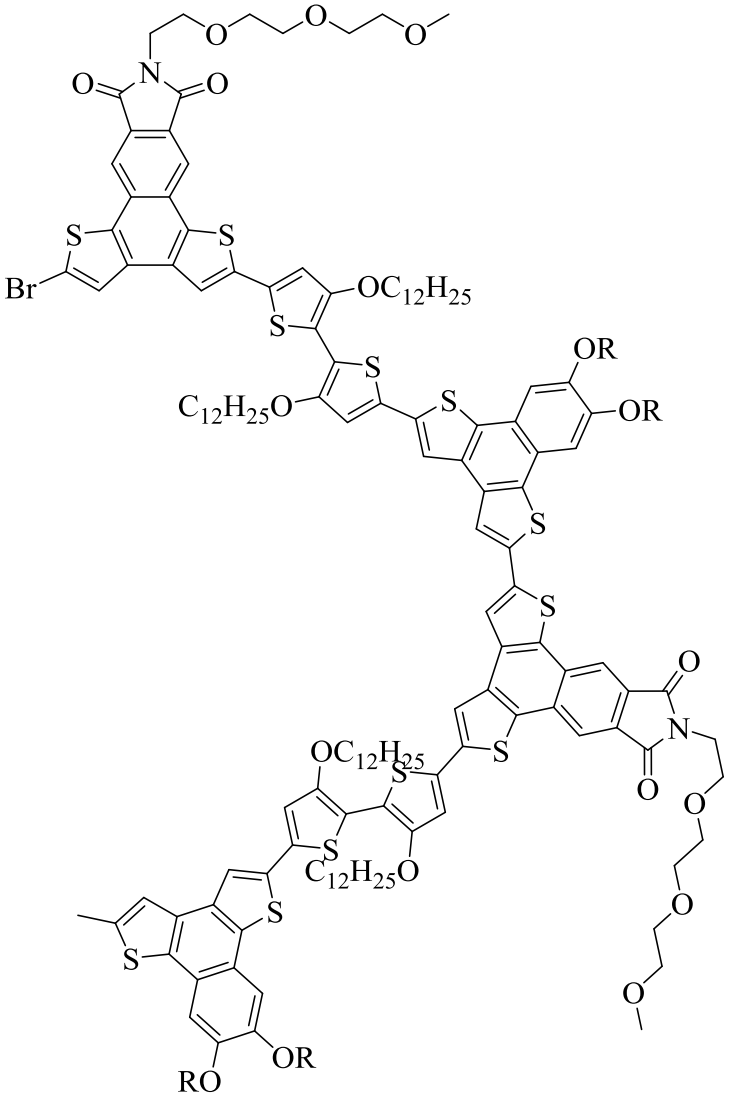

Figure 121: Proposed folded structure of a polymer with higher pitch radius.

4.8 Experimental

Solvents were distilled from appropriate drying agents under inert conditions prior to use. Unless otherwise stated, all other chemicals were purchased from commercial sources and used without further purification. All reactions were carried out under nitrogen using standard Schlenk techniques. ^{1}H-NMR and ^{13}C-NMR spectra were collected using a Varian INOVA 400 MHz NMR spectrometer. Polymer molecular weights were determined at 30^{0}C on a Tossoh EcoSec HLC 8320GPC system equipped with a differential refractometer, UV detector, and styragel column with THF as the eluent versus polystyrene standard. All samples were referenced to the deuterated solvents. UV-Vis absorption spectra were measured using a Hewlett-Packard 8452A diode array spectrophotometer. Cyclic voltammetry (CV) studies were carried out under argon atmosphere using BAS Epsilon EC electrochemical station employing a Pt working electrode, a silver wire reference electrode and a Pt wire as the counter electrode. A 0.1 M tetra-n-butylammonium hexafluorophosphate solution in acetonitrile as supporting electrolyte and the scan rate was 20 mVs^{-1}. Fc/Fc^{+} was used as reference for all measurements and assigned an absolute energy of -4.8 eV versus vacuum.

Compound 5

In a 25 mL RBF, compound **4** (1.00 g, 3.41 mmol) was added and dissolved in methanol (20 mL). To this solution, hydrazine hydrate (0.64 mL, 10.5 mmol) was added slowly, and the reaction mixture was refluxed at 65 °C for 3 h. The solvent was evaporated and later washed with 10% KOH solution. It was then extracted with DCM, and the organic layers were dried with $MgSO_4$. It was filtered, and solvent was evaporated under vacuum to give dark yellow oily liquid of compound **5** (0.37 g, 2.29 mmol, 67%). ^{1}HNMR (400 MHz, $CDCl_3$): δ 3.3 (m, 6H, $-OCH_2-$), 3.2 (t, *J*= 4 Hz, 2H, $-OCH_2-$), 3.1 (t, *J*= 6 Hz, 2H, $-OCH_2-$), 3.0 (s, 3H, $-OCH_3$),

2.5 (t, *J*= 6 Hz, 2H, -NCH_2-), 2.0 (br, 2H, -NH_2) ppm. ^{13}CNMR (400 MHz, DMSO-d_6): δ 73.3, 71.6, 70.0, 69.9, 58.3, 41.6 ppm.

Compound 32

In a 50 mL RBF, compound **27** (1.00 g, 2.06 mmol) was added. To this flask, an excess of acetic anhydride (30 mL) was added, and the reaction mixture was heated to 150 °C overnight. It was then cooled to room temperature and was concentrated by removing the solvent under reduced pressure to give the yellow-brown crude product. It was then recrystallized from DCM: methanol to give compound **32** as a yellow solid (0.63 g, 1.34 mmol, 65%). ^{1}HNMR (400 MHz, DMSO-d_6): δ 8.8 (s, 2H, Ar-H), 8.4 (s, 2H, Ar-H) ppm.

Compound 33

In a three neck RBF, compound **32** (1.00 g, 2.14 mmol) was added. The flask was subjected to three cycles of pump/ purging with N_2 gas. It was followed by addition of compound **5** (0. 52 g, 3.20 mmol) and acetic acid (50 mL). The resulting reaction mixture was refluxed at 110 °C for 4 h. The solvent was then removed to give crude yellow product. It was recrystallized from DCM: MeOH to give buff colored solid of compound **33** (0.92 g, 1.50 mmol, 70%). ^{1}HNMR (400 MHz, DMSO-d_6): δ 8.5 (s, 2H, Ar-H), 8.3 (s, 2H, Ar-H), 3.8 (t, *J*= 6 Hz, 2H, -NCH_2-), 3.7 (t, *J*= 6 Hz, 2H, -OCH_2-), 3.5 (t, *J*= 6 Hz, 2H, -OCH_2-), 3.4 (t, *J*= 4 Hz, 2H, -OCH_2-), 3.4 (t, *J*= 6 Hz, 4H, -OCH_2-), 3.1 (s, 3H, -OCH_3) ppm.

Polymer 54

In a two neck schlenk flask under argon protection, compound **33** (100 mg, 0.16 mmol), compound **44** (181 mg, 0.16 mmol), tris(dibenzylideneacetone)dipalladium(0) (7.47 mg, 0.008 mmol), and tri(o-tolyl)phosphine (19.9 mg, 0.065 mmol) were added. The flask was subjected to three cycles of pump and purge with argon gas. To this flask, oxygen free *N*,*N*-

dimethylformamide (5 mL) was added, and the reaction mixture was refluxed at 150 °C for 60 h. It was then cooled to room temperature, and the reaction mixture was poured into a solvent mixture containing methanol (45 mL) and 12 N HCl (5 mL). It was stirred for an additional 3 h. The precipitate was collected by centrifugation and poured into solvent mixture containing methanol (45 mL) and chloroform (5 mL). It was again stirred for 3 h, and precipitate was collected by centrifugation. The collected precipitates were dried under reduced pressure to give polymer **54** as dark purple solid (143 mg, 0.14 mmol, 88%). ^{1}HNMR (400 MHz, $CDCl_3$): δ 3.2- 4.2 (br, 17H, -OCH_2 on the comonomer, H's on the ethylene oxide side chain), 1.0- 1.5 (br, 40H,- CH_2 H's on dodecyloxy chain), 0.8 (br, 6H, -OCH_3) ppm. Molecular weights from GPC measurements: Mn= 9.8 kDa, Mw= 21.5 kDa, PDI= 2.19.

Polymer 55

Polymer **55** was prepared by the same procedure following the stille co-polymerization from comonomers (compound **30** and **33**) in DMF for 60 h to give dark brown solid. Yield (0.09 g, 0.15 mmol, 90%). ^{1}HNMR (400 MHz, DMSO-d_6): δ 8.4 (s, 2H, Ar-H), 6.3 (s, 2H, Ar-H), 4.2-4.4 (br, 4H, -OCH_2 on comonomer), 3.2- 4.0 (br, 15H, H's on ethylene oxide chain) ppm. Molecular weights from GPC measurements: Mn= 29 kDa, Mw= 52 kDa, PDI= 1.79.

CHAPTER 5

MAIN-CHAIN POLYOXOMETALATE CONTAINING D/A CONJUGATED POLYMERS

5.1 Introduction to polyoxometalates

In the past few decades, conjugated polymer-based solar cells (PSCs) have gathered tremendous attention due to their potential to generate low-cost, clean energy with the added advantages of being light weight and having mechanical flexibility.[200-202] Among the electron accepting and transporting materials in PSCs, fullerene derivatives are the most commonly used due to their good electron affinity and high electron mobility (up to 1 $cm^2V^{-1}s^{-1}$ measured by field effect transistors).[203,204] They are often blended with conjugated polymers to form bulk-heterojunction (BHJ) structures.[205] In order to form separate pathways for both electrons and holes, the weight percentage of fullerene in the composite is often 50% or higher.[205,206] However, fullerene derivatives have certain drawbacks, and the first one is very expensive to synthesize.[207,208] Another disadvantage of using fullerene derivatives as acceptor materials is that they also have tendency to undergo post-fabrication crystallization. This leads to morphological instability and evolution that would ultimately lower the device performance and long-term stability.[206,209] Hence, it is necessary to look for alternative acceptor materials.

With this regard, various other non-fullerene electron acceptors have been explored,[210-214] among which inorganic materials, such as ZnO,[215] TiO_2,[216] and CdSe,[217] etc., have drawn significant attention. These hybrid solar cells maintain the benefits of organic photovoltaic devices but also bring some other advantages of inorganic materials. There are various advantages of using these organic-inorganic hybrid materials, such as, these inorganic materials are more stable upon exposure to light or oxygen.[218] They also have higher light

absorption as compared to PCBM.[218] Additionally, some of these materials would be able to form well aligned nanostructures, which would provide pathways for the charge transportation.[219] There has been continuous progress in this area, however, it is still not comparable in terms of PCE of polymer/fullerene blends, which would be due to the incompatibility between the organic and inorganic materials.[220] Since, during the blending process, the content of both donor and acceptor materials need to be in very high blending ratios,[205,206] and the structural and property differences between the organic and inorganic counterparts tend to form unstable morphologies in such high blending ratios.[218,220] In order to resolve this issue of incompatibility between organic and inorganic materials, surface modification process can be used where the inorganic surface can be capped with dyes or small molecules containing inorganic-binding groups or ligands.[221,222] Another option to resolve this incompatibility issue between the two counterparts would be to covalently connect them through chemical bonds.[223,224] The covalent incorporation of inorganic building blocks into a polymer matrix to obtain a stable, robust materials is widely used concept in the field of organic-inorganic hybrid materials. They encompass the use of different inorganic systems including but not limited to nanoparticles, mono and poly nuclear metal complexes and clusters, polyhedral oligomeric silsesquioxanes (POSS), polyoxometalates (POM), layered inorganic systems, inorganic fibers, and whiskers to name few.[225] When they are connected through covalent linkage, it is possible to achieve controllable morphologies, compatibility can be improved, and there is closer electronic interaction between the donor and acceptor material.[220] In this chapter, structurally well-defined inorganic building block, polyoxometalates (POMs) were studied and combined with organic material to make hybrid polymers.

Among various inorganic electron acceptors, POMs, early transition metal oxygen anion are especially attractive.[225] The discovery of POMs can be dated back to the last third of the XIX century, when early transition metals of groups V and VI were found to form polynuclear oxyanions in aqueous solutions at acidic pH. In these conditions, they can form molecular compounds of variable dimensions ranging from few angstroms to tens of nanometers.[226-230] The metal oxygen polyhedral that make up POM structures have the general formula $[MO_x]_n$, where M is the early transition metal, O is the oxygen atom, x is usually between 4-7, and n is the number of repeated polyhedral units. They are usually negatively charged, and the negative charge is balanced by small counter ion like Na^+, K^+, and NH_4^+.[231] These POMS can be generally classified into isopolyanions $[M_mO_y]^{p-}$ and heteropolyanions $[X_xM_mO_y]^{q-}$ based on their compositions, where X is non-metal like P, Si, As, and Sb, another element of the p-block or a different transition metal.

Among the heteropolyanions when different transition metals are incorporated, they are called Transition Metal Substituted Polyoxometalates (TMSP). Mostly, the structures of POMs is derived from the aggregation of octahedral units MO_6, although tetrahedral units MO_4 can be present as well. Oxygen atom acts as bridging unit for the condensation between two octahedral units via μ-oxo bridges between two metal ions. Their molecular structure is built through three different ways, corner-sharing, edge-sharing, or face-sharing of early transition metal, such as Mo, W, Nb, Ta, V, or Pd oxygen polyhedra into larger architectures with high symmetry.[232] These early transition metals are in their higher oxidation state with a wide range of properties, such as photonic, electronic, and magnetic properties. Due to these multitude of properties, they have been widely used in various fields and various applications such as in

molecular magnetism,[233] protein sequencing,[234] solar cells,[235] stimuli responsive material,[236] catalysis,[237] medicine,[238] and storage devices.[239]

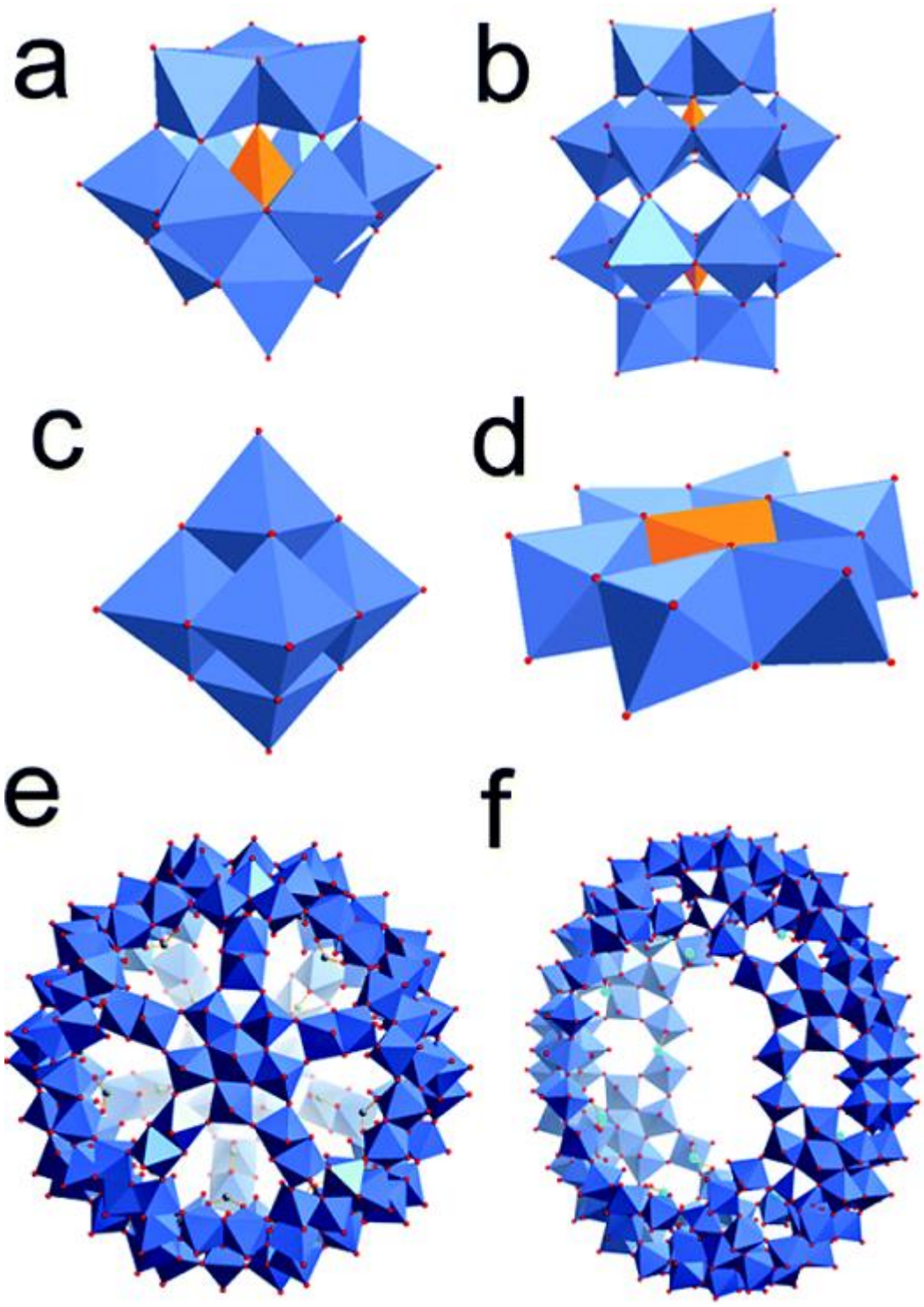

Figure 122: Different illustration of POM anions (a) Keggin anion (b) Dawson anion (c) Lindqvist anion (d) Anderson anion (e), (f) polyhedral illustation of POM anions, ball shaped cluster and wheel structure, respectively.[240]

A number of categories were developed to classify POMs clusters[240] that were synthesized with different physical and chemical properties (Figure **122**). Some of the examples of POM inorganic clusters with low charge density include Anderson, Keggin, Dawson, and Lindqvist POMs, as well as, some noble metal based POMs.[240]

Keggin POMs: These are among the most important classes of heteropolyanions having the general formula $[XM_{12}O_{40}]^{n-}$, where M can be Mo or W, and X is a heteroatom like P^{5+} and Si^{4+}. It was first proposed by Linus Pauling, where he suggested they are made of tetrahedral $[XO_4]^{n-8}$ units that are surrounded by 12 MO_6O_h units to create overall tetrahedral (T_d) symmetry.[241] Keggin later obtained the structure of hexahydrated dodecatungstophosphoric acid by X-ray crystallography investigation.[242] The structure of Keggin POMs consist of central PO_4 tetrahedron, which is surrounded by 12 octahedra WO_6, and these octahedral arrange themselves in four triplets M_3O_{13} where the three octahedral units are aggregated by edge sharing. The four different triplets condense each other by corner sharing. Another feature of these Keggin structures is their instability to the higher pH. In the alkaline condition, the acidic Keggin POM will be able to transform into mono, di, or tri- lacunary Keggin POMs by the removal of M-O unit.[243] These lacunary POM complexes[230, 244] can be used as ligands for transition metals and organometallic groups or as the building blocks for the preparation of POM aggregates.

Wells-Dawson POMs: They are also another type of heteropolyoxoanions having the general formula $[X_2M_{18}O_{62}]^{n-}$, where M is usually a W atom. These POMs are composed by condensation of two XM_9O_{34} units by sharing of six oxygen atoms. These type of POMs have primary applications in the field of catalysis or water splitting because of their higher stabilities in bulk and solution states.[245]

Anderson POMs: These POMs are also another type of heteropolyoxoanions having the general formula $[XO_6M_6O_{24}]^{n-}$, where X can be transition metal like Mn, Cr or Pt. The geometry of these POMS is planar with D_{3d} symmetry, where, the six edge sharing MO_6 octahedral units surround the central XO_6 octahedron. These kind of POMs too have applications in the fields of catalysis where these POMs can be functionalized with organic tails to create organic-inorganic hybrid materials.[246]

Lindqvist POMs: They are the type of isopolyoxoanions having the general formula $[M_6O_{19}]^{n-}$ where M can be Mo, W, Ta, Nb, or V, and n = 2. These POMs are composed of six MO_6 units connected via edge sharing to form octahedral symmetry. Due to the various applications of these isopolyoxometalates in electrochemistry, photovoltaics, optoelectronics. A significant effort has been towards the functionalization of these Lindquvist POMs with organic tails to create materials with different crystallinity.[247] The structure of hexamolybdate anion is shown in Figure **123** consisting of a central oxygen atom surrounded by six molybdenum atoms in an octahedral fashion.[248] In this general structure of hexamolybdate anion, each central oxygen atom (O_c) is surrounded by six molybdenum atoms (bond length, Mo – O_c = 2.32 Å). Each molybdenum atom then connects to terminal oxygen (O_t) (Mo – O_t = 1.68 Å) and shares additional four bridge oxygen atoms (O_b) (Mo – O_b = 1.93 Å) with adjacent molybdenum atoms. The end-to-end overall size of hexamolybdate anion is about 8 Å, which is comparable to fullerene C_{60} which is about 7.1 Å.[249]

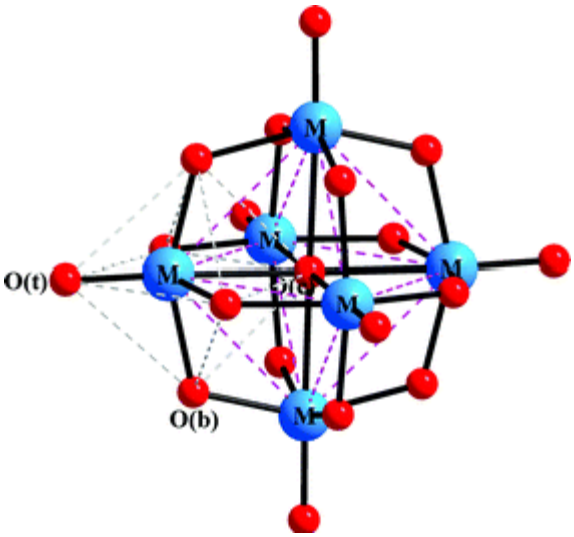

Figure 123: General structure of hexamolybdate anion.

Another advantage of hexamolybdates, is the stability which could be seen in Table **13** below. They undergo reversible one electron reduction ($E_{1/2}$= -830 mV) and are highly stable.[249] As seen in the Table **13**, the bond lengths between Mo and O are only slightly altered before and after reduction, confirming the stable nature of them.[250] Bridgman *et al* also calculated charge distribution of hexamolybdate anion during the reduction process and reported that the negative charges and added electron in the reduction process are distributed over all types of atoms as shown in Table **14**.[251]

Table 13: Mo-O bond lengths of hexamolybdate anion (a) experimental and (b) calculated data.

	Molecule	**Mo- O_c (Å)**	**Mo- O_b (Å)**	**Mo- O_t (Å)**
Before reduction	$[(Mo_6O_{19})^{2-}]^a$	2.32	1.93	1.68
	$[(Mo_6O_{19})^{2-}]^b$	2.32	1.93	1.71
After reduction	$[(Mo_6O_{19})^{3-}]^b$	2.33	1.93	1.73

Table 14: Calculated charges of hexamolybdate anion.

	Molecule	Mo	Ot	Ob	Oc
Before reduction	$[(Mo_6O_{19})^{2-}]^a$	2.19	-0.66	-0.83	-1.19
After reduction	$[(Mo_6O_{19})^{3-}]^b$	2.11	-0.72	-0.85	-1.18

POMs are a large group of rigid, stable, well-defined and gigantic anionic clusters and are well known oxidants that can accept multiple electrons.[251, 252] In addition, they are also robust and structurally stable.[253] Among the various metal-oxygen clusters, POMs not only have unmatched structural and compositional diversity,[254] but also have discrete molecular structures that allow surface functionalization in a controlled manner.[255] One of the POMs, the hexamolybdate cluster, is particularly appealing as seen previously due its approximately spherical shape with a diameter about 0.8 nm which is close to that of C_{60} (0.7 nm).[256] It has a reversible one electron reduction process at potentials (~-3.5 eV in LUMO) close to that of a fullerene (~-3.7 eV in LUMO);[257] hence have electron accepting capability similar to fullerene but at much lower cost and are easy to synthesize.[258]

More importantly, the hexamolybdate cluster can be conveniently and efficiently functionalized with one or two organo imido groups.[259] Since the π electrons can extend their conjugation into the inorganic framework which results in stronger d- π interactions the organoimido derivatives have been of keen interest among various organic derivatives. The terminal O atom can be replaced by N atom, allowing the preparation of covalently-bonded organic–inorganic small-molecule hybrids and POM containing polymer hybrids.[259] There are typically three types of reactions that have been developed for the synthesis of organoimido derivatives as shown in Scheme **18**.

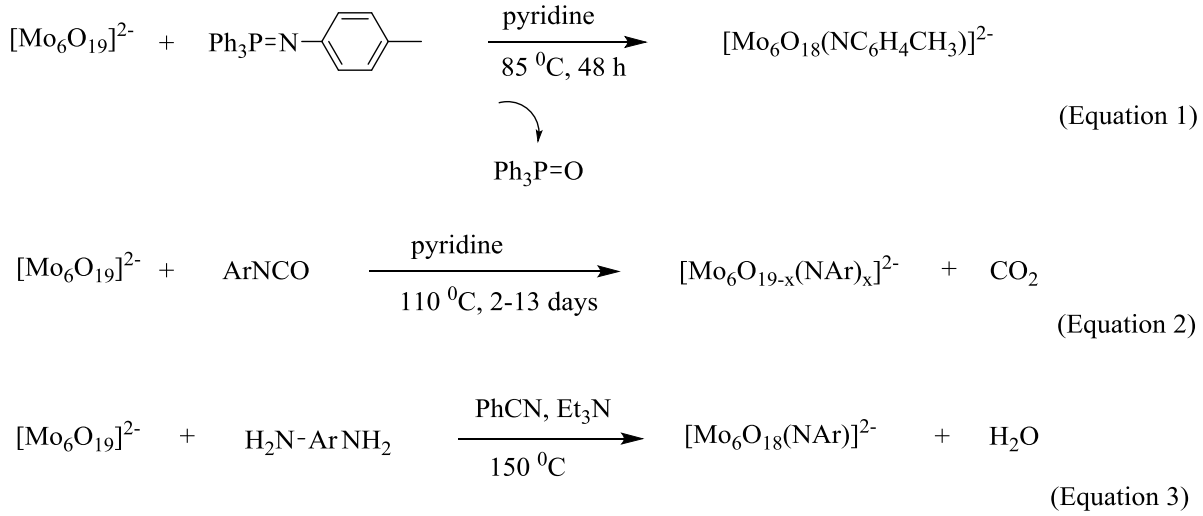

Scheme 18: Different routes for the synthesis of organoimido derivatives.

The pioneering work in synthesis of organoimido derivatives was done by Sprout,[259,260] Matta[261-263] and Errington.[264] Due to their efforts in synthesizing these derivatives from phosphinimines, isocyanates and aromatic amines, respectively, organoimido derivaties of POMs can now be prepared with various imido releasing reagents.[265] The synthesis involved in equation 1 is the reaction of phosphinimines with hexamolybdate leading to direct functionalization of the parent cluster. In the second equation discovered by Errington and Matta, the reaction was performed between hexamolybdate and various isocyanates under anhydrous conditions (pyridine) for several hours. Although Strong and Matta could isolate higher substituted derivatives from a mixture containing lower substituted by-products via one pot reaction of aryl isocyanates, only the terminal (Ot) atoms in hexamolybdate could be replaced by arylimido ligands. This limited the broad application of Matta's protocol. The third equation also involved harsh conditions developed by Errington *et al* between hexamolybdate and aromatic diamines, and also was unable to yield pure imidoderivative.[264] To this date,

polysubstituted organoimido derivatives of POMs, especially with bridging oxo group (O_b) replacement are rare, hence, leaves a scope to develop this field of chemistry of POM derivatives.

Alternatively, Peng and Wei's groups achieved controlled synthesis of mono and disubstituted organoimido derivatives of hexamolybdate by employing dicyclohexylcrbodiimide (DCC) dehydarating protocol.[266-275] The use of DCC can facilitate the reaction of various aromatic amines with hexamolybdate in refluxing acetonitrile avoiding all the harsh conditions of temperature and are much faster. As shown in Scheme **19**, the revised scheme where DCC is used has faster rate due to the activation of Mo-O_t bond. The terminal O atom can be efficiently replaced by N atom with a shorter Mo-N bond (~1.7 Å) and near linear Mo-N-C bond angle, which is greater than 170 °C, allowing the preparation of covalently bonded organic-inorganic hybrids. Unlike those conjugated systems containing one or more covalently bonded fullerene units in the molecule that have been well reported in the literature,[277-279] hybrid-conjugated polymers containing covalently bonded POMs are still rare and have not been extensively explored as photovoltaic materials.[280]

$$[Mo_6O_{19}]^{2-} + Ar{-}NH_2 \xrightarrow[\text{reflux}]{\text{DCC, } CH_3CN} [Mo_6O_{18}(NAr)]^{2-}$$

Scheme 19: Hexamolybdate reaction with aromatic amines using DCC.

5.2 Objective of synthesis of POM containing hybrid polymers

There are generally three different types of hybrid materials that can be synthesized with POMs (Figure **124**).

1) Charge transfer hybrids where organic donor and POM cluster are connected through conjugated linkage
2) POM containing rod-coil diblock copolymers where POM clusters are connected to the coil block on sides as pendants
3) POM containing main chain conjugated polymers where POM clusters are embedded in the main conjugated backbone of the system.

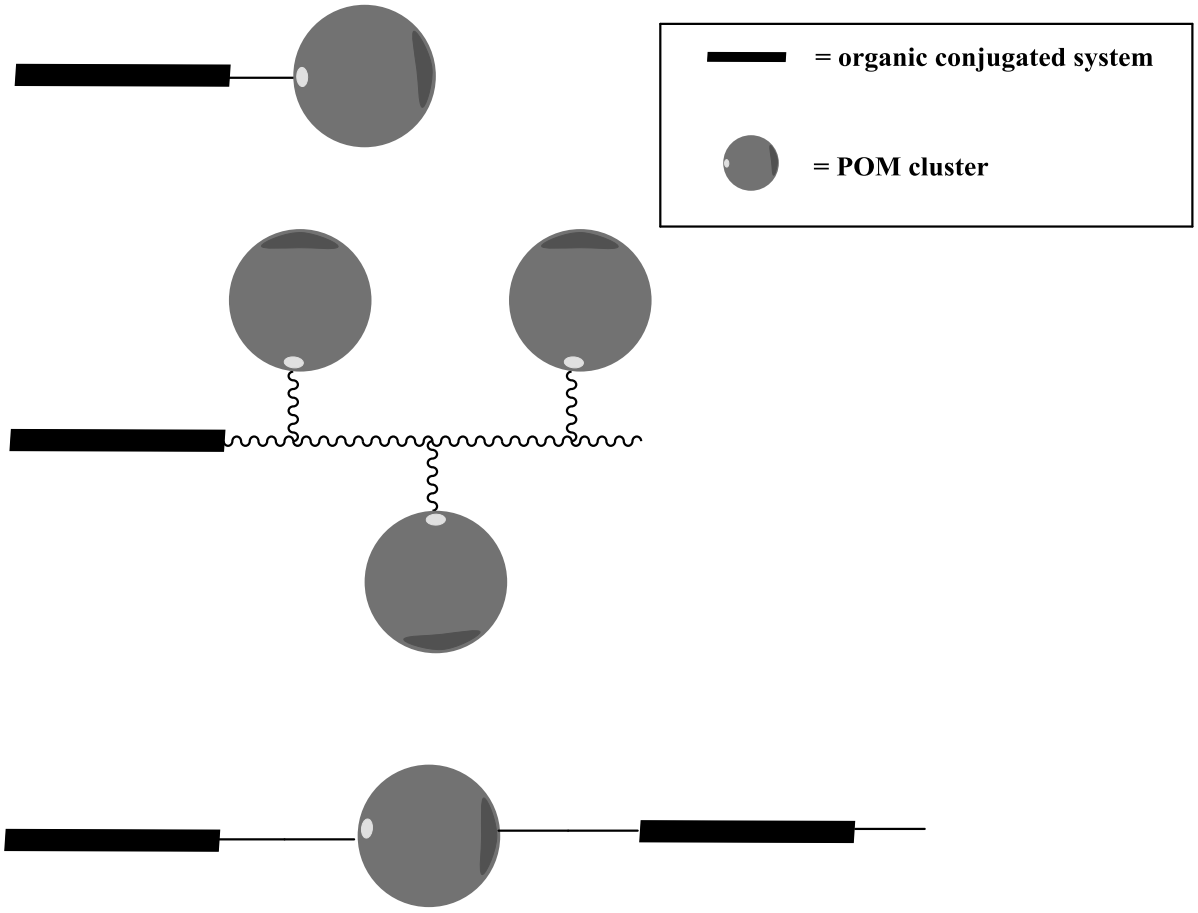

Figure 124: Different types of POM containing hybrid polymers.[282]

We have shown previously that the charge transfer process becomes inefficient if the organic molecules are connected to the POM clusters through non-conjugated linkage, hence it is advisable to have a conjugated linkage between them. This result would then improve the charge transfer from photo excited organic system towards the POM clusters that are excellent electron acceptors.

Main chain POM containing conjugated polymers where the organic π conjugated molecules are directly connected to the POM clusters show efficient charge transporting and are hence can be excellent photovoltaic materials. Although few conjugated polymers have been reported thus far having main chain POM containing conjugated polymer backbone, they have shown better device performance than other POM containing hybrid polymers. These hybrid polymers having different blocks may self-assemble into various morphological structures[283] such as spheres, gyroids, and cylinders. These may also fold as shown in the following Figure **125** to create a cavity wherein guest molecules could be encapsulated as discussed in the previous chapters and would become novel tool in nanofabrication, nanolithography.[283]

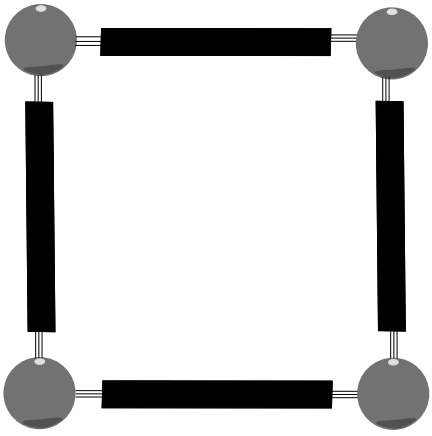

Figure 125: Proposed self-organization of POM containing hybrid polymers into foldamers.

We have reported recently,[284] synthesis of two new main chain POM containing donor-acceptor conjugated copolymers with single component solar cells based on **P10**. It is without addition of any electron acceptor showing respectable PCE upto 0.31%. In this contribution, we report the synthesis, characterization, and optoelectronic properties of new main-chain hexamolybdate-containing conjugated copolymers, namely **Polymer 56**.

5.3 Target molecule

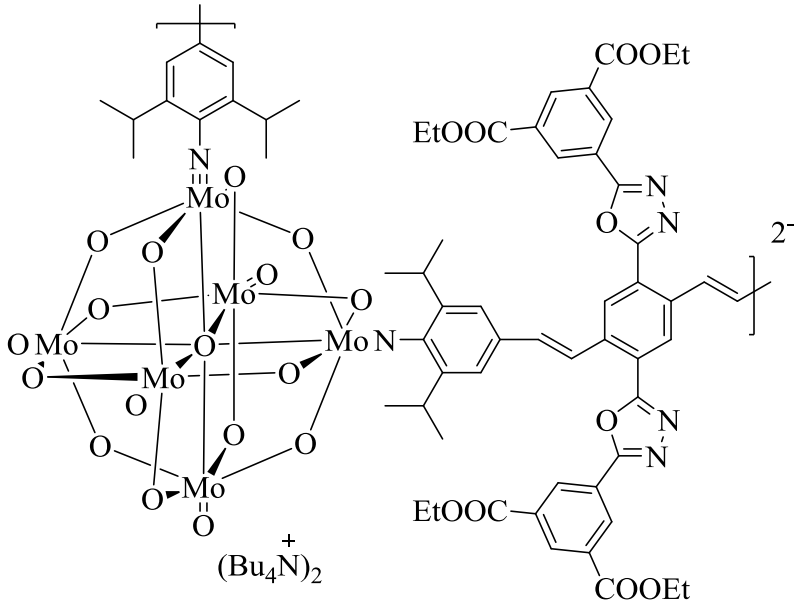

Figure 126: Chemical structure of the target main-chain POM containing hybrid conjugated copolymer.

The polymer **56** was synthesized following the Mizoroki-Heck cross coupling reaction with the previously synthesized bifunctionalized POM compound[285] and the divinyl comonomer[286] in our laboratory. The catalyst, dichloro{bis[1,1',1''-(phosphinetriyl)tripiperidine]}palladium, used for this polymerization was also synthesized following the reported literature procedure by Oberholzer and Frech.[287]

5.4 Results and Discussion

The Mizoroki-Heck cross coupling reaction was used to synthesize this main chain POM containing hybrid conjugated polymer. The coupling reaction was carried out using dichloro{bis[1,1',1"-(phosphinetriyl)tripiperidine]}palladium [$(P(NC_5H_{10})_3)_2Pd(Cl)_2$] (**53**) as a catalyst under milder conditions to give the polymer in good yields. The catalyst was synthesized following the reported procedure[287] by Oberholzer and Frech as shown in Scheme **20**.

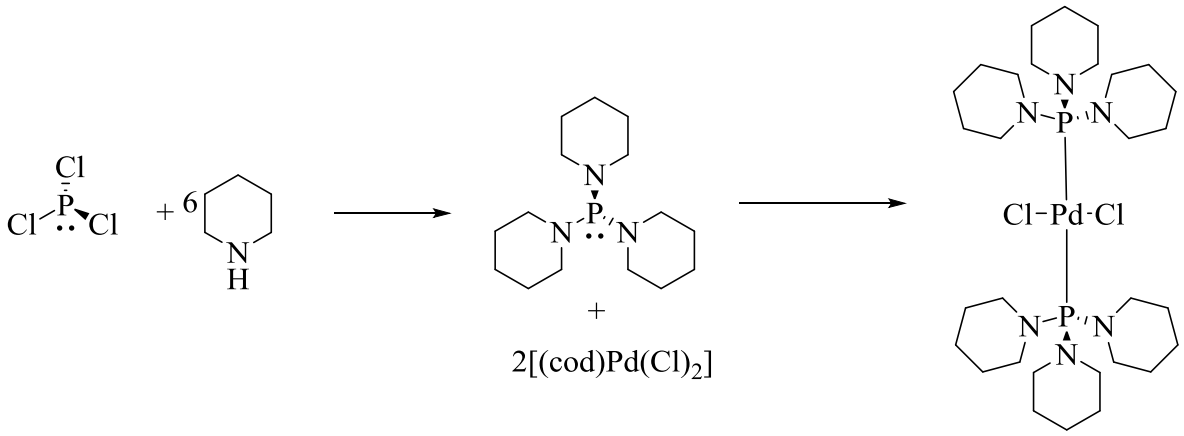

Scheme 20: Synthesis of Heck catalyst for polymerization.

The Heck reaction has shown good applicability both in total syntheses of natural products in academia and for the synthesis in pharmaceutical and agro industries.[288] Although recent developments have considerable scope for Heck catalysts, they often require high reaction conditions, higher catalyst loading ratios, and longer reaction times. Also, the catalyst used require multiple steps in the preparation and hence they are often time consuming and low yielding processes. Compound **53** was prepared in a two-step process, and the first step involved synthesis of a ligand, (1,1',1"-(phosphinetriyl)tripiperidine) made by a reaction between phosphorus trichloride and piperidine. It was then prepared within few minutes by treatment of THF suspensions of [$Pd(Cl)_2(cod)$] with the prepared ligand under air atmosphere

at 25 °C. The purity of the prepared compound **53** was confirmed by the P^{31}-NMR spectroscopy that showed sharp signal at 92.5 ppm due to the central phosphorus atom present in its structure (Figure **127**).

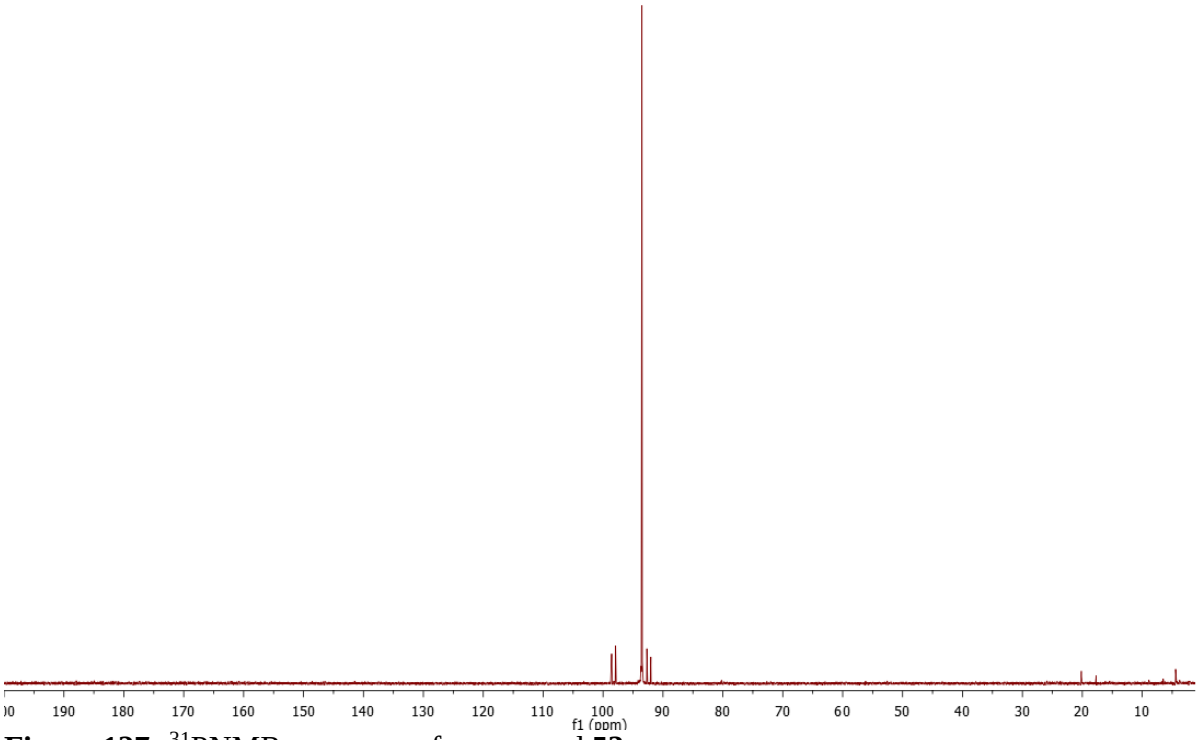

Figure 127: ^{31}PNMR spectrum of compound **53**.

Bifunctionalized polyoxometalate cluster was also prepared following the previously published literature[285] in our group as depicted in the following Scheme **21** and its purity was checked by ^{1}H-NMR (Figure **128**).

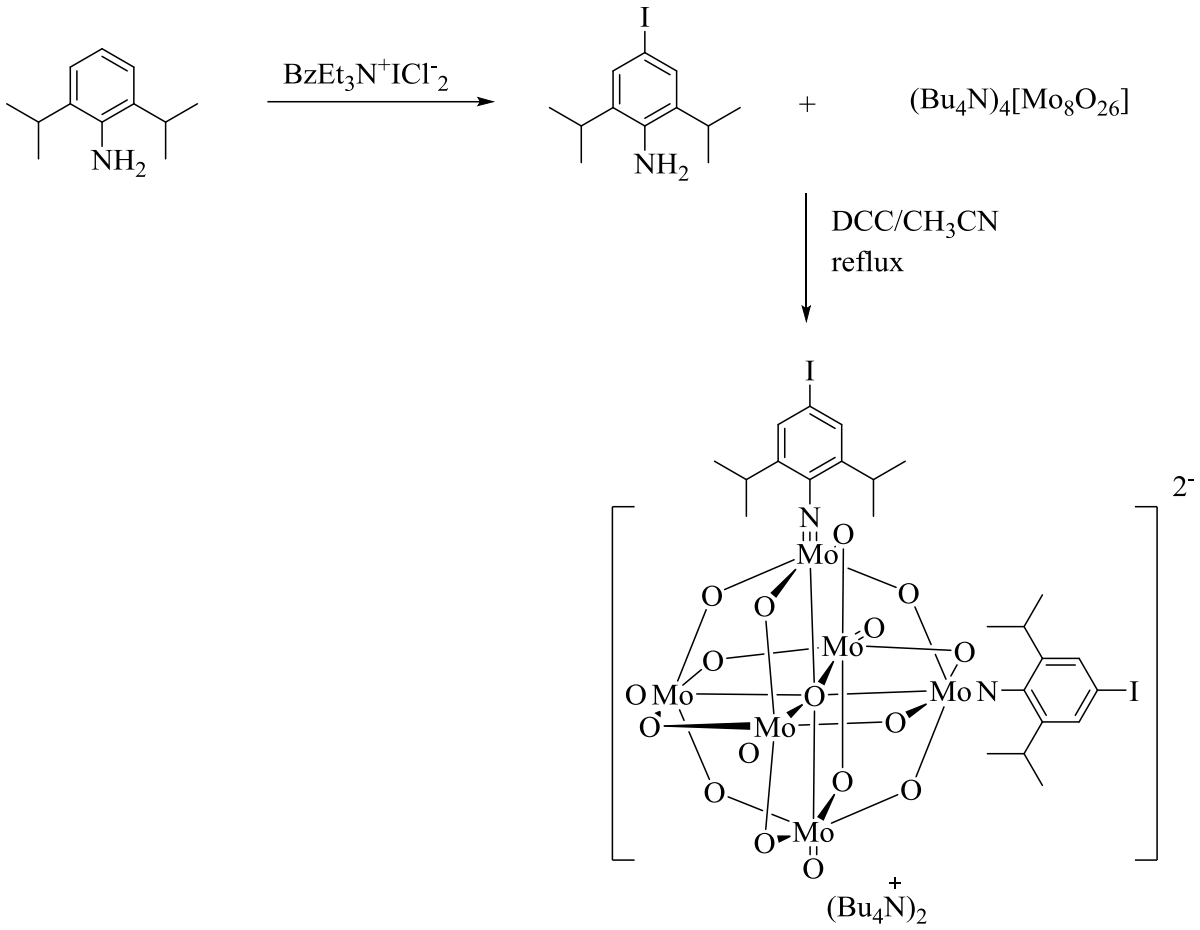

Scheme 21: Synthesis of bifunctionalized POM cluster.

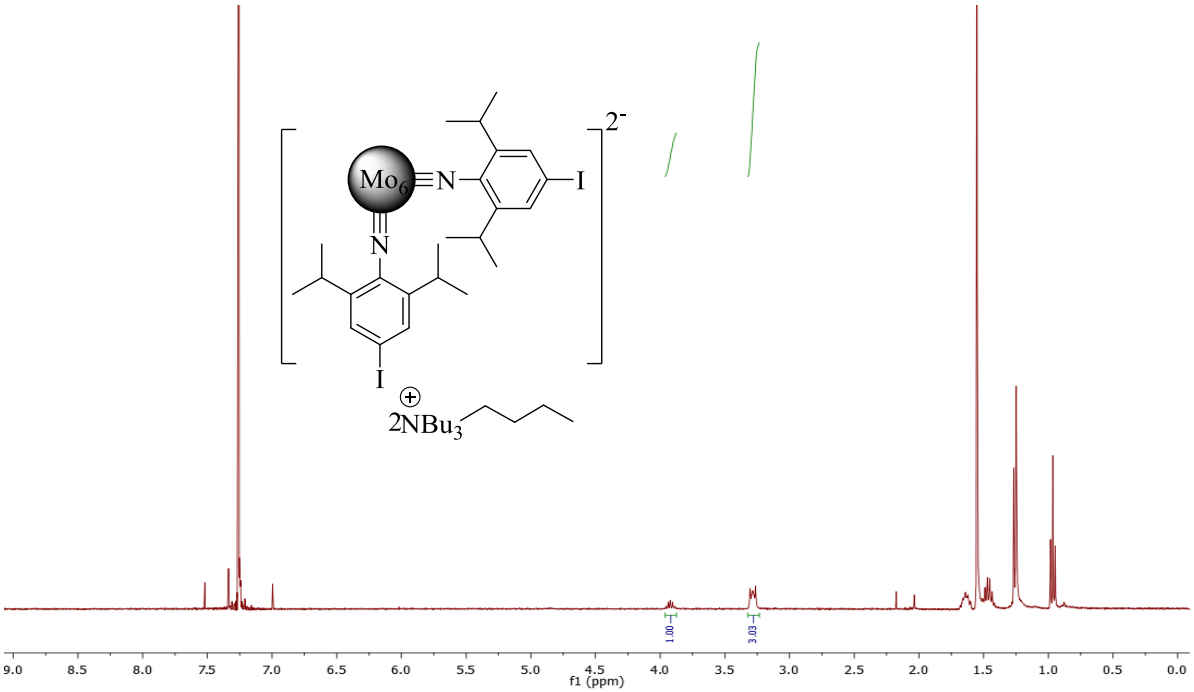

Figure 128: ^{1}H-NMR spectrum of bifunctionalized POM cluster.

The polymerization performed following the previously mentioned protocol for Mizoroki-Heck cross coupling reaction and the polymerization was carried out at a lower temperature as compared to usual harsh conditions (scheme **22**).[287] Compound **56** was obtained as a dark red/ brown solid and purified by precipitation in insoluble solvents such as methanol/ hexane. The molecular weight of the polymer was obtained by gel permeation chromatography (GPC) with THF as the eluent and polystyrene as the standard. The polymer was only partially soluble in THF, and hence it was passed through a 0.45 µm filter. The number average molecular weight (Mn) and weight average molecular weight (Mw) were found to be 4.13 kDa and 9.29 kDa, respectively. The polymer had relatively broader polydispersity index of 2.25 possibly due to the poor solubility in THF. The ^{1}HNMR spectrum (Figure **129**) for polymer **56** showed the broadening of aromatic signals around 8.50–9.00 ppm as well as from 0.50-2.00

ppm for the aliphatic protons, and also a broad peak at 4.0 ppm was indicative of the signals due to -OCH_2- protons.

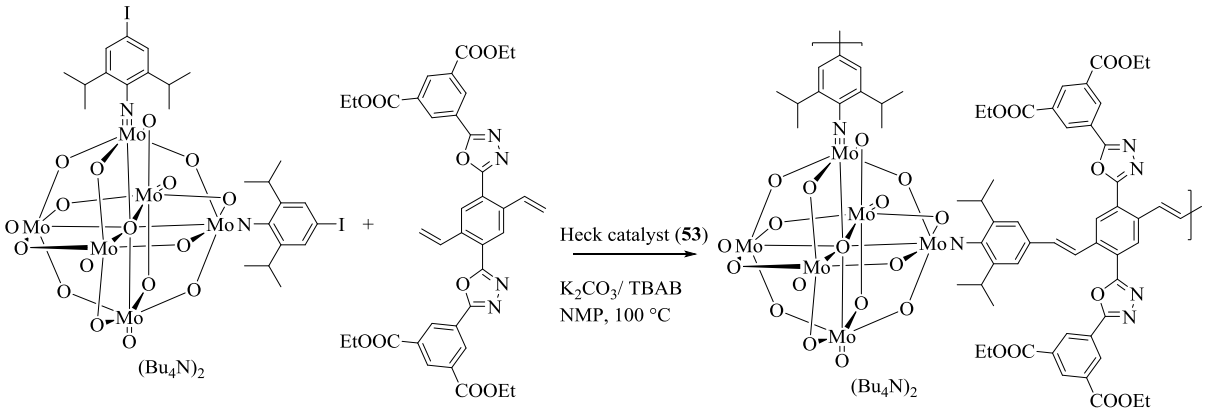

Scheme 22: Synthesis of the target molecule **56** from bifunctionalized POM and diene.

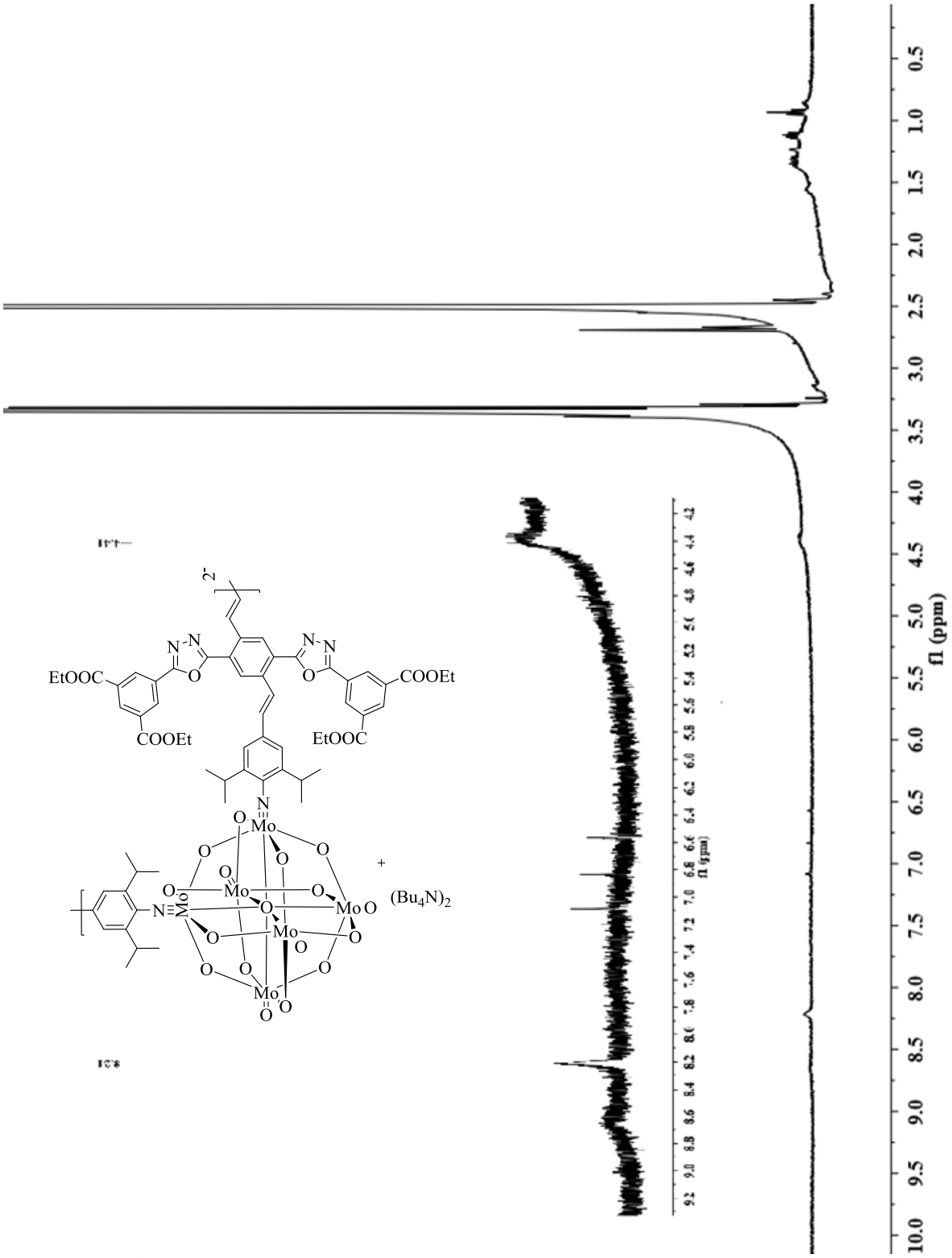

Figure 129: ^{1}H-NMR spectrum of polymer **56**.

5.5 Electrochemical studies

The electrochemical studies of polymer **56** was performed by preparing thin films of its solution in THF using CV measurements. The polymer showed irreversible oxidation and reduction waves in the anodic and cathodic scan during the CV measurements (Figure **130**). Using the first onset oxidation potential in anodic scan and first onset reduction potential in the cathodic scan, the HOMO and LUMO energy levels were estimated to be -5.72/-3.18 eV respectively. The E_g obtained by CV measuremnts was 2.54 eV.

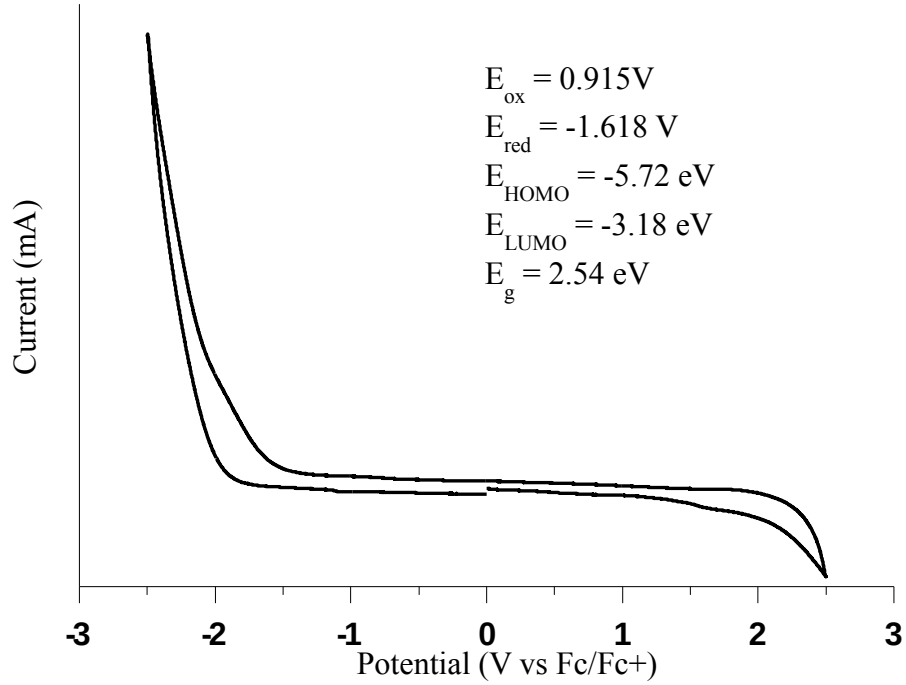

Figure 130: Cyclic volatammogram of polymer **56**, and the scale referenced to Fc/ Fc+ redox couple.

5.6 Optical studies

The optical data of polymer **56** was observed in THF as shown in Figure **131**. The polymer had very low solubility in most of the organic solvents, hence the solution was prepared by dissolving in *N*,*N*-dimethylformamide. The absorbance spectra of polymer **56** showed absorption maxima at 302 nm with a shoulder peak at 340 nm. When the solution was excited at those wavelengths of 302 and 340 nm, they resulted in similar emission spectra at 531 nm with different intensity. The E_g obtained from the λ_{max}^{abs} was calculated to be 3.30 eV. Since the polymer had limited solubility in THF and other organic solvents, it is possible that the low molecular weight oligomers are soluble in THF/ DMF and dominates the emission spectrum. We have to investigate further details on the optical data of the polymer and study their emission and absorbance data in various other possible solvents.

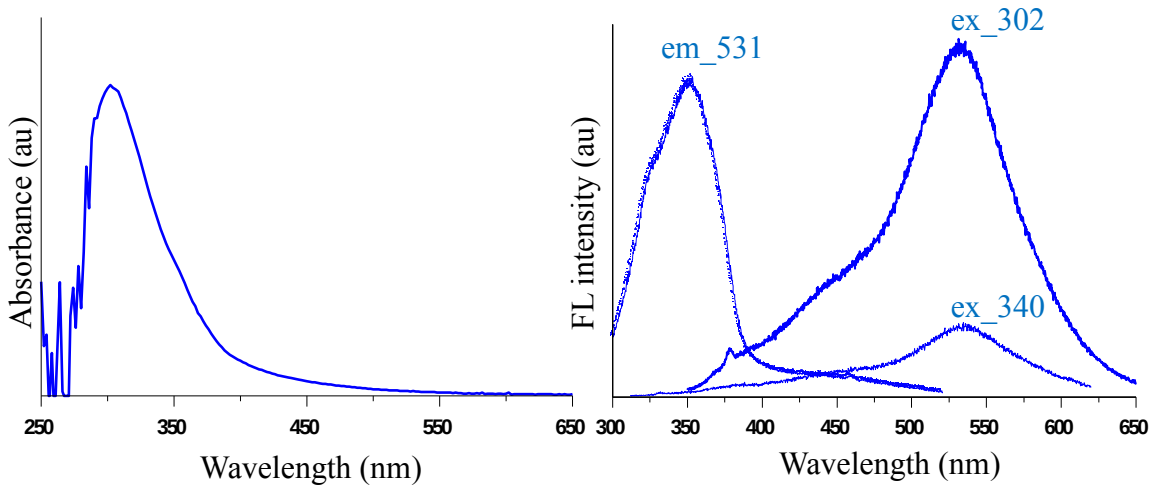

Figure 131: Absorption spectra of polymer **56** in THF (left) emission spectra (right).

5.7 Conclusion and future directions

We have synthesized organic-inorganic hybrid conjugated copolymer **56** wherein hexamolybdate clusters are covalently embedded in the main chain with diene and have characterized its optical and electrical properties. The incorporation of hexamolybdate cluster into polymer backbone is confirmed by ^{1}HNMR spectroscopy and GPC data. The ^{1}HNMR spectrum of the polymer was measured in DMSO-d_6, and the presence of characteristic signals associated with the bifunctionalized POM cluster due to isopropyl CH proton at δ 4.00 ppm and N^{+}-CH_2 protons at δ 3.30 ppm confirmed the successful incorporation of POM clusters into polymer. The number average molecular weight (Mn) and weight average molecular weight (Mw) for polymer **56** were found to be 4.13 kDa and 9.29 kDa, respectively. These molecular weights of POM containing hybrid polymer based on GPC relative to polystyrene standards should not be taken literally. However, they are clearly different and separated from their monomers which indicate the covalent attachment of POM cluster in the hybrid copolymers.

This is an ongoing project, and we will be further investigating morphological, photovoltaic properties of this polymer. We would also like to incorporate other comonomers in the polymer backbone and increase the length of conjugation and alter the cluster ratio in the polymer backbone and study its effect on the photocurrent efficiency measurements.

5.8 Experimental

Solvents were distilled from appropriate drying agents under inert conditions prior to use. Unless otherwise stated, all other chemicals were purchased from commercial sources and used without further purification. All reactions were carried out under nitrogen using standard Schlenk techniques. ^{1}HNMR and ^{31}PNMR spectra were collected using a Varian INOVA 400 MHz NMR spectrometer. Polymer molecular weights were determined at 30°C on a Tossoh EcoSec HLC 8320GPC system equipped with a differential refractometer, UV detector, and styragel column with THF as the eluent versus polystyrene standard. All samples were referenced to the deuterated solvents. UV-Vis absorption spectra were measured using a Hewlett-Packard 8452A diode array spectrophotometer. Cyclic voltammetry (CV) studies were carried out under argon atmosphere using BAS Epsilon EC electrochemical station employing a Pt working electrode, a silver wire reference electrode and a Pt wire as the counter electrode. A 0.1 M tetra-n-butylammonium hexafluorophosphate solution in acetonitrile as supporting electrolyte and the scan rate was 20 mVs^{-1}. Fc/Fc^{+} was used as reference for all measurements and assigned an absolute energy of -4.8 eV versus vacuum.

Compound 52

In a 500 ml RBF, dry diethyl ether (75 mL) and phosphorus trichloride (2.50 mL, 28.65 mmol) were added. The reaction mixture was cooled to 0°C. To this mixture, a solution of piperidine (19.8 mL, 200.6 mmol) dissolved in diethyl ether (anhydrous) (50 mL) was added dropwise. The reaction mixture was brought to room temperature and stirred for additional 45 min after which a white thick solid of piperidinum chloride precipitated. The reaction mixture was filtered, and washed with diethyl ether. The filtrate collected was subjected to evaporation to get clear thick liquid as compound **52**. (6.50 g, 23.0 mmol, 80.2%)

Compound 53

In a 100 mL RBF, dichloro(1,5-cyclooctadiene)palladium(II) (0.10 g, 0.35 mmol) and tetrahydrofuran (anhydrous) (10 mL) were added. In another flask, compound **52** (0.25 g, 0.88 mmol) was dissolved in tetrahydrofuran (anhydrous) (10 mL) to make a clear solution and was added to the previous solution and stirred for 1 min. It was then passed through a glass-frit funnel, and the filtrate was evaporated to give crude product. It was washed with pentane (3 x 5 mL), and the solvent was decanted. The remaining solid on drying gave the pure compound **53** as a yellow solid. Yield (0.45 g, 0.25 mmol, 70.8%). $^{31}P\{^{1}H\}$NMR: δ 92.5 ppm in $CDCl_3$.[287]

Compound 56

In a two neck schlenk flask under argon conditions, compound **53** (1.95 mg, 0.05 mmol) and anhydrous THF (1 mL) were added to prepare the catalyst solution. The flask was subjected to three cycles of pumping and purging with N_2 gas. In another schlenk flask, tetrabutylammonium bromide (16.7 mg, 1 mmol) and potassium carbonate (143 mg, 20 mmol) were added and dissolved in N-methyl-2-pyrrolidone (NMP) (3 mL). It was also subjected three cycles of pump/ purge with N_2 gas. To this flask, bifunctionalized POM (100 mg, 12.5 mmol) and diene (44 mg, 15 mmol) were added, and the solution was heated at 100 °C for 5 min. In this reaction mixture, the catalyst solution was added dropwise under N_2, and the reaction mixture was stirred at the same temperature for 40 h. The reaction was stopped and quenched by adding in solvent mixture containing methanol (45 mL) and 12 N HCl (5 mL). It was stirred for an additional 3 h. The precipitate was collected by centrifugation and was poured into solvent mixture containing methanol (45 mL) and chloroform (5 mL). It was again stirred for 3 h, and the precipitate was collected by centrifugation. The collected crude precipitate of polymer was dried under reduced pressure to give the dark brown solid. Yield:

(75 mg, 7.50 mmol, 60%). ^{1}HNMR: δ 8.00-9.00 (br, Ar-H, 13H), 6.50- 7.20 (br, -CH=CH-, 2H), 4.20- 4.80 (br, 4H, isopropyl H's and 8H, -OCH_2-), 3.30-3.50 (br, 4H, -NCH_2-), 1.00-1.70 (br, 42H, -CH_3) ppm. Molecular weights from GPC measurements: Mn = 4.13 kDa, Mw = 9.29 kDa, PDI = 2.25.

REFERENCES

1. Flexible electronics market by components (Display, battery, sensors, memory) by application (consumer electronics, automative, healthcare, industrial) and segment forecast to 2024, May **2016**.

2. VanSlyke, S. A.; Tang, C. W. *Appl. Phys. Lett.* **1987**, *51*, 913-915.

3. http://reviews.cnet.com/oled/sony-xel-1-oled/4505-13948_7-32815284.html.

4. http://ces.cnet.com/8301-33379_1-57353040/samsung-announces-its-own-55-inch-oled-tv/

5. https://www.cnet.com/news/lg-says-white-oled-gives-it-ten-years-on-tv-competition/

6. Shirakawa, H.; Ikeda, S. *Polym. J.* **1971**, *2*, 231-244.

7. Heeger, A. J. *Rev. Mod. Phys.* **2001**, *73*, 681-700.

8. Meyer, G. J. *Nano Focus* **2010**, *4*, 4337-4343.

9. taf.fi/en/millennium-technology-prize/winners-2010/

10. Zhong, C.; Duan. C.; Huang, F.; Wu, H.; Cao, Y. *Chem. Mater.* **2011**, *23*, 326-340.

11. Wang, C.; Dong, H.; Hu, W.; Liu, Y.; Zhu, D. *Chem. Rev*. **2012**, *112*, 2208-2267.

12. Li, G.; Zhu, R.; Yang, Y. *Nat. Photonics*. **2012**, *6*, 153-161.

13. Ji, Y.; Lee, S.; Cho, B.; Song, S.; Lee, T. *ACS Nano*, **2011**, *5*, 5995-6000.

14. Bagher, A. M. *Int. J. of Renewable and Sustainable Energy* **2014**, *3*, 53-8.

15. Becquerel, E. *Comptes Rendus* **1839**, *9*, 561-7.

16. Fritts, C. E. *Am. J. Sci.* **1883**, *26*, 465-472.

17. Chapin, D. M.; Fuller, C. S.; Pearson, G. L. *J. Appl. Phys.* **1954**, *25*, 676-677.

18. Kibria, M. T.; Ahammed, A.; Sony, S. M.; Hossain, F.; Islam, S.-U. *Proc. of 5th Intl. Conf. on Environ. Aspects of Bangladesh* **2014**, 51-3.

19. Ferry, V. E.; Vwerschuuren, M. A.; Lare, C. Van; Schropp, R. R. I.; Atwater, H. A.; Polman, A. *Nano Lett.* **2011**, *11*, 4239-45.

20. Sites, J.; Pan, J. *Thin Solid Films* **2007**, *515*, 6099-6102.

21. Chopra, K. L.; Paulson, P. D.; Dutta, V. *Prog. Photovoltaics Res. Appl.* **2004**, *12*, 69-92.

22. Green, M. A.; Emery, K.; Hishikawa, Y.; Warta, W.; Dunlop, E. D. *Prog. Photovoltaics Res. Appl.* **2011**, *19*, 565-72.

23. Abdulrazzaq, O. A.; Saini, V.; Bourdo, S.; Dervishi, E.; Biris, A. S. *Part. Sci. Technol.* **2013**, *31*, 427-42.

24. Scharber, M. C.; Sariciftci, N. S. *Prog. Polym. Sci.* **2013**, *38*, 1929-40.

25. (a) Irwin, M. D.; Buchholz, B.; Hains, A. W.; Chang, R. P. H.; Marks, T. J. *P. Natl. Acad. Sci. USA* **2008**, *105*, 2783-7. (b) Shrotriya, V.; Li, G.; Yao, Y.; Chu, C. W.; Yang, Y. *Appl. Phys. Lett.* **2006**, *88*, 253503(1-3).

26. Tang, C. W. *Appl. Phys. Lett.* **1986**, *48*, 183-5.

27. (a) Block, M. A. B.; Kaiser, C.; Khan, A.; Hecht, S. *Top. Curr. Chem.* **2005**, 89-150. (b) Sanford, A. R.; Yamato, K.; Yang, X.; Han, Y.; and Gong, B. *Eur. J. Biochem.* **2004**, *271*, 1416-25. (c) Huc, I. *Eur. J. Org. Chem.* **2004**, 17-29. (d) Schmuck, C. *Angew. Chem. Int. Ed.* **2003**, 2448-52. (e) Hill, D. J.; Mio, M. J.; Prince, R. B.; Hughes, T. S.; Moore, J. S. *Chem. Rev.* **2001**, *101*, 3893-4011. (f) Gellman, S. H. *Acc. Chem. Res.* **1998**, *31*, 173-180.

28. (a) Kritzer, J. A.; Tirado-Rives, J.; Hart, S. A.; Lear, J. D.; Jorgensen, W. L.; and Schepartz, A. *J. Am. Chem. Soc.* **2005**, *127*, 167-78. (b) Dill, K. A.; Chan, H. S. *Nat. Struct. Biol.* **1997**, *4*, 10- 9. (c) Levinthal, C. *J. Chim. Phys.* **1968**, *65*, 44-5.

29. Zimm, B.H.; Bragg, J.K. *J. Chem. Phys.* **1959**, *31*, 526-35.

30. Pauling, L.; Corey, R. B.; Branson, H. R. *Proc. Natl. Acad. Sci. USA.*, **1951**, *37*, 205-11.

31. Watson, J. D.; Crick, F. H. C. *Nature* **1953**, *171*, 737-38.

32. Natta, G.; Pino, P.; Corradini, P.; Danusso, F.; Mantica, E.; Nazzanti, G.; Moraglio, G. *J. Am. Chem. Soc.* **1955**, *77*, 1708-10.

33. (a) Doty, P.; Lundberg, R. D. *J. Am. Chem. Soc.* **1956**, *78*, 4801-6. (b) Doty, P.; Lundberg, R. D. *J. Am. Chem. Soc.* **1957**, *79*, 2338-39.

34. Pino, P.; Lorenzi, G. P. *J. Am. Chem. Soc.* **1960**, *82*, 4745-47.

35. Millich, F.; Baker, G. K. *Macromolecules* **1969**, *2*, 122-28.

36. Nolte, R. J. M.; van Beijnen, A. J. M.; Drenth, W. *J. Am. Chem. Soc.* **1974**, *96*, 5932-33.

37. Green, M. M.; Gross, R. A.; Crosby, C., III.; Schilling, F. C. *Macromolecules* **1987**, *20*, 992-99.

38. Kollmar, C.; Hoffman, R. *J. Am. Chem. Soc.* **1990**, *112*, 8230-38.

39. Pini, D.; Iuliano, A.; Salvadori, P. *Macromolecules* **1992**, *25*, 6059-62.

40. Schmidt, E. *Angew. Makromol. Chem.* **1970**, *14*, 185-202.

41. Chen, F.; Lepore, G.; Goodman, M. *Macromolecules* **1974**, *7*, 779-83.

42. Yuki, H.; Okamoto, Y.; Taketani, Y.; Tsubota, T.; Marubayashi, Y. *J. Polym. Sci. Polym. Chem. Ed.* **1978**, *16*, 2237-51.

43. Fernandez-Santin, J. M.; Aymami, J.; Rodriguez-Galan, A.; Munoz-Guerra, S.; Subirana, J. A. *Nature* **1984**, *311*, 53-4.

44. Okamoto, Y.; Suzuki, K.; Ohta, K.; Hatada, K.; Yuki, H. *J. Am. Chem. Soc.* **1979**, *101*, 4763-65.

45. (a) Okamoto, Y.; Honda, S.; Okamoto, I.; Yuki, H.; Murata, S.; Noyori, R.; Takaya, H. *J. Am. Chem. Soc.* **1981**, *103*, 6971-73 (b) Okamoto, Y.; Hatada, K. *J. Liq. Chromatogr.* **1986**, *9*, 369-84 (c) Nakano, T. *J. Liq. Chromatogr. A* **2001**, *906*, 205-25.

46. (a) Martinek, T. A.; Fulop, F. *Eur. J. Biochem.* **2003**, *270*, 3657-66 (b) Cheng, R. P.; Gellman, S. H.; DeGrado, W. F. *Chem. Rev.* **2001**, *101*, 3219-32 (c) Degrado, W. F.; Schneider, J. P.; Hamuro, Y. *Peptide Res.* **1999**, *54*, 206-17.

47. Appella, D. H.; Christianson, L. A.; Klein, D. A.; Powell, D. R.; Huang, X.; Barchi Jr, J. J.; Gellman, S. H. *Nature*, **1997**, *387*, 381-4.

48. (a) Reuping, M.; Mahajan, Y. R.; Jaun, B.; Seebach, D. *Chem. Eur. J.* **2004**, *10*, 1607-15 (b) Seebach, D.; Matthews, J. L. *Chem. Commun.* **1997**, 2015-22.

49. Newman, M. S.; Lutz, W. B.; Lednicer, D. *J. Am. Chem. Soc.* **1955**, *77*, 3420-1.

50. Wynberg, H.; Groen, M. B. *J. Am. Chem. Soc.* **1968**, *86*, 727-38.

51. Han, S.; Bond, A. D.; Disch, R. L.; Holmes, D.; Shculman, J. M.; Teat, S. J.; Vollhardt, K. P. C.; Whitener, G. D. *Angew. Chem. Int. Ed.* **2002**, *41*, 3223-7.

52. Lehn, J.-M.; Rigault, A.; Siegel, J.; Harrowfield, J.; Chevrier, B.; Moras, D. *Proc. Natl. Acad. Sci. U. S. A.* **1987**, *84*, 2565-9.

53. Hanan, G. S.; Lehn, J.-M.; Kyritsakas, N.; Fischre, J. *J. Chem. Soc. Chem. Commun.* **1995**, 765-6.

54. Nelson, J. C.; Saven, J. G.; Moore, J. S.; Wolynes, P. G. *Science* **1997**, *277*, 1793-6.

55. Ohkita, M.; Lehn, J.-M.; Baum, G.; Fenske, D. *Chem. Eur. J.* **1999**, *5*, 3471-81.

56. Cuccia, L. A.; Lehn, J.-M.; Homo, J.-C.; Schmutz, M. *Angew. Chem. Int. Ed.* **2000**, *39*, 233-7.

57. Petitjean, A.; Cuccia, L. A.; Lehn, J.-M.; Nierengarten, H.; Schmutz, M. *Angew. Chem. Int. Ed.* **2002**, *41*, 1195-8.

58. Yang, X.; Yuan, L.; Yamato, K.; Brown, A. L.; Feng, W.; Furukawa, M.; Cheng Zeng, X.; Gong, B. *J. Am. Chem. Soc.* **2004**, *126*, 3148-62.

59. Cary, J. M.; Moore, J. S. *Org. Lett*. **2002**, *4*, 4663-6.

60. Yang, X.; Brown, A. L.; Furukawa, M.; Li, S.; Gardinier, W. E.; Bukowski, E. J.; Bright, F. V.; Zhen, C.; Zeng, X. C.; Gong, B. *Chem. Commun.* **2003**, 56-7.

61. Jones, T. V.; Slutsky, M. M.; Laos, R.; de Greef, T. F. A.; Tew, G. N. *J. Am. Chem. Soc.* **2005**, *127*, 17235-40.

62. Tashiro, K.; Kobayashi, M.; Tadokoro, H. *Macromolecules* **1977**, *10*, 413-420.

63. Burch, R. R.; Manring, L. E. *Macromolecules* **1991**, *24*, 1731-5.

64. Tanatani, A.; Yokoyama, A.; Azumaya, I.; Takakura, Y.; Mitsui, C.; Shiro, M.; Uchiyama, M.; Muranaka, A.; Kobayashi, N.; Yokozawa, T. *J. Am. Chem. Soc.* **2005**, *127*, 8553-61.

65. Jiang, H.; Legar, J.-M.; Huc, I. *J. Am. Chem. Soc.* **2003**, *125*, 3448-9.

66. Sanford, A. R.; Yamato, K.; Yang, X.; Yuan, L.; Han, Y.; Gong, B. *Eur. J. Biochem.* **2004**, *271*, 1416-25.

67. Van Gorp, J. J.; Vekemans, J. A. J. M.; Meijer, E. W. *Chem. Commun*. **2004**, 60-1.

68. Tanatani, A.; Kagechika, H.; Azumaya, I.; Fukutomi, R.; Ito, Y.; Yamaguchi, K.; Shido, K. *Tetrahedron Lett.* **1997**, *38*, 4425-8.

69. Yamaguchi, K.; Matsumura, G.; Kagechika, H.; Azumaya, I.; Ito, Y.; Itai, A.; Shido, K. *J. Am. Chem. Soc.* **1991**, *113*, 5474-5.

70. Corbin, P. S.; Zimmerman, S. C.; Thiessen, P. A.; Hawryluk, N. A.; Murray, T. J. *J. Am. Chem. Soc.* **2001**, *123*, 10475-88.

71. Chou, C.-E.; Wang, D.; Bagui, M.; Hsu, J.; Chakraborty, S.; Peng, Z. *Jr. of Luminescence* **2010**, *130*, 986-94.

72. Eickhoff, C. V.; He, S.-X.; Gobas, F. A. P. C.; Law, F. C. P. *Environ. Toxicology and Chem.* **2003**, *22*, 50-58.

73. Abdel-Shafy, H. I.; Mansour, M. S. M. *Egyptian Jr. of Petroleum* **2016**, *25*, 107-123.

74. J. Masih, R. Singhvi, K. Kumar, V.K. Jain, A. Taneja, *Aerosol Air Qual Res* **2012**, *12*, 515–25.

75. Akyuz, M.; Cabuk, H. *Sci Total Environ.* **2010**, *408*, 5550–58.

76. Kaminski, N. E.; Faubert, Kaplan, B. L.; Holsapple, M. P. 7th ed., in: Curtis D. Klaassen (Ed.), Casarett and Doull's Toxicology, the basic science of poisons, vol. 526, Mc-Graw Hill, Inc, (**2008**).

77. (a) Watson, M. D.; Fechtenkotter, A.; Mullen, K.; *Chem. Rev.* **2001**, *101*, 1267-1300 (b) Wu, J.; Pisula, W.; Mullen, K.; *Chem. Rev*. **2007**, *107*, 718-47.

78. Scholl, R.; Seer, C. *Justus Liebigs Annalen Der Chemie* **1912**, *394* (1/3), 111-77.

79. Scholl, R.; Seer, C. *Ber. Dtsch. Chem. Ges.***1911**, *44*, 1233-40.

80. Scholl, R.; Seer, C.; Weitzenbock, R. *Ber. Dtsch. Chem. Ges.***1910**, *43*, 2202-9.

81. Clar, E. *Ber. Dtsch. Chem. Ges.* **1929**, *62*, 1574-82.

82. Clar, E. *Ber. Dtsch. Chem. Ges.* **1929**, *62*, 350-359.

83. Clar, E.; John, F.; Hawran, B. *Ber. Dtsch. Chem. Ges.* **1929**, *62*, 940-50.

84. Clar, E.; Wallenstein, H.; Avenarius, R. *Ber. Dtsch. Chem. Ges.* **1929**, *62*, 950-55.

85. Clar, E.; Zander, M. *J. Chem. Soc*. **1958**, 1577-79.

86. Clar, E.; Zander, M. *J. Chem. Soc*. **1957**, 4616-19.

87. Clar, E.; Ironside, C. T.; Zander, M. *Tetrahedron* **1959**, *6* (4), 358-63.

88. Elbs, K.; Larsen, E. *Ber. Dtsch. Chem. Ges.* **1884**, *17*, 2847-49.

89. Fieser, L. F. Seligman, A. M. *J. Am. Chem. Soc*. **1935**, *35*, 228.

90. LeHoullier, C. S.; Gribble, G. W. *J. Org. Chem*. **1983**, *48*, 1682-85.

91. Davies, W.; Porter, Q. N. *J. Chem. Soc*. **1957**, 4967-70.

92. Grubbs, R. H.; Chang, S. *Tetrahedron* **1998**, *54*, 4113-450.

93. Iuliano, A.; Piccioli, P.; Fabbri, D. *Org. Lett*. **2004**, *6*, 3711-14.

94. Scholl, R.; Mansfeld, J. *Ber. Dtsch. Chem. Ges*. **1910**, *43*, 1734-46.

95. Hammerich, O.; Parker, V. D. *In Advances in Physical Organic Chemistry; Gold, V., Bethell, D., Eds.; Academic Press* **1984**, *20*, 55-189.

96. Simpson, C. D.; Mattersteig, G.; Martin, K.; Gherghel, L.; Bauer, R. E.; Rader, H. J.; Mullen, K. *J. Am. Chem. Soc.* **2004**, *126*, 3139-47.

97. Kovacic, P.; Jones, M. B. *Chem. Rev.* **1987**, *87*, 357-79.

98. (a) Laarhoven, W. H. *Recl. Trav. Chim. Pays-Bas* **1983**, *102*, 185−204 (b) Mallory, F. B.; Mallory, C. W. *Org. Reactions* **1984**, *30*, 1−456. (c) Jørgensen, K. B. *Molecules* **2010**, *15*, 4334−58.

99. De Vries, J. G.; Hubbard, S. A. *J. Chem. Soc. Commun.* **1988**, 1172-3.

100. Kar, S.; Lahiri, S. *J. Chem. Soc. Commun*. **1995**, 957-8.

101. Banerjee, S.; Sinha, S.; Pradhan, P.; Caruso, A.; Liebowitz, D.; Parrish, D.; Rossi, M.; Zajc, B. *J. Org. Chem*. **2016**, *81*, 3983-93.

102. Floyd, A.J.; Dyke, S. F; Ward, S. E. *Chem. Rev.* **1976**, *76*, 509-62.

103. Yang, C.; Yang, D. T. C.; Harvey, R. G. *Synlett* **1992**, 799-800.

104. Scott, L. T.; Boorum, M. M.; McMahon, B. J.; Hagen, S.; Mack, J.; Blank, J.; Wegner, H.; de Meijere, A. *Science* **2002**, *295* (5559), 1500-3.

105. Berliner, E. *Org. React.* **1948**, *5*, 229-289.

106. Diederich, F.; Staab, H. A. *Angew. Chem., Int. Ed. Engl.* **1978**, *17* (5), 372-374.

107. Krieger, C.; Diederich, F.; Schweitzer, D.; Staab, H. A. *Angew. Chem., Int. Ed. Engl.* **1979**, *18* (9), 699-701.

108. Staab, H. A.; Diederich, F. *Chem. Ber.-Rec.* **1983**, *116* (10), 3487-3503.

109. Crispi, X.; Cornil, J.; Friedlein, R.; Okudaira, K. K.; Lemaur, V.; Crispin, A.; Krestmont, G.; Lehmann, M.; Fahlman, M.; Lazzaroni, R.; Geerts, Y.; Wendin, G.; Ueno, N.; Bredas, J.-L.; Salaneck, W. R. *J. Am. Chem. Soc.* **2002**, *126*, 11889-99.

110. Warman, J. M.; de Haas, M. P.; Dicker, G.; Grozema, F. C.; Piris, J.; Debije, M. G. *Chem. Mater*. **2004**, *16*, 4600-09.

111. Jaiswal, M.; Menon, R. *Polym. Int.* **2006**, *55*, 1371-84.

112. Heiney, P. A. *Structure and Physical Properties of Columnar Liquid Crystals. In Handbook of Liquid Crystals*; Goodby, J. W., Collings, P. J., Kato, T., Tschierske, C., Gleeson, H. F., Raynes, P., Eds.; Wiley-VCH: Weinheim, **2014**, *4*, 521−68.

113. Steed, J. W.; Turner, D. R.; Wallace, K. J. *Core Concepts in Supramolecular Chemistry and Nanochemistry, John Wiely & Sons, Ltd., Chichester, UK*, **2007**.

114. Wohrle, T., Wurzbach, I., Kirres, J., Kostidou, A., Kapernaum, N., Litterscheidt, J., Haenle, J. C., Staffield, P., Baro, A., Giesselmann, F. Laschat, S. *Chem. Rev*. **2016**, *116*, 1139−241.

115. Van de Graats, AM; Warman, JM; Fechtenkötter, A; Brand, JD; Harbison, MA; Müllen, K. *Adv. Mater* **1999**, *11*, 1469–72.

116. Christ, T.; Glusen, B.; Greiner, A.; Kellner, A.; Sander, R., Stumpflen, V.; Tsukruk, V.; Wendorff, J. H. *Adv. Mater*. **1997**, *9*, 48-52.

117. Schmit-Mende, L.; Fechtenkotter, A.; Mullen, K.; Moons, E.; Friend, R.; McKenzie, J. D. *Science* **2001**, *293*, 1119-22.

118. Schmidt-Mende, L.; Watson, M. D.; Mullen, K.; Friend, R. H. *Mol. Cryst. Liq. Cryst.* **2003**, *396*, 73-90.

119. Dyreklev, P; Gustafsson, G; Inganäs, O; Stubb, H. *Solid State Commun*. **1992**, *82*, 317–20.

120. Sirringhaus, H.; Wilson, R. J.; Friend, R. H.; Inbasekaran, M.; Wu, W.; Woo, E. P.; Grell, M.; Bradley, D. D. *Appl. Phys. Lett*. **2000**, *77*, 406-8.

121. Adam, D.; Schuhmacher, P.; Simmerer, J.; Haussling, L.; Siemensmeyer, K.; Etzbach, K. H.; Rinsdorf, H.; Harrer, D. *Nature* **1994**, *371*, 141-3.

122. Grelet, E.; Dardel, S.; Bock, H.; Goldmann, M.; Lacaze, E.; Nallet, F. Eur. Phys. J. E.: *Soft Matter Biol. Phys*. **2010**, *31*, 343-9.

123. Kaafarani, B. R. *Chem. Mater*. **2010**, *23*, 378-96.

124. Ompong, D.; Yeboah, D.; Narayan, M.; Singh, J. *Organic solar cells research at Charles Darwin University*, **2016**.

125. Zhao, H.; He, Z.; Xu, M.; Liang, C.; Kumar, S. *Phys. Chem. Chem. Phys*. **2016**, *18*, 8554-60.

126. Carsten, B.; Szarko, J. M.; Son, H. J.; Wang, W.; Lu, L.; He, F.; Rolczynski, B. S.; Lou, S. J.; Chen, L. X.; Yu, L. *J. Am. Chem. Soc.* **2011**, *133*, 20468-75.

127. Dutta, Tanmoy. *Polycylic Aromatic Hydrocarbon (PAH)-Based Conjugated Macrocycles and Polymers For Electronic Applications.* Ph. D. Thesis. University of Missouri-Kansas City, **2014**.

128. Rempala, P.; Kroulik, J.; King, B. T. *J. Org. Chem.* **2006**, *71*, 5067-81.

129. Xin, H.; Guo, X.; Kim, F. S.; Ren, G.; Watson, M. D.; Jenekhe, S. A. *J. Mater. Chem.* **2009**, *19*, 5303-10.

130. Perepichka, I. F.; Perepichka, D. F. *Handbook of Thiophene-Based Materials: Applications in Organic Electronics and Photonics, John Wiley & Sons, Ltd*, **2009**.

131. Bao, Z.; Chan, W. K.; Yu, L. *J. Am. Chem. Soc.* **1995**, *117*, 12426-35.

132. Frisch, M. J. *et al. Gaussian 03, Revision C.02, Gaussian, Inc., Wallingford CT*, **2004**.

133. Blouin, N.; Michaud, A.; Gendron, D.; Wakim, S.; Blair, E.; Neagu-Plesu, R.; Belletête, M.; Durocher, G.; Tao, Y.; Leclerc, M. *J. Am. Chem. Soc.* **2007**, *130*, 732-42.

134. Belletête, M.; Blouin, N.; Boudreault, P.-L. T.; Leclerc, M.; Durocher, G. *J. Phys. Chem. A* **2006**, *110*, 13696-704.

135. Belletete, M.; Durocher, G.; Hamel, S.; Cote, M.; Wakim, S.; Leclerc, M. *J. Chem. Phys.* **2005**, *122*, 104303-9.

136. Kurashige, Y.; Nakajima, T.; Kurashige, S.; Hirao, K.; Nishikitani, Y. *J. Phys. Chem. A* **2007**, *111*, 5544-8.

137. Osuna, R. M.; Ortiz, R. P.; Okamoto, T.; Suzuki, Y.; Yamaguchi, S.; Hernández, V.; López Navarrete, J. T. *J.Phys. Chem. B* **2007**, *111*, 7488-96.

138. Chiang, C. K.; Fincher, C. R., Jr.; Park, Y. W.; Heeger, A. J.; Shirakawa, H.; Louis, E. J.; Gau, S. C.; MacDiarmid, A. G. *Phys. Rev. Lett.* **1977**, *39*, 1098-101.

139. Shirakawa, H.; Louis, E. J.; MacDiarmid, A. G.; Chiang, C. K.; Heeger, A. J. *J. Chem. Soc., Chem. Commun.* **1977**, 578-80.

140. Skotheim, T. A.; Reynolds, J. R.; Elsenbaumer, R. L. *Handbook of Conducting Polymers. Marcel Dekker Inc., New York, 2nd edition*, **1998**, 1-11.

141. Janata, J.; Josowicz, M. *Nat. Mater.* **2003**, *2*, 19-24.

142. Yu, H.; Shao, S.; Yan, L.; Meng, H.; He, Y.; Yao, C.; Xu, P.; Zhang, X.; Hu, W.; Huang, W. *J. Mater. Chem.* **2016**, *4*, 2269-73.

143. (a) Irwin, M. D.; Buchholz, B.; Hains, A. W.; Chang, R. P. H.; Marks, T. J. *P. Natl. Acad. Sci. USA* **2008**, *105*, 2783-7 (b) Shrotriya, V.; Li, G.; Yao, Y.; Chu, C. W.; Yang, Y. *Appl. Phys. Lett.* **2006**, *88*, 073508(1-3).

144. Tang, C. W. *Appl. Phys. Lett.* **1986**, *48*, 183-5.

145. Scharber, M. C.; Wuhlbacher, D.; Koppe, M.; Denk, P.; Waldauf, C.; Heeger, A. J.; Brabec, C. L. *Adv. Mater.* **2006**, *18*, 789-94.

146. (a) Peumans, P.; Yakimov, A.; Forrest, S. R. *J. Appl. Phys.* **2003**, *93*, 3693-723 (b) Peumans, P.; Forrest, S. R. *Chem. Phys. Lett.* **2004**, *398*, 27-31.

147. Roncali, J. *Macromol. Rapid Commun.* **2007**, *28*, 1761-75.

148. Wudl, F.; Kobayyashi, M.; Heeger, A. J. *J. Org. Chem.* **1984**, *49*, 3382-84.

149. Bredas, J. L.; Heeger, A. J.; Wudl, F. *J. Chem. Phys.* **1986**, *85(8)*, 4673-4678.

150. Jenekhe, S. A. *Nature* **1986**, *322*, 345-7.

151. Kertsez, M.; Choi, C. H.; Yang, S.; *Chem. Rev.* **2005**, *105*, 3448-81.

152. Roncali, J. *Chem. Rev.* **1997**, *97*, 173-206.

153. Kurti, J.; Surjan, P. R.; Kertesz, M.; Frapper, G. *Synth. Met.* **1993**, *55-57*, 4338-43.

154. Ou, P.; Shen, W.; He, R.; Xie, X.; Zeng, C.; Li, M. *Polym Int.* **2011**, *60*, 1408-18.

155. Brisset, H.; Thobie-Gautier, C.; Gorgues, A.; Jubault, M.; Roncali, J. *J. Chem. Soc., Chem. Commun.* **1994**, 1305-6.

156. Roncali, J.; Thobie-Gautier, C. *Adv. Mater.* **1994**, *6*, 846-8.

157. Blanchard, P.; Brisset, H.; Riou, A.; Hierle, R.; Roncali, J. *J. Org. Chem*, **1998**, *63*, 8310-9.

158. Roncali, J.; Thobie-Gautier, C.; Elandaloussi, E.; Frere, P. *J. Chem. Soc., Chem. Commun.* **1994**, 2249-50.

159. Lee, J. S.; Son, S. K.; Song, S.; Kim, H.; Lee, D. R.; Kim, K.; Ko, M. J.; Choi, D. H.; Kim, B.; Cho, J. H. *Chem. Mater* **2012**, *24*, 1316-23.

160. Jen, K. Y.; Maxfield, M. R.; Shacklette, L. W.; Elsenbaumer, R. L. *J. Chem. Soc., Chem. Commun*. **1987**, 309-11.

161. Waltman, R. J.; Bargon, J.; Diaz, A. F. *J. Phys. Chem.* **1983**, *87*, 1459-63.

162. Lambert, T. L., Ferraris, J. P. *J. Chem. Soc., Chem. Commun.* **1991**, 752-4.

163. Lambert, T. L., Ferraris, J. P. *J. Chem. Soc., Chem. Commun.* **1991**, 1268-70.

164. Roncali, J.; Garreau, R.; Yassar, A.; Marque, P.; Garnier, F.; Lemaire, M. *J. Phys. Chem.* **1987**, *91*, 6706-14.

165. Kirchmeyer, S.; Reuter, K. *J. Mater. Chem.* **2005**, *15*, 2077-88.

166. Roncali, J.; Blanchar, P.; Frere, P. *J. Mater. Chem*. **2005**, *15*, 1589-610.

167. Hendriks, K. H.; Li, W.; Wienk, M. M.; Janssen, R. A. J. *Adv. Energy Mater*. **2013**, *3*, 674-9.

168. Liang, Y.; Feng, D.; Wu, Y.; Tsai, S.- T.; Li, G.; Ray, C.; Yu, L. *J. Am. Chem. Soc.* **2009**, *131*, 7792-9.

169. Zhang, Q. T.; Tour, J. M. *J. Am. Chem. Soc.* **1998**, *120(2)*, 5355-62.

170. (a) Greenham, N. C.; Moratti, S. C.; Bradley, D. D. C.; Friend, R. H.; Holmes, A. B. *Nature*, **1993**, *365*, 628-30 (b) Demanze, F.; Yassar, A.; Garnier, F. *Macromolecules*, **1996**, *29*, 4267-73.

171. Crossley, D. L.; Cade, I. A.; Clark, E. R.; Escande, A.; Humphries, M. J.; King, S. M.; Victoria-Yrezabal, I.; Ingleson, M. J.; Turner, M. L. *Chem. Sci.* **2015**, *6*, 5144-51.

172. Zhang, M.; Gu, Y.; Guo, X.; Liu, F.; Zhang, S.; Huo, L.; Russell, T. P.; Hou, J. *Adv. Mater.* **2013**, *25*, 4944-9.

173. Liang, Y.; Xu, Z.; Xia, J.; Tsai, S.-T.; Wu, Y.; Li. G.; Ray, C.; Yu, L. *Adv. Mater.* **2010**, *22*, E135-8.

174. He, Z.; Zhong, C.; Huang, X.; Wong, W.-Y.; Wu, H.; Chen, L.; Su, S.; Cao, Y. *Adv. Mater.* **2011**, *23*, 4636-43.

175. Peng, Q.; Huang, Q.; Hou, X.; Chang, P.; Xu, J.; Deng, S. *Chem. Commun.* **2012**, *48*, 11452-4.

176. Badgujar, S.; Song, C. E.; Shin, W. S.; Moon, S.-J.; Kang, I.-N.; Lee, J.; Cho, s.; Lee, S. K.; Lee, J.-C. *Macromolecules* **2012**, *45*, 6938-45.

177. Uy, R. L.; Price, S. C.; You, W. *Macromol. Rapid Commun.* **2012**, *33*, 1162-77.

178. Zhou, H.; Yang, L.; Price, S. C.; Knight, K. J.; You, W. *Angew. Chem. Int. Ed.* **2010**, *49*, 7992-5.

179. Zhao, X.; Yang, D.; Lv, H.; Yin, L.; Yang, X. *Polym. Chem.* **2013**, *4*, 57-60.

180. Sirringhaus, H.; Fiend. R. H.; Wang, C.; Leuninger, J.; Mullen, K. *J. Mater. Chem.* **1999**, *9*, 2095-101.

181. Chou, C.-E.; Li, Y.; Che, Y.; Zang, L.; Peng, Z. *RSC Adv*. **2013**, *3*, 20666-72.

182. Dutta, T.; Li, Y.; Thornton, A. L.; Zhu, D.-M.; Peng, Z. *J. Polym. Sci., Part A: Polym. Chem.* **2013**, *51*, 3818-28.

183. Chen, F.; Zhang, J.; Wan, X. *Chem. Eur. J.* **2012**, *18*, 4558-4567.

184. Tovar, J. D.; Rose, A.; Swager, T. M. *J. Am. Chem. Soc.* **2002**, *124*, 7762-9.

185. Cho, D. M.; Parkin, S. R.; Watson, M. D. *Org. Lett.* **2005**, *7*, 1067-8.

186. Jørgensen, K. B. *Molecules* **2010** *15*, 4334-58.

187. Mallory, F. B.; Mallory, C. W. *Org. React.* **1984**, *30*, 1-456.

188. Kauffmann, T.; Torii, S.; Inokuchi, T. *Encyclopedia of Reagents for Organic Synthesis, J. Wiley & Sons, New York.* **2004**.

189. Abdo, N. I.; Ku, J.; El-Shehawy, A. A.; Shim, H.-S.; Min, J.-K.; El-Barbary, A. A.; Jang, Y. H.; Lee, J.-S. *J. Mater. Chem. A* **2013**, *1*, 10306-17.

190. Guo, X.; Zhou, N.; Lou, S. J.; Hennek, J. W.; Ponce Ortiz, R.; Butler, M. R.; Boudreault, P.-L. T.; Strzalka, J.; Mortin, P.-O.; Leclerc, M.; Lopez Navarrete, J. T.; Ratner, M. A.; Chen, L. X.; Chang, R. P. H.; Facchetti, A.; Marks, T. J. *J. Am. Chem. Soc.* **2012**, *134*, 18427-39.

191. Chou, C.-E.; Wang, D.; Bagui, M.; Hsu, J.; Chakraborty, S.; Peng, Z. *J. Lumin.* **2010**, *130*, 986-94.

192. Johnson, B. G.; Gill, P. M. W.; Pople, J. A. *J. Chem. Phys.* **1993**, *98*, 5612-26.

193. Lee, C.; Yang, W.; Parr, R. G. *Phys. Rev. B.* **1988**, *37*, 785-9.

194. Becke, A. D. *J. Chem. Phys.* **1993**, *98*, 1372-7.

195. Li, Y.; Dutta, T.; Gerasimchuk, N.; Wu, S.; Shetye, K.; Lu, J.; Wang, R.; Zhu, D.-M.; Peng, Z. *ACS Appl. Mater. Interfaces* **2015**, *7*, 9372-84.

196. Homyak, P. D.; Liu, Y.; Harris, J. D.; Liu, F.; Carter, K. R.; Russell, T. P.; Coughlin, E. B. *Macromolecules* **2016**, *49*, 3028-37.

197. Meyer, F. *Prog. Polym. Sci.* **2015**, *47*, 70-91.

198. Kawamato, K.; Grindy, S. C.; Liu, J.; Holten-Andersen, J.; Johnson, J. A. *ACS Macro Lett.* **2015**, *4*, 458-61.

199. Tour, J.; Huq, R.; Mann, J. A.; Jalilov, A.; Nilewski, L.; Kent, T.; Beeton, C. *U. S. Pat. Appl. Publ.*, **2016**, 20160175292.

200. Yu, G.; Gao, J. C.; Hummelen, F.; Wudl, F.; Heeger, J. *Science* **1995**, *270*, 1789-91.

201. Guo, X.; Facchetti, A.; Marks, T. J. *Chem. Rev.* **2014**, *114*, 8943-9021.

202. Liu, C.; Wang, K.; Gong, X.; Heeger, A. J. *Chem. Soc. Rev.* **2016**, *45*, 4825-46.

203. Singh, T. B.; Marjanovic, N.; Matt, G. J.; Gunes, S.; Sariciftci, N. S.; Ramil, A. M.; Sitter, H.; Schwodiauer, R.; Bauer, S. *Org. Electron.* **2005**, *6*, 105-10.

204. Cai, W.; Gong, X.; Cao, Y. *Sol. Energy Mater. Sol. Cells* **2010**, *94*, 114-27.

205. Lu, L.; Zheng, T.; Wu, Q.; Schneider, A. M.; Zhao, D.; Yu, L. *Chem. Rev.* **2015**, *115*, 12666-731.

206. Dennler, G.; Scharber, M. C.; Brabec, C. J. *Adv. Mater.* **2009**, *21*, 1323-38.

207. Po, R.; Bernardi, A.; Calabrese, A.; Carbonera, C.; Corso, G.; Pellegrino, A. *Energy Environ. Sci.* **2014**, *7*, 925-43.

208. Meng, D.; Sun, D.; Zhong, C.; Liu, T.; Fan, B.; Huo, L.; Li, Y.; Jiang, W.; Choi, H.; Kim, T.; Kim, J. Y.; Sun. Y.; Wang, Z.; Heeger, A. J. *J. Am. Chem. Soc.* **2016**, *138*, 375-80.

209. Nielsen, C. B.; Holliday, S.; Chen, H.-Y.; Cryer, S. J.; McCulloch, I. *Acc. Chem. Res.* **2015**, *48*, 2803-12.

210. Zhan, X.; Facchetti, A.; Barlow, S.; Marks, T. J.; Ratner, M. A.; Wasielewski, M. R.; Marder, S. R. *Adv. Mater.* **2011**, *23*, 268-84.

211. Lin, Y.; Li, Y.; Zhan, X. *Chem. Soc. Rev.* **2012**, *41*¸4245-72.

212. Li, C.; Wonneberger, H. *Adv. Mater.* **2012**, *24*, 613-36.

213. Kozma, E.; Catellani, M. *Dyes Pigm.* **2013**, *98*, 160-79.

214. Hwang, Y.-J.; Courtright, B. A. E.; Ferreira, A. S.; Tolbert, S. H.; Jenekhe, S. A. *Adv. Mater.* **2015**, *27*, 4578-84.

215. Huang, J.; Yin, Z.; Zheng, Q. *Energy Environ. Sci.* **2011**, *4*, 3861-77.

216. Wang, X.; Li, Z.; Shi, J.; Yu. Y. *Chem. Rev.* **2014**, *114*, 9346-84.

217. Zhou, Y.; Eck, M.; Kruger, M. *Energy Environ. Sci.* **2010**, *3*, 1851-64.

218. Wright, M.; Uddin, A. *Sol. Energy Mater. Sol. Cells* **2012**, *107*, 87-111.

219. Li, Y.; Lu, P.; Jiang, M.; Dhakal, R.; Thapaliya, P.; Peng, Z.; Jha, B.; Yan, X. *J. Phys. Chem. C* **2012**, *116*, 25248-56.

220. Mathias, F.; Fokina, A.; Landfester, K.; Tremel, W.; Schmid, F.; Char, K.; Zentel, R. *Macromol. Rapid Commun.* **2015**, *36*, 959-83.

221. Hsu, S.-C.; Liao, W.-P.; Lin, W.-H.; Wu, J.-J. *J. Phys. Chem. C* **2012**, *116*, 25721-6.

222. Li, Y.; Li, S.; Jin, L.; Murrowchick, J. B.; Peng, Z. *RSC Adv.* **2013**, *3*, 16308-12.

223. Zhao, L.; Pang, X.; Adhikary, R.; Petrich, J. W.; Lin, Z. *Angew. Chem. Int. Ed.* **2011**, *50*, 3958-62.

224. Li, S.; Li, Y.; Wisner, C. A.; Jin, L.; Leventis, N.; Peng, Z. *RSC Adv.* **2014**, *4*, 35823-32.

225. Gouzerh, P.; Proust, A. *Chem. Rev.* **1998**, *98*, 77-112.

226. Yamase, T.; Pope, M. T. *Polyoxometalate Chemistry for Nano-composite design: Kluwer Academic/ Plenum Publishers:* Boston, MA, USA **2002**, 4763-8.

227. Pope, M. T.; Muller, A. *Polyoxometalate Chemistry From Topology via Self-Assembly to Applications; Kluwer Academic Publishers:* Boston, MA, USA **2001**, 1-6.

228. Pope, M. T.; Muller, A. *Heteropoly and Isopoly Oxometalates; Springer Verlag:* New York, NY, USA **1983**, 1-227.

229. Pope, M. T.; Muller, A. *Topics in Molecular Organization and Engineering; Series: Polyoxometalates*; Kluwer Academic Publishers: Alphen and den Rijn, The Netherlands **1994**, *10*, 117.

230. Pope, M. T.; Muller, A.; *Polyoxometalates: Oxoanion Clustersof the Early Transition Elements. In Molecula Engineering*; Kluwer Academic Publishers: Alphen and den Rijn, The Netherlands **1993**, *3*, 118.

231. Pope, M. T.; Muller, A. *Angew. Chem. Int. Ed. In Eng.* **1991**, *30*, 34-48.

232. Long, D.-L.; Tsunashima, R.; Cronin, L. *Angew. Chem. Int. Ed.* **2010**, *49*, 1736-58.

233. Coronado, E.; Day, P. *Chem. Rev.* **2004**, *104*, 5419-48.

234. Sap, A.; Absillis, G.; Parac-Vogt, T. N. *Dalton Trans.* **2015**, *44*, 1539-48.

235. Wang, R.; Li, Y.; Shetye, K.; Dutta, T.; Jin, L.; Li, S.; Peng, Z. *Eur. Jr. of Inorg. Chem.* **2015**, *4*, 656-63.

236. Tong, U.; Chen, W.; Ritchie, C.; Wang, X.; Song, Y.-F. *Chem. A Eur. Jr.* **2014**, *20*, 1500-4.

237. Schreiber, R. E.; Cohen, H.; Leitus, G.; Wolf, S. G.; Zhou, A.; Que, L.; Neumann, R. *J. Am. Chem. Soc.* **2015**, *137*, 8738-48.

238. Rhule, J. T.; Hill, C. L.; Judd, D. A.; Schinazi, R. F. *Chem. Rev.* **1998**, *98*, 327-58.

239. Busche, C.; Vila-Nadal, L.; Yan, J.; Miras, H. N.; Long, D.-L.; Georgiev, V. P.; Asenov, A.; Pedersen, R. H.; Gadegaard, N.; Mirza, M. M.; Paul, D. J. Poblet, J. M.; Cronin, L. *Nature* **2014**, *515*, 545-49.

240. Ritchie, C.; Bryant, G. *Dalton Trans.* **2015**, *44*, 20826-29.

241. Lopez, X.; Carbo, J. J.; Bo.; C.; Poblet, J. M. *Chem. Soc. Rev.* **2012**, *41*, 7537-71.

242. Pauling, L. *J. Am. Chem. Soc.* **1929**, *51*, 2868-80.

243. Keggin, J. F. *Proc. R. Soc. London Ser. A* **1934**, *144*, 75-100.

244. Neyman, A.; Wang, Y.; Sharet, S.; Varsano, N.; Botar, B.; Kogerler, P.; Meshi, L.; Weinstock, I. A. *Chem. Commun.* **2012**, *48*, 2207-9.

245. Canny, J.; Teze, A.; Thouvenot, R.; Herve, G. *Inorg. Chem.* **1986**, *25*, 2114-19.

246. Dawson, B. *Acta Crystall.* **1953**, *6*, 113-26.

247. James, F.; Anderson, J.; Briscoe, H. *Nature* **1937**, *139*, 109.

248. Jeannin, Y. P. *Chem. Rev.* **1998**, *98*, 51-76.

249. Strong, J. B.; Yap, G. P. A.; Ostrander, R.; Liable-Sands, L. M.; Rheingold, A. L.; Thouvenot, R.; Gouzerh, P.; Matta, E. A. *J. Am. Chem. Soc.* **2000**, *122*¸ 639-49.

250. Hirsch, A. *Synthesis* **1995**, 895-913.

251. Bridgeman, A. J.; Cavigliasso, G. *Inorg. Chem.* **2002**, *41*, 1761-70.

252. Bi, L.-H.; Zhou, W.-H.; Jiang, J.-G.; Dong, S.-J. *J. Electroanal. Chem.* **2008**, *624*, 269-74.

253. Gao, W.; Ma, H.; Zheng, D.; Dong, Z.; Wu, L.; Bi, L. *Dalton Trans.* **2015**, *44*, 14763-70.

254. Zhou, C.; Li, S.; Zhu, W.; Pang, H.; Ma, H. *Electrochim. Acta* **2013**, *113*, 454-63.

255. Carraro, M.; Gross, S. *Materials* **2014**, *7*, 3956-89.

256. a) Hill, C. L. *Chem. Rev.* **1998**, *98*, 1-2 b) Cotton, F. A.; Wilkinson, G. A.; Murillo, C. A.; Bochman, M. *Advanced Inorganic Chemistry*; John Wiley & Sons. Inc.: New York, NY **1999** c) Long, D.-L.; Burkholder, E.; Cronin, L. *Chem. Soc. Rev.* **2007**, *36*, 105-21.

257. Xu, L.; Lu, M.; Xu, B.; Wei, Y.; Peng, Z.; Powell, D. R. *Angew. Chem., Int. Ed.* **2002**, *41*, 4129-32.

258. Li, Y.; Jin, L.; Chakraborty, S.; Li, S.; Lu, P.; Zhu, D.-M.; Yan, X.; Peng, Z. *J. Polym. Sci., Part B: Polym. Phys.* **2014**, *52*, 122-33.

259. Peng, Z. *Angew. Chem., Int. Ed.* **2004**, *43*, 930-5.

260. Proust, A. *Inorg. Chim. Acta* **1994**, *224*, 81-95.

261. Gouzerh, P.; Proust, A. *Chem. Rev.* **1998**, *98*, 77-111.

262. Strong, J. B. *J. Am. Chem. Soc.* **2000**, *122*, 639-49.

263. Strong, J. B.; Haggerty, B. S.; Rheingold, A. I.; Matta, E. A. *Chem. Commun.* **1997**, 1137-38.

264. Strong, J. B.; Ostrander, R.; Rheingold, A. I.; Matta, E. A. *J. Am. Chem. Soc.* **1994**, *116*, 3601-2.

265. Clegg, W.; Errington, R. J.; Fraser, K.; Holmes, S. A.; Schafer, A. *J. Chem. Soc., Chem. Commun.* **1995**, 455-6.

266. Huang, Y.; Zhang, J.; Hao, J.; Wei, Y. *Sci. Rep.* **2016**, *6*, 24759(1-10).

267. Xu, L.; Lu, M.; Xu, B.; Wei, Y.; Peng, Z.; Powell, D. R. *Angew. Chem. Int. Ed. Engl.* **2002**, *41*, 4129-32.

268. Xu, B.; Lu, M.; Kang, J.; Wang, D.; Brown, J.; Peng, Z. *Chem. Mater.* **2005**, *17*, 2841-51.

269. Lu, M.; Wei, Y.; Xu, B.; Cheung, C. F.-C.; Peng, Z.; Powell, D. R. *Angew. Chem. Int. Ed. Engl.* **2002**, *41*, 1566-8.

270. Kang, J.; Xu, B.; Peng, Z.; Zhu, X.; Wei, Y.; Powell, D. R. *Angew. Chem. Int. Ed. Engl.* **2005**, *44*, 6902-5.

271. Yin, P. C.; Wu, P. F.; Xiao, Z. C.; Li, D.; Bitterlich, E.; Zhang, J.; Cheng, P.; Vezenov, D. V.; Liu, T. B.; Wei, Y. G. *Angew. Chem. Int. Ed.* **2011**, *50*, 2521-25.

272. Wei, Y.; Xu, B.; Barnes, C. L.; Peng, Z. *J. Am. Chem. Soc.* **2001**, *123*, 4083-4.

273. Xiao, F.; Hao, J.; Zhang, J.; Lv, C.; Yin, P.; Wang, L.; Wei, Y. *J. Am. Chem. Soc.* **2010**, *132*, 5956-7.

274. Yin, P.; Zhang, J.; Li, T.; Zuo, X.; Hao, J.; Warner, A. M.; Chattopadhyay, S.; Shibata, T.; Wei, Y.; Liu, T. *J. Am. Chem. Soc.* **2013**, *135*, 4529-36.

275. Zhang, J.; Hao, J.; Wei, Y.; Xiao, F.; Yin, P.; Wang, L. *J. Am. Chem. Soc.* **2010**, *132*, 14-15.

276. Zhu, Y.; Yin, P.; Xiao, F.; Li, D.; Bitterlich, E.; Xiao, Z.; Zhang, J.; Hao, J.; Liu, T.; Wang, Y.; Wei, Y. *J. Am. Chem. Soc.* **2013**, *135*, 17155-17160.

277. Roncali, J. *Adv. Energy Mater.* **2011**, *1*, 147-60.

278. Chen, T. L.; Zhang, Y.; Smith, P.; Tamayo, A.; Liu, Y.; Ma, B. *ACS Appl. Mater. Interfaces* **2011**, *3*, 2275-80.

279. Cao, J.; Du, X.; Chen, S.; Xiao, Z.; Ding, L. *Phys. Chem. Chem. Phys.* **2014**, *16*, 3512-4.

280. Azcarate, I.; Huo, Z.; Farha, R.; Goldmann, M.; Xu, H.; Hasenknopf, B.; Lacute, E.; Ruhlmann, L. *Chem.-Eur. J.* **2015**, *21*, 8271-2.

281. Jin, Lu *Studies of Conjugated Small Molecules, Polymers and Organic-inorganic Hybrid Materials for Photovoltaic Applications.* Ph. D. Thesis. University of Missouri-Kansas City, **2015**.

282. Haso, F.; Wang, R.; Yin, P.; Zhou, J.; Lu, J.; Peng, Z.; Liu, T. *Eur. J. Inorg. Chem.* **2014**, 4589-92.

283. Li, Y.; Shetye, K.; Baral, K.; Lu, J.; Oster, J. D.; Zhu, D.-M.; Peng, Z. *RSC Adv.* **2016**, *6*, 29909-19.

284. Xu, L.; Lu, M.; Xu, B.; Wei, Y.; Powell, D. R.; Peng, Z. *Angew. Chem. Int. Ed.* **2002**, *41*, 4129-4132.

285. Xu, B.; Pan, Y.; Zhang, J.; Peng, Z. *Synthetic Metals* **2000**, *114*, 337-345.

286. Oberholzer, M.; Frech, C. M. *Journal of visual experiments* **2014**, *85*, doi: 10.3791/51444.

287. Bolliger, J. L.; Frech, C. M. *Chem. Eur. J.* **2010**, *16*, 11072-81.

288. Tietze, L. F.; Kettschau, G.; Heuschert, U.; Nordmann, G. *Chem. Eur. J.* **2001**, *7*, 368-73.

VITA

Kuldeep Shetye was born on March 4, 1982 in Pune, Maharashtra, and completed his education including high school, bachelors, and Master's degree from University of Mumbai, India. He earned his batchelors degree in Chemistry with First class, and chose Organic chemistry for his research during M.Sc. He completed it successfully in 2008 by defending the thesis in the topic of "Synthesis of new spiro heteroycles". He joined the Department of Chemistry at University of Missouri-Kansas City in August 2011 and started working for Prof. Peng research laboratory by the end of December 2011.

During the Ph. D. study, the emphasis of his research was mainly on the synthesis of conjugated polymers that are capable of rearranging themselves in favorable folding conformations, especially having triphenylene, imide-functionalized naphathalenedithiophenes, and hybrid conjugated polymers. The list of publications and presentations at various meetings are shown below.

PUBLICATIONS

- Li, Yong; **Shetye, Kuldeep**; Baral, Khagendra; Jin, Lu; Oster, John, Zhu, Da-Ming, Peng, Zhonghua 'Main-chain polyoxometalate-containing donor–acceptor conjugated copolymers: synthesis, characterization, morphological studies and applications in single-component photovoltaic cells' *RSC Adv*. **2016,** *6(36)*, 29909-19.

- Li, Yong; Dutta, Tanmoy; Gerasimchuk, Nikolay; Wu, Shijie; **Shetye, Kuldeep**; Jin, Lu; Wang, Ruixin; Zhu, Da-Ming; Peng, Zhonghua 'Conjugated Foldamers with Unusually High SCLC Hole Mobilities' *ACS Applied Materials Interfaces* **2015**, *7(18)*, 9372-84.

- Wang, Ruixin; Li, Yong; **Shetye, Kuldeep**; Dutta, Tanmoy; Jin, Lu; Li, Shaohua; Peng, Zhonghua 'Luminescent Polythiophene-Based Main-Chain Polyoxometalate-Containing Conjugated Polymers with Improved Solar-Cell Performance' *Eur. Jr. Inorg. Chem.* **2015**, *4*, 656-63.

ORAL AND POSTER PRESENTATIONS

- **Shetye, K.;** Li, Y.; Dutta, T.; Peng, Z. 'Rational design of conjugated foldamers for advanced optoelectronic applications' Abstracts, 51st Midwest Regional Meeting of the American Chemical Society, Manhattan, KS, United States, October 26-28, **2016**.

- Li, Y.; **Shetye, K.**; Oster, J.; Peng, Z. 'Synthesis, characterization, and photovoltaic applications of near-infrared absorbing main-chain polyoxometalate-containing conjugated copolymers' Abstracts, 51st Midwest Regional Meeting of the American Chemical Society, Manhattan, KS, United States, October 26-28, **2016**.

- **Shetye, K**.; Dutta, T.; Li, Y.; Lu, J.; Peng, Z. 'Synthesis and optical properties of conjugated foldamers' Abstracts, 48th Midwest Regional Meeting of the American Chemical Society, Springfield, MO, United States, October 16-19, **2013**.

- Dutta, T.; Li, Y.; **Shetye, K.**; Lu, j.; Peng, Z. 'Naphthodithiophene-based conjugated polymers for electronic applications' Abstracts, 48th Midwest Regional Meeting of the American Chemical Society, Springfield, MO, United States, October 16-19, **2013**.

- **Shetye, K.**.; Dutta, T.; Li, Y.; Lu, J.; Peng, Z. 'Synthesis of conjugated foldamers for solar cells' Abstracts, 47th Midwest Regional Meeting of the American Chemical Society, Omaha, NE, United States, October 24-27, **2012**.

- Dutta, T.; Li, Y.; **Shetye, K**.; Lu, J.; Peng, Z. 'Imide functionalized naphthadithiophene based conjugated polymers for photovoltaic applications' Abstracts, 47th Midwest Regional Meeting of the American Chemical Society, Omaha, NE, United States, October 24-27, **2012**.